ALFRED-WEGENER-INSTITUT
HELMHOLTZ-ZENTRUM FÜR POLAR- UND MEERESFORSCHUNG

764
2022

Berichte
zur Polar- und Meeresforschung
Reports on Polar and Marine Research

The Expedition PS128 of the Research Vessel POLARSTERN to the Weddell Sea, Lazarew Sea, Riiser-Larsen Sea, Cosmonaut Sea and Cooperation Sea in 2022

Edited by
Ralf Tiedemann and Juliane Müller
with contributions of the participants

HELMHOLTZ

Die Berichte zur Polar- und Meeresforschung werden vom Alfred-Wegener-Institut, Helmholtz-Zentrum für Polar- und Meeresforschung (AWI) in Bremerhaven, Deutschland, in Fortsetzung der vormaligen Berichte zur Polarforschung herausgegeben. Sie erscheinen in unregelmäßiger Abfolge.

Die Berichte zur Polar- und Meeresforschung enthalten Darstellungen und Ergebnisse der vom AWI selbst oder mit seiner Unterstützung durchgeführten Forschungsarbeiten in den Polargebieten und in den Meeren.

Die Publikationen umfassen Expeditionsberichte der vom AWI betriebenen Schiffe, Flugzeuge und Stationen, Forschungsergebnisse (inkl. Dissertationen) des Instituts und des Archivs für deutsche Polarforschung, sowie Abstracts und Proceedings von nationalen und internationalen Tagungen und Workshops des AWI.

Die Beiträge geben nicht notwendigerweise die Auffassung des AWI wider.

Herausgeber
Dr. Horst Bornemann

Redaktionelle Bearbeitung und Layout
Susan Amir Sawadkuhi

Alfred-Wegener-Institut
Helmholtz-Zentrum für Polar- und Meeresforschung
Am Handelshafen 12
27570 Bremerhaven
Germany

www.awi.de
www.awi.de/reports

Der Erstautor bzw. herausgebende Autor eines Bandes der Berichte zur Polar- und Meeresforschung versichert, dass er über alle Rechte am Werk verfügt und überträgt sämtliche Rechte auch im Namen seiner Koautoren an das AWI. Ein einfaches Nutzungsrecht verbleibt, wenn nicht anders angegeben, beim Autor (bei den Autoren). Das AWI beansprucht die Publikation der eingereichten Manuskripte über sein Repositorium ePIC (electronic Publication Information Center, s. Innenseite am Rückdeckel) mit optionalem print-on-demand.

The Reports on Polar and Marine Research are issued by the Alfred Wegener Institute, Helmholtz Centre for Polar and Marine Research (AWI) in Bremerhaven, Germany, succeeding the former Reports on Polar Research. They are published at irregular intervals.

The Reports on Polar and Marine Research contain presentations and results of research activities in polar regions and in the seas either carried out by the AWI or with its support.

Publications comprise expedition reports of the ships, aircrafts, and stations operated by the AWI, research results (incl. dissertations) of the Institute and the Archiv für deutsche Polarforschung, as well as abstracts and proceedings of national and international conferences and workshops of the AWI.

The papers contained in the Reports do not necessarily reflect the opinion of the AWI.

Editor
Dr. Horst Bornemann

Editorial editing and layout
Susan Amir Sawadkuhi

Alfred-Wegener-Institut
Helmholtz-Zentrum für Polar- und Meeresforschung
Am Handelshafen 12
27570 Bremerhaven
Germany

www.awi.de
www.awi.de/en/reports

The first or editing author of an issue of Reports on Polar and Marine Research ensures that he possesses all rights of the opus, and transfers all rights to the AWI, including those associated with the co-authors. The non-exclusive right of use (einfaches Nutzungsrecht) remains with the author unless stated otherwise. The AWI reserves the right to publish the submitted articles in its repository ePIC (electronic Publication Information Center, see inside page of verso) with the option to "print-on-demand".

Titel: Schelfeis-Abbruch im Südpolarmeer 70°42'0.11'' S 9°25'14.63'' W
(Foto: C.R. Rohleder, DWD)

Cover: Ice shelf breakup in the Southern Ocean 70°42'0.11'' S 9°25'14.63'' W
(Photo: C.R. Rohleder, DWD)

The Expedition PS128 of the Research Vessel POLARSTERN to the Lazarew Sea, Riiser-Larsen Sea, Cosmonaut Sea, and Cooperation Sea in 2022

Edited by

Ralf Tiedemann and Juliane Müller
with contributions of the participants

Please cite or link this publication using the identifiers

https://hdl.handle.net/10013/epic.4b73adb3-b8b6-40c9-889e-78d0acb4b311

https://doi.org/10.48433/BzPM_0764_2022

ISSN 1866-3192

PS128

6 January 2022 – 28 February 2022

Cape Town – Cape Town

Chief scientist
Ralf Tiedemann

Co-chief scientist
Juliane Müller

Coordinator
Ingo Schewe

Contents

1. ÜBERBLICK UND FAHRTVERLAUF

Ralf Tiedemann[1], Juliane Müller[1], [1]DE.AWI
Sonja Berg[2] [2]DE.UNI-Köln

Überblick

Die Expedition EASI-1 (**E**ast **A**ntarctic Ice **S**heet **I**nstability) ist die erste von drei durchzuführenden Expeditionen, die sich mit der erdgeschichtlichen Instabilität des ostantarktischen Eisschildes (EAIS) und ihrer Wechselwirkung mit Zirkulationsänderungen im Südpolarmeer befassen. Die Reaktion des EAIS auf die anthropogene Erwärmung ist mit großen Unsicherheiten für die Vorhersage des zukünftigen Meeresspiegelanstiegs behaftet, weil die Eis-Ozean-Klima Rückkopplungen kaum verstanden sind. Ihre Rekonstruktion, insbesondere für Zeiten in denen es wärmer war als heute, soll helfen, die Grundlagen für die Vorhersage zukünftiger Änderungen zu verbessern. Unsere Arbeiten konzentrierten sich auf die Region zwischen dem Weddellmeer und der Kooperationssee. Ziel war die Gewinnung von marinen und terrestrischen Sedimentkernen und die Erfassung von ozeanographischen, marin-geophysikalischen und kontinental-geodätischen Daten. Dieses Ziel konnte erfolgreich umgesetzt werden. Mit der zukünftigen Bearbeitung der Proben und Daten sollen neue Erkenntnisse über die Änderungen in folgenden Bereichen gewonnen werden: Bildung und Export von Antarktischem Bodenwasser vor Cape Darnley, ozeanischer Wärmetransport unter das Eisschelf der *Neumayer-Station III*, Verhalten der Eisaufsetzlinie, Meereisbedeckung, Schmelzwassereintrag und ozeanische Stratifizierung. Die Gewinnung langer Sedimentkerne und -oberflächen wurde von bathymetrischen Kartierungen, sediment-echografischen und hydrografischen Untersuchungen (inkl. Beprobung der Wassersäule) begleitet. Ebenfalls erfolgreich abgeschlossen wurde die Kampagne zur Verbindung mariner und kontinentaler Seismikprofile vor *Neumayer-Station III*

Die wichtigsten Ergebnisse der geologischen, geophysikalischen, geochemischen und ozeanographischen Arbeiten während PS128 sind:

Während aller Transitstrecken und Stationssuchfahrten in den Arbeitsgebieten wurden HYDROSWEEP und PARASOUND-Daten aufgezeichnet (insgesamt ca. 7.000 nm). Diese Daten lieferten die wichtigste Grundlage, um geeignete Sedimentkern-Lokationen zu identifizieren. Die PARASOUND-Daten dokumentierten lokal sehr unterschiedliche Sedimentbedeckungen und Mächtigkeiten von relativ jungen, quartären Sedimenten. Das Sedimentkerntransekt vom Bungenstockplateau zum oberen Kontinentalhang vor der Atka-Bucht zeichnet sich durch hohe Sedimenteindringungen > 50 m aus. In der Kooperationssee lagen die Eindringungen deutlich darunter, mit Ausnahme des Nielsen Basins. Selbst die Sedimentdrift am Edward VIII Rise lässt im Vergleich zum Bungenstockplateau geringere spätquartäre Sedimentationsraten vermuten.

- Oberflächensedimente konnten mit dem Multicorer an 22 Stationen und mit dem Großkastengreifer an 3 Stationen, insgesamt sehr erfolgreich gewonnen werden. 38 Schwereloteinsätze (35 erfolgreich), 9 Kolbenloteinsätze (8 erfolgreich) und 1 Kastenloteinsatz erbrachten insgesamt ca. 344 m Sedimentkernmaterial. Der längste Kern war 23,84 m lang.

- Eines der wichtigsten geologischen Ergebnisse ist die Gewinnung von Sedimentkernen entlang eines Nord-Süd Profiles vom oberen Kontinentalhang nahe der Atka-Bucht bis auf das Bungenstockplateau. Dieses Transekt deckt einen Wassertiefenbereich von 1600 m bis 3000 m ab. Erste sedimentphysikalische Messungen und lithostratigraphische Einstufungen an Bord deuten auf zeitlich relativ hochauflösende Sedimentabfolgen hin, die mehrere Glazial-Interglazial Zyklen abdecken. Eine Besonderheit dieses Sedimentkern-Transekts ist der relativ hohe Anteil an Biogenkarbonat (Foraminiferenschalen). Damit wird die zur Verfügung stehende Bibliothek an Proxyanwendungen zur Rekonstruktion ozeanographischer und klimatischer Veränderungen deutlich vergrößert.

- Die unprozessierten seismischen Daten lassen schon jetzt erkennen, dass die neuen seismischen Offshore-Profile qualitativ hochwertige Bilder von glazial transportierten und abgelagerten Sedimentabfolgen auf dem Kontinentalschelf vor der Ekström-Schelfeisregion liefern. Das wichtigste Ziel, die bereits bestehenden kontinentalen Vibroseis-Linien vom Ekström-Schelfeis mit den seismischen Profilen vom marinen Schelf und der Tiefsee miteinander zu verbinden konnte erfolgreich umgesetzt werden. Die stratigraphische Anbindung der marinen seismischen Sequenzen über die Sedimentkernbohrungen von ODP Leg 113 könnte damit auch die stratigraphische Einstufung der Vibroseis-Linien vom Ekström-Schelfeis erlauben.

- Auf dem Kontinentalschelf vor dem Ekström-Schelfeis im westlichen Teil unseres Arbeitsgebietes, sowie in zwei Glazialtrögen des Schelfes vor dem im östlichen Bereich des Arbeitsgebietes konnte durch Auskartierung prominenter pro- und subglazialer Strukturen am heutigen Meeresboden der Eisfluss während der letzten maximalen glazialen Ausbreitung, sowie der Beginn des Eisrückzugs von diesem Maximalstand verdeutlicht werden. Mehrere Sedimentkerne von diesen Strukturen werden wichtigen Aufschluss darüber geben können, wann das Eis seine maximale Ausbreitung in diesen Bereichen erreicht hat, wann in der Folge das Zurückweichen der Aufsetzlinie des Eisschildes eingeleitet wurde und in welchem Muster sich der Eisschild seitdem in Richtung der heutigen Aufsetzlinie zurückgezogen hat. Wir hoffen außerdem in der Lage zu sein, die Antriebsmechanismen zu charakterisieren, die zu den unterschiedlichen Rückzugsphasen geführt haben.

- Das Hauptziel der physikalischen Ozeanographie war es, die Grenzen des unteren zirkumpolaren Tiefenwassers (LCDW) und des antarktischen Bodenwassers (AABW) sowie die Wassermassen von der Oberfläche und vom Schelf als Quelle für die Bildung des AABW zu bestimmen. Aus diesem Grund haben wir einen zonalen Schnitt mit 17 CTD-Stationen (Conductivity, Temperature, Depth) von 9° West bis 66° Ost angelegt. Für jede Station wurde die CTD so eingesetzt, dass sie das Maximum der Wassertiefe abdeckte, um die Parameter in Bodennähe zu erreichen, die Werte der neutralen Dichte zu berechnen und die Grenzen der in diesem Gebiet der Ostantarktis vorhandenen Wassermassen abzugrenzen.

- An insgesamt 17 Stationen wurde die Wassersäule im antarktischen Sektor des Südozeans auf deren hydrologische Eigenschaften (Temperatur, Salinität, Dichte), der gelösten Sauerstoffkonzentration, Spurenmetall-Konzentrationen und Neodymium-Isotopen-Signaturen, sowie auf deren Kohlenstoff-Budget, Radiokarbongehalt und gelöste Nährstoffe beprobt. Ziel dieser Arbeiten ist die geochemische Charakterisierung einzelner Wassermassen des Südozeans, vertikaler Umwälzbewegungen sowie die Identifizierung der Fließpfade neu gebildeter Tiefenwassermassen. An einigen dieser Stationen wurde zusätzlich das Überstandswasser aus Multicorern gewonnen, um chemische Austauschprozesse am Meeresboden besser zu verstehen. Besonderes Augenmerk galt der Neubildung Antarktischen Bodenwassers vor Cape Darnley.

- An fünf Stationen wurden aus Multicorer-Sedimenten in Argonatmosphäre spurenmetallsauber Porenwasser aus Sedimenten extrahiert für die geochemische Charakterisierung des Ablagerungsmilieus, der Quantifizierung erwarteter in situ Verwitterungsprozesse am Meeresboden und lokaler Redox-Prozesse in antarktischen Tiefenwasser-Sedimenten.
- An drei landbasierten Stationen entlang des Kontinentalrandes der Ostantarktis wurde Sedimente enthaltenes Gletschereis gewonnen. Isotopengeochemische Untersuchungen an diesen Proben gewähren einerseits feinskaligere Einblicke in die Geologie der Herkunftsgebiete detritischer mariner Sedimente im Arbeitsgebiet. Vor allem werden diese Eisproben aber wichtige Rückschlüsse auf das physikalisch-chemische Verwitterungsverhalten ausgewählter Spurenmetalle (Nd, Pb, Sr) erlauben. Dies sind Untersuchungen, die aufgrund anthropogener Überprägung heutzutage nur an sehr wenigen Orten der Erde noch möglich sind.

Im Zeitraum vom 2. Februar bis 14. Februar 2022 haben die beiden Arbeitsgruppen der Universität zu Köln und der TU Dresden in den Thala Hills (*Station Molodezhnaya*) geologische und geodätische Untersuchungen durchgeführt.

- Zielsetzung der geologischen Arbeiten war es, Sedimentkerne aus den dortigen Seen zu gewinnen und glaziale Ablagerungen zu untersuchen, um die Spätpleistozäne bis Holozäne Eisrückzugsgeschichte und die nachfolgenden Umweltbedingungen in den Thala Hills zu rekonstruieren. Es konnten Sedimente aus insgesamt sechs Seen beprobt werden. In allen untersuchten Seen ist die postglaziale Sedimentation durch Ablagerungen aus mikrobiellen Matten im Zentimeter bis Dezimeter Bereich charakterisiert, die entweder klastische Sedimente überlagern oder direkt auf Festgestein liegen. Desweiteren wurden entlang von zwei Profilen glazial transportierte Ablagerungen beprobt, deren Ablagerungsalter eine Datierung des Eisrückzugs mittels der Analyse kosmogener Nuklide erlauben wird.
- Die geodätischen Feldarbeiten beinhalteten wiederholte GNSS-Messungen (Global Navigation Satellite Systems) an drei bereits im Festgestein vermarkten Punkten. Mit Hilfe der geodätischen GNSS-Messungen kann die Deformation der festen Erde bestimmt werden, welche durch vergangene und derzeit stattfindende Eismassenänderungen hervorgerufen wird. Im gesamten Enderby-Land sind präzise GNSS-Messungen auf Fels nur spärlich vorhanden, so dass die Messungen in den Thala-Bergen unerlässliche Daten zur Analyse des glazial-isostatischen Ausgleichs (GIA) und zur Validierung entsprechender Modelle darstellen. Die drei Messpunkte wurden für eine Dauer von sieben bis zehn Tage besetzt. Die Analyse der neu gewonnenen Daten erfolgt nach Beendigung der Expedition am Institut mittels sog. Postprocessing mit der Berner GNSS-Software. Damit kann die Zeitbasis für die abzuleitenden Deformationsraten entscheidend erweitert werden (auf über 15 Jahre), womit auch deren Genauigkeit verbessert wird.

Fahrtverlauf

Die *Polarstern*-Expedition PS128 startete am 6. Januar leicht verspätet gegen 18:00 Uhr in Kapstadt. An Bord befanden sich 44 Besatzungsmitglieder sowie 53 Wissenschaftler/innen, Techniker/innen und Hubschrauberpersonal. Außerdem hatten wir in den ersten 10 Tagen das AWI-Überwinterungsteam (9 Personen) für die *Neumayer-Station III* dabei. Alle hatten die Quarantänezeit in Kapstadt gesund überstanden. Die wissenschaftlichen Expeditionsteilnehmer aus 6 Arbeitsgruppen unterschiedlicher geologischer, geophysikalischer, ozeanographischer und geodätischer Disziplinen, darunter 16 Frauen, waren international gemischt. So waren

Kolleginnen und Kollegen aus Argentinien, Brasilien, Dänemark, Deutschland, Frankreich, England, Singapur, Spanien und China an Bord. Zwei Wissenschaftler erfüllten dabei Aufgaben als professionelle Wal-/Säugetierbeobachter. Zum Schutz der Wale und Robben wurden bei ihrer Sichtung die Stationsarbeiten unterbrochen.

Die recht ruhige Überfahrt Richtung *Neumayer-Station III* wurde vor allem zum Einrichten der Labore und für den Aufbau der Geräte genutzt. Unser erstes Arbeitsgebiet, das Bungenstockplateau (Abb. 1.1), erreichten wir am 16. Januar. Während der Anfahrt wurde der Streamer der Geophysik abgetrommelt und zu Wasser gelassen, um Messmodule am Streamer zu installieren. Die Meereissituation am Bungenstockplateau und in der angrenzenden Atka-Bucht vor *Neumayer III* stellte zu diesem Zeitpunkt kein großes Problem dar. Ziel der geologischen Arbeiten war es lange relativ karbonatreiche Sedimentkerne (20 –25 m) zu ziehen, die insbesondere durch erhöhte Sedimentationsraten in den vergangenen pleistozänen Warmzeiten charakterisiert sind. Leider war der Schiffskran, der zum Bewegen des Kernabsatzgestells benötigt wurde, nicht einsatzfähig. Es wurden daher zunächst an zwei Stationen nur kurze Sedimentkerne mit Längen von 4,4 – 5,4 m gewonnen (PS128_1, PS128_2). An beiden Stationen konnte der MUC zur Gewinnung ungestörter Sedimentoberflächen und Bodenwasserproben eingesetzt werden. Der begleitende Einsatz der CTD musste wiederholt werden, da verschiedene Sensoren der CTD zunächst ausgefallen war (PS128_1). Die anschließende Reparatur war erfolgreich. Am 17. Januar setzten wir unsere Fahrt Richtung Atka-Bucht fort und nutzten die Zeit zur Suche von Sedimentkern-Stationen mit HYDROSWEEP und PARASOUND. So arbeiteten wir uns im Zickzack-Kurs nach Süden vor, um möglichst weite Bereiche des Kontinentalhanges abzufahren. Wir wussten bereits von vorherigen Expeditionen, dass sich die Sedimentarchive dieser Region besonders für zeitlich hochauflösende Umweltrekonstruktionen eignen. Wir identifizierten vier Sedimentstationen (PS128_14 bis PS128_17), die wir zu einem späteren Zeitpunkt wieder anliefen. Am Nachmittag waren wir in Flugdistanz zur *Neumayer-Station III* und begannen mit dem Transfer des Überwinterer-Teams bei besten Flugwetterbedingungen. Insgesamt waren 7 Flüge notwendig.

Im Anschluss setzten wir unsere geologischen Untersuchungen am oberen Kontinentalschelf nordwestlich von *Neumayer III* fort. Ziel war es, die Ausdehnung des Eisschildes während des letzten Glazials sowie die Dynamik der Eisrückzüge zu erfassen. Dazu wurden hydroakustische Verfahren eingesetzt (HYDROSWEEP, PARASOUND) um die Morphologie des Meeresbodens und die Beschaffenheit der obersten Sedimentschichten zu erfassen. Anhand dieser Daten wurden 7 Lokationen ausgewählt (PS128_4 bis _10), an denen der Meeresboden mit kurzen Sedimentkernen oder mit dem Kastengreifer beprobt wurde. Begleitend wurde an der Station PS128_4 zur Charakterisierung der Wassermassensignaturen und der Beprobung der Wassersäule die CTD/Rosette eingesetzt (PS128_4). Die Arbeiten konnten am 18. Januar erfolgreich abgeschlossen werden.

An den folgenden Stationen PS128_11 bis PS128_13 (19.–20. Januar) sollten tertiäre Sedimentschichten mit dem Schwerelot beprobt werden. Seismische Profile zeigen an diesen Stationen, nördlich der Atka-Bucht, alte, dicht unter der Sedimentoberfläche ausbeißende Sedimentschichten, bzw. angeschnittene tertiäre Sedimentabfolgen im Bereich von Canyon-Flanken. An der ersten Station begannen wir mit einem ozeanographischen Profil (CTD/Rosette). Leider konnten die exakten Koordinaten zur Kernentnahme aufgrund der schwierigen Eisbedingungen nicht mehr angefahren werden. Der Schiffskran konnte zwischenzeitlich repariert werden und ermöglichte nun den Einsatz langer Kolben- und Schwerelote. Trotzdem konnten an den Stationen PS128_12 und PS128_13 nur kurze Sedimentkerne gewonnen werden. Leider waren die älteren Sedimentschichten so hart, dass ein tiefes Eindringen scheiterte und eines der Schwerelote sogar verbogen wurde (PS128_13).

Am 20. Januar erreichten wir wieder unser Arbeitsgebiet am Kontinentalhang zwischen Atka-Bucht und Bungenstockplateau und arbeiteten die vier bereits zuvor identifizierten Sedimentstationen PS128_14 bis PS128_17 erfolgreich mit Multicorer, Kolbenlot und Schwerelot ab. An jeder Station wurden zwei Sedimentkerne gezogen um ausreichend Probenmaterial für spätere Proxy-Messungen zur Verfügung zu haben. Das Transekt von Sedimentkernen deckt einen Wassertiefenbereich von ca. 1600 m bis 2300 m ab. Erste Messdaten und Kernbeschreibungen zeigen, dass sich die Sedimentprofile lithostratigraphisch gut miteinander korrelieren lassen. Nach Abschluss der Arbeiten führten wir am 22. Januar einen Seismiktest durch (PS128_18). Der Streamer wurde ausgebracht, die Luftkanonen getestet und die eingehenden Signale überprüft. Obwohl der Test positiv verlief, erlaubten die Meereisbedingungen keine daran anschließende Profilfahrt im geplanten Untersuchungsgebiet. Da wir wieder lange Lote einsetzen konnten, entschieden wir uns dafür nochmals das Bungenstockplateau anzusteuern um dort an zwei Stationen (PS128_19 und PS128_20) lange Sedimentkerne zu gewinnen. Nur die langen Sedimentkerne erlauben es uns, weit genug in der Erdgeschichte “zurückzureisen“ um an Zeitintervallen zu arbeiten, in denen es global wärmer war als heute. Mit der Station PS128_20 wurde die Station PS128_2 gedoppelt (ca. 1.700 m Wassertiefe). Die Station PS128_19 befindet sich am nördlichen Ende des Plateaus in etwa 3.000 m Wassertiefe. Die Arbeiten wurden am 24. Januar erfolgreich beendet.

Obwohl die Meereisbedingungen immer noch nicht optimal für den Einsatz der Seismik waren, wurde der Streamer am 24. Januar gegen 19:30 UTC ausgebracht. Die Navigation der Profilfahrten durch das Eis wurde durch Helikopter-Erkundungsflüge unterstützt. Obwohl nur ein geringer Teil der angedachten Profilstrecken abgefahren werden konnte, wurden die seismischen Untersuchungen am 27. Januar dennoch erfolgreich beendet. Mit großer Wahrscheinlichkeit wurde das Hauptziel erreicht, nämlich die Anbindung bereits existierender mariner Seismikprofile an die kontinentalen Seismikprofile bei *Neumayer III*.

Nach Abschluss aller Arbeiten am Schelf und Kontinentalhang vor *Neumayer III* dampften wir mit voller Kraft ostwärts in Richtung der russischen Station *Molodezhnaya,* um dort unser Landteam abzusetzen. Auf dem langen Transit von ca. 1.200 nm haben wir an 5 CTD Stationen ozeanographische Profile erstellt und Wasserproben genommen. An zwei dieser Stationen wurde auch die Sedimentoberfläche mithilfe des MUC beprobt.

Am frühen Morgen des 2. Februar erreichten wir die eisbedeckten Küstengewässer vor *Molodezhnaya*. *Polarstern* konnte sich bis auf 35 km der Küste nähern. Die Flugwetter-bedingungen waren optimal: gute Sicht, strahlend blauer Himmel, kaum Wind. Nach 11 Helikopterflügen (3 davon mit Außenlast für den Transport der Ausrüstung) war das Landteam (6 Personen) nach *Molodezhnaya* gebracht worden, wo die belarussischen Kollegen von der nahe von *Molodezhnaya* gelegenen Station am Mount Vechernyaya, sie unter Wahrung der Corona-Maßnahmen begrüßten.

Am Abend des 2. Februar machten wir uns auf den Weg in unser zweites Hauptarbeitsgebiet, die Kooperationssee. Kurz nach der Abfahrt kreuzte der chinesische Forschungseisbrecher *Xuelong 2* unseren Weg, mit dem wir Funk- und Sichtkontakt hatten. Am 4. Februar erreichten wir die Kooperationssee. Aufgrund eines Orkantiefs, welches in den Vorhersagen und in den Wettermodellrechnungen nicht so stark vorausgesagt wurde, mussten wir den Forschungsbetrieb vom 4. – 6. Februar einstellen und abwettern. Im Mittel lag die Windstärke bei 10 Bft mit Böen bis 12 Bft (Abb. 1.2). Die Windsee erreichte ihr Maximum bei 10 – 12 m. Da wir mit etwa 3 – 4 kn Fahrt nach Südosten gegen den Wind abwetterten, entfernten wir uns während der zwei Tage zunehmend von den ursprünglich anvisierten Kernstationen. Aus Zeitgründen verzichteten wir auf eine erneute Anfahrt sowie auf zwei weitere küstenferne Stationen weiter nördlich. Stattdessen konzentrierten wir unsere HYDROSWEEP- und PARASOUND-Suchen nach geeigneten Sedimentarchiven auf die küstennäheren Bereiche am Daly Rise und Wild West

Rise. Im Bereich des Daly Rise wurden MUC und zwei Schwerelote erfolgreich an Station PS128_34 eingesetzt. Etwas versetzt dazu wurde die CTD/Rosette Station (PS128_35) in den Daly Canyon verlegt, um den Ausstrom des Antarktischen Bodenwassers (AABW) aus seinem Bildungsgebiet vor Cape Darnley zu erfassen. Die anschließende Suche nach geeigneten Sedimentarchiven am oberen Kontinentalhang blieb leider erfolglos. Weiter südlich, in unmittelbarer Nähe zum Bildungsgebiet des AABW, wurde der Bodenwasser-Ausstrom mit einer weiteren CTD/Rosette Station am oberen Kontinentalhang erfasst (PS128_36).

Am 8. Februar erreichten wir das Nielsen Basin am kontinentalen Schelf des Mac. Robertson Land (Abb. 1.1), das durch glaziale Erosion entstanden ist. Das Nielsen Basin besteht aus bis zu 1.000 m tiefen, großflächigen Trögen, die durch flache Schwellen voneinander getrennt sind. Diese Tröge beinhalten zeitlich sehr hochauflösende deglaziale Sedimentarchive, die vorwiegend aus gewarvten, diatomeenreichen Sedimenten bestehen. Ziel war es einerseits diese hochauflösenden Archive zu beproben und andererseits die Ausdehnung des Eisschildes während des letzten Glazials sowie die Dynamik der Eisrückzüge zu erfassen. Mit HYDROSWEEP und PARASOUND wurde die Morphologie des Meeresbodens kartiert und die Beschaffenheit der obersten Sedimentschichten erfasst. Diese Untersuchungen waren Basis für die erfolgreiche Beprobung der Sedimentschichten mit Schwerelot und MUC und den Einsatz der CTD/Rosette zur Charakterisierung der Wassermassensignaturen und der Beprobung der Wassersäule (PS128_38 bis PS128_45). Am 10. Februar haben wir unsere Untersuchungen mit zwei weiteren Stationen auf die westlich gelegene Iceberg Alley ausgeweitet (PS128_46, PS128_47). Während der Stationsarbeiten wurden drei Helikopterflüge entlang der Küstenlinie zur Sichtung und Beprobung von sedimentreichen Gletscherlagen in der Nähe von Nunataks durchgeführt. Das Beprobungsprogrammem konnte am Neill Peak und am Painted Peak in der Nähe der *Mawson Station* erfolgreich umgesetzt werden.

Am 11. Februar setzten wir unsere geologischen und ozeanographischen Untersuchungen weiter westlich im Bereich der Stefanssons Bay fort. Dort zeigen die bathymetrischen Karten eine südliche Einbuchtung des oberen Kontinentalhangs mit einer nach Norden angelegten Beckenstruktur. Wir hatten gehofft, dass die dortigen Sedimente die Dynamik des westwärts setzenden Antarktischen Küstenstroms abbilden und haben an drei Stationen Multicorer, Schwerelot und CTD eingesetzt (PS128_48 bis PS128_51). Die bathymetrischen Daten haben allerdings offenbart, dass es sich nicht um ein Sedimentbecken handelt, sondern um ein dynamisches Canyonsystem, durch das die Sedimente in die Tiefsee transportiert werden.

Am 12. Februar erreichten wir weiter westlich den Edward VIII Rise. Leider musste wegen stürmischer Wetterbedingungen (Abb. 1.2) und hoher Windsee der versuchte Einsatz eines Schwerelotes abgebrochen werden. Stattdessen wurden PARASOUND und HYDROSWEEP Profilfahrten zur Erkundung von Sedimentarchiven im Bereich des Edward VIII Rise durchgeführt, bevor wir uns auf den Weg in Richtung *Molodezhnaya* machten, um unser Landteam abzuholen. Aufgrund der Wetterprognosen für *Molodezhnaya* haben wir den Abholtermin um zwei Tage vorverlegt. Dennoch konnten wir die Landexpedition alle geplanten Aufgaben in der verbliebenen Zeit erledigen.

Am Vormittag des 14. Februar erreichten wir die Bucht vor *Molodezhnaya*. Die Eisverhältnisse waren günstig, so dass wir bis auf ca. 2 Seemeilen an die Station herankamen. Die Flugbedingungen waren perfekt, wenig Wind und strahlend blauer Himmel. Die sechs Personen und die gesamte Ausrüstung konnten in sieben Heli-Flügen an Bord geholt werden. Im Vorfeld hatte das Landteam Corona-Schnelltests durchgeführt. Nach Ankunft an Bord wurde in sofortiger Isolation ein PCR-Test durchgeführt. Alle Testergebnisse waren negativ. Während der Flugoperationen haben wir mithilfe von Zodiac-Booten Gesteinsproben entlang der Küste entnommen. Diese sollen, wie auch die vorangegangenen Beprobungen an Nunataks, verbesserte Rückschlüsse auf die Herkunftsgebiete von eistransportiertem Schutt

in das Südpolarmeer zulassen. Nachdem das Landteam und ihre Ausrüstung an Bord waren, wurde beim Verlassen der Bucht noch eine CTD/Rosette-Station durchgeführt (PS128_52).

Im Anschluss war eigentlich ein Forschungsprogrammem im Bereich der Lützow Holm Bay und der *Syowa-Station* geplant, bevor wir uns auf den Weg Richtung Kapstadt machten. Aufgrund der dortigen sehr schlechten Wetterverhältnisse und Prognosen für die nächsten Tage, sind wir wieder nach Osten zurückgefahren, um in der Kooperationssee am Edward VIII Rise die ausgefallenen Sedimentkernbeprobungen (schlechtes Wetter) nachzuholen. Auf dem Weg dorthin kreuzte der japanische Forschungseisbrecher *Shirase* unseren Weg. Nach einem kurzen Rendezvous und Gesprächsaustausch (per Funk) haben wir im Bereich der Amundsen Bay, nördlich von White Island, einen Sedimentkern aus 1.000 m Wassertiefe gezogen (PS128_53). Dieses Sedimentarchiv, das wir bereits auf dem vorangegangenen Transit nach *Molodezhnaya* entdeckten, sollte Hinweise auf die deglaziale Dynamik des Beaver Gletschers und des Antarktischen Küstenstromes liefern.

Am 16. Februar erreichten wir den Edward VIII Rise. Die PARASOUND Daten weisen auf eine Sedimentdrift hin, die ihre höchsten Mächtigkeiten zwischen 3.400 und 4.000 m erreicht. Insgesamt gab es vier Einsätze von Schwerelot und Multicorer und eine CTD/ Rosette Station (PS128_54 bis PS128_58). Die CTD/Rosette wurde in einem Canyon an der östlichen Flanke bis auf ca. 4.120 m Wassertiefe abgesenkt und lieferte Wasserproben und Wassermassensignaturen (Temperatur, Salinität) zum Ausstrom des AABW in die nördliche Tiefseeebene des Indischen Ozeans. Von den Sedimentkernen versprechen wir uns Einsichten in die Veränderlichkeit der Strömungsdynamik und der Bildung von AABW während der letzten Glazial/Interglazial-Zyklen.

Am 17. Februar traten wir die Rückreise nach Kapstadt an. Auf dem Weg lag eine weitere Station im Bereich des Atlantisch-Indischen Rückens (ca. 52.5° S), die wir am 22. Februar erreichten. Die dortigen Sedimentarchive ermöglichen erdgeschichtliche Rekonstruktionen zur Breitenverlagerung der Polarfront und der winterlichen antarktischen Meereisausdehnung infolge von Klimaschwankungen. Während der Parasound-Profilfahrt wurde ein zeitlich sehr hochauflösendes Sedimentarchiv aufgespürt (bis zu 200 m mächtig). Anfangs waren Windstärke und Windsee zu hoch, um einen Schwereloteinsatz durchzuführen (Abb. 1.2). Nach ein paar Stunden besserten sich die Verhältnisse. Die Windstärke lag bei ca. 5 Bft, die Windsee bei etwa 3 m. Dennoch war aus Sicherheitsgründen kein Einsatz des Schwerelotes möglich. Die Einsatzmöglichkeiten des Haupt-Krans zur Montage des Kernabsatzgestells auf den Haltebolzen des Quer-Schiebebalkens wurden als zu gefährlich eingestuft. Auf der Weiterfahrt waren wir gezwungen einem Orkantief auszuweichen. Am 28. Februar erreichte *Polarstern* den Hafen von Kapstadt und beendete die Expedition PS128.

Verlauf der Landexpedition

Am frühen Morgen des 2. Februars erreichten wir die eisbedeckten Küstengewässer vor *Molodezhnaya*. Mit dem ersten Helikopterflug wurden die zwei Geodät:innen unserer Landgruppe zum Abendberg geflogen, wo sie den ersten GNSS Messpunkt (ABE1) aufbauten. Der Messpunkt befindet sich in der Nähe der belarussischen Station und die Mitglieder der belarussischen Antarktisexpedition (BAE) hatten für unsere Ankunft einen Helikopterlandeplatz vorbereitet. Die weiteren Personen unserer Landgruppe und unsere gesamte Ausrüstung wurden darauffolgend zur russischen Antarktisstation *Molodezhnaya* gebracht. Dort konnten wir ein Stationsgebäude als Unterkunft nutzen, welches durch die BAE unterhalten wird. Von dem Leiter der BAE, A. Gaidashov, und seinem Team wurden wir unter Wahrung der Corona-Maßnahmen begrüßt. Die Flugoperationen konnten am Nachmittag beendet werden.

Am 3. Februar, als wir mit unserem Arbeitsprogrammem begannen, war es bewölkt und windig. Die Geodät:innen besuchten den zweiten GNSS Messpunkt (GRA1), wo wir das GNSS

Equipment der russischen Kollegen von Aerogeodeziya für die Zeitspanne unserer Messung abbauten und das eigene GNSS Equipment montierten. Die Geolog:innen begannen die Seen Lagernoye und Glubokoye zu untersuchen. Beide Seen waren mit 3 m dickem Eis bedeckt. Die ersten Versuche Sediment mit dem Schwerelot zu beproben waren aufgrund einer sehr dünnen Sedimentdecke nicht erfolgreich. Für geochemische Analysen nahmen wir an einer 22,4 m tiefen Stelle des Sees Glubokoye Wasserproben aus verschiedenen Tiefen.

Die Wetterbedingungen am Morgen des 4. Februars waren gut (weniger windig, keine Wolken, gute Sicht, guter Kontrast) und die Geodät:innen fuhren zur Halbinsel Blisnetzov, um den dritten GNSS Messpunkt (BLIS) aufzubauen. Die Geolog:innen setzten ihre Arbeit am See Glubokoye fort. Wir entnahmen mehrere Proben mit 20 cm dicken Ablagerungen von Algen/ mikrobiellen Matten mit Hilfe des Schwerelotes an einer > 30 m tiefen Stelle. Gegen Mittag nahm der Wind zu und es wurde bewölkt. Am Nachmittag mussten wir aufgrund von sehr starken Winden im Gebäude verweilen.

Am 5. Februar verbesserte sich das Wetter und wir fuhren mit der Arbeit am See Ovalnoye fort, wo bis zu 70 cm lange Sedimentkerne erbohrt wurden. Zu zweit besuchten wir einige kartografisch eingezeichnete GNSS Punkte, die als potentielle Messpunkte zum vorübergehenden Aufbau der russischen GNSS Ausrüstung hätten dienen können. Jedoch fanden wir keine passenden Vermarkungen vor. Am späten Vormittag trafen zwei Kollegen der BAE bei *Molodezhnaya* ein und übergaben uns Sedimentproben, die sie für uns im See Niznee in der Nähe der belarussischen Station genommen hatten (und einen sehr schönen *Polarstern* Kuchen).

Das Wetter verbesserte sich weiter und der 6. Februar war ein windstiller, sonniger Tag. Zwei Personen unserer Gruppe begannen entlang der des Eisschilds nächsten Erhebungen mit der Beprobung von glazial transportierten Ablagerungen zur Datierung des Eisrückzugs. Desweiteren beprobten wir am Nachmittag Gletschereis mit eingeschlossenem Sediment am Rande des Eisschildes. Die anderen Personen setzten die Beprobungen am See Lagernoye fort und konnten erfolgreich mehrere Schwerelotkerne von bis zu 20 cm Länge gewinnen.

Am 7. Februar war das Wetter windig, aber mit guter Sicht und gutem Kontrast. Daher fuhren die Geodät:innen am Morgen mit dem Schneemobil zu dem GNSS Messpunkt ABE1, um die Geräte zu überprüfen. Wir benutzen die existierende, markierte Route über den Eisschild zum Abendberg und sind mittags nach *Molodezhnaya* zurückgekehrt. Wir beobachteten, dass sich das Meereis vor dem Abendberg gelöst hatte, während wir vor *Molodezhnaya* nach wie vor eine geschlossene Meereisbedeckung vorfanden. Die Geolog:innen fuhren mit der Beprobung der glazialen Findlinge und der Sedimente am See Lagernoye and Glubokoye fort. Zwei Personen machten sich am Nachmittag auf dem Weg zu den nahegelegenen Rücken, um biologische Bodenkrusten zu beproben.

Wir setzten sowohl die Sediment- als auch die Wasserbeprobung am See Glubokoye am 08. Februar fort und nahmen zusätzlich eine Sedimentprobe am See Promeoye. Weiterhin bereiteten wir das Equipment zur Benutzung des Kolbenlotes am See Glubokoye für den folgenden Tag vor. Mit dem Einsetzen des Kolbenlotes konnten wir jedoch nicht tiefer als mit dem Schwerelot in das Sediment eindringen, da sich entweder sehr hartes Sediment oder Festgestein unter den postglazialen Sedimentablagerungen befindet. Am Nachmittag besuchten wir den nordwestlichen Teil von *Molodezhnaya*, um die Gerätschaften des GNSS Messpunktes GRA1 zu überprüfen und glazial transportierte Ablagerungen zu sammeln.

Das Wetter am 10. Februar war sonnig (gute Sicht und guter Kontrast), jedoch sehr windig. Wir fuhren zu der Halbinsel Blisnetzov und folgten dabei der bereits am 4. Februar benutzten Route, die gut zu befahren war. Bei Blisnetzov kontrollierten wir den Messpunkt BLIS und beprobten ein Profil mit glazialen Findlingen von der Küste bis hin zum heutigen Eisschildrand. Außerdem nahmen wir Sedimentproben von einem See und an einem Standort Bodenkrustenproben.

Da für den 12. und 13. Februar Sturm vorhergesagt wurde, holten wir die GNSS Ausrüstung des Messpunktes BLIS bereits am Morgen des 11. Februars ein. Daraufhin fuhren wir zum Abendberg, um auch den GNSS Messpunkt ABE1 abzubauen und Sedimentbeprobungen am Niznee See durchzuführen. Die Traverse zum Abendberg wurde mit den belarussischen Kollegen koordiniert, die uns mit ihrem Kettenfahrzeug begleiteten. Dies war insbesondere beim Hinauf- und Herabfahren vom Land auf den Eisschild und umgekehrt hilfreich, da an diesen Hängen teils keine Schneebedeckung mehr vorhanden war und Blaueisstellen überquert werden mussten. Die Arbeit am Abendberg führten wir erfolgreich durch und die Kollaboration mit den Kollegen der BAE war, unter Einhaltung aller Coronaregelungen, sehr herzlich.

Mit der Beprobung von glazial transportierten Ablagerungen entlang eines nordsüdlichen Profils durch *Molodezhnaya* beendeten wir am Nachmittag des 12. Februars unser wissenschaftliches Programmem. Wir begannen unser Equipment für den Transport zurück zu *Polarstern* vorzubereiten und verbrachten den folgenden Tag mit den Aufräumarbeiten unseres Lagers. Der Helikopter von *Polarstern* kam am Morgen des 14. Februars an und das Zurückbringen der Personen und der Ausrüstung zu *Polarstern* konnte ohne Verspätungen ausgeführt werden.

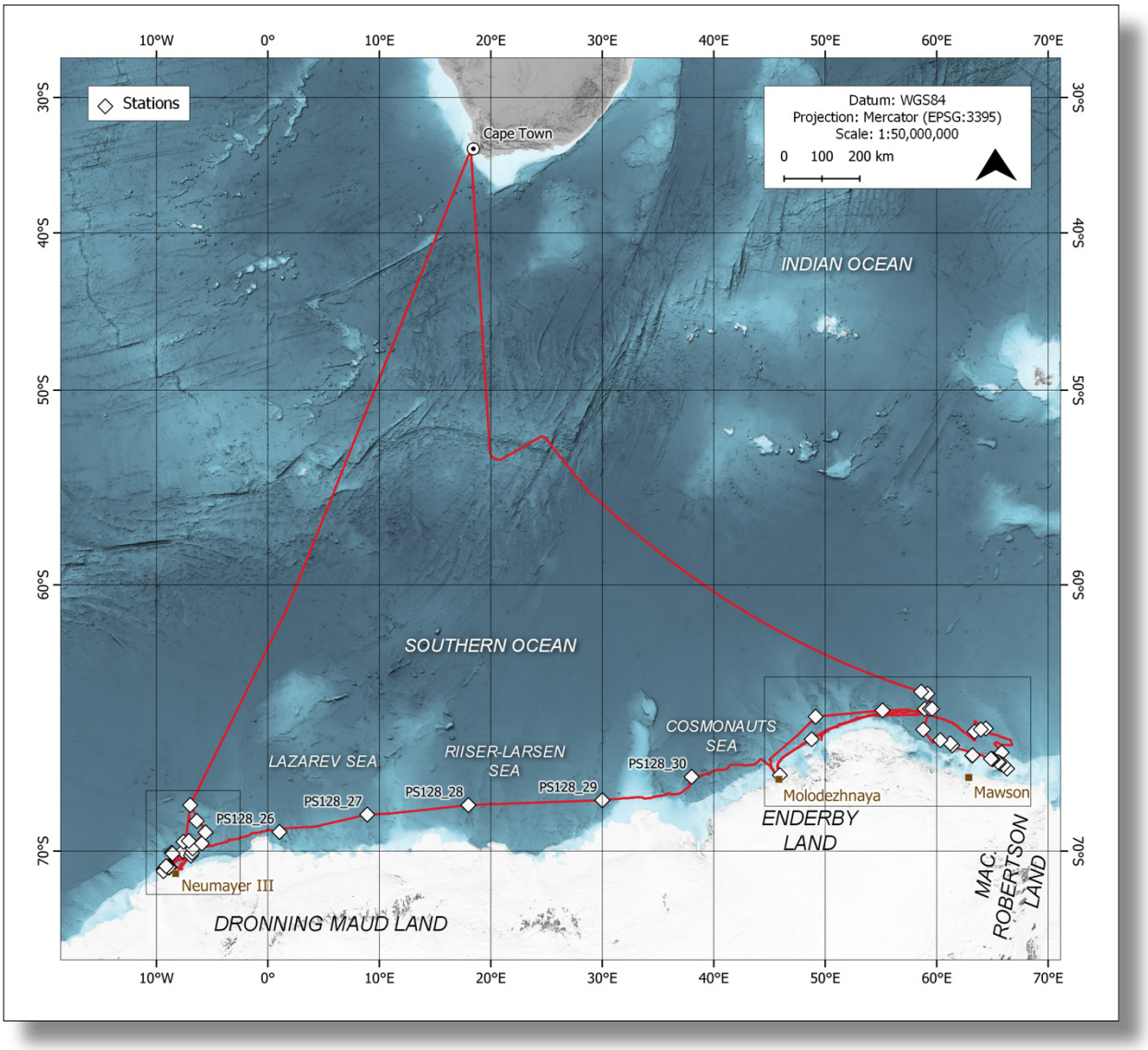

Abb. 1.1: Fahrtroute und Stationen der Polarstern während der Expedition PS128 von Kapstadt, entlang des antarktischen Kontinentalhangs von Dronning Maud Land bis zum Mac. Robertson Land und zurück nach Kapstadt. Siehe https://doi.pangaea.de/10.1594/PANGAEA.944833 für eine Darstellung des master tracks in Verbindung mit der Stationsliste für PS128.

Fig. 1.1: Cruise track and stations of Polarstern during expedition PS128 from Cape Town, along the Antarctic continental margin from Dronning Maud Land to Mac. Robertson Land and back to Cape Town. See https://doi.pangaea.de/10.1594/PANGAEA.944833 to display the master track in conjunction with the station list for PS128.

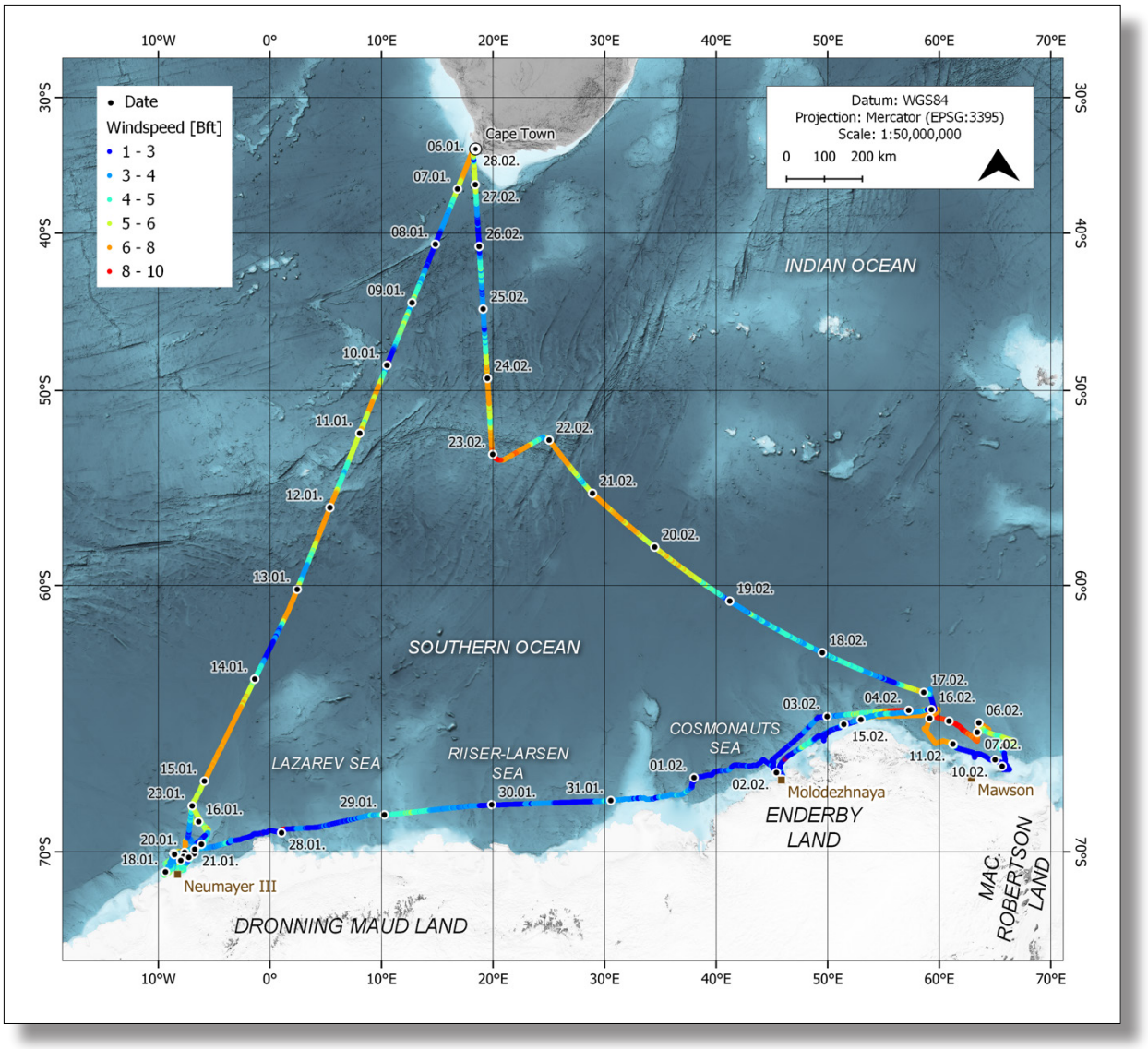

Abb. 1.2: Zeitlicher Fahrtverlauf und Windstärke entlang der Fahrtroute der Polarstern Expedition PS128

Fig. 1.2: Timing and wind strength along the route of Polarstern expedition PS128

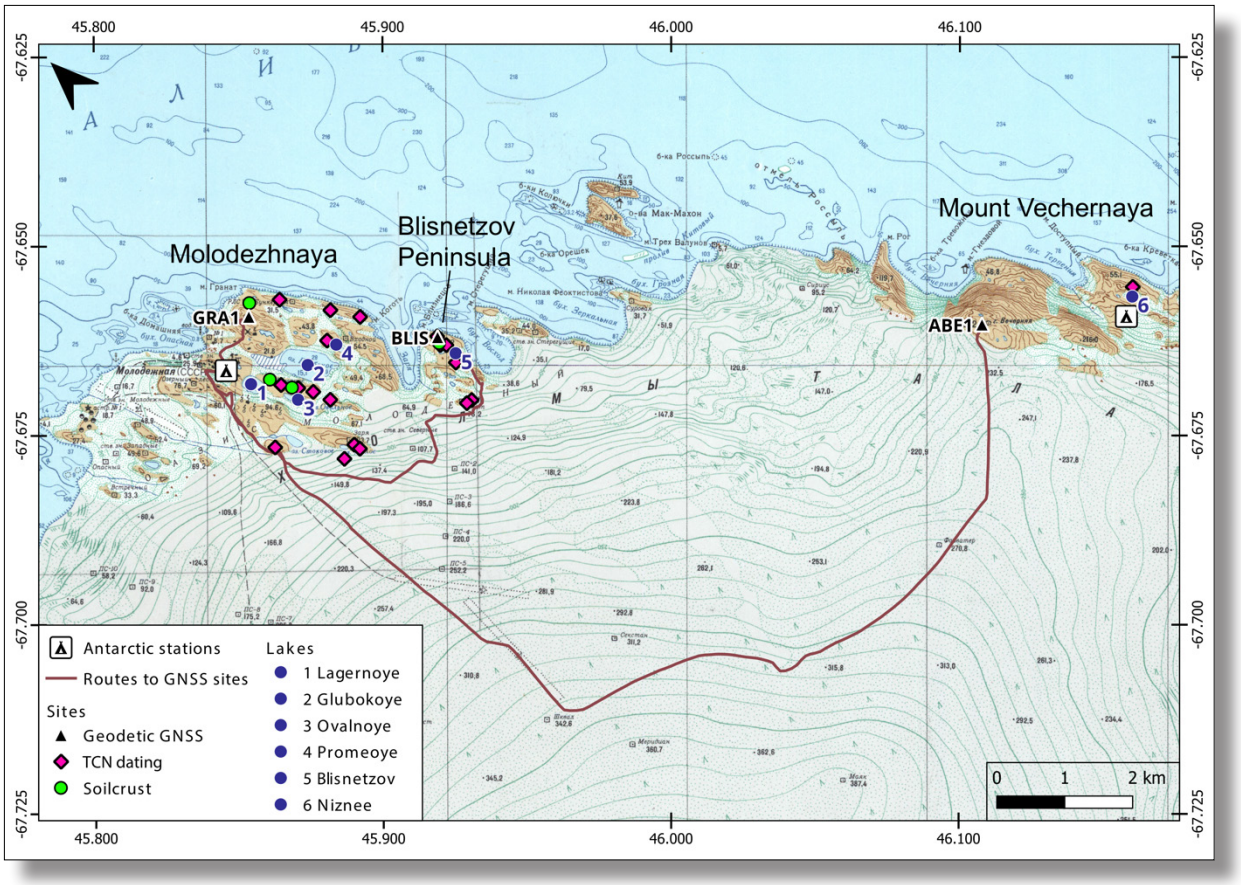

Abb. 1.3: Karte des Untersuchungsgebietes Thala Hills; Probenahmepunkte sind farblich hervorgehoben.

Fig. 1.3: Map showing Thala Hills; sampling sites and respective sample types are indicated.

SUMMARY AND ITINERARY

Summary

- Expedition EASI-1 represents the first of three scheduled expeditions that will examine the history of **E**ast **A**ntarctic Ice **S**heet **I**nstability and its interaction with changes in Southern Ocean (SO) circulation. The behaviour of the East Antarctic Ice Sheet (EAIS) under projected anthropogenic warming is a key uncertainty in predicting future sea level rise due to the influence of strong ice-ocean feedbacks, which are poorly understood. Reconstructing and disentangling these feedbacks during past warmer-than-present climate states is considered to provide an enhanced basis for improved prediction of future changes in the ice-ocean-climate system. Our goal was to acquire marine and terrestrial sediment records, in combination with oceanographic, marine-geophysical and continental-geodetic data. Our work focused on the Antarctic continental margin between the Weddell and Cooperation Seas. This goal was successfully achieved. Future processing of the samples and data should enhance our knowledge about

changes in: Antarctic bottom water formation and export at Cape Darnley, ocean heat transport to the ice-shelf cavity below *Neumayer Station III*, grounding-line behaviour, sea ice-cover, meltwater supply and oceanic stratification. The recovery of long sediment records and surface sediments was accompanied by bathymetric, sediment echo-sounding, and hydrographic surveys (including water column sampling). The campaign to connect marine and continental seismic profiles of *Neumayer Station III* was also successfully completed.

- The most important results of the geological, geophysical, geochemical and oceanographic work during PS128 are:

- HYDROSWEEP and PARASOUND data were recorded during all transit routes and coring site surveys (in total about 7,000 nm). These data provided the main basis for identifying suitable sediment core locations. The PARASOUND data documented locally very different sediment cover and thicknesses of relatively young Quaternary sediments. The sediment core transect from the Bungenstock Plateau to the upper continental slope off Atka Bay is characterised by PARASOUND signals that reveal a nice succession of parallel sediment reflectors more than > 50 m thick. In the Cooperation Sea, the PARASOUND penetration was well below this, with the exception of Nielsen Basin. Even the sediment drift at Edward VIII Rise suggests lower Late Quaternary sedimentation rates compared to the Bungenstock Plateau.

- Surface sediments were recovered very successfully with the Multicorer at 22 stations and with the Giant Box Corer at 3 stations. 38 Gravity Corer deployments (35 successful), 9 Piston Corer deployments (8 successful) and 1 Box Corer deployment yielded a total of approx. 344 m of sediment core material. The longest core had a length of 23,84 m.

- One of the most important geological achievements is the recovery of sediment cores along a north-south profile from the upper continental slope near Atka Bay to the Bungenstock Plateau. First shipboard sediment-physical measurements and lithostratigraphic assignments indicate relatively high-resolution sedimentary sequences covering several glacial-interglacial cycles. This transect covers a water depth range from 1,600 m to 3,000 m and thus allows to reconstruct changes in water mass structures, such as the influence of warm deep-water masses on the upper continental slope that can penetrate into the cavities below the ice shelf. Another special characteristic of this sediment core transect is the relatively high proportion of biogenic carbonate (*foraminifera* shells). This significantly increases the available library of proxies for reconstructing oceanographic and climatic changes off *Neumayer Station III.*

- The unprocessed seismic data already indicate that the new offshore seismic profiles will provide high quality images of glacially transported and deposited sedimentary sequences on the continental shelf off the Ekström Ice Shelf region. The main goal of connecting the already existing continental vibroseismic lines from the Ekström Ice Shelf with the seismic profiles from the marine shelf and the deep sea was successfully achieved. The stratigraphic calibration of the marine seismic sequences via the sediment records of ODP Leg 113 could thus also allow the assignment of ages to the vibroseismic sequences of the Ekström Ice Shelf.

- Within glacial troughs on the continental shelf offshore the Ekström Ice Shelf as well as on the shelf offshore the Mac. Robertson Land in the eastern part of the study area, we were able to map prominent pro- and subglacial morphological structures on the seafloor that allow characterisation of past ice flow during the last maximum extent and subsequent retreat dynamics of the grounding line. Several sediment cores from these structures will 1) provide important insights as to when the ice reached its maximum

extent in these areas, 2) when the subsequent retreat of the ice sheet's grounding line was initiated, and 3) how the ice sheet has retreated towards the present grounding line thereafter. We also hope to be able to characterise the driving mechanisms that led to the different phases of retreat.

- The main goal of Physical Oceanography was to establish the boundaries of the Lower Circumpolar Deep Water (LCDW) and the Antarctic Bottom Water (AABW) as well as the water masses from the surface and shelf water masses as sources for the formation of the AABW. For that reason, we made a zonal section with 17 CTD (Conductivity, Temperature, Depth) stations from 9° West to 66° East. For each station, the CTD was deployed to cover the full water column in order to reach the parameters near the bottom, compute neutral density values, and delineate the boundaries of the water masses present in this area of East Antarctica.

- The water column in the Atlantic/Indian sector of the Southern Ocean was sampled at 17 stations in total for its hydrologic parameters (temperature, salinity, density), the dissolved oxygen concentration, trace metal abundances and neodymium isotopic composition, as well as their carbon budget, radiocarbon content and dissolved nutrients. The aim of these analyses is the geochemical characterisation of individual water masses within the Southern Ocean, assessment of vertical exchange processes, as well as the identification of flow pathways of newly formed Antarctic Bottom Water. Additionally, multicore water was sampled at several of these stations in order to better understand chemical exchange processes at the seafloor. The water column work centered around the study of Antarctic Bottom Water formation in the Cape Darnley area.

- Marine porewater was extracted at a total of five deep water multicore stations along the East Antarctic margin under argon atmosphere. This approach allows retrieval of marine porewaters under oxygen-free and trace metal clean conditions for the geochemical characterisation of the depositional environment, quantification of expected *in-situ* chemical weathering processes at the seafloor, as well as investigation of the intensity of local redox processes in Antarctic deep sea sediments.

- Sediment-bearing Antarctic continental ice was sampled at three stations along the East Antarctic margin. Isotope geochemical analyses on these samples will provide fine-scaled insights into the geology of the source areas of these sediments. Moreover, these archives will allow a critical new assessment of the effect of glacial physico-chemical weathering processes on the release of selected trace metals (Nd, Pb, Sr), a mechanism termed "incongruent weathering" among isotope geochemists. Nowadays, these kinds of analyses can only be carried out at very few pristine locations around the globe due to anthropogenic activity elsewhere.

From 2 Febuary to 14 Febuary 2022 the working groups from the University of Cologne and the TU Dresden successfully carried out geological and geodetical field work in Thala Hills.

- The aim of the geological study was to collect lake sediment cores and glacial deposits in order to reconstruct the timing of the late Pleistocene to Holocene deglaciation and the subsequent environmental history of Thala Hills. Sediment coring was conducted on six lakes. We found that post-glacial sedimentation in all lakes is dominated by biogenic sedimentation, which is reflected in centimeter- to multi-decimeter-thick deposits of microbial/algae mats that overlay clastic sediments or bedrock. Glacial erratics for cosmogenic nuclide dating were collected along two transects from the ice sheet margin to the coast to infer the timing of ice sheet retreat. Further analyses will

provide information on the age of lake sediments and glacial deposits and lead to a first comprehensive deglaciation history of the area.

- The geodetic field work included repeated GNSS (Global Navigation Satellite Systems) measurements at three points already marked in bedrock. The geodetic GNSS measurements can be used to determine the deformation of the solid earth caused by past and present ice mass changes. Throughout Enderby Land, precise GNSS measurements on bedrock are sparse, so the measurements in the Thala Hills provide indispensable data for analyzing glacial isostatic adjustment (GIA) and validating corresponding models. The three measurement points were occupied for a period of seven to ten days. After the end of the expedition, the newly acquired data will be analyzed at the institute by means of so-called post-processing with the Bernese GNSS software. This allows the time base for the deformation rates to be derived to be decisively extended (to over 15 years), which also will improve their accuracy.

Itinerary

Polarstern expedition PS128 departed Cape Town on 6 January, slightly delayed, at about 18:00. On board were 44 crew members and 53 scientists, technicians and helicopter personnel. We also had the AWI overwintering team (9 people) for *Neumayer Station III* with us for the first 10 days. All had passed the quarantine period in Cape Town in good health. The scientific expedition participants from 6 working groups of different geological, geophysical, oceanographic and geodetic disciplines, including 16 women, were internationally mixed. Colleagues from Argentina, Brazil, Denmark, Germany, France, England, Singapore, Spain, Switzerland and China were on board. Two scientists fulfilled tasks as professional whale/mammal observers. To protect the whales and seals, station work was interrupted during their sightings.

The rather calm crossing towards *Neumayer Station III* was mainly used for setting up the laboratories and the equipment. We reached our first working area, the Bungenstock plateau (Fig. 1.1), on 16 January. During the approach, the geophysics streamer was unwound and lowered into the water to install measurement modules on the streamer. The sea ice-situation on the Bungenstock plateau and in the adjacent Atka Bay off *Neumayer Station III* did not pose a major problem at this point. The aim of the geological work was to retrieve long relatively carbonate-rich sediment cores (20 – 25 m), characterised in particular by increased sedimentation rates during the past Pleistocene warm periods. Unfortunately, the ship's main crane, which was needed to move the "core handling rack", was not operational. Therefore, only short sediment cores could be recovered at two stations, with lengths of 4,4 and 5,4 m (PS128_1 and _2 respectively). At both stations, the MUC could be used to obtain undisturbed sediment surfaces and bottom water samples. The accompanying deployment of the CTD/Rosette had to be repeated as various sensors initially failed (PS128_1). The subsequent repair was successful. On 17 January we continued towards Atka Bay and used HYDROSWEEP and PARASOUND for a site survey to identify potential coring locations. We zigzagged southwards to cover as much of the continental slope as possible. We already knew from previous expeditions that the sedimentary archives of this region are particularly suitable for high temporal resolution environmental reconstructions. We identified four sediment stations (PS128_14 to PS128_17), which we returned to at a later date. In the afternoon we were within flying distance to *Neumayer Station III* and started the transfer of the overwintering team in excellent flying weather conditions. A total of 7 flights were necessary

We then continued our geological investigations on the upper continental shelf northwest of *Neumayer Station III*. The aim was to record the extent of the ice sheet during the last glacial period as well as the dynamics of the ice retreats. For this purpose, hydroacoustic methods

(HYDROSWEEP, PARASOUND) were used to record the morphology of the sea floor and the composition of the uppermost sediment layers. Based on these data, 7 locations were selected (PS128_4 to _10) where glaciogenic sediment features were sampled with short sediment cores or with the box corer. An accompanying CTD/Rosette was deployed at station PS128_4 to characterise the water mass signatures and sample the water column. The work was successfully completed on 18 January.

At the following stations PS128_11 to PS128_13 (19 – 20 January), Tertiary sediment layers were to be sampled with the gravity corer. Seismic profiles at these stations, north of Atka Bay, show old sedimentary layers striking out just below the sediment surface, or Tertiary outcrops of sediment sequences in the area of canyon flanks. At the first station we started with an oceanographic profile (CTD/Rosette). Unfortunately, the exact coordinates for coring could no longer be approached due to difficult ice conditions. The ship's crane was repaired in the meantime and now allowed the use of long piston and gravity corers. Nevertheless, only short sediment cores could be obtained at stations PS128_12 and PS128_13. Unfortunately, the older sediment layers were too hard for deep penetration with the gravity corer and one of the gravity corers was even bent (PS128_13).

On 20 January, we returned to our working area on the continental slope between Atka Bay and Bungenstock Plateau and successfully accomplished the four previously identified sediment stations PS128_14 to PS128_17 with deployments of multicorer, piston corer and gravity corer. Two sediment cores were taken at each station to ensure sufficient sample material for later proxy measurements. The transect of sediment cores covers a depth range from about 1,600 m to 2,300 m water depth. Initial magnetic susceptibility data and core descriptions show that the sediment profiles can be well correlated lithostratigraphically. After completion of the work, we carried out a seismic test on 22 January (PS128_18). The streamer was deployed, the air guns tested and the incoming signals checked. Although the test was positive, the sea ice-conditions did not allow a subsequent profile run in the planned study area. Since we were able to deploy long gravity cores again, we decided to go to the Bungenstock Plateau once more to collect long sediment records at two stations (PS128_19 and PS128_20). Only the long sediment cores allow us to "travel" far enough back in Earth's history to work on time intervals when it was globally warmer than today. With station PS128_20, station PS128_2 was doubled (approx. 1,700 m water depth). Station PS128_19 is located at the northern end of the plateau in about 3,000 m water depth. The work was successfully completed on 24 January.

Although sea ice-conditions were still not optimal for seismic operations, the streamer was deployed around 19:30 UTC on 24 January. Navigation of the profiling transects through the ice was supported by several helicopter reconnaissance flights. Although only a small part of the intended profile routes could be covered, the seismic surveys were nevertheless successfully completed on 27 January. It is very likely that the main goal was achieved, i.e., the connection of these new and already existing marine seismic profiles to the continental seismic profiles around *Neumayer III*.

After completion of all work on the shelf and continental slope off *Neumayer Station III*, we sailed full steam eastwards towards the Russian station *Molodezhnaya* to drop off our shore team there. On the long transit of about 1,200 nm we took oceanographic profiles and water samples at 5 CTD stations. At two of these stations, we also sampled the sediment surface using the MUC.

In the early morning of 2 February, we reached the ice-covered coastal waters off *Molodezhnaya*. *Polarstern* was able to approach within 35 km of the coast. The flying weather conditions were optimal: good visibility, bright blue sky, hardly any wind. After 11 helicopter flights (3 of them with external loads for transporting the equipment) the shore team (6 persons) was brought to

Molodezhnaya, where colleagues from the Belarusian station (Mount Vechernyaya) located in close vicinity to *Molodezhnaya* welcomed them while respecting the Corona measures.

On the evening of 2 February, we set off for our second main area of work, the Cooperation Sea. Shortly after departure, the Chinese research icebreaker *Xuelong 2* crossed our path with whom we had radio and visual contact. We reached the Cooperation Sea on 4 February. Due to a low-pressure cyclone, which was not predicted to be so strong in the forecasts and in the weather model calculations, we had to stop research operations from 4 – 6 February. The average wind force was 10 Bft with gusts up to 12 Bft (Fig. 1.2). The wind sea reached its maximum at 10 – 12 m. Since we were weathering against the wind at about 3 – 4 knots to the southeast, we increasingly moved away from the originally targeted core stations during the two days. Due to time constraints, we decided against another approach and two more offshore stations further north were cancelled likewise. Instead, we concentrated our HYDROSWEEP and PARASOUND surveys on the areas closer to shore on Daly Rise and Wild West Rise to identify suitable sediment archives. In the Daly Rise area, MUC and two gravity cores were successfully deployed at station PS128_34. The CTD/Rosette station (PS128_35) was relocated to Daly Canyon to record the outflow of Antarctic Bottom Water (AABW) from its formation area off Cape Darnley. The subsequent search for suitable sediment archives on the upper continental slope was unfortunately unsuccessful. Further south, in the immediate vicinity of the AABW formation area, the bottom water outflow was recorded with another CTD/ Rosette station on the upper continental slope (PS128_36).

On 8 February we reached the Nielsen Basin on the continental shelf of Mac. Robertson Land (Fig. 1.1), which was formed by glacial erosion. The Nielsen Basin consists of large-scale troughs up to 1,000 m deep, separated by shallow sills. These troughs contain deglacial sedimentary archives with exceptionally high temporal resolution consisting mainly of varved, diatom-rich sediments. The aim was to sample these high-resolution archives to record the extent of the ice sheet during the last glacial period and the dynamics of ice retreat. With HYDROSWEEP and PARASOUND, the morphology of the seafloor was mapped and the structure of the uppermost sediment layers was recorded. These investigations provided the basis for the successful sampling of the sediment layers with the gravity corer and MUC. In addition, the CTD/Rosette was used to characterise the water mass signatures and sample the water column (PS128_38 to PS128_45). On 10 February, we extended our surveys to the west with two additional stations in Iceberg Alley (PS128_46, PS128_47). During the station work, three helicopter flights were made along the coastline to sight and sample sediment-rich glacial layers near nunataks. The sampling programmeme was successfully implemented at Neill Peak and Painted Peak near *Mawson Station*.

On 11 February we continued our geological and oceanographic investigations further west in the area of Stefanssons Bay. There, the bathymetric maps show a southern offset of the upper continental slope with a basin structure in the north. We hoped that the sediments there would reflect the dynamics of the westward-setting Antarctic Slope Current and deployed multicorer, gravity corer and CTD at three stations (PS128_48 to PS128_51). However, our bathymetric survey revealed that it is not a sediment basin, but a dynamic canyon system that transports sediments into the deep sea.

On 12 February we reached Edward VIII Rise further west. Unfortunately, due to stormy weather conditions and high wind seas (Fig. 1.2), the attempted deployment of the gravity corer had to be aborted. Instead, PARASOUND and HYDROSWEEP site surveys were conducted to explore the sediment archives in the area of Edward VIII Rise before heading towards *Molodezhnaya* to pick up our shore team. Due to the weather forecast for *Molodezhnaya*, we brought the pick-up date forward by two days. Nevertheless, the landing expedition was able to complete all planned tasks in the remaining time.

On the morning of 14 February, we reached the bay off *Molodezhnaya*. The ice conditions were favourable, so we were able to approach to within about 2 nautical miles of the station. The flying conditions were perfect: little wind and bright blue skies. The six people and all the equipment could be brought on board in seven helicopter flights. Beforehand, the landing team had carried out Corona quick tests. After arrival on board, PCR tests were carried out in immediate isolation. All test results were negative. During the flight operations, we collected rock samples along the coast using Zodiac boats. These, as well as the previous sampling at nunataks, will be used for sediment provenance studies to improve our understanding from a parent rock of the Antarctic source area to detritus that is deposited in the adjacent Southern Ocean. After the shore team and their equipment were on board, a CTD/Rosette station was carried out on leaving the bay (PS128_52).

Afterwards, a research programmeme in the area of Lützow Holm Bay and Syowa Station was originally planned before we set off towards Cape Town. As very bad weather conditions prevailed there and were also forecast for the next few days, we abandoned the initial plan and travelled back east again to make up for the cancelled sediment core sampling (bad weather) in the Cooperation Sea at Edward VIII Rise. On the way there, the Japanese research icebreaker *Shirase* crossed our path. After a short rendezvous and exchange of greetings (by radio), we recovered a sediment core from 1,000 m water depth in the area of Amundsen Bay, north of White Island (PS128_53). This sediment archive, which we already discovered on the previous transit to *Molodezhnaya*, should provide clues to the deglacial dynamics of the Beaver Glacier and the Antarctic Coastal Current.

We arrived at Edward VIII Rise on 16 February. The PARASOUND data indicated a sediment drift reaching its highest thicknesses between 3,400 and 4,000 m water depth. In this area we had 4 stations in total (PS128_54 to PS128_58) with deployments of gravity corer, multicorer and CTD/Rosette. The CTD/Rosette was lowered in a canyon on the eastern flank to a water depth of about 4,120 m and provided water samples and water mass signatures (temperature, salinity) characterising the outflow of the AABW into the Indian Ocean. The sediment records are thought to contain insights into the variability of the current dynamics and the formation of AABW during the last glacial/interglacial cycles.

On 17 February we started our return journey to Cape Town. On the way, on 22 February, we reached another planned station in the area of the Atlantic-Indian Ridge (approx. 52.5° S), which we reached on 22 February. The sediment archives there allow reconstructions of the latitudinal shift of the polar front and the boundary of winter sea ice-extent due to past climate fluctuations. The PARASOUND survey identified a coring location that was marked by a 200 m thick sediment sequence. Initially, wind strength and wind seas were too high to deploy the gravity corer. After a few hours, conditions improved. The wind strength was about 5 Bft, the wind sea about 3 m. Nevertheless, for safety reasons, it was not possible to use the gravity corer. The use of the main crane to assemble the “core handling rack” onto the holding pin of the transverse sliding beam was deemed too dangerous. On the onward journey we were forced to avoid a stormy cyclone. On 28 February, *Polarstern* reached the port of Cape Town and ended expedition PS128.

Itinerary land expedition

In the early morning of 2 February, we reached the ice-covered coastal waters off *Molodezhnaya*. With the first helicopter flight the two geodesists of our team were flown to Mount Vechernaya, where we set up the first GNSS site (ABE1). The site is close to the Belarusian station and before our arrival the members of the Belarusian Antarctic Expedition (BAE) had prepared a landing site for the helicopter. The rest of the land team and the equipment were subsequently

brought to the *Molodezhnaya* area. There we could use one of the station's buildings for accommodation maintained by the BAE. We were welcomed by the head of the BAE A. Gaidashov and his team. Flight operations were finished by mid-afternoon.

The weather was cloudy and windy on 3 February, when we started our working programme. The geodesists visited the second GNSS site (GRA1), where they unmounted the GNSS equipment of the Russian colleagues from Aerogeodeziya for the duration of our measurement and set up the GNSS site GRA1. The geologists started investigating Lake Lagernoye and Lake Glubokoye. Both lakes were covered by 3 m thick ice and first attempts of sediment sampling with a gravity corer were not successful due to very thin sediment coverage at the investigated sites. From a 22.4 m deep site at Lake Glubokoye we sampled a water profile for geochemical analyses.

On 4 February weather conditions were good in the morning (less windy, no clouds and good visibility and contrast) and the geodesists drove to the Blisnetzov to set up the third GNSS site (BLIS). The geologists continued work on Lake Glubokoye. At a site with a water depth > 30 m we recovered several samples of 20 cm thick algae mat deposits with the gravity corer. Around noon the wind strengthened and clouds came up and, in the afternoon, we had to stay inside the building due to very strong winds. The equipment stored in front of the building was rearranged to prevent lighter boxes flying off.

On 5 February weather improved and we continued work on Lake Ovalnoye, where up to 70 cm long sediment cores were collected. We visited several mapped GNSS sites as potential places to install the Russian GNSS equipment. However, no suitable fixings (anchored bolts) were present. In the late morning two BAE colleagues came to *Molodezhnaya* and brought sediment samples, which they cored for us in Lake Niznee in the proximity to the Belarusian station (and a very nice *Polarstern* cake).

Weather further improved and we had a calm, sunny day on the 6 February. We started sampling of glacial deposits (boulders) for exposure dating along the hill tops/crests closest to the ice sheet margin and sampled glacier ice containing sediments in the afternoon. The others continued coring on Lake Lagernoye and successfully recovered several gravity cores of up to 20 cm length.

The weather was windy but with good visibility and contrast on 7 February. The geodesists drove to the GNSS site ABE1 by snowmobile in the morning to check if the device was properly working. We used the existing, marked route to Mount Vechernaya across the ice sheet and were back to the *Molodezhnaya* area by noon. We observed that sea ice had broken up off Mount Vechernaya, while we still had closed sea ice-cover off *Molodezhnaya* and in the marine bays to the east of *Molodezhnaya*. We continued sampling glacial erratics and sediment coring on Lake Lagernoye and Lake Glubokoye. Two of us undertook soil crust sampling on the nearby ridges in the afternoon.

On 8 February we continued sediment coring and water sampling on Lake Glubokoye and took sediment cores at Lake Promeoye. We also prepared the equipment to start piston coring on Lake Glubokoye on the 9 February. We deployed one run with the piston corer, but did not reach deeper into the sediments compared to gravity coring due to very stiff sediment or bedrock below the postglacial sediment deposits. In the afternoon we visited the north-western part of *Molodezhnaya* to check the GNSS device at GRA1 and to collect glacial deposits.

On 10 February weather was sunny (good visibility and contrast) but very windy. We drove to the Blisnetzov Peninsula, following the track we used on 4 February, which worked without any problems. At Blisnetzov we checked the GNSS site BLIS, which was working properly. We sampled a transect of glacial erratics from the coast to the present-day ice sheet margin,

took sediment samples from one of the lakes, and sampled soil crusts at one site. We also observed that sea ice-break up was progressing westwards into the marine bay in direction of *Molodezhnaya*.

Since a storm was forecast for the 12 and 13 February, we retrieved the BLIS GNSS station in the morning of 11 February. Afterwards, we drove to Mount Vechernaya to retrieve the ABE1 GNSS station and to conduct lake sediment coring on Lake Niznee. The traverse to Mount Vechernaya was coordinated with the Belarusian colleagues, who joined us with their track-vehicle. This was particularly helpful during the ascent and descent from land onto the ice sheet and vice versa, where snow coverage was partly gone on the slopes and areas of blue ice had to be crossed. We were warmly welcomed at the Mount Vechernaya by the BAE colleagues and had a successful collaboration on conducting our work, while still respecting all Corona (Covid-19) measures.

In the afternoon of 12 February, we completed sampling for glacial erratics along the north-south transect through *Molodezhnaya* and finalized our scientific programme. We started to prepare our equipment for transport back to *Polarstern* and spent the next day clearing the camp. The *Polarstern* helicopter arrived in the morning of 14 February and retrieval of persons and equipment to *Polarstern* was accomplished without any delays.

2. WEATHER CONDITIONS DURING PS128

Markus Eifried, Christian Rohleder DE.DWD

Overview

The expedition PS128 mainly served to explore the marine areas of the East Antarctic coast starting from the *Neumayer Station III* region in the west via the *Molodezhnaya* region and the Cooperation Sea in the east. During the expedition, geological, geophysical, geochemical, and oceanographic surveys were conducted. During our work off the coast of *Neumayer Station III*, the team of the AWI overwinterers was flown out to their “new home”.

On our way to the second major study area, the Cooperation Sea, we dropped off a six-member land-team at the Russian Station *Molodezhnaya* for 12 days. During this time, *Polarstern* sailed to the Cooperation Sea. There, marine geological work was carried out on the continental margin and on the shelf in the Nielsen Basin off Mac. Robertson Land. In addition, we also used helicopters to take rock samples and ice samples along Mawson Coast in the vicinity of Nunataks. After the land-team was picked up at *Molodezhnaya*, marine geological work continued in the Cooperation Sea. A final marine geological Station was planned on the way back to Cape Town in the area of the Indian submarine Atlantic Ridge. Due to the weather the station had to be cancelled.

Section Cape Town – *Neumayer Station III*

At departure on Thursday, 6 January 2022, around 16 UTC, the position of *Polarstern* was between a trough extending from Namibia to the Western Cape and a large high-pressure zone running along about 40° S. Around the Cape, easterly to southeasterly winds of around 6 Bft were blowing (Chapter 1, Fig. 1.2). With a southwesterly swell a cross sea established. As the vessel moved into the high-pressure zone, which shifted its centre eastwards over the next few days, the easterly to southeasterly winds decreased hesitantly. Cloud cover was often low due to stratocumuli and cirrus clouds, occasionally there were cloud-free sections. With the passage of the ridge axis of the high on its western flank on the weekend of 8/9 January, the now weak to moderate inflow over northeast and northwest turned to southwest. As a result, *Polarstern* was on the front side of a trough running southwestwards of its cruising position. On Sunday, the cloud coverage increased and, in the evening, drizzle reduced the visibility and the cloud base of the stratus considerably, so that partly foggy conditions prevailed temporarily. With the passage of the trough, the initially fresh inflow turned to southwest to south on Monday, 10 January 2022, with a decrease. A small high provided almost cloud-free weather on this day.

From Tuesday, 11 January 2022, wind and weather conditions changed significantly. *Polarstern* advanced into the westerly wind zone on its way. A stormy low-pressure system approaching from the southwest with a core pressure of about 969 hPa moved eastwards further south of the cruising area, i.e. in front of *Polarstern*. Thus, *Polarstern* was initially on the northeast flank of this low, and by midweek on the northwest to west flank. Mostly northwesterly winds of 6 to 7 Bft prevailed, with occasional slight decreases to 5 to 6 Bft (Fig.1.2). It was mostly

cloudy to overcast with stratocumulus fields and overlying mid-level clouds, with precipitation changing to snow by Wednesday, 12 January 2022, also due to underlying stratus. *Polarstern* then moved away from this gale and got into the front of a trough of the next low approaching from the northwest. For a short time, the wind shifted to west to southwest and increased to about 7 Bft, before southeasterly wind directions set in again via north. The winds were mostly around 6 Bft with occasional decreases to 4–5 Bft and increases to 7 Bft. The weather pattern was characterised by low stratus and stratocumulus clouds. As the trough approached, visibility deteriorated significantly to foggy conditions. Until the weekend 15/16 January 2022, the storm low moved northwards, i.e. behind the track of *Polarstern*, eastwards. Thus, the southeasterly winds with 6 to 7 Bft continued on the southwestern flank of the gale.

Research area around *Neumayer Station III*

At the beginning of the new week, the next low considerably increased its influence on the weather in the vicinity of *Polarstern*. Disturbed by a massive high-pressure ridge directed southwards out of the Indian Ocean and an overlying ridge in higher altitudes in a similar position, it was forced to move southwards out of the westerly wind zone in the coming days, deepening considerably towards the coast off the central part of Antarctic Dronning-Maud Land. For *Polarstern*, this meant a reversal of the wind to southwest with strengths around 5 Bft and intermittent break-ups of the low stratocumulus and overlying altocumulus clouds. This meant the most favourable conditions for Monday, 17 January 2022, to conduct a helicopter flight operation to *Neumayer Station III* lasting several hours until late in the evening. The sea state was meanwhile considerably dampened by increasing ice cover. On Tuesday, the cloud cover increased from the east, the reason for this was a new gale coming from the south-east Atlantic Ocean, which developed into a hurricane and moved southwards off the central coast of Dronning-Maud Land, making a requested inner-Antarctic helicopter flight connection from Neumayer to Førstefjell, the first nunatak in the south-east, difficult due to limited visual contrast, which ultimately could not be realised for other reasons either. This hurricane became weather-dominating from Wednesday, 19 January 2022. The winds shifted to the east and freshened up strongly – on average Bft 7 and Bft 8 were recorded (Fig. 1.2). From compact frontal cloud cover with low-lying stratus below, it snowed at times with a considerable reduction in visibility. This weather situation did not improve until Saturday, 22 January 2022, when the low pressure weakened and moved southeast.

As a result, a weak high-pressure area developed from a high-pressure ridge directed from the north into the eastern part of the Weddell Sea. On its southeastern flank, the southwesterly flow freshened up considerably. The weather was characterised by low stratocumulus and partly stratus fields, partly with fog patches.

Section *Neumayer Station III – Molodezhnaya*

From Wednesday, 26 January 2022, *Polarstern* entered the sphere of influence of small-scale lows that developed north of the East Antarctic coast and formed a trough north of the cruising area in the direction of *Molodezhnaya*. This meant a moderate to fresh and partly strong easterly to southeasterly flow in mostly heavy stratocumulus clouds under a subsidence inversion. The clouds did not clear until the weekend, but the trough structure in the weather situation did not change significantly at the beginning of the next week. On the approach to the ice edge off *Molodezhnaya*, *Polarstern* repeatedly got into areas of significantly warmer water on the southern flank of the above-mentioned trough from 1 February 2022, which produced sea fog in calm wind conditions. This was advected from the southwest into the area selected as the target area for helicopter flights to *Molodezhnaya*, but dissipated in the morning of 2 February 2022. Visibility was always good in the direction of the ice shelf-edge. Thus, 2 February was characterised by cloudless skies and almost no wind (Fig. 1.2).

Research area Cooperation Sea and return to *Molodezhnaya*

From the sea area around 50° South 20° East, a gale developed from 2 February 2022 onwards, which moved north of the eastern part of the Cosmonauts Sea into the Cooperation Sea with strong deepening as a hurricane and influenced the weather on *Polarstern*. Especially when bypassing Cape Ann and Cape Batterbee, as well as to the east of them, an inflow from east to southeast prevailed with mean winds up to 9 – 10 Bft (Fig. 1.2), the gusts repeatedly reached hurricane-like strengths. Two hurricane-force gusts of 33.0 m/s (64 knots) each were recorded on 4 February 2022 at about 17:34 and 18:23 board time. Snow fell with moderate to heavy intensity from compact frontal cloud cover, with the cloud base partly 100 metres above sea level. The wind sea reached heights of over 8 metres, with swell waves of 2 to 3 metres, the significant swell peaked at about 9 metres. *Polarstern* had to weather in the southern cooperation sea from 4 to 6 February 2022. It was striking that the available runs of the global models from ICON and ECMWF had significantly underestimated what was happening; the regional Antarctic AMPS model could not be accessed in Iridium satellite operation mode, this data would certainly have been interesting.

Heading into the Cooperation Sea, a southeasterly, at first strong, later moderate flow prevailed between low-pressure areas coming from the northern Cosmonauts Sea and moving eastwards into the northern Davis Sea, and northeastward shifting ridges of the high over the polar plateau. The cloud cover was characterised by varying proportions of strato- and altocumuli. In the second half of the week, from 9 February 2022 onwards, high air pressure dominated offshore of the Mawson coast with sinking inversions and good weather conditions, but locally pronounced katabatic winds in the area of the ice shelf edge. When moving out of denser into thinner sea ice, there was a shallow ground fog directly above the sea ice on the evening of 10 February 2022 due to an influx of moisture, which did not exceed a height of 2 metres. Towards the weekend, a low-pressure trough close to the East Antarctic coast with small-scale marginal lows embedded in; it was established by a low-pressure system lying to the northeast of the area of operation. On the southern flank of the trough, a freshening southeasterly to easterly flow prevailed with a mean of 8 to 9 Bft on Saturday, 12 February 2022 (Fig. 1.2). The swell increased to 5 to 6 metres. Snow fell intermittently from low-lying clouds. On the way west to *Molodezhnaya*, the weather calmed down a bit. The trough north of the coast of Enderbyland and eastern Dronning-Maud Land remained almost unchanged, temporarily moving slightly inland to the south.

Monday, 14 February 2022, turned out to be the best day for helicopter flights to *Molodezhnaya*. Around *Molodezhnaya* the ridge of high pressure over the polar plateau was effective, so that only a few stratocumuli affected visibility, contrast and horizon east and north of *Molodezhnaya*.

For the further course of the voyage from 14 February 2022, the large-scale weather situation was a major cause. Originally, research investigations in the Lützow-Holm Bay near Syowa west of *Molodezhnaya* were scheduled. Unfavourable sea ice-conditions and even more unfavourable weather conditions – to the east of an extensive gale north-northwest of *Neumayer Station III*, a trough formed with forecast easterly winds of 7 to 8 Bft in combination with widespread low clouds garnished with large areas of moderate snowfall – reduced the probability of further flight options due to icing and poor visual contrast as well as horizon to the point of virtual impossibility, thus making important investigations almost unfeasible. In contrast, the weather conditions were much better eastwards in the Cooperation Sea. Accordingly, we returned to the Cooperation Sea to continue our work, which previously had to be repeatedly canceled due to bad weather conditions. Still in the late evening of 14 February 2022, the crossing of the trough off the coast of Enderby Land resulted in significantly less wind and more precipitation with moderate snow than foreseen in the few available model forecasts. The subsequent weather pattern was characterised by a trough of low pressure, which originated

from a gale over the Lazarev Sea and lay over the coastal area of Enderby Land. Under heavy cloud cover with intermittent snow, fresh to strong southwesterly winds prevailed on the way to the Cooperation Sea. Approaching the area of operation in the Cooperation Sea, weak high-pressure influence temporarily prevailed on 16 February 2022, before the trough from the now approaching storm low, already over the Cosmonauts Sea on 17 February 2022, again became weather-dominating. The flow was initially from a northeasterly, later northwesterly direction. Initially low and later increasingly compact frontal cloud cover provided snow from time to time.

Section Cooperation Sea – Cape Town

On Friday, 18 February 2022, *Polarstern*, on its way to the last area of operations on the Atlantic-Indian Ridge, first came into contact with the northeast flank of the low-pressure system now weakening over the Cosmonauts Sea. With heavy cloud cover and a strong northwesterly to westerly flow, snowfall occurred at times. At the same time, the next low-pressure system established itself over the Riiser-Larsen Sea, and *Polarstern* was on its northeastern flank in an increasingly near-gale northwesterly flow over the weekend. At this time, a small depression appeared for the first time far off the southern Brazilian coast in the central southwest Atlantic Ocean, whose development in the following days took on that of a rapid cyclogenesis. With strong deepening, it subsequently moved east-southeastwards towards the research area on the Indian-Atlantic Ridge. At the beginning of the week, *Polarstern* was still on the northern flank of a low north of the Cosmonauts Sea in an often near-gale northwest to west flow. The originally small-scale low off Brazil mentioned above has now developed into a fast-moving low and was still far to the north-west of *Polarstern*, which was, however, on a north-westerly course. From Tuesday onwards, *Polarstern* came into its sphere of influence in the area of the research area in the Indian-Atlantic Ridge. Because of imprecise model ranges, it crystallised that the low core was to be expected close to the south of the area of operations on Wednesday morning. Immediately before that, on the late evening of Tuesday, 22 February 2022, the weak ridge of a subtropical high caused the wind direction to shift to the northeast with a temporary decrease, but the swell component in the waves remained too strong to allow sampling without danger. Wind peaks of over 75 kt were forecast in common global models for the planned onward journey to the north. This high lability was due to the mixing down of higher air masses, but without corresponding weather. Also in satellite images, especially in infrared and water vapour channels, a dry air layer was recognisable, as corresponds to a dryslot in the development process of a Shapiro-Keyser cyclone – some images also showed structures that indicated a break-off of the cold front. The modelling of the gusts mentioned above was within the range of the expected sting jet. Since waiting would have meant waiting in the area of the research area due to only slightly lower wind speeds (west to southwest 9 Bft with gusts 12 Bft at 65 to 70 kt, wind sea 7 to 8 metres; Fig. 1.2), the course was changed to southwest and, with passage of the core at about 961 hPa, to west, northwest and north-northwest in order not to have to pass the full back of the hurricane-like low.

On Thursday, 24 February 2022, weather conditions improved significantly, but a trough to the west of the cruising area still caused near-gale winds from the west and a significant swell. On Saturday, 26 February 2022, *Polarstern* entered the subtropical high-pressure zone. The wind decreased considerably, but a moist-unstable boundary layer provided cumuli and stratocumuli below a subsidence inversion, from which a few droplets fell. On Sunday, 27 February 2022, a low-pressure system originally coming from Namibia and moving across the Western Cape Province to the area west of Cape Town first caused a significantly freshening easterly and then northerly flow before entering Cape Town, which occurred in the morning hours of 28 February 2022.

3. BATHYMETRIC MAPPING

Yvonne Schulze Tenberge[1], Maybrit Gießler[1], [1]DE.AWI
Ellen Unland[1],Boris Dorschel[1] (not on board)

Grant-No. AWI_PS128_02

Objectives

Accurate knowledge of the seafloor topography, hence high-resolution bathymetry data, is key basic information necessary to understand many marine processes. It is of particular importance for the interpretation of scientific data in a spatial context. Bathymetry, hence geomorphology, is furthermore a basic parameter for the understanding of the general geological setting of an area and geological processes such as erosion, sediment transport and deposition. Even information on tectonic processes can be inferred from bathymetry.

While global bathymetric maps give the impression of detailed knowledge of the seafloor topography, most of the world's ocean floor remains unmapped by hydroacoustic systems. In these areas, bathymetric information is derived from satellite altimetry with corresponding low resolutions – too coarse to resolve small- to meso-scale geomorphological features (e.g. sediment waves, glaciogenic features and small seamounts). Ship-borne multibeam data provide bathymetry information in a resolution sufficient to resolve those features, and therefore can be used to select sites for accurate scientific sampling.

Accordingly, the main tasks of the bathymetry/geophysics group on board of *Polarstern* during PS128 were:

- collection of bathymetric data, including calibration and correction of the data for environmental circumstances
- post processing and cleaning of the data
- data management for on-site map creation
- support of other working groups for sampling sites selection and station planning
- collection of sound velocity data for calibration of the multibeam echosounder system

Work at Sea

Technical description

During expedition PS128, bathymetric surveys were conducted with the hull-mounted multibeam echosounder (MBES) Teledyne Reson Hydrosweep DS3 (HSDS3). The Hydrosweep is a deep water system for continuous mapping with the full swath potential. It operates on a frequency of ~14 kHz with chirped pulses. On *Polarstern*, the MBES transducer arrays are arranged in a Mills cross configuration of 3 m (transmit unit) by 3 m (receive unit). Combined motion, position (Trimble GNSS), and time information is provided by an iXBlue Hydrins motion reference unit (MRU). MRU data is directly transferred into the Processing Unit (PU) of the MBES for real-

time motion compensation (Pitch, Roll and Yaw). With a combination of phase and amplitude detection algorithms the PU computes the water depth from the returning backscatter signal. The maximum opening angel is 140° (70° to each side of the nadir). In water depths deeper than 2,000 m, the maximum opening angle is reduced to approx. 50° to each side of the nadir.

Data acquisition and processing

Bathymetric data acquisition was carried out throughout the entire expedition, as long as the ship was sailing in international waters or the Southern Ocean (south of 60°S). There, the acquisition was only interrupted during station work. Then the Hydrosweep was switched off. South of 60° S the system was also switched off, if marine mammals were sighted within a 100 m zone around the ship. Data acquisition was resumed, if an observer did not sight a marine mammal within the 100 m zone for 15 minutes.

The Hydrosweep was operated with Hydromap Control and for online data visualisation, Teledyne PDS was used. Data were stored in ASD, PDS and S7K raw files in the shipboard file system for later transfer into the long-term data archive PANGAEA. Subsequent data processing was done with Caris HIPS and SIPS. For generating maps onboard, the data were exported as XYZ ASCII files and gridded using mb-system. The grids were imported to QGIS in the GeoTIFF raster format.

Sound velocity profiles

For best survey results and to correct Hydrosweep depths for changes of the sound velocity (SV) in the water column, SV profiles were generated from CTD data that were collected and provided by the Marine Geochemistry group. SV correlates with the density of a water mass and thus is depending on pressure, temperature and salinity of the seawater in a given location at a given depth. Wrong or outdated SV profiles lead to refraction errors and reduced data quality.

Were no CTD data were available, SV profiles were obtained by the Bathymetry group using a Valeport MIDAS Sound Velocity Profiler (SVP). The Valeport was attached to the winch cable of sampling instruments such as the Multi Corer (MUC) or the Giant Box Corer (GKG). Table 3.1 lists all stations were the Valeport was used and the devices it was attached to.

The SV profiles obtained by the CTD and the Valeport were immediately processed and applied within the MBES for correct beamforming during the survey. Before ingestion, they were extended to full ocean depth with WOA13 (World Ocean Atlas 2013) data.

During PS128, a total of 105 SV profiles were applied to the MBES. They include 16 SV profiles from the CTD data and 6 SV profiles recorded with the Valeport. The remaining 83 profiles were generated using the WOA13.

Stations

Data collection with the Hydrosweep received the number PS128_0_Underway-13 throughout the expedition. All additional bathymetry stations are listed in Table 3.1.

Tab. 3.1: List of bathymetric stations during PS128

Station Number	Description	Device	Start [UTC]	End [UTC]
PS128_1-2	sound velocity profile; lowered with MUC	Valeport MIDAS SVP	2022-01-16 03:26:31	2022-01-16 05:06:20
PS128_3-1	MBES survey	Hydrosweep DS3	2022-01-17 21:57:55	2022-01-18 10:31:24
PS128_4-2	sound velocity profile; lowered with GKG	Valeport MIDAS SVP	2022-01-18 11:25:13	2022-01-18 12:03:37
PS128_6-2	sound velocity profile; lowered with GKG	Valeport MIDAS SVP	2022-01-18 18:17:02	2022-01-18 18:35:26
PS128_14-3	sound velocity profile; lowered with MUC	Valeport MIDAS SVP	2022-01-20 18:57:00	2022-01-20 19:55:32
PS128_17-3	sound velocity profile; lowered with MUC	Valeport MIDAS SVP	2022-01-22 09:56:07	2022-01-22 11:23:21
PS128_19-1	sound velocity profile; lowered with MUC	Valeport MIDAS SVP	2022-01-23 01:03:49	2022-01-23 03:05:19
PS128_37-2	MBES survey	Hydrosweep DS3	2022-02-08 22:55:54	2022-02-09 06:29:18
PS128_48-1	sound velocity profile; lowered with MUC	Valeport MIDAS SVP	2022-02-11 07:13:45	2022-02-11 08:13:29

Preliminary results

During 52 days of survey, a track length of 8,687 nm (16,088 km) was surveyed with the Hydrosweep. The raw data volume of bathymetric data (S7K, PDS and ASD) was 600 GB broken up in 1,014 separated survey track lines. Figure 3.1 shows the coverage of the bathymetric data collected during transit and dedicated surveys in the research areas. See chapter 5 for details on the MBES surveys.

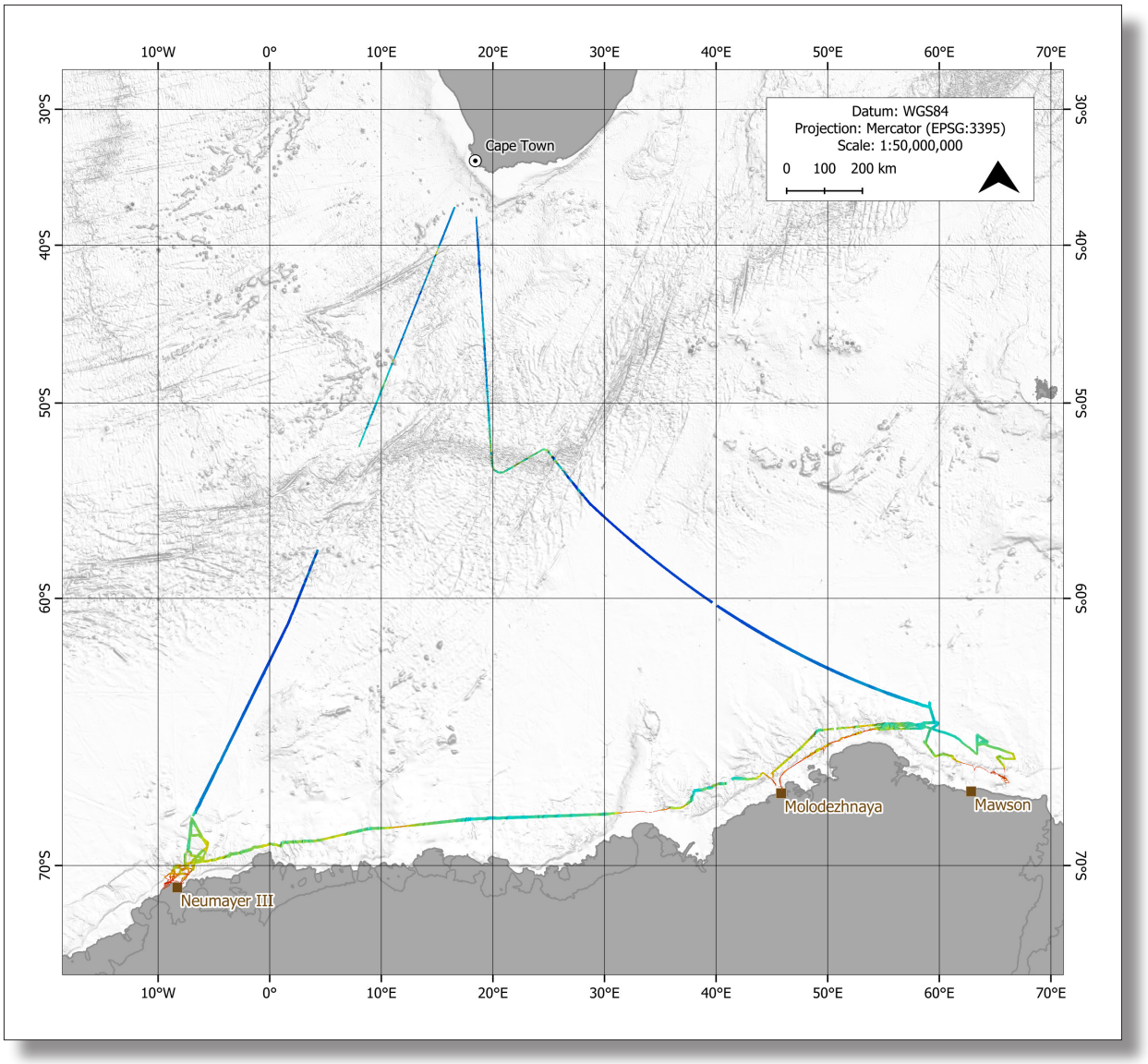

Fig. 3.1: Overview of the bathymetric data coverage acquired during PS128

Data management

Bathymetric data and sound velocity data collected by the Bathymetry group during PS128 will be stored and made publicly available in the PANGAEA data repository in accordance with the AWI research data guideline and directive (https://hdl.handle.net/10013/epic.be2ebee5-fb98-4144-9e74-aa1d38378c5e). The data will be provided to mapping projects such as the International Bathymetric Chart of the Southern Ocean (IBCSO), the General Bathymetric Chart of the Oceans (GEBCO), and the Nippon Foundation – GEBCO Seabed 2030 Project.

This expedition was supported by the Helmholtz Research Programme "Changing Earth – Sustaining our Future" Topic 2, Subtopic 2.3.

In all publications based on this expedition, the **Grant No. AWI_PS128_02** will be quoted and the following publication will be cited:

Alfred-Wegener-Institut Helmholtz-Zentrum für Polar- und Meeresforschung (2017) Polar Research and Supply Vessel POLARSTERN Operated by the Alfred-Wegener-Institute. Journal of large-scale research facilities, 3, A119. http://dx.doi.org/10.17815/jlsrf-3-163.

4. MARINE GEOPHYSICS/PARASOUND

Karsten Gohl[1], Estella Weigelt[1], [1]DE.AWI
Christoph Gaedicke[2], Adalbert Pfeiffer[1], [2]DE.BGR
Jakob Hamann[1], Henning Bauch[3], [3]DE.GEOMAR
Alejandro Cammareri[4], Juan Manuel Salazar[4] [4]DE.MARYBIO

Grant No. AWI_PS128_04

4.1 The continental-marine seismic link of Dronning Maud Land: Reconstructing the long-term evolution of the Ekström ice streams

Objectives

The ice stream system feeding into the Ekström Ice Shelf represents one of the numerous small outlet glacier systems of East Antarctica. Considering that the behaviour of the EAIS with increasing global temperature is hardly known, a thorough assessment of glacial dynamics of such a small outlet glacier system can provide important constraints on large proportions of the EAIS. A joint project between the Bundesanstalt für Geowissenschaften und Rohstoffe (BGR) and the AWI, named Sub-Ekström Ice Shelf (Sub-EIS), studies the potential of the sedimentary archive below the Ekström Ice Shelf for reconstructing Antarctic ice history and paleoclimate from warm greenhouse climates to the latest icehouse era. A network of seismic profiles, most of them by vibroseis technique, was acquired on the Ekström Ice Shelf in various previous seasons (Figure 4.1.1), revealing a sequence of northward dipping, pre-glacial sediments overlain by glacial deposits showing near-seafloor and deeper buried features of glacial transport processes such as truncational discontinuities, grounding zone wedges and over-deepened sub-basins (Kristoffersen et al., 2014; Smith et al., 2020; Oetting et al., 2021). As most of these pre-glacial and glacial deposits are likely to continue offshore across the continental shelf, slope and further into the deep sea, we aim to connect the seismic ice shelf network to the inner and outer continental shelf and continental rise with additional seismic profiles in order to map the offshore continuation of the sequences. Some seismic units and horizons are expected to be dated via seismic horizon correlation along pre-existing seismic profiles (Fig. 4.1.1) to the distal Ocean Drilling Project (ODP) Leg 113 drill sites on the Explora Escarpment of the southeastern Weddell Sea and on Maud Rise (Barker et al., 1988; Lindeque et al., 2013). This will allow a seismostratigraphic analysis from oldest (Jurassic-Cretaceous-Paleocene) pre-glacial sedimentation to early glacial periods (Eocene-Oligocene) and up to the Miocene-Pliocene-Pleistocene cold-house periods. A quantification of glacially induced variations in sediment transport during relevant warm times and colder periods within this Dronning Maud Land sector may be representative of many small glacier outlet regions along the East Antarctic margin. Accordingly, the major goal of our seismic survey and data analysis is to decipher the sediment transport processes for deriving ice-sheet dynamics from early to recent Antarctic glaciation, and in particular during major past warm periods from the Ekström Ice Shelf region.

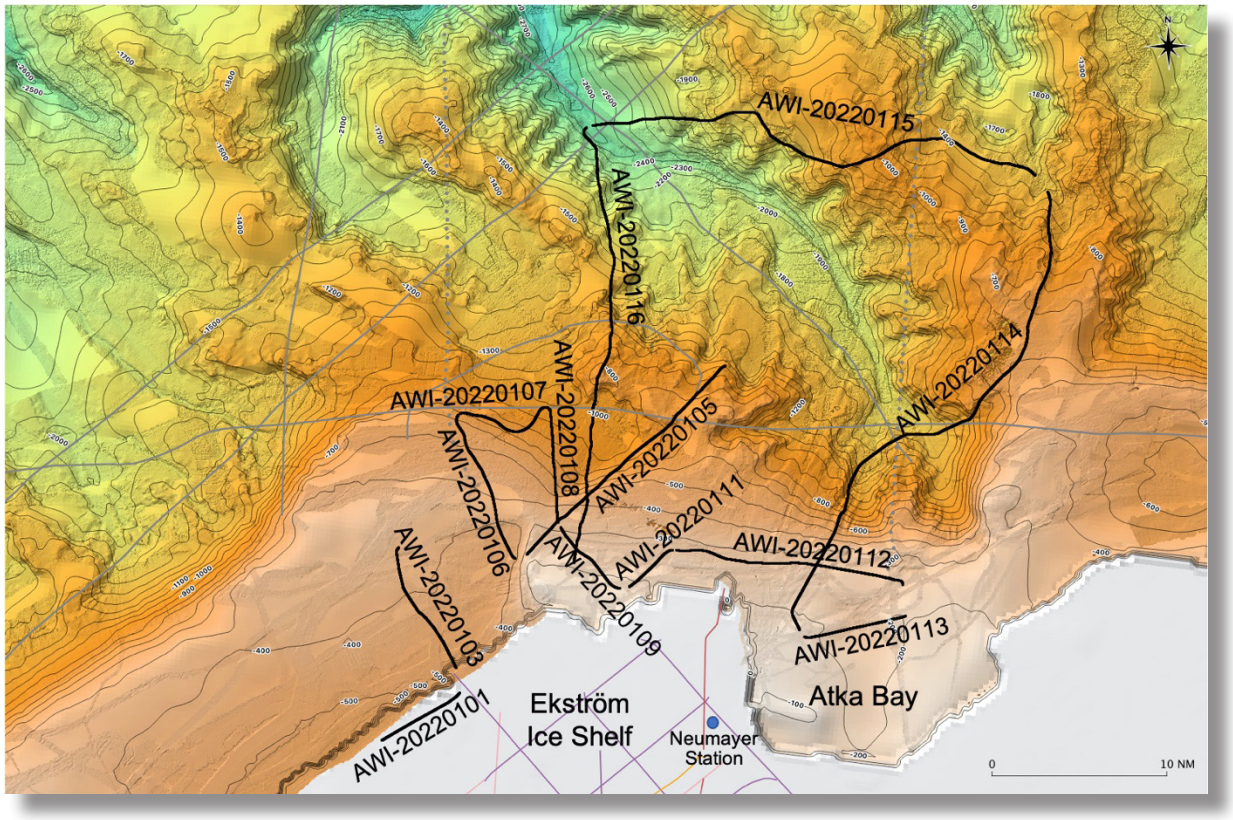

Fig 4.1.1: Bathymetric map showing the marine seismic profiles off the Ekström Ice Shelf of Dronning Maud Land collected during PS128 (bold black lines) as well as pre-existing marine seismic lines collected since 1978 by various organisations (thin grey solid and dotted lines); the Ekström Ice Shelf was previously surveyed with vibroseis profiles (thin coloured lines). Note that the ice shelf edge – compared to that in this map – was located further south in the area of profile AWI-20220101.

Work at sea

For the extension and connection of the pre-existing seismic networks offshore Ekström Ice Shelf, we collected 310 km (167 nm) of multi-channel seismic reflection profiles on the continental shelf, slope and rise (Fig. 4.1.1; Tab. 4.1.1).

Fig. 4.1.2: Photos of GI-Gun cluster (left), winch with 600 m long digital seismic streamer (middle) and recording system monitors (right)

Instruments

We used a cluster of 4 GI-Guns™ as seismic source (Fig. 4.1.2) to resolve the sedimentary layers as best as possible and by achieving depth penetration down to basement in places at the same time. A single GI-Gun™ is in principle constructed of two gun components within the same cylindric body. The primary gun (named “Generator”) produces the primary pulse, while the secondary gun (named “Injector”) is fired shortly after the primary gun to control the oscillation of the bubble produced by the “Generator”. We used the “Generator” with a volume of 0.72 litres (45 in^3) and triggered the “Injector” (1.68 litres = 105 in^3) with a delay of 33 ms. This led to an almost bubble-free signal. The GI-Guns were towed 15 **m behind the** stern of the vessel in nominally 2 **m** water depth and triggered every 10 s (~25.7 **m shot interval)** at an operational air pressure of nominally 170 bar.

For seismic signal recording, we used the integrated digital seismic streamer and recording system by SERCEL consisting of several equipment units. As severe sea ice-conditions were to be expected in the survey area, we had shortened AWI’s 3,000 m long Sentinel Solid Streamer to only 600 m (48 channels at 12.5 m group interval) of active lengths for this expedition (Fig. 4.1.2), because this shortened streamer can be towed without the depth-control devices (‘birds’) which could potentially damage the streamer in sea ice conditions. The data collected by the hydrophone groups (16 hydrophones per group) of the streamer are amplified and converted from an analogue to a digital signal by various modules placed along the streamer. The coupling of the streamer to the SEAL 428™ on-deck recording system is made via the Deck Cable Crossing Unit (DCXU) and Control Module (CMXL). The CMXL decompresses, demultiplexes and then performs IEEE 32-bit conversion to the data. The data are collected via a network switch and converted to SEG-D format by the PRM, the PRM being a processor software module.

The navigation data needed for airgun firing control and the seismic trace headers come from the SERCEL SeaPro Nav™ system which is used to pre-define the profiles. Airgun firing control was exercised by the BigShot™ unit.

Integrated into the Sentinel Solid Streamer and the SEAL 428™ systems, the passive acoustic monitoring (PAM) system SERCEL QuietSea™ performs an automatic detection of marine mammal vocalisation as part of the marine mammal mitigation procedure. This system was employed during the whole seismic operation.

All recording system parameters can be set manually. The system’s activity are continuously displayed (Fig. 4.1.2) together with log data entries, graphic displays of single shots and single-trace plots for quality control through the SERCEL e-SQCPRO unit. The seismic recording parameters were set to 1 ms sample interval and 9.5 s recording length for all profiles.

Seismic profiling

The scheduled start of seismic survey was delayed due to technical issues with the navigation header data transfer from the SeaPro Nav to the Seal 428. Shortly after the beginning of the survey, severe sea ice hampered the profiling progress and forced us to focus the survey mainly to the eastern part of the originally planned survey area, collecting a series of profiles across the inner and outer shelf, the slope and rise north and northeast of the Ekström Ice Shelf (Fig. 4.1.1; Tab. 4.1.1). The restriction to these areas of less severe sea ice cover and open-water polynyas shortened the seismic survey programme substantially. However, we still achieved the main objectives in connecting the vibroseis survey profiles of the Sub-EIS project on the Ekström Ice Shelf to the older seismic lines north of the shelf. By crossing the continental shelf on several locations to the north and northeast of the ice shelf and, therefore, closing - for the first time - the continuous seismic link to the ODP Leg 113 drill sites 692 and

693 on the Explora Escarpment, we are now able to derive a seismic stratigraphic model for the sub-ice shelf sequences observed from the vibroseis profiles.

After solving the initial problem of navigation header data transfer, other technical issues were almost negligible. Only a few shutdowns of airgun operations, due to visual detection of one whale and two seals within the 1,000 m safety zone around the ship, caused some minor data gaps along some profiles. The QuietSea PAM system did not record any mammal vocalisation events. The seismic data quality is generally at a high level due to relatively favourable weather conditions with calm seas despite the sea ice.

Tab. 4.1.1: Seismic profile summary

Profile No.	Start/ End	Date [UTC]	Time (UTC)	Longitude	Latitude	Ffids, No. of Shots	Profile Length	No. Guns	Remarks
AWI-20220100	start	22.01.22	16:28	7°07.933`W	69°35.605`S	160662-	2.8 nm	4	16:28 Start of softstart,
test profile	end	22.01.22	17:09	7°14.545`W	69°34.454`S	161033, 372	5.2 km		16:59 full power
AWI-20220101	start	24.01.22	20:45	9°13.835´W	70°39.174´S	161034-	5.3 nm	4	
	end	24.01.22	21:56	8°59.860´W	70°36.566´S	161822, 789	9.9 km		
AWI-20220103	start	24.01.22	22:15	9°00.417´W	70°35.119´S	161824-	8.0 nm	4	
	end	24.01.22	23:55	9°09.611´W	70°28.029`S	163029, 1206	14.9 km		
AWI-20220105	start	25.01.22	13:40	8°12.361´W	70°18.022‘S	163056-	15.8 nm	4	13:40 Start of softstart,
	end	25.01.22	17:02	8°47.450´W	70°28.685´S	164227, 1172	29.2 km		14:10 full power
AWI-20220106	start	25.01.22	17:12	8°49.451´W	70°28.885´S	164313-	9.3 nm	4	
	end	25.01.22	19:08	8°58.438´W	70°20.442´S	164957, 645	17.2 km		
AWI-20220107	start	25.01.22	19:10	8°58.126´W	70°20.371´S	165030-	6.0 nm	4	
	end	25.01.22	20:41	8°43.057`W	70°20.204`S	165582, 552	11.1 km		
AWI-20220108	start	25.01.22	20:43	8°42.789´W 8°41.802´W	70°20.281´S	165583-	6.5 nm	4	
	end	25.01.22	22:09		70°26.886´S	166102, 519	12.1 km		
AWI-20220109	start	25.01.22	22:13	8°41.423´W	70°27.177´S	166104-	5.0 nm	4	
	end	25.01.22	23:16	8°31.431´W	70°30.810´S	166492, 388	9.3 km		
AWI-20220111	start	25.01.22	23:23	8°29.778´W	70°30.715´S	166493-	3.3 nm	4/3	23:30 Gun 2 deactivated due to air loss
	end	26.01.22	00:06	8°22.079´W	70°28.654´S	166765, 272	6.2 km		

Profile No.	Start/ End	Date [UTC]	Time (UTC)	Longitude	Latitude	Ffids, No. of Shots	Profile Length	No. Guns	Remarks
AWI-20220112	start end	26.01.22 26.01.22	00:09 02:59	8°21.416´W 7°42.200´W	70°28.679´S 70°30.911´S	166766- 167808, 1043	13.4 nm 24.8 km	3	
AWI-20220113	start end	26.01.22 26.01.22	03:25 04:50	7°41.861´W 7°59.484´W	70°32.722´S 70°33.835´S	167811- 168329, 518	6.0 nm 11.1 km	3	
AWI-20220114	start end	26.01.22 26.01.22	04:57 12:21	8°00.305´W 7°16.685´W	70°33.435´S 70°08.170´S	168355- 171122, 2768	32.1 nm 59.5 km	3	12:21 MMO alarm: shutdown at end of profile
AWI-20220115	start end	26.01.22 26.01.22	12:36 18:32	7°18.801´W 8°33.934'W	70°07.214´S 70°03.895'S	171141- 173255, 2115	27.6 nm 51.2 km	3	12:58 Reactivation of 3 guns at full pressure after shutdown 15:24 MMO alarm: failed shutdown; 15:39 Delayed shutdown 15:59 Reactivation of 3 guns at full pressure after shutdown 16:33-16:35 Shutdown due to false MMO alarm
AWI-20220116	start end	26.01.22 27.01.22	18:37 00:11	8°35.052'W 8°39.326'W	70°04.015'S 70°29.258'S	173256- 175281, 2026	25.9 nm 48.0 km	3	00:11 MMO alarm: shutdown at end of profile
					Number of shots along recorded profiles =	14385	Total:		
					Number of shots during turns not recorded on profiles =	428	167.0 nm		
					Total number of shots =	14813	309.7 km		

Mitigation for marine mammals

The mitigation regulations for seismic operations consisted of visual observations for marine mammals within a predefined exclusion zone by marine mammal observers (MMOs). MMOs followed the mitigation protocol predefined by Germany's Federal Environment Agency (*Umweltbundesamt*).

The marine mammal observation was coordinated and conducted by the two professional, JNCC-PSO qualified MMOs Alejandro Cammareri and Juan Manuel Salazar Sierra with the

support of 17 voluntary observers drafted from the various science teams of PS128 and trained by A. Cammareri and J.M. Salazar Sierra during the expedition. During seismic operations, a constant visual watch for marine mammals was conducted by four marine mammal observers (MMOs) per shift to detect any marine mammals within the predefined safety zone of 1,000 m around the ship. Visual observations were conducted by one MMO from the bridge deck, by two MMOs from the winds of the port and starboard sides, respectively, and one MMO observed the infrared (IR) monitoring system. The observers scanned 360° around the vessel. The primary observation technique to spot marine mammals was to scan the sea around the vessel and within the exclusion zone using the naked eye and scanning with reticulated binoculars (Fujinon 7x50) continuously. Areas of interest on the water (breaking wave crests, splashes, blows, footprints, dark shapes, bird activity, etc.) were used as visual cues to investigate.

To ensure that most of the perimeter of the seismic sources was observed continuously, an IR thermal imaging sensor (FIRST Navy), installed in the crow's nest of *Polarstern* (Zitterbart et al., 2013), was used. The IR sensor constantly monitors its environment within a field of view of 360° horizontally by 28.8° vertically. The recorded image shows the thermographic signatures of marine mammals (*e.g.* blow) and provides the observer in the IR observation room with detected cues on the monitor to give further assistance to the MMOs in a potential shut-down situation. The IR thermal imaging system worked during seismic operation times without any flaws.

As the QuietSea PAM system is integrated in the seismic recording system, it's monitors and acoustic alarms in cases of any events were continuously observed by the seismic watch team. However, no detection event occurred during the seismic survey.

Pre-watch observations started at least 60 minutes before scheduled seismic operations were to begin to ensure that no marine mammal was detected within the safety zone when seismic operations were due to start. Clearance for the 30-minute soft-start procedure (a gradual increase of energy and number of the air pulsers) was given when there was no detection of marine mammals in the water of the safety zone. Airgun shutdown occurred when a marine mammal was detected in the water within the safety zone.

During seismic operations, we recorded three detections of marine mammals within the safety zone, of which all were initial visual sightings, all were additional IR detections and there was none QuietSea PAM event. In all of these encounters, mitigation actions such as shut-downs of airguns were conducted. Besides detections of animals in the water, we also recorded seals resting on ice floes. The sightings within the safety zone (in water) are summarised in Table 4.1.2.

Tab. 4.1.2: Marine mammal sightings within mitigation/safety zone (MZ) during seismic profiling

Date [UTC]	**Time** [UTC]	**Visual / IR**	**Species**	**Within MZ [y/n]**	**Mitigation action**
26/01/2022	12:21	visual	minke whale	y	shutdown
26/01/2022	15:24	visual/IR	crabeater seal	y	delayed shutdown
27/01/2022	00:11	visual/IR	crabeater seal	y	shutdown

Preliminary results

Shipboard seismic data processing included only initial steps such as seismic line geometry definition, filtering, single-channel displays and brute stacking. Advanced processing of the seismic data will be performed at AWI in Bremerhaven with particular emphasis to suppress

of the strong seafloor multiples in the shelf profile data. From single-channel displays, it can already be seen that our new offshore seismic profiles provide good quality images of glacially transported and deposited sediment sequences on the continental shelf off the Ekström Ice Shelf region (Fig. 4.1.3). In connection to pre-existing seismic profiles on the continental rise and deep sea with links to ODP Leg 113 drill sites as well as to the pre-existing vibroseis lines on the Ekström Ice Shelf, we expect to delineate preglacial to glacial stratigraphic sequences and dominant periods of past EAIS dynamics in this Dronning Maud Land sector.

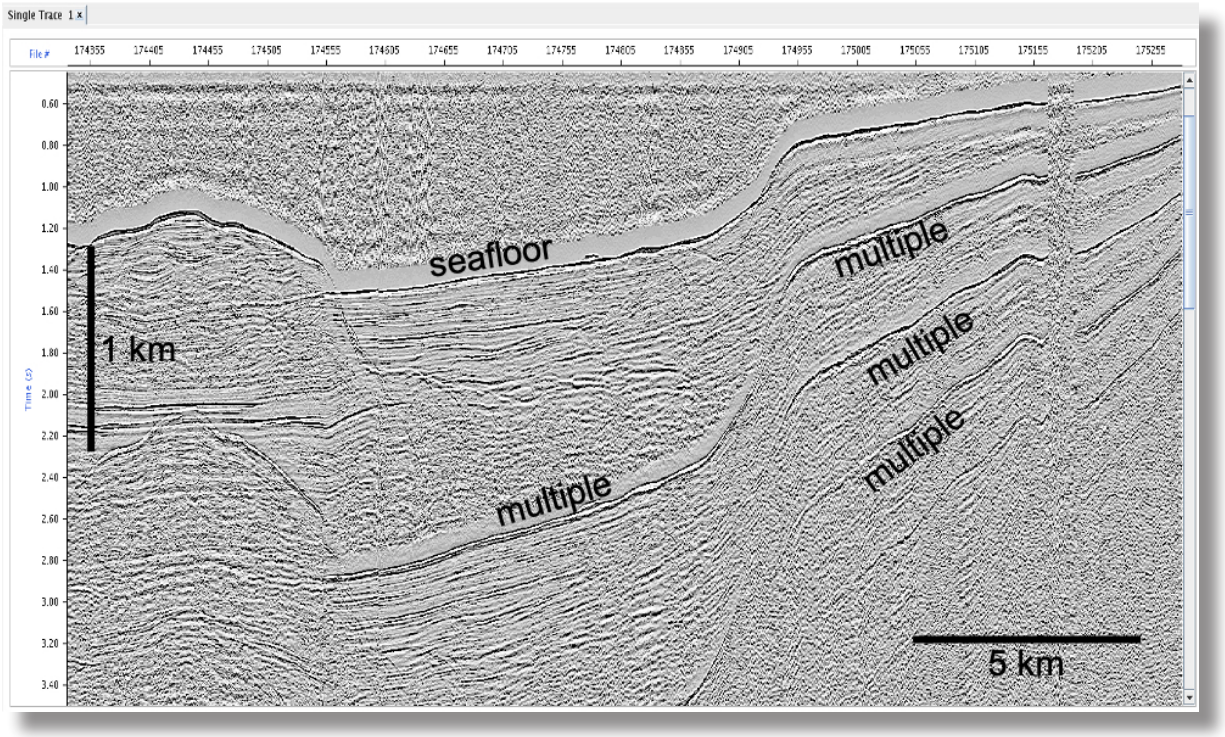

Fig. 4.1.3: Example of a single-channel quality-control display of recorded seismic data

Data management

Seismic data will be submitted to the SCAR Antarctic Seismic Data Library System (SDLS) from which they will be made available to other users four years after data acquisition. Access for the science community will also be provided via the geoscientific database PANGAEA, once the data are published or latest three years after the end of the expedition (moratorium period).

References

Barker PF, Kennett JP et al. (1988) 1. Introduction and Objectives. Proceedings ODP, Initial Reports, 113, College Station, TX, (Ocean Drilling Program).

Kristoffersen Y, Hofstede C, Diez A, Blenkner R, Lambrecht A, Mayer C, Eisen O (2014) Reassembling Gondwana: A new high-quality constraint from vibroseis exploration of the sub-ice shelf geology of the East Antarctic continental margin. J. Geophys. Res. Solid Earth 119:9171-9182. https://doi.org/10.1002/2014JB011479.

Lindeque A, Martos Y, Gohl K, Maldonado A (2013) Deep-sea pre-glacial to glacial sedimentation in the Weddell Sea and southern Scotia Sea from a cross-basin seismic transect. Marine Geology 336:61-83. https://doi.org/10.1016/j.margeo.2012.11.004.

Oetting A, Smith EC, Arndt JE, Dorschel B, Drews R, Ehlers TA, Gaedicke C, Hofstede C, Klages JP, Kuhn G, Lambrecht A, Läufer A, Mayer C, Tiedemann R, Wilhelms F, Eisen O (2021) Geomorphology and shallow sub-sea floor structures underneath the Ekström Ice Shelf, Antarctica. The Cryosphere Discussions. https://doi.org/10.5194/tc-2021-305.

Smith EC, Hattermann T, Kuhn G, Gaedicke C, Berger S, Drews R, Ehlers TA, Franke D, Gromig R, Hofstede C, Lambrecht A, Läufer A, Mayer C, Tiedemann R, Wilhelms F, Eisen O (2020) Detailed seismic bathymetry beneath Ekström Ice Shelf, Antarctica: Implications for glacial history and ice-ocean interaction. Geophysical Research Letters 47. https://doi.org/10.1029/2019GL086187.

Zitterbart DP, Kindermann L, Burkhardt E, Boebel O (2013) Automatic round-the-clock detection of whales for mitigation from underwater noise impacts. PLoS ONE 8. https://doi.org/10.1371/journal.pone.0071217.

4.2 Sediment echo-sounding (Parasound) in the Indian Ocean sector of the Southern Ocean and along the Antarctic continental margin

Objectives

Accurate knowledge of the upper sedimentary strata via sub-bottom profiling data is necessary to study glacial-marine sedimentation processes of the younger past. The data provide basic information on the upper meters of subsoil for the understanding of geological processes such as erosion, sediment transport and deposition, or even tectonic processes. Glacially formed structures (*e.g.* moraines) preserved in the sub-bottom can help to reconstruct the dynamic history of East Antarctic ice sheet, and can shed light on its retreat since its maximum extent during the last glacial maximum. In turn, understanding the processes of this past ice sheet retreat can provide important information for predictions of future responses of the East Antarctic ice sheet to changing climate conditions and oceanographic settings.

Imaging the upper few tens of meters, the sediment echography presents an important link between bathymetry (mapping the surface morphology) and reflection seismics (imaging the deep structures down to several km depth). Further, the integration of these three data sets is of particular importance for the interpretation of geological data in a spatial context.

The survey by sediment echography “Parasound” is essential to identify (1) core locations ideally containing undisturbed sediment sequences, (2) sites with high sediment supply, (3) outcrops and slope structures to recover older sediments close to the surface.

Work at sea

Instruments

Sub-bottom profiles were recorded with the hull-mounted Deep-Sea Sediment Echo Sounder PARASOUND (Teledyne Reson, Bremen, Germany), system PS3-P70. This system generates two primary, high-frequency acoustic signals with slightly differing frequencies selectable in a range of 18-24 kHz (PLF, PHF). Due to the non-linear acoustic behaviour of water, the so-called “Parametric Effect”, two secondary harmonic frequencies (SLF, SHF) are generated in the water column of which one is the difference (SLF) and the other the sum (SHF), respectively. As a result of the longer wavelength, the secondary low frequency signal (SLF) is able to penetrate the sediment column as deep as *e.g.* a 4 kHz signal (up to 100 m depending on sediment conditions), whereas the vertical resolution still corresponds to the primary high-

frequency signal (PHF), and thus about some decimeters in sediments. The secondary high frequency (SH) can be used for detection of bubbles in the water column.

The primary signals are submitted in a narrow beam of 4°, but at high power. That has the advantage that the sediment-penetrating pulse is generated within the narrow beam of the primary frequencies, and thereby providing a very high lateral resolution.

The system, however, finds limitations on imaging a rough sea floor topography or submarine ridges with gradients and slopes steeper than 4°. Here, the signal energy reflected from the small inclined footprint on the seafloor is scattered out of the lateral range of the receiving transducers in the hull of the vessel. As a consequence, only poor reflections from the seafloor are recorded, and much less from the sub-bottom.

Survey settings

During expedition PS128, 20 kHz were used as the Primary High Frequency (PHF), and 4 kHz as the Secondary Low Frequency (SLF). Depending on the properties of the sea-floor surface and sediments our settings enabled an imaging of the sub-bottom down to more than 100 m, and with a vertical resolution of about 30 cm. The combined signal has a beam width of ~4°. The resulting beam's footprint on the sea bottom is about 7 % of the water depth.

Concerning signal frequencies, a deviation was noted between the auxiliary log-files (PHF = 18 kHz and SLF = 4 kHz) and values selected in the "Control PARASOUND Sensor" > "Basic settings" (PHF = 20 kHz and SLF = 4 kHz).

The system was controlled using the program Hydromap Control. Live data visualisation and data storage was performed with the Parastore software. Every 30 min, screenshots of the profiles were stored and made directly accessible on a public directory.

Several times, operators of Teledyne (Jörn Ewert) logged in remotely to the system performing maintenance work and system updates. These actions are documented in Appendix A.5.1 (PS128 Parasound Log).

Sub-bottom profiling

During expedition PS128 digital data acquisition and storage were switched on after *Polarstern* left the EEZ of South Africa on 7 January 2022 at 14:43 UTC and was switched off on 27 February 2022 at 04:01 UTC when the ship reached the South African EEZ again after expedition. An interruption of recording was made during passage of the EEZ of Bouvet Island from 11 January 2022 at 13:25 to 12 January 2022 at 21:18 UTC

Data acquisition took place during all times during transit, and of surveys in the study areas to provide information for station planning and sediment sampling sites. For some specific surveys, and during seismic reflection measurements, the ship's speed was reduced from 10 kn in average to only 5 kn, to achieve undisturbed and high-resolution profiles as possible. Profiling was carried out in a 24-hour/7-day shift mode, and the data recorded were promptly made available for site selection and cruise planning.

The daily routine included the subsequent processing steps that are meanwhile established as a standardised workflow consisting of (a) acquisition of data in the internal PARASOUND ASD and PS3 formats, (b) conversion of PS3 to standard SGY format, (c) extraction of navigation data and conversion to standard UKOOA format, (d) preparation for storage in Pangaea, and (e) performance of a preliminary processing of data and visualisation with Kingdom software (Appendix A.5.2, PS128 Parasound Station Profiles).

Mitigation for marine mammals

The mitigation regulations for profiling operations consisted of visual observations for marine mammals by observers, following the mitigation protocol predefined by Germany's Federal Environment Agency (Umweltbundesamt).

In detail, the mitigation actions comprised:

1. Continuous marine mammal observer (MMO) watches by two persons before start of sounding, and during station time.
2. Start of sounding only after at least 15 min whale watching without sightings of marine mammals.
3. Start of sounding only at daylight and good visibility, whenever scientific missions and ship's security allowed.
4. Stop sounding whenever marine mammals were sighted in the water closer than 100 m to the ship (opportunistic during ship's run, and by watches during stations).
5. Compliance with a minimum distance of > 500 m to icebergs, shelf-ice edges, and coasts during the operation of the sediment echo sounder.
6. Stop of sounding during station time if scientific missions and ship security allowed to break.
7. Reduce sounding rate to 10 s during station time, when the location of small sub-bottom structures was necessary, or water depths were less than 1,000 m.
8. Instruction of trained observers by experienced marine mammal observers.

Summary

All actions and reasons concerning switching on and off the system, system parameters, actions on stations, and events concerning MMO calls are documented in Appendix A.5.1 (PS128-Parasound Log).

Preliminary (expected) results

In total ~18,000 km (~9,700 nm) of sub-bottom profiles were acquired during 52 days of operation. South of 60° our working comprised 38 days, and about 1,080 km (5,835 nm) of sub-bottom profiles (Chap. 1, Fig. 1.2: Route of *Polarstern* expedition PS128). The profile names, sub-bottom penetration range, advices for geological sampling, and other notes are listed in Appendix 4.2.3 (PS128-Parasound-files).

The acquired data set provide geomorphological information on the upper 50 m of sedimentary sequences of the research area. The recorded profiles serve as a compilation of high-resolution seabed maps along the cruise track and from the target research sites. These sub-bottom maps image glacial-geomorphological features (*e.g.* grounding zone wedges), erosional structures, and depositional features (*e.g*. slumps, slides, fans) (Fig. 4.2.1). Linked to the findings of sampling, the net of sub-bottom profiles offers an important tool for the interpretation of geological data in a spatial context. Expected outcomes aim towards a better understanding of ice-sheet dynamics and geological processes in the research area.

For the selection of coring locations, the sub-bottom profiles enabled to identify areas of high and low sedimentation rates, outcrops, and to avoid areas of sediment redeposition or erosion (Fig. 4.2.2).

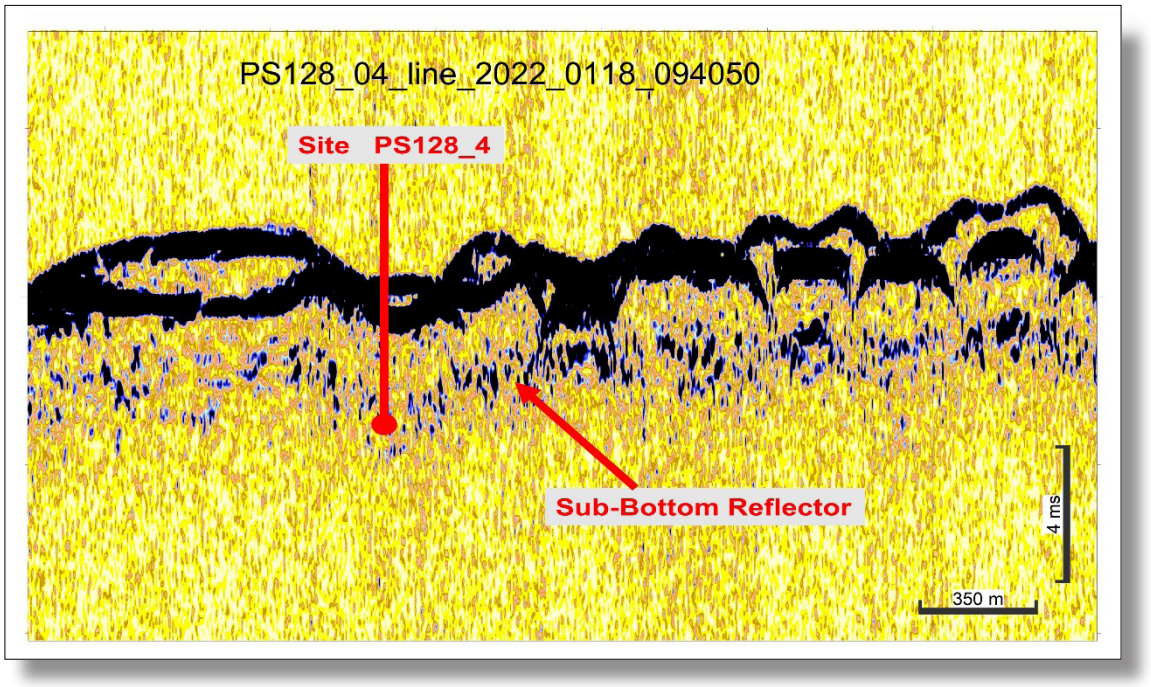

Fig. 4.2.1: Section of a sub-bottom profile along the outer continental shelf close to Neumayer III Station and location of sampling site PS128_4. The profile images clearly a sub-bottom reflector at 4 m depth (~ 3 mbsf). This reflector indicates the surface of a subglacial till, i.e., the surface of mega-scale glacial lineations, that was likely penetrated by geological sampling.

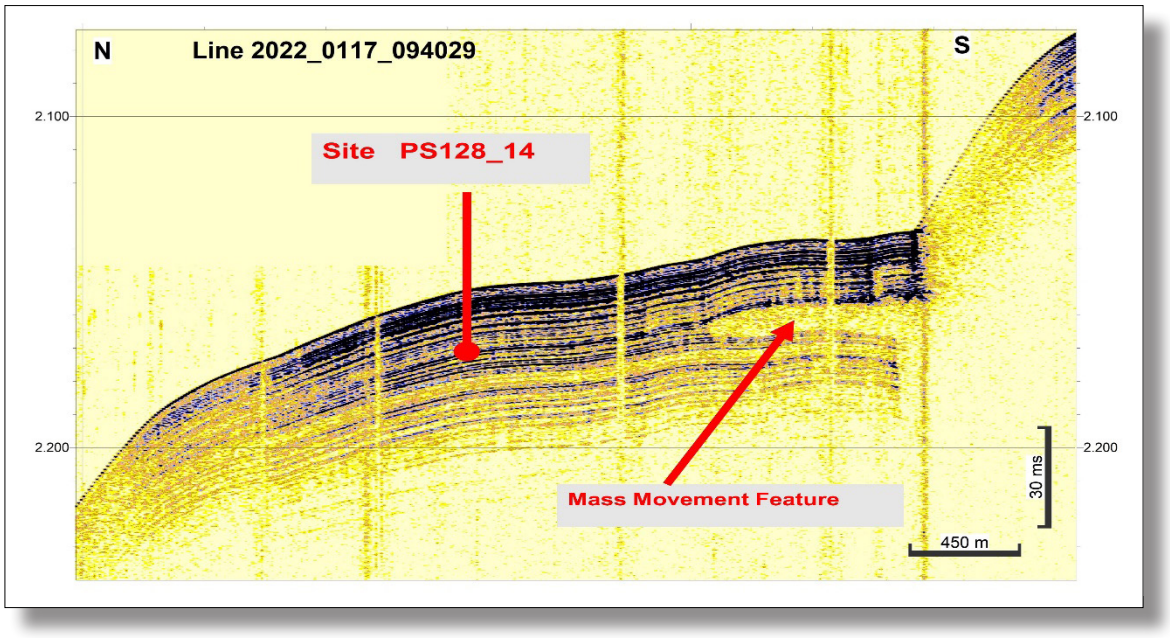

Fig. 4.2.2: Section of a sub-bottom profile imaging undisturbed, well-stratified ~50 m thick sedimentary sequences as example for a favourable sampling location (PS128_14); close to site however, a transparent, lens-like structure indicates useless slumping and mass movement features.

Data management

Sub-bottom profiling data collected during PS128 were copied to the *Polarstern* data base, from where they will be transferred to the data mass storage at AWI Bremerhaven and linked to the World Data Center PANGAEA Data Publisher for Earth & Environmental Science (https://www.pangaea.de) at AWI.

This expedition was supported by the Helmholtz Research Programme "Changing Earth – Sustaining our Future" Topic 2, Subtopic 2.1.

In all publications based on this expedition, the **Grant No. AWI_PS128_04** will be quoted and the following publication will be cited:

Alfred-Wegener-Institut Helmholtz-Zentrum für Polar -und Meeresforschung (2017) Polar Research and Supply Vessel POLARSTERN Operated by the Alfred-Wegener-Institute. Journal of large-scale research facilities, 3, A119. http://dx.doi.org/10.17815/jlsrf-3-163.

5. MARINE GEOLOGY AND PALEOCEANOGRAPHY

Ralf Tiedemann[1], Juliane Müller[1], Johann Klages[1], Dirk Nürnberg[2], Lester Lembke-Jene[1], Bernhard Diekmann[1], Henning Bauch[1], Gesine Mollenhauer[1], Thomas Arney[3], Matthieu Civel-Mazens[4], Tainã Pinho[1], Wee Wei Khoo[1], Vincent Rigalleau[1], Hinner Preckel[5], Ebbe Nürnberg[6], Alina Ivanova[5], Laura Kattein[5], Lea Fuchs[5], Patricia Sonnemann[7], Denise Diekstall[1], Valea Schumacher[1], Lisa Schönborn[1], Pascal Daub[1], Norbert Lensch[1]
Not on board: Frank Lamy[1], Oliver Esper[1], Thorsten Bauersachs[8], Claus-Dieter Hillenbrand[9], Alix Post[10], Helen Bostock[11], Guiseppe Cortese[12]

[1]DE.AWI,
[2]DE.GEOMAR,
[3]UK.UNI-SOUTHAMPTON-SOES,
[4]JP.KOCHI-U.AC,
[5]DE.UNI-BREMEN
[6]DE.UNI-GREIFSWALD
[7]AT.UNI-INSBRUCK
[8]DE.CAU-GEOWISS
[9]UK.BAS,
[10]AU.GA.GOV,
[11]AU.UQ.EDU.SEES,
[12]NZ.GNS.CRI

Grant-No. AWI_PS128_01

5.1 Objectives

The overall goal is to enhance our understanding on the late Paleogene to Quaternary processes as well as the orbital to submillennial-scale evolution of ice-ocean-climate interactions during deglacial warming and climate intervals that were warmer than today. Therefore, we plan to probe marine sediment archives along the continental margin of Dronning Maud Land, Enderby Land and Mac. Robertson Land. Particular attention will be paid to processes that are related to basal ice shelf melting, including Warm Deep Water (WDW) intrusions into the ice shelf cavities and feedback mechanisms (e.g. freshening, sea ice cover) that control the formation and extent of Antarctic Bottom Water (AABW). Key hypotheses we will address in this context are:

- Marine ice-based portions of the Antarctic ice sheet collapsed during warmer than present times at a temperature anomaly threshold of 2–3° C.
- The marine-based East Antarctic ice portions are similarly unstable as the West Antarctic Ice Sheet.
- The frequency, duration and extent of cross-continental shelf intrusions of Warm Deep Water control the instability of ice sheets during past interglacials.
- Antarctic sea ice varied asynchronously with Arctic sea ice extent over centennial to millennial times scales and synchronously on orbital times scales.
- Sea ice retreat favours the destabilisation of ice shelves, accelerating continental ice mass loss.
- Changes in ice sheet melt and freshwater input affect Southern Ocean circulation and ecosystem processes, *e.g.* through fundamental changes in formation rates and physical and biogeochemical characteristics of abyssal AABW.

An important backbone to validate these hypotheses is the development of high-resolution age models. Precise timeframes are required to allow for comparisons with other existing high-resolution climate proxy records derived from sediment and ice cores. We will apply a variety of stratigraphic methods, including marine oxygen isotope stratigraphy, ^{14}C-dating techniques, ^{230}Thex, ^{231}Paex/^{230}Thex methods, cross-correlation of proxy records with other well-dated records, paleomagnetics and tephrachronology. Other options (yet to be tested) include correlating proxy records from sediment and ice cores, that indicate changes in sea ice variability (*e.g.* Abram et al., 2013) by assuming synchronous variability. This could anchor the sediment stratigraphy to *e.g.* the ice core chronology of the EPICA DML ice core (EPICA Community Members, 2006).

The sediment archive at the continental margin off *Neumayer Station III* provides large quantities of well-preserved planktonic and benthic foraminifers (Grobe and Mackensen 1992) and thus, the opportunity to reconstruct glacial/interglacial temperature variations on centennial/millennial to orbital timescales from the surface into the deep water. Temperatures will be reconstructed by means of Mg/Ca paleothermometry on planktic and benthic foraminifers (Nürnberg et al., 2000), the organic biomarker-based indices TEX^{L}_{86} and RI-OH' (Ho et al., 2014; Lamping et al., 2021; Park et al., 2019) and diatom/radiolarian transfer functions (Gersonde et al., 2005; Civil-Mazens et al., in prep.). Sea ice reconstructions will be based on analyses and intercomparisons of specific biomarker lipids (highly branched isoprenoids) and diatom assemblages. These studies will allow to assess the role of "Warm Deep Water" in ice-shelf melting and the response of the SO and sea ice to meltwater-induced freshening.

The sediment archives proximal and distal to the Cape Darnley Polynya offer an excellent opportunity to assess past changes in Cape Darnley Bottom Water/AABW formation, which is of global significance. A multi-proxy approach is required to reconstruct and understand the system (Borchers et al., 2016; Vorrath et al., 2019; Rickli et al., 2014). We will reconstruct changes in sea ice production, biogenic productivity, Nd isotopes and Rare Earth Elements indicative of the provenance of current-derived and ice-transported material as well as past regional changes in overturning circulation.

Our studies also aim to significantly improve our understanding of past EAIS extent, its flow and retreat patterns, and the related bed processes that controlled ice flow primarily since the last glacial to the Holocene (Klages et al., 2016; 2017). We will integrate and link bathymetric, seismic, marine geological, and modelling competence to map and document temporal changes in grounding line dynamics since the LGM.

5.2 Work at sea

5.2.1 Surface sediment sampling

Work at sea

Undisturbed surface sediments, reflecting the most recent sedimentary and environmental conditions in our study area, provide an important avenue for the calibration of microfossil and geochemical proxies against observational data. This is important as new proxies evolve continuously, and testing their applicability and reliability, *e.g.* as sea surface temperature or sea ice proxies, is a crucial step within paleoceanographic and paleoclimate research. The multicorer permits the recovery of up to 12 surface sediment samples and the uppermost 30 to 40 cm of sediment, which encompass the most recent geological history. The surface sediments recovered during *Polarstern* Expedition PS128 in the Dronning Maud and Enderby Land continental shelf and slope areas constitute a highly valuable reference data set for the evaluation of different proxies' response to varying polar oceanic domains and polar

frontal connected sea ice – glacier – ocean systems. Additionally, these near-surface samples are indispensable for generating uninterrupted records up to the most recent past, in cases where the uppermost part of a gravity or piston core is disturbed or missing. By combining proxy records from both the multicorer and the piston/gravity corer, a complete sedimentary sequence and hence, stratigraphy can be established.

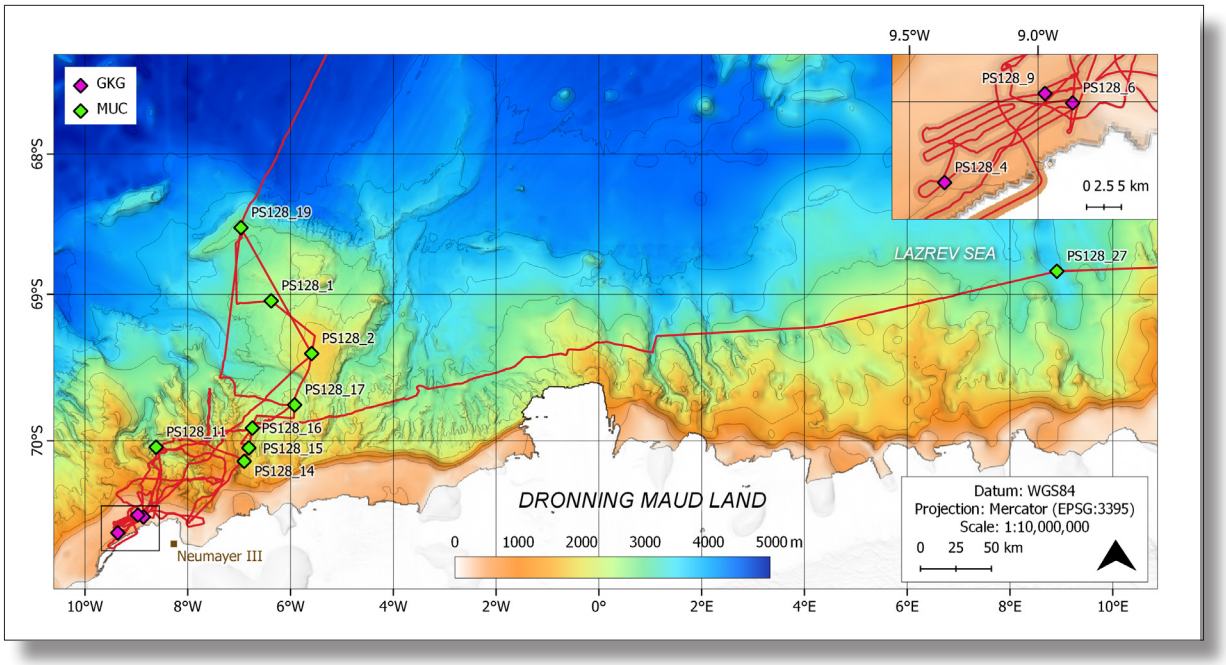

Fig. 5.2.1.1: Overview of multicorer (MUC) and giant box corer (GKG) stations off Dronning Maud Land. Insert shows multicorer and giant box corer stations at the continental shelf off Neumayer.

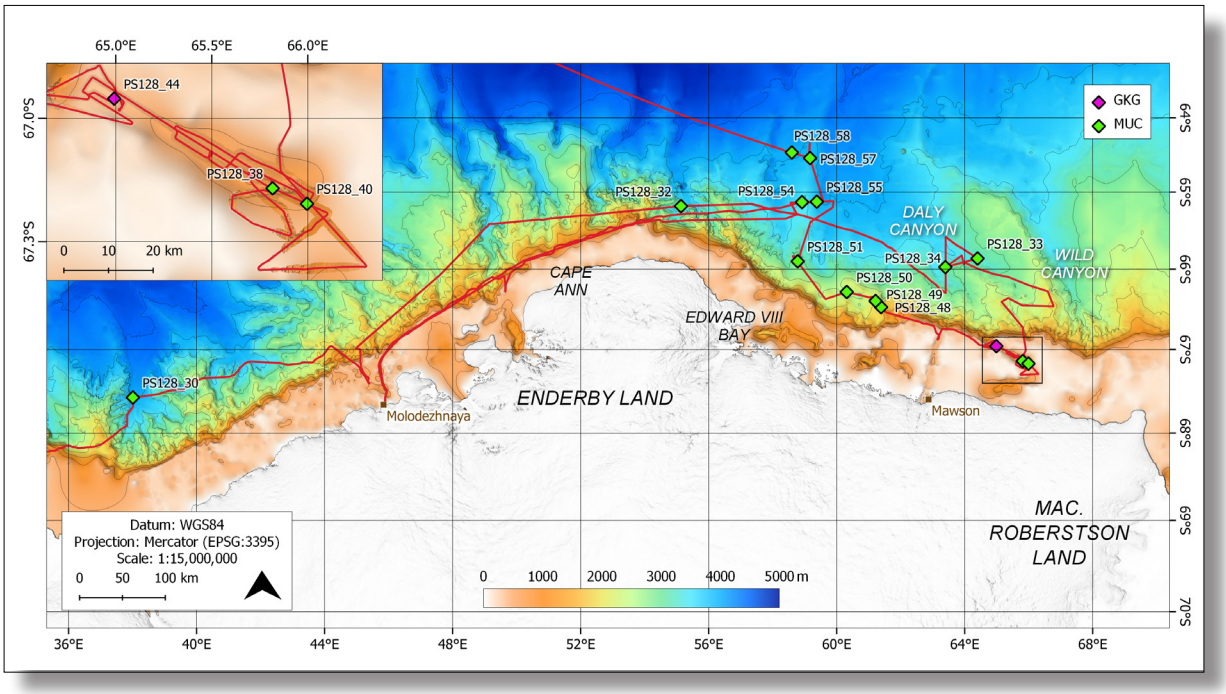

Fig. 5.2.1.2: Overview of multicorer (MUC) and giant box corer (GKG) stations off Enderby Land and Mac. Robertson Land. Insert shows multicorer and giant box corer stations within Nielsen Basin.

Surface and near-surface sediment sampling during PS128 was carried out at 26 stations with a Multicorer (MUC) or a Giant Box Corer (GBC; Figs. 5.2.1.1 and 5.2.1.2).

The 12-tubes multicorer (MUC67; manufactured by Fa. Wuttke, Henstedt-Ulzburg, Germany), with an inner tube diameter of 6 cm and a length of 60 cm, was deployed at 24 stations and usually recovered undisturbed surface sediments and overlying bottom water. Apart from an initial test run, all MUC deployments successfully recovered surface sediments.

On average, all 12 tubes recovered intact sediments, with average penetration depths between 10 and 35 cm (Fig. 5.2.1.3). Overpenetration of the MUC67 occurred at station PS128_40-3, and was likely related to the occurrence of very soft, biosiliceous sediments. On this station, only four MUC cores were deep-frozen as entire cores designated as ARC I – IV.

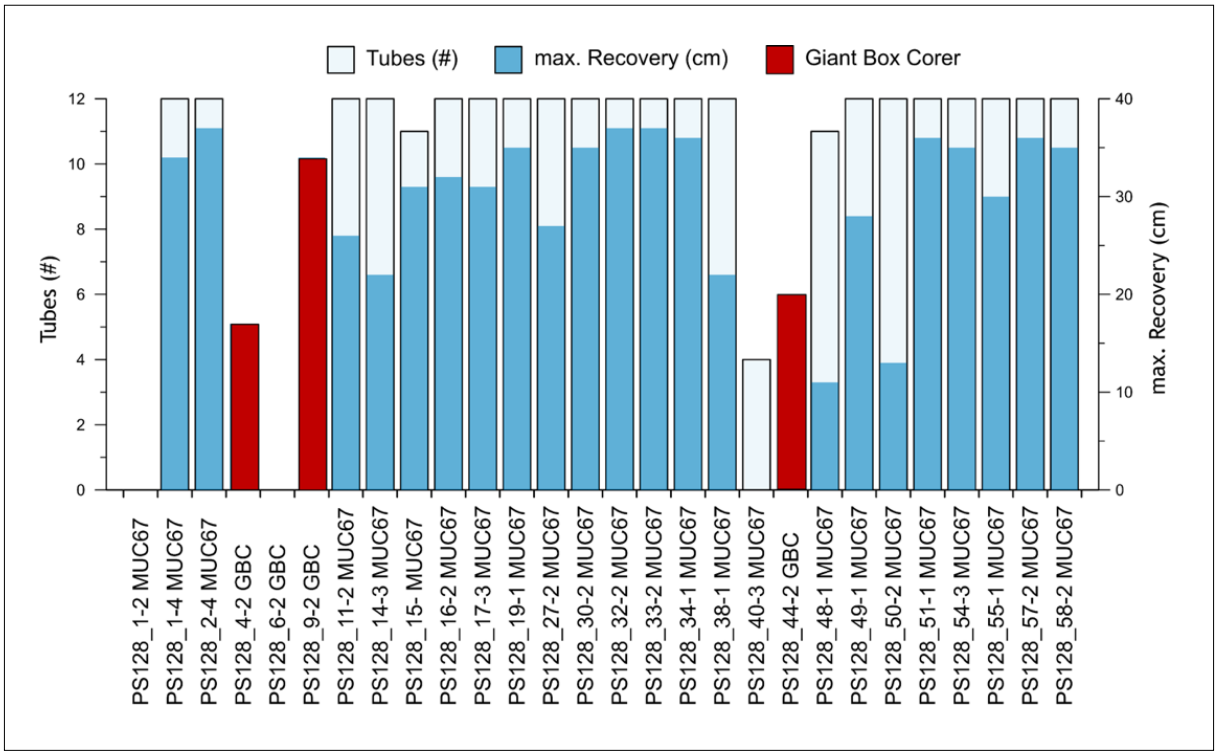

Fig. 5.2.1.3: Recovery of 12-tubes Multicorer (MUC67) and Giant Box Corer (GBC) on PS128 stations; light blue and red bars show the number of tubes that recovered sediment (left axis), the dark blue bars indicate the maximum recovery (right axis).

Immediately after recovery of the device, supernatant water was sampled at each station for stable isotopes ($\delta^{13}C$ and $\delta^{18}O$) and ^{14}C from the two assigned Benthos (BEN I and II) tubes. Stable isotope samples were collected as duplicates in 50 and 100 ml glass bottles with screw tops. For radiocarbon analyses, 2 x 5 ml of water from the same MUC tube were sampled in pre-combusted glass vials, which were poisoned with $HgCl_2$ and closed gas tight using crimp lids immediately after sampling. From the remaining tubes the supernatant water was transferred to a 10 L cubitainer plastic bag for further analysis. For documentation, all MUC tubes were photographed (Fig. 5.2.1.4).

Fig. 5.2.1.4: MUC tubes retrieved at station PS128_17-3

Except the MUC tubes designated as Archive-MUCs, all MUC tubes were sampled immediately after recovery to avoid degradation of organic compounds. For multidisciplinary investigations of the recovered sediments, the multicorer tubes were sampled according to the following scheme:

Tab. 5.2.1.1: Allocation and sampling of MUC tubes for the different post-cruise investigations

#Tubes	Working Group	Sampling	Storage
1	Sedimentology (SED)	1 cm slices in Whirlpack bags	4°C
2	Benthos (BEN I+II)	1 cm slices in Kautex bottles (0-10 cm) & Whirlpack bags (10 cm to bottom)	4°C
2	Biomarker (BIO I and II)	0-1 cm and 1-2 cm slices in Petri dishes (BIO MUC I+II combined); remaining material in 1 cm slices in glass vials covered with Al foil	-20°C
1	Plankton (PLA)	1 cm slices in Whirlpack bags	4°C
1	Micropaleontology (MPAL)	1 cm slices in Whirlpack bags	4°C
2	Porewater (PW I + II)	1 cm slices in Whirlpack bags if not sampled by MG	4°C
1	Paleo DNA (DNA)	Entire MUC tube deep frozen, stored wrapped in aluminum foil in evacuated and sealed plastic bag	–20°C
1	Physical properties (PP)	1 cm slices in Whirlpack bags	4°C
1	Archive (ARC)	Entire MUC tube deep frozen, stored wrapped in aluminum foil in evacuated and sealed plastic bag	-20°C

The giant box corer (GBC; volume of sample 50*50*60 cm (manufactured by Fa. Wuttke, Henstedt-Ulzburg, Germany) was successfully deployed at three stations on the continental shelf off *Neumayer* and Mac. Robertson Land. Deployment at station PS128_6-2 failed, which is probably related to the very consolidated sediments on the shelf. Surface sediments and usually two archive tubes (diameter 12 cm) were taken for organic geochemical, micropaleontological and sedimentological studies (Fig. 5.2.1.5), while the remaining sediment has been sieved and sampled for investigations (see Chapter 5.3).

Fig. 5.2.1.5: Sedimentary structure (a) of the GBC obtained at station PS128_4-2 and sampling (b) of the GBC obtained at station PS128_9-2

5.2.2 Sediment coring and core documentation

Work at sea

During PS128, 10 piston corers (PC) with a gear length between 15 and 25 m, 39 gravity corers (GC) with a gear length between 3 and 20 m, and 1 Kasten corer (KAL) with a device length of 2 x 5.75 m were used to recover long sedimentary sequences (Tab. 5.2.2.1). The different coring systems were deployed via *Polarstern*'s core handling rack (Kernabsatzgestell) using cable #2 with a diameter of 180 mm. 46 deployments were successful and resulted in a total core recovery of ca 344 m (Tab. 5.2.2.1). In addition, 6.32 m were recovered by the pilot corer (TC) triggering the PC. The gear types and the length of the coring devices were chosen based on sediment acoustic profiles with the PARASOUND echo-sounding system, considering acoustic patterns such as the strength of characteristic reflectors, their spacing, and the total sub-bottom penetration (Chapter 4.2).

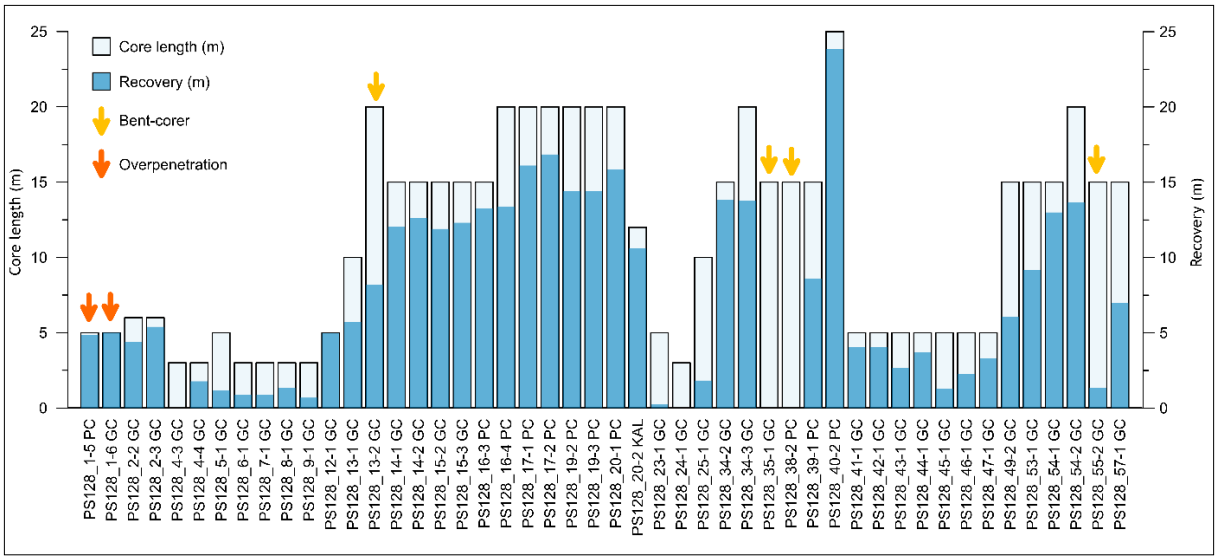

Fig. 5.2.2.1: PS128 sediment core recovery (m) in consecutive order of stations. Light blue shading: Length of deployed coring device (m). Dark blue shading: Absolute core recovery in (m). Yellow and orange arrows indicate occasions of bent-corers and overpenetration, respectively.

The main sediment coring device applied during cruise PS128 was a gravity corer, which consists of a 2.3 t weight and an up to 25 m long steel pipe (in 5 m-barrel-increments). The gravity corer was lowered to depth at a speed of 1.2 m/s. The device remained in the sediments for ~30 seconds to allow for penetration until it was heaved with a speed of 0.2 m/s out of the seafloor and with 1.2 m/s back to the ship´s working deck. Penetration into and release from the sediments were monitored through the cable tension.

For *ad hoc* deployments in order to gain a quick impression of the sediment consistency, we used a short gravity corer, with 3 m to 6 m steel pipe length. We here did not make use of the ship's core handling rack (Fig. 5.2.2.2).

Fig. 5.2.2.2 (see left): Deployment of an ad hoc gravity corer (3–6 m) during PS128, without Polarstern´s core handling rack (Kernabsatzgestell).

In addition to gravity coring, we applied the AWI piston corer (PC) of the Fa. Kawohl-Marinetechnik (Fig 5.2.2.3). Equipped with a split piston, the maximum length of the piston corer pipe aboard *Polarstern* is 25 m (in 5 m increments). The pipe diameter is 12.5 cm. The barrel´s weight is ca. 2.8 t. The piston corer was lowered and heaved at a winch speed of 1.2 m/s. A 1 m-long pilot (trigger) core is attached to the piston corer by a steel rope via a release mechanism (Fig. 5.2.2.4). Upon contact with the seafloor, the pilot core triggers the release of the main device, which then free-falls into the sediment and allows deeper penetration into the sediments, rather than a gravity corer. To allow for a deep penetration, the piston corer was left at the seafloor for about 30 seconds, then hieved with 0.2 m/s until it was pulled out of the sediment. Hieving activates the split piston, which produces an underpressure

within the steel pipe and allows for better core recovery (Fig. 5.2.2.4). Overall, the sediment pile within the gravity core is significantly compressed during the coring process, and core recovery is consistently lower than for a piston corer.

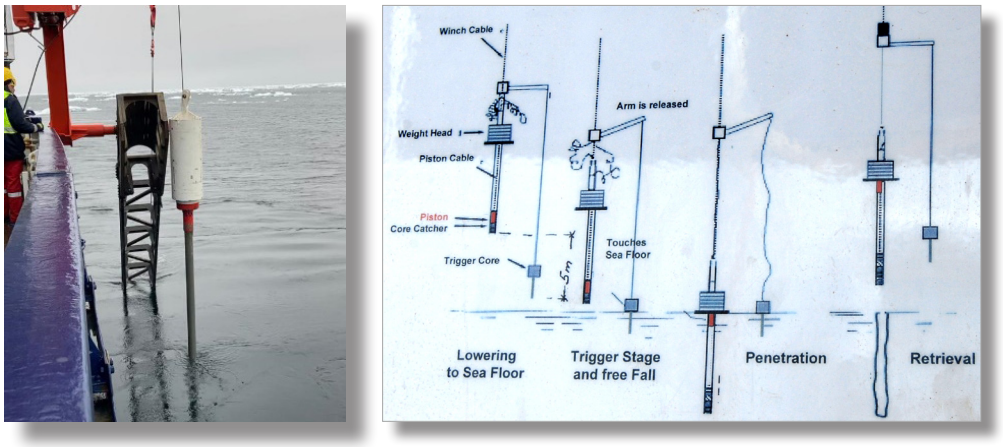

Fig. 5.2.2.3 (left): Polarstern´s core handling rack system to deploy long coring devices, here the AWI piston corer; Fig. 5.2.2.4 (right): Functioning of the piston corer (PC) from Fa. Kawohl-Marinetechnik

The largest-in-diameter coring device deployed during PS128 was a 11.5 m Kasten corer (KAL) consisting of two 5.75 m segments (Fig. 5.2.2.5). The KAL´s rectangular shape has a footprint of 30*30 cm and is attached to a 2.8 t weight barrel. Due to its large diameter, the KAL has a four-times higher sediment recovery compared to the PC. Upon recovery, one of the two angle sections of the KAL were removed to allow access to the sediments. Prior to sampling, the outermost sediments layers were removed, which might have been disturbed by the coring process. To sample the recovered KAL-sediments, 5 rows of rectangular plastic boxes (98*15*7 cm), 1 row of smaller rectangular plastic boxes (98*7*7 cm) and 1 row of U-channels (for paleomagnetic studies) were pushed into the sediments (Fig. 5.2.2.6).

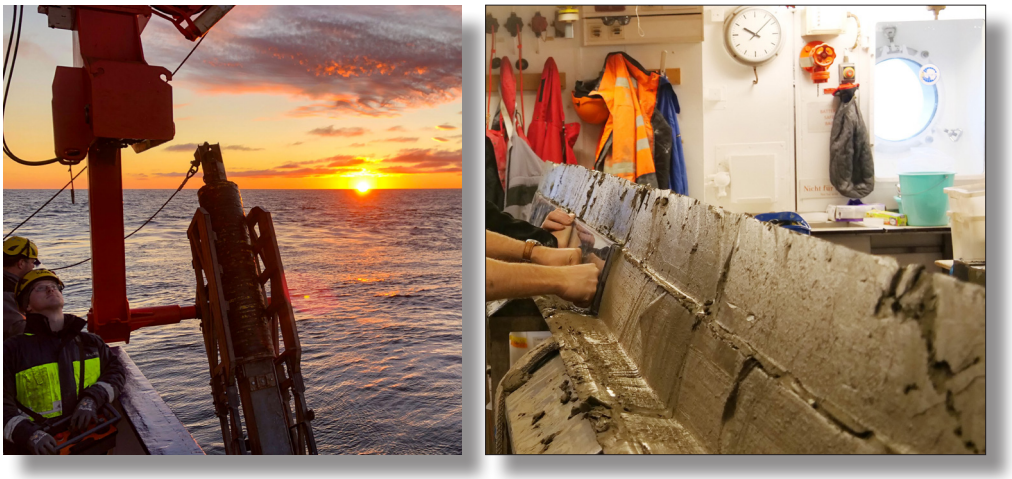

Fig. 5.2.2.5 (left): Deployment of the Kasten corer; Fig. 5.2.2.6 (right): Sampling of the Kasten core

Coring statistics are given in Figure 5.2.2.7. The lengths of the sediment cores recovered by the gravity corer (GC) ranged from 0.25 m to 13.84 m with on average 5 m. The average core recovery was 57 %. The piston corer (PC) deployments gained core recoveries of 8.59 m

to 23.84 m with on average 13.6 m, which is 72 % m core recovery. The only deployment of the Kasten corer (KAL) yielded a recovery of 10.62 m (92.3 %). In total, the sediment core recovery was at ~ 63 %, with an overall sediment core recovery of 344 m.

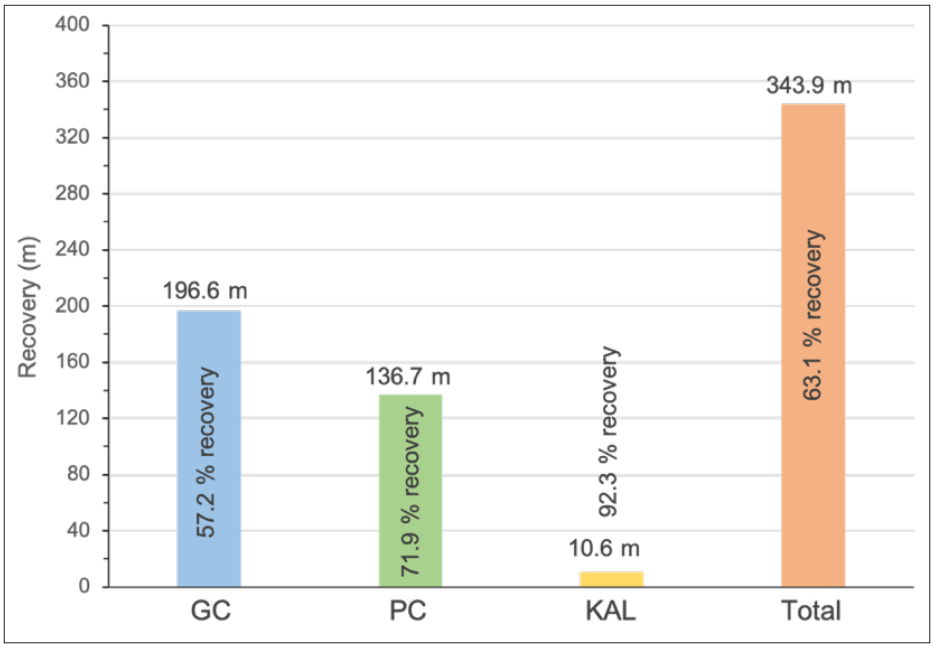

Fig. 5.2.2.7: Total sediment core recovery during PS128 in (m) and (%). GC = gravity corer; PC = piston corer; KAL = Kasten core

Sediment core handling

After being placed on deck, the core catcher of the coring device was removed, with its sediment material being stored in labeled plastic bags. The 5 m-PVC-liner sections were pulled out of the steel pipes. The numbered sections were brought into the laboratory and cut into 1 m round sections. Alternatively, the PVC-liners were cut into 1-m PVC-sections directly in the core handling rack (Kernabsatzgestell). Labeling of the 1-m PVC-sections is according to the following scheme that was also used for the storage containers (D-tubes) and their caps (Fig.5.2.2.8):

- Cruise number; station number; number of device at station (*e.g.* PS128_07-2)
- Label A for archive half; label W for working half
- Arrow, pointing to the bottom of the section
- Depth interval (in cm)
- Label Top/Base

The sediment cores taken with piston and gravity corers were cut into 1 m long segments on board of *Polarstern*. Before closing the core segments with plastic caps, smear slides were taken from each segment base in order to conduct biostratigraphic analyses.

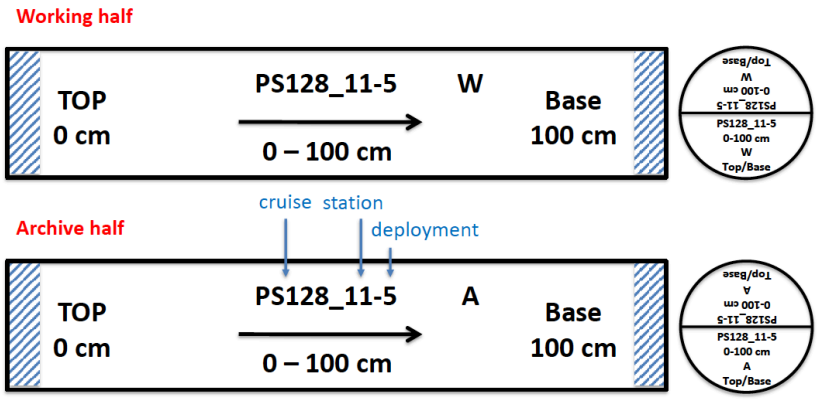

Fig. 5.2.2.8: Labeling scheme for liners, D-tubes, and liner caps; bluish hatched areas indicate place for caps and tapes.

After the measurement of the physical properties using a GEOTEK multi-sensor core logger (MSCL; Chapter 5.2.3) for un-split core sections, cores were selected for opening and sampling based on initial biostratigraphic and physical property analyses.

Routinely, the 1 m-core sections were split lengthwise into a working (W) and an archive (A) half (Figs. 5.2.2.8 and 5.2.2.9).

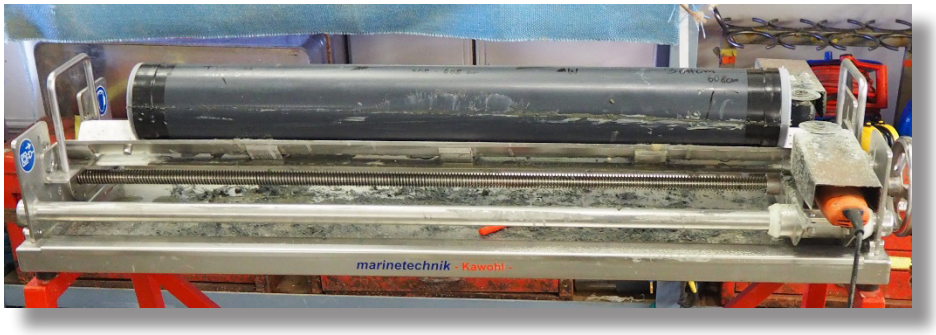

Fig. 5.2.2.9: Splitting of a core section in working and archive halves, using the Fa. Marinetechnik Kawohl vibration saw tool

After opening and splitting of the cores, the core sections were photographed (Appendix A.6.1). The archive halves were described visually (see below). Sediment colours were determined using the “Munsell Soil Colour Chart“. Samples (~3 cc) designated for measurements of the physical sediment properties were taken each 10 cm from the working half. As a last step, all core sections were wrapped in transparency foil, placed into D-tubes or vacuum bags, sealed and stored in reefer-containers at ~4°C.

Visual core description

The sediment core descriptions, visualised as lithologs (Appendix A.6.2), comprise information on lithogenic and biogenic sediment composition, as well as the inventory of sediment textures and structures. Lithologs were generated according to observations from visual core inspection in verification with shipboard core logging, core photography, and findings from microscopic smear-slide analysis. Based on the standard IODP classification scheme and following the

lithological classification of Mazullo et al. (1998), we used the APPLECORE software package with a custom-made lithological file to digitise all visual core descriptions.

According to the classification of Mazzullo et al., (1998), the hemipelagic to pelagic sediments are mainly of terrigenous origin and comprise mainly siliciclastic lithogenic matter. Pure biogenic sediments are rare. The siliciclastic components consist of common rock-forming minerals, mainly quartz, feldspar, mica, as well as rock fragments of the sand, silt, and clay size fractions. Sand- and gravel-sized material of glaciogenic origin (ice-rafted debris, IRD or “dropstones”) is common, but regionally enriched, and unexpectedly low in the overall amount. For siliciclastic sediments, the principal name describes the texture (gravel, sand, mud (silt+clay)) based on the Udden-Wentworth grain-size scale (Wentworth, 1922). Biogenic sediments are composed of skeletal remains of marine calcareous and siliceous microfauna and microflora, *e.g.* foraminifers, coccoliths, diatoms, and radiolarians as well as minor amounts of sponge spicules and silicoflagellates. Moreover, we found rather unconsolidated siliceous biogenic sediments (oozes).

We used a principal name, which is preceded by additional minor or major modifiers to describe the composition, texture and features of the sediments. The principal name identifies the degree of consolidation (induration) as well as the granular sediment class. Further characteristics like macro and microfossils, ichnofossils, dropstones, shell fragments, tephra layers, laminae, pyrite or iron sulfides etc. were additionally reported in the core descriptions (Appendix A.6.2).

Microscopic smear slides, sand fraction analyses, gravel petrography

Visual core description was complemented by microscopic analysis of sediment smear slides (Appendix A.6.3) and coarse fraction analyses (Appendix A.6.4) from all major lithologies found in the individual cores. Smear slides were prepared and examined under transmitted light with a Leica Laborlux 11POL petrographic microscope (100 to 630x magnification), allowing mineral determination under both plane-polarized and cross-polarized light. Smear-slide analysis of bulk sediment was undertaken to check sediment composition and for the identification of diatoms and radiolarians that bear biostratigraphic information. Where possible, maximum ages were determined from core catcher samples at the base of each core, and in some cases, samples within cores were examined to refine age determination. By combining magnetic susceptibility with shipboard diatom biostratigraphic findings, preliminary age-models for some of the recovered cores were established.

The sieve fraction > 63 µm was watched with reflected light, using a Wild-Heerbrugg Binocular at 6 – 25x magnification. The sand fraction was studied to confirm the presence of foraminifera and to look on heavy minerals as provenance indicators. At two shelf locations off *Neumayer* (PS128_4, PS128_9) and off Mac. Robertson Land (PS128_44), remains of sediment from giant box corer were sieved through 2-mm, 4-cm and 8-cm meshes on the working deck and used for the qualitative petrographic characterization of the gravel fraction (grit, pebbles, and cobbles).

Sediment sampling

On-board DNA sampling of closed core sections

To investigate the occurrence of ancient DNA in shelf proximal sediment cores, the undisturbed sediment at the bottom of each sub-section of the cores taken at stations PS128_14-1, PS128_15-3, PS128_39-1, PS128_49-2 were sampled. A total of 38 discrete sediment DNA samples was obtained. After cutting the core in 1 m segments, the sediment surface at the segment’s bottom was scraped away with a Japanese spatula to clean the sampling location.

Subsequently 5 – 10 g of the sediment were sampled with a sterile spoon into sterile Whirlpack bags. The bags were sealed carefully, placed into additional Whirlpack bags and stored at –20° C until analysis at home laboratories.

Sampling of opened cores

Further sampling was carried out on the work half and samples for bulk parameter (water content, density, contents of $CaCO_3$, C_{org}, and biogenic silica) studies were taken. The bulk parameter samples (~6–10 cm^3 in volume each) were taken with syringes and stored in pre-weighed glasses. In total, ~114 core meters were opened and sampled. Sediment cores PS128_2–3 and PS128_17–1 were completely sampled (work and archive half) at high-resolution (each cm) for immediate availability of the sample material for foraminiferal analyses at home laboratories. Core PS128_2–3 was sampled to the end of the core, while only the upper 6 m of core PS128_17–1 were sampled. Samples were stored in Whirlpack bags at 4° C until air-freight transport to Germany after the end of the expedition. Core segments, which were not opened during the expedition, were stored in a reefer container at a temperature of 4° C for transport to Bremerhaven.

Tab. 5.2.2.1: Gravity and piston core stations during PS128 along the continental margin off Dronning Maud Land and along the continental margin off Enderby and Mac. Robertson Land

Station Number	Gear [Type/ Length]	Latitude [°]	Longitude [°]	Water depth [Hydro-sweep[	Core recovery [m]	TC recovery [m]	Opened/ described
Continental Margin off Dronning Maud Land							
PS128_1-5	GC (5 m)	69°2.9‘ S	6°23.05‘ W	2674	4.86		x
PS128_1-6	GC (5 m)	69°2.83‘ S	6°22.68‘ W	2674	5.10		
PS128_2-2	GC (6 m)	69°24.69‘ S	5°35.38‘ W	1839	4.39		
PS128_2-3	GC (6 m)	69°24.64‘ S	5°35.34‘ W	1839	5.40		x
PS128_4-3	GC (3 m)	70°36.29‘ S	9°21.77‘ W	462	0.00		
PS128_4-4	GC (3 m)	70°36.26‘ S	9°21.73‘ W	462	1.78		
PS128_5-1	GC (5 m)	70°33.01‘ S	9°20.61‘ W	389	1.19		
PS128_6-1	GC (3 m)	70°30.11‘ S	8°51.88‘ W	420	0.89		
PS128_7-1	GC (3 m)	70°29.01‘ S	8°51.58‘ W	442	0.89		
PS128_8-1	GC (3 m)	70°29.12‘ S	8°53.41‘ W	442	1.33		
PS128_9-1	GC (3 m)	70°29.36‘ S	8°58.34‘ W	442	0.69		
PS128_10-1	GC (3 m)	70°27.9‘ S	8°51.27‘ W	426	0.58		
PS128_12-1	GC (5 m)	69°42.52‘ S	7°34.455‘ W	3031	4.97		
PS128_13-1	GC (10 m)	70°0.08‘ S	7°37.73‘ W	1732	5.72		
PS128_13-2	GC (20 m)	70°0.078‘ S	7°37.709‘ W	1732	8.21		
PS128_14-1	GC (15 m)	70°8.184‘ S	6°54.162‘ W	1586	12.04		x
PS128_14-2	GC (15 m)	70°8.21‘ S	6°54.12‘ W	1586	12.63		

Station Number	Gear [Type/ Length]	Latitude [°]	Longitude [°]	Water depth [Hydro-sweep[	Core recovery [m]	TC recovery [m]	Opened/ described
PS128_15-2	GC (15 m)	70°2.881‘ S	6°48.727‘ W	1876	11.90		
PS128_15-3	GC (15 m)	70°2.866‘ S	6°48.724‘ W	1876	12.31		
PS128_16-3	PC (15m)	69°54.94‘ S	6°44.59‘ W	2099	13.24	0.91	
PS128_16-4	PC (20 m)	69°54.96‘ S	6°44.57‘ W	2099	13.40	0.78	x
PS128_17-1	PC (20 m)	69°45.62‘ S	5°55.207‘ W	2268	16.11	0.96	x
PS128_17-2	PC (20 m)	69°45.522‘ S	5°54.807‘ W	2268	16.85	0.91	
PS128_19-2	PC (20 m)	68°31887‘ S	6°57.895‘ W	2918	14.41		x
PS128_19-3	PC (20 m)	68°31.877‘ S	6°58.004‘ W	2918	14.41	0.86	
PS128_20-1	PC (20 m)	69°24.687‘ S	5°35.326‘ W	1832	15.84	0.80	x
PS128_20-2	KAL	69°24.68‘ S	5°35.32‘ W	1832	10.62		x
PS128_23-1	GC (5 m)	70°27.367‘ S	9°7.225‘ W	356	0.25		
PS128_23-2	GC (3 m)	70°27.366‘ S	9°7.229‘ W	356	0.45		
PS128_24-1	GC (3 m)	70°27.548‘ S	9°8.182‘ W	358	0.00		
PS128_25-1	GC (10 m)	70°4.53‘ S	8°33.095‘ W	2619	1.83		x
Continental Margin off Enderby Land and Mac Robertson Land							
PS128_34-2	GC (15 m)	65°58520‘ S	63°24‘ E	3090	13.84		
PS128_34-3	GC (20 m)	65°58508‘ S	63°24.059‘ E	3090	13.78		x
PS128_35-1	GC (15 m)	65°53.31‘ S	63°57.41‘ E	3289	0.00		
PS128_38-2	PC (15 m)	67°8536‘ S	65°49.035‘ E	525	0.00	0.10	
PS128_39-1	PC (15 m)	67°6950‘ S	65°41.763‘ E	661	8.59	0.00	
PS128_40-2	PC (25 m)	67°10.4‘ S	65°59.81‘ E	816	23.84	1.00	
PS128_41-1	GC (5 m)	67°5.54‘ S	65°35.99‘ E	584	4.06		
PS128_42-1	GC (5 m)	67°4.065‘ S	65°29.9‘ E	581	4.07		
PS128_43-1	GC (5 m)	66°58253‘ S	65°2.91‘ E	391	2.67		
PS128_44-1	GC (5 m)	66°57.6‘ S	64°59.4‘ E	400	3.69		
PS128_45-1	GC (5 m)	66°57.16‘ S	64°51.53‘ E	357	1.29		
PS128_46-1	GC (5 m)	66°50614‘ S	63°11.294‘ E	376	2.26		
PS128_47-1	GC (5 m)	66°49.71‘ S	63°12.48‘ E	390	3.29		
PS128_49-2	GC (15 m)	66°24.052‘ S	61°13.027‘ E	2193	6.08		x
PS128_53-1	GC (15 m)	66°15.418‘ S	48°46.662‘ E	1072	9.17		
PS128_54-1	GC (15 m)	65°7.979‘ S	58°55.979‘ E	3457	13		
PS128_54-2	GC (20 m)	65°7.976‘ S	58°55.108‘ E	3457	13.66		x
PS128_55-2	GC (15 m)	65°7.603‘ S	59°22.856‘ E	3770	1.36		
PS128_57-1	GC (15 m)	64°32.805‘ S	59°10.233‘ E	3864	7		x

5.2.3 Multisensor core logging and physical properties measurements

Work at sea

Multi Sensor Core Logging (MSCL) was performed as a first non-destructive measurement on all obtained sediment cores. These measurements were used to compare and correlate cores within the same work areas, or to established reference records. Major lithological changes can usually be already seen in logging data and provide information on variations in terrigenous or biogenic (mostly biogenic opal, or carbonate) sediment components. Furthermore, sound velocity and density measurements could be used to calculate synthetic seismograms, which can be compared to sub-bottom profiling data obtained with the ATLAS PARASOUND sediment echo sounder (Chapter 4.2) or with air-gun reflection seismics (Chapter 4.1) during the cruise. Subsequently, these results enable the calculation of key parameters *e.g.* the true sediment thickness and distribution around coring locations and for core-to-core correlations as well.

At sea, we measured the following parameters on whole-round core sections: magnetic susceptibility, sound velocity of the pressure wave (vP), and the gamma ray attenuation density, later calibrated as wet bulk density (WBD). Physical properties of the sediments expressed as wet bulk density, p-wave velocity and magnetic susceptibility were measured on all collected sediment cores using a GEOTEK multi-sensor core logger (MSCL). In addition, core diameter and ambient temperature were measured for data processing. The parameters listed in the logger settings of the MSCL software (version 6) and given in Table 5.2.3.1 were used for calibration that was conducted after the Geotek MSCL manual and after Gunn & Best (1998) and Best & Gunn (1999). An AWI MSCL device was used for continuous whole-round core section measurements with a 1 cm resolution. All physical property data were qualitatively controlled on board, and faulty values, *e.g.* at core section boundaries, were flagged in output files. In order to obtain true volume corrected $\varkappa$ (Kappa) magnetic susceptibility in (10^{-6} SI-units) values, the processed magnetic susceptibility sensor data were processed drift and volume corrected and multiplied by the correction factor (Tab. 5.2.3.1).

To verify the MSCL measurements, individual sediment samples were taken from all opened cores with 10 cubic centimetre plastic syringes at 10 cm sample spacing for physical property measurements (water content, sediment density) and further geochemical, sedimentological and mineralogical investigations. To calculate sediment fluxes and mass accumulation rates of specific compounds, the water content and the sediment density will be measured on individual samples taken from the cores that were opened during the cruise. Onshore at AWI, all individual physical properties samples shall be weighed, freeze-dried and milled. Water content, bulk-, grain-, wet-, and dry-bulk-densities, and the porosity shall be determined.

Initial, uncorrected magnetic susceptibility values were used to check core-to-core consistency on stations with double coring. In general, all double-cored stations showed close correlation patterns and high consistency throughout their individual susceptibility patterns (Fig. 5.2.3.1), thus allowing for shipboard opening and complete sampling of one of two respective cores (PS128_2-3 and -4), while the respective other core remained unopened.

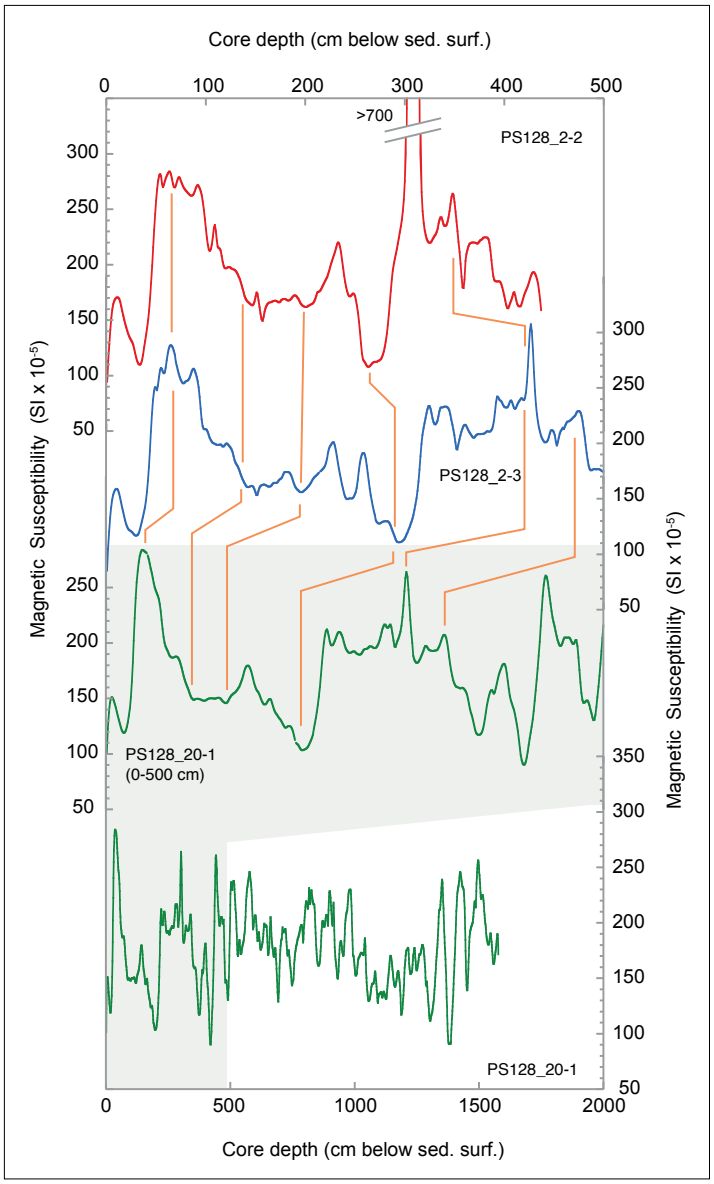

Fig. 5.2.3.1: Downcore changes in magnetic susceptibility (κ, 10-6 SI-units of gravity cores PS128_2-2 (red), PS128_2-3 (blue), and piston core PS128_20-1 from slightly different water depth (green, upper curve, excerpt of upper 5 m), all taken at the same geographical location; tentative correlation lines drawn in orange

Magnetic susceptibility correlation, however showed depth offsets between double cores in correlation patterns, usually restricted to 10 – 20 cm, but at times increasing with core depth to up to 80 – 100 cm. Reasons for these discrepancies can be assigned to system-inherent differences between gravity and piston coring, with the former usually leading to compressed sediment sections, dependent on the sedimentary facies and its water content and compressibility. We also observed smaller offsets between two gravity core deployments on a number of double coring stations. These offsets are harder to explain but are most likely related to differences in penetration speed on the seafloor through combined winch speed, heave, etc. variations. In some cases, high depth differences occurred, e.g. in PS128_16-3 vs. -4, with offsets reaching nearly 200 cm (Fig. 5.2.3.2). In these cases, different piston settings on 15 m vs. 20 m corer setup may have contributed to the features.

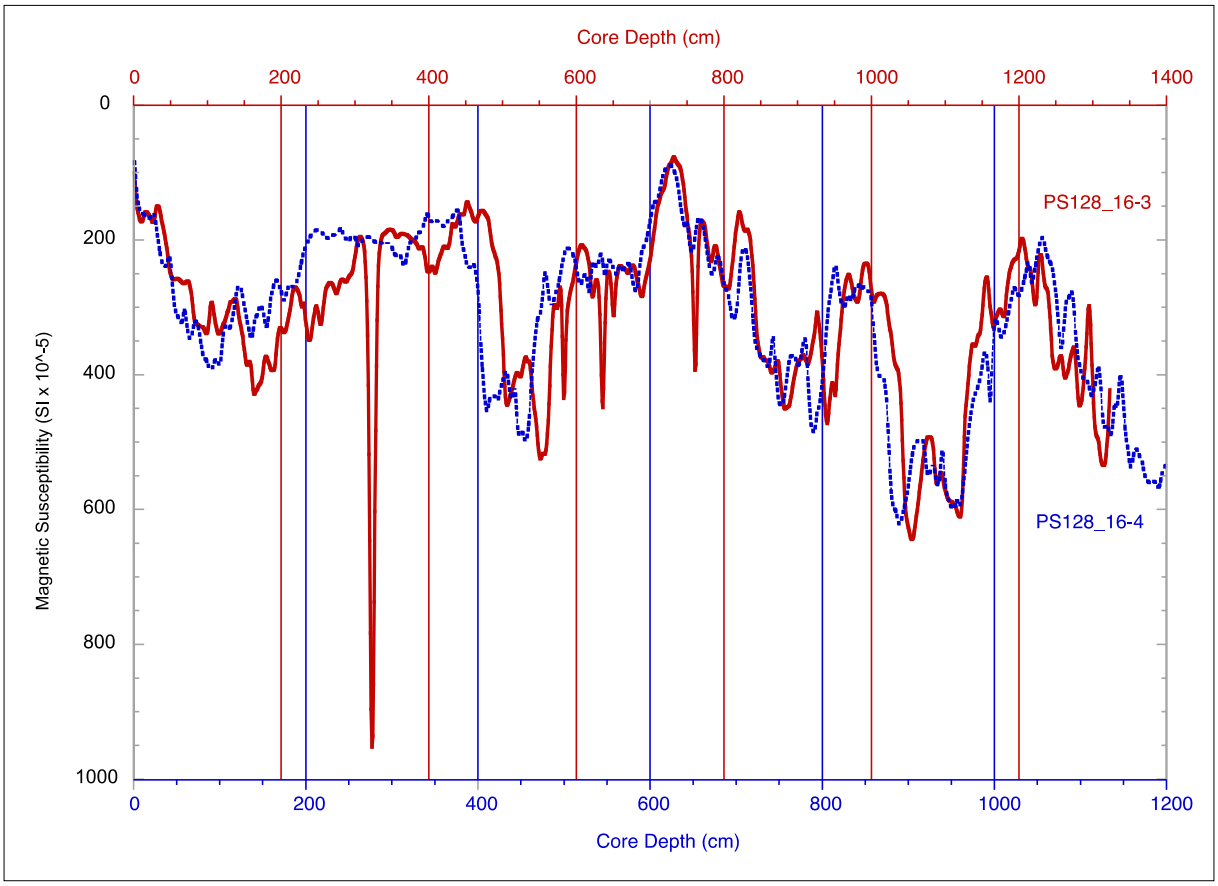

Fig. 5.2.3.2: Comparison of downcore changes in magnetic susceptibility (κ, 10-6 SI-units) between two piston cores retrieved from same location PS128_16-3 PC15 (red) and PS128_16-4 PC20 (blue); note the different core depths on upper (PS128_16-3) vs. lower x-axis (PS128_16-4) to increase visual alignment between both cores. The depth offset remains relatively constant but is significant, on average 150-180 cm, while both cores yielded nearly similar recoveries of 1,324 cm (PS128_16-3) and 1,340 cm (PS128_16-4), respectively.

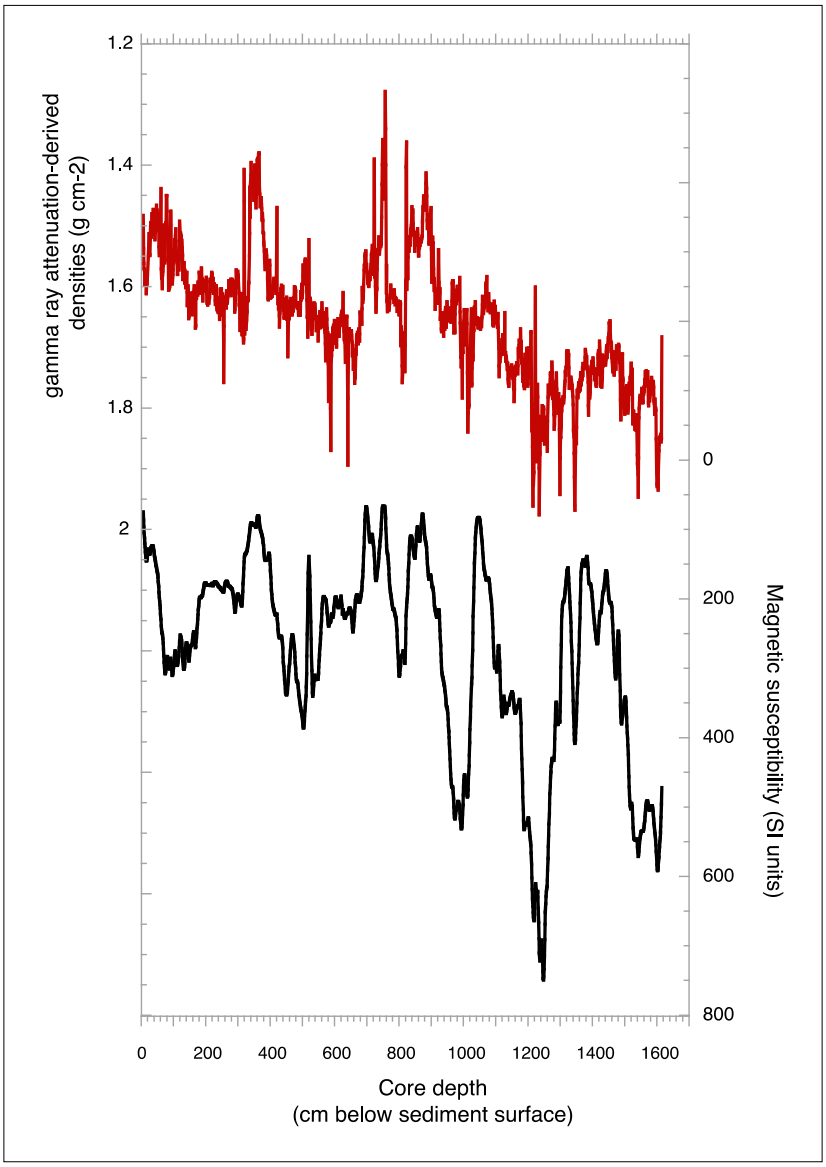

Fig. 5.2.3.3: Example of measured basic parameters on sediment core PS128_17-1; from top to bottom: Gamma Ray Attenuation (GRA)-derived wet bulk density, magnetic susceptibility

Tab. 5.2.3.1: Sensors and parameter settings for measurements with the GEOTEK multi-sensor core logger during PS128

P-wave velocity and core diameter plate-transducers diameter: 4 cm transmitter pulse frequency: 500 kHz pulse repetition rate: 1 kHz recorded pulse resolution: 50 ns gate: 900 µs delay: 10 µs P-wave travel time offset: 21.72 µs (PC125, 125 cm outer diam., 2*3.7 mm liner thickness) P-wave travel time offset: 21.72 µs (GC125, 125 cm outer diam., 2*2.5 mm liner thickness) temperature = 20 °C, salinity = 35 psu, not corrected for water depth and in situ temperature; calibrated with water core of known temperature and theoretical sound velocity.
Temperature bimetal sensor, calibrated with Hg-thermometer
Density gamma ray source: Cs-137; activity: 370 MBq, Serial No. 0874/13 aperture diameter: 5.0 mm (PC and GC) gamma ray detector: Gammasearch2, Serial no. DET S1AA5480; count time 10 s Gamma ray attenuation measurement and density calculation with equation type $y=Ax^2+Bx+C$, (Coefficients A, B, and C determined with measurements on calibration cores.
Fractional porosity Mineral grain density = 2.65, water density = 1.026
Magnetic susceptibility (MS) coil sensors: BARTINGTON MS-3, Ser. Nr. 0582, and Ser. Nr. SN716 (coil sensor) nominal inner coil diameter: 14 cm coil diameter: 14.8 cm (factors B, Den and LD were deactivated in the GEOTEK processing software). alternating field frequency: 565 Hz, count time 10 s, precision $0.1 * 10^{-5}$ (SI) magnetic field strength: ca. 80 A/m RMS Krel: 1.73 (PC, 11.76 core-ø); 1.56 (GC, 12 cm core-ø) coil sensor MS volume ($\varkappa$) correction factor for 10^{-6} (SI): 5.778 (PC125); 5.4378 (GC125)
Core thickness measurement Penny + Giles, Type HLP 190, calibrated with distance pieces

5.3 Preliminary (expected) results

5.3.1 Continental Margin off Dronning Maud Land

Paleoceanography

The working area between the Antarctic continental margin and the Bungenstock Plateau extends from ~68.5°S to ~70.6°S, and 4°W to 10°W (Fig. 5.3.1.1) and includes the Antarctic continental shelf and margin off Dronning Maud Land, Bungenstock Plateau itself and areas further offshore. Within this area, 6 gravity cores (GC), 4 piston cores (PC), and 1 Kasten core (KAL) were recovered from a large range of water depths between ~1,550 and ~3,060 m. At most of these stations, surface sediments were additionally collected with the MUC. The sampling stations, the gear types and the lengths of the coring devices were chosen based on sediment acoustic profiles with the PARASOUND echo-sounding system.

Coring operations in the Bungenstock Plateau area focused on the recovery of sedimentary records spanning late Pleistocene glacial-interglacial cycles and high-resolution Holocene sequences. In the following, we subdivide the working area in i) the Outer Bungenstock Plateau comprising sediment coring stations PS128_20, _2, _1, and _19; ii) the Eastern Bungenstock Slope Area comprising sediment coring stations PS128_14, _15, _16, and _17; iii) the Western Bungenstock Channel comprising sediment coring stations PS128_12 and _13; and iv) the continental shelf off *Neumayer* (Fig. 5.3.1.1). In parts, double coring was accomplished.

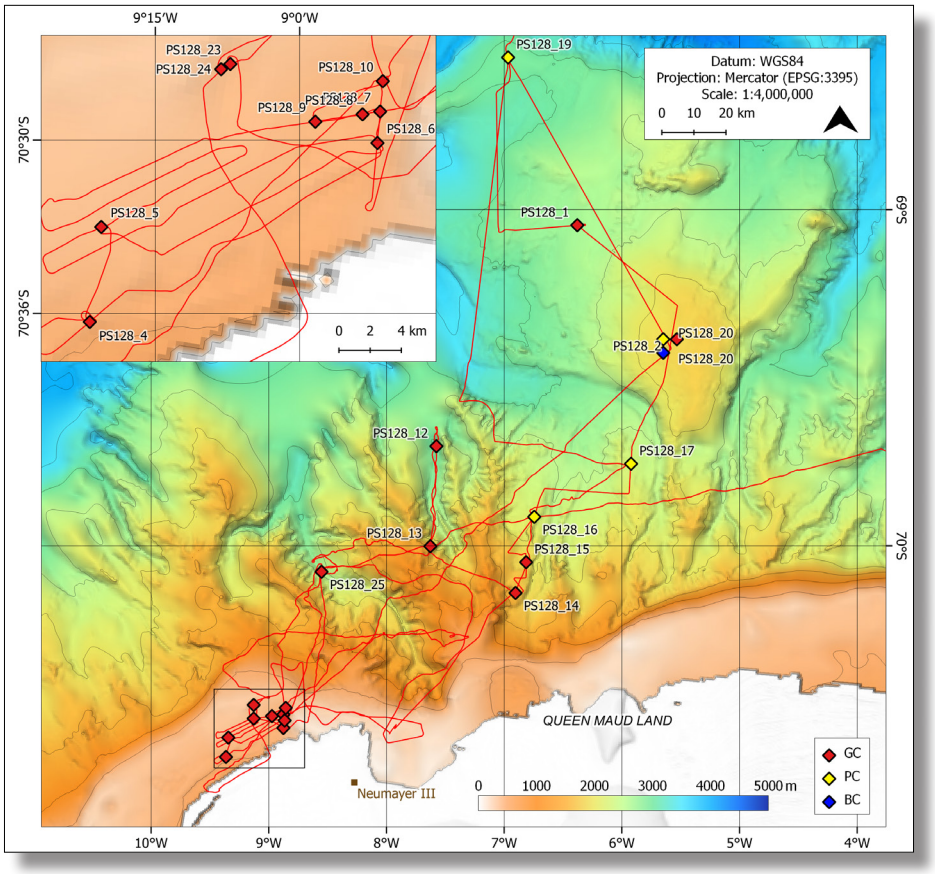

Fig. 5.3.1.1: Overview of GC, PC and KAL coring sites in the Bungenstock Plateau area, subdivided into the Outer Bungenstock Plateau, the Eastern Bungenstock Slope Area and the Western Bungenstock Channel. The insert shows GC stations on the continental shelf off Neumayer.

Outer Bungenstock Plateau

At Outer Bungenstock Plateau, four gravity cores (PS128_1-5, 2,674 m water depth, 4.86 m recovery; PS128_1-6, 2674 m water depth, 5.10 m recovery; PS128_2-2, 1,839 m water depth, 4.39 m recovery; PS128_2-3, 1,839 m water depth, 5.4 m recovery), 3 piston cores (PS128_20-1, 1,832 m water depth, 15.84 m recovery; PS128_19-2, 2,918 m water depth, 14.41 m recovery; PS128_19-3, 2,918 m water depth, 14.41 m recovery), and 1 Kasten corer (PS128_20-2, 1,832 m water depth, 10.62 m recovery) were successfully recovered from a NW-SE-oriented depth transect covering water depths from ~3,000 m to ~1,700 m. In the following we refer to those cores, which were opened, described, photographed, and logged with the MSCL system during the expedition.

Sediment core PS128_19-2 was taken at 2,918 m water depth from the outer rim of the Bungenstock Plateau. It consists of grayish to olive lithogenic mud with variable amounts of foraminifera and very few silica remains. It is faintly layered moderately bioturbated and includes dispersed clasts, with occasional sandy layers. Foraminifera occur as intact specimens and as calcareous detritus in the ground mass of the sediment. Fluctuations in magnetic susceptibility follow carbonate concentrations and grain-size variations, with coarse grain size of siliciclastic silt and higher carbonate concentrations in intervals of low magnetic susceptibility (Appendix A.6.2).

Sediment core PS128_1-6 was recovered from 2,674 m water depth (Figs. 5.3.1.1 and 5.3.1.2). The ~5 m long sequence comprises a variety of sediment types, with typically light greenish gray to light olive gray clayey silt with abundant sand in the uppermost and lowermost sections (Appendix A.6.2). The sand component is from either fine lithogenic sand and/or planktic foraminifers. The magnetic susceptibility is low. The middle part of the core consists of clearly darker sediment, ranging between silty clay and clayey silt with varying colors, grain sizes and magnetic susceptibilities. Dropstones are rather common.

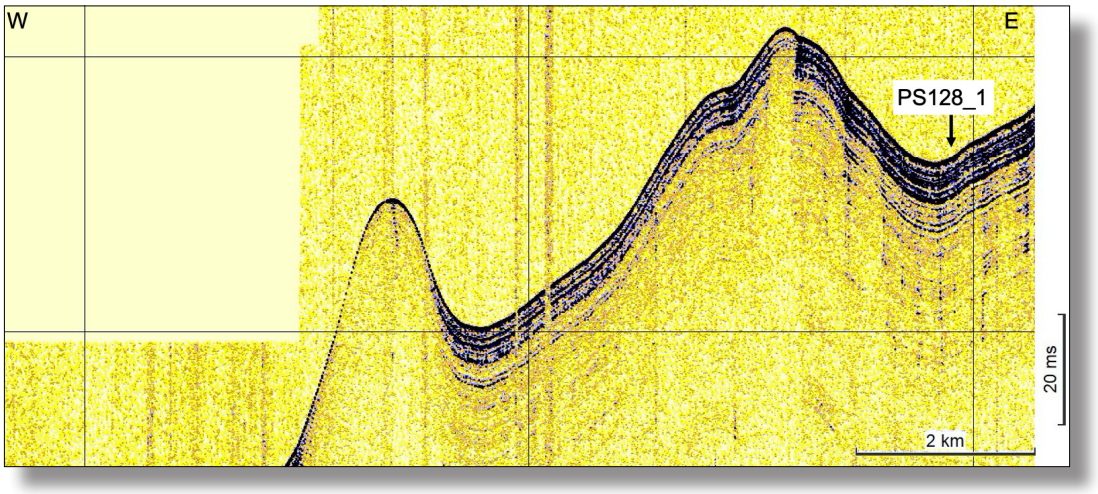

Fig. 5.3.1.2: Sediment acoustic profile of the deeper NW Bungenstock Plateau with coring site PS128_1 at ~2,670 m water depth

Sediment core PS128_2-2 is from 1,839 m water depth (Figs. 5.3.1.1 and 5.3.1.3). The ~4.4 m long core contains sedimentary sequences which are rather similar to those described in core PS128-1-6: light greenish gray to light olive gray clayey silt with abundant sand and foraminifers but low magnetic susceptibility values change to dark and very dark gray, clearly finer, less sandy, less bioturbated silty clays and clays (Appendix A.6.2). Large parts of the core are of sediments transitional between both types.

Sediment core PS128_20-1 from 1,832 m water depth is with 15.84 m the longest record and the shallowest of the transect (Figs. 5.3.1.1 and 5.3.1.3). It consists of many lithological changes, with main lithologies resembling those of the deeper cores (Appendix A.6.2). Low magnetic susceptibilities accompany light greenish gray, partly brownish to light olive gray clayey silt, which contains abundant sand and foraminifers. High magnetic susceptibilities are paralleled by mostly dark to very dark gray silty clays and clays, being clearly finer, less sandy, and less bioturbated. Foraminifers are rare to absent. Similar as in core PS128_2-2, large parts of the core are of transitional sediments of medium magnetic susceptibilities.

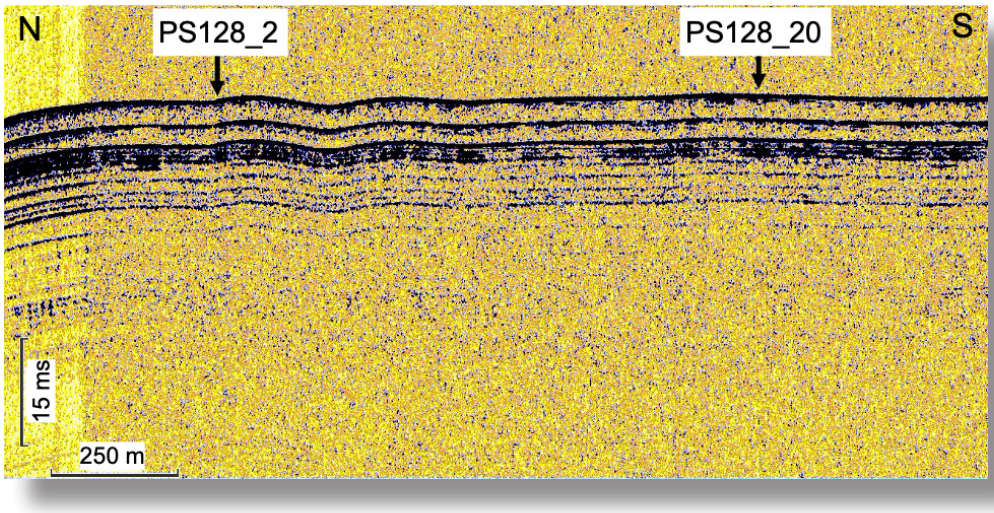

Fig. 5.3.1.3: North-south oriented sediment acoustic profile of the summit of Bungenstock Plateau. Coring locations PS128_2 and PS128_20 at ~1830 m are in well-stratified sediments.

Figure 5.3.1.4 shows a tentative correlation of magnetic susceptibility records of cores from the outer Bungenstock Plateau, thereby taking into account the lithological information derived from the visual inspection of cores PS128_20-1, 2-2, 1-6, and 19-3. Exemplarily in core PS128-20-1, three major facies types were differentiated (Appendix A.6.2). The greenish shadings in Figure 5.3.1.4 mark the light greenish gray, partly brownish to light olive gray clayey silt sequences, the high planktonic foraminifer and diatom abundances of which point to enhanced marine productivity. The common bioturbation and brownish colour shading implies well-oxygenated bottom waters. Such conditions likely persisted during warm (interglacial and interstadial) periods.

The second facies-type comprises mostly dark to very dark gray silty clays and clays, being clearly finer, less sandy, and rarely bioturbated. Although surprisingly low in absolute values, the enhanced magnetic susceptibilities (Fig. 5.3.1.4) point to less dilution by biogenic components rather than higher lithogenic supply. Ice-rafted debris (IRD) is mostly absent. We hypothesise that environmental conditions were rather cool, with a persistent and perennial sea ice cover at Bungenstock Plateau, and strongly reduced marine productivity. Both facies-types describe most extreme environmental and climatic conditions. The transitional third facies-type, instead, predominates with intermediate magnetic susceptibilities, varying grainsizes, abundant IRD, and common bioturbation, suggesting intermediate climate condition with varying sea ice coverage.

Although the different facies-types were also observed in the deeper and further offshore-cores, the correlation of magnetic susceptibility records is not yet straight-forward. Further stratigraphical work is needed.

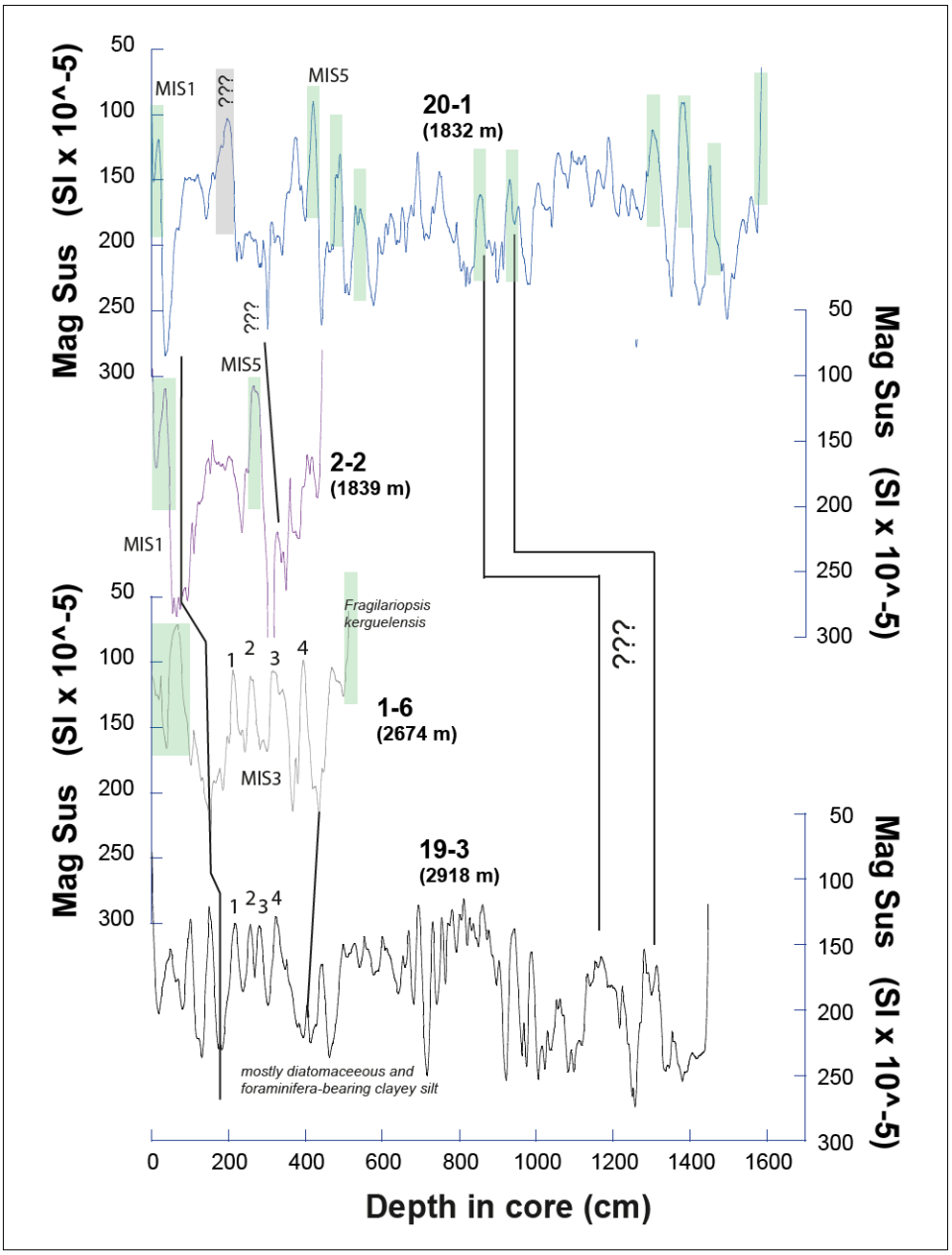

Fig. 5.3.1.4: Tentative correlation of magnetic susceptibility records from the outer Bungenstock Plateau area, from shallow (top: PS128_20-1) to greater depth (bottom: PS128_19-3); green shading indicates relatively warmer climate condition (Facies-type 1).

Eastern Bungenstock Slope Area

In the Eastern Bungenstock Slope area, 7 gravity cores (PS128_12-1, 3,031 m water depth, 4.97 m recovery; PS128_13-1, 1,732 m water depth, 5.72 m recovery; PS128_13-2, 1,732 m water depth, 8.21 m recovery; PS128_14-1, 1,586 m water depth, 12.04 m recovery; PS128_14-2, 1,586 m water depth, 12.63 m recovery; PS128_15-2, 1,876 m water depth, 11.90 m recovery; PS128_15-3, 1,76 m water depth, 12.31 m recovery), and 4 piston cores (PS128_16-3, 2,099 m water depth, 13.24 m recovery; PS128_16-4, 2,099 m water depth, 13.40 m recovery; PS128_17-1, 2,268 m water depth, 16.11 m recovery; PS128_17-2, 2,268 m water depth, 16.85 m recovery) were successfully recovered from a NNE-SSW-oriented

depth transect across the Antarctic continental slope covering water depths from ~3,070 m to ~1,550 m (Fig. 5.3.1.1). In the following we refer to those cores, which were opened, described, photographed, and logged onboard during the expedition.

Sediment core PS128-17-1 was taken at ~2,268 m water depth from a ridge south of the Bungenstock Plateau, situated ~75 km offshore the coast (Fig. 5.3.1.1). It includes grayish lithogenic mud with variable amounts of diatoms and very low amounts of foraminifera. Fluctuations in magnetic susceptibility follow variations in the presence of biosiliceous remains (diatoms, radiolarians, sponge spicules) and grain-size variations, with low magnetic susceptibility values related to silica-rich intervals with coarser grain sizes of siliciclastic silt (Appendix A.6.2). Variations in colour are not clearly related to lithological variations. Diatom-rich intervals show weakly expressed layering. Dispersed microclasts with occasional ice-rafted debris (IRD) appear occasionally. Two important features are two erosive contacts at 849 cm and at 1,336 cm core depth, respectively, and the almost absence of biosiliceous remains below 914 cm.

Sediment core PS128_16-4 has been taken at ~2,099 m water depth (Fig. 5.3.1.5). Its lithology is similar to that found in Bungenstock summit core PS128_20-1. Also, the shallower cores PS128_15-3 and core PS128_14-1 from 1,876 m and 1,586 m water depth, respectively, reveal the facies-types 1-3 defined in the area (Fig. 5.3.1.5). Light greenish gray, partly brownish to light olive gray clayey silt with abundant sand and foraminifers (Facies-type 1) differ clearly from the dark to very dark gray fine-grained silty clays and clays of Facies-type 2. Large parts of the cores are from transitional sediments of medium magnetic susceptibilities, varying grain sizes and colours (Facies-type 3).

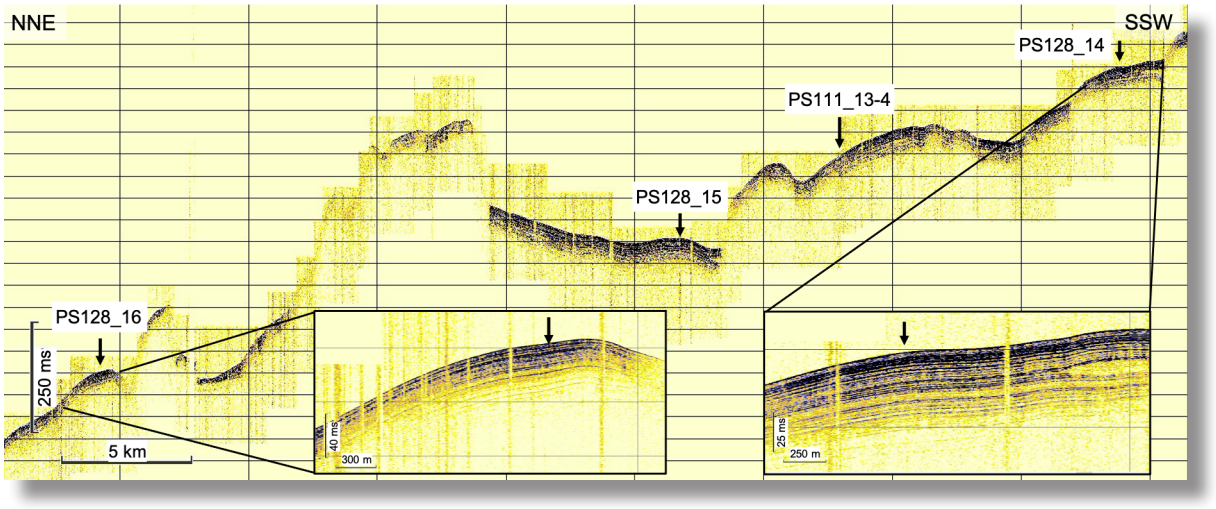

Fig. 5.3.1.5: Sediment acoustic profile of the Eastern Bungenstock Slope area (c.f. Fig. 5.3.1.1 station map). The coring locations PS128_14 (~1,580 m water depth), _13 (~1,730 m), _15 (~1,880 m) to _16 (2,100 m) from SSW to NNE reveal highly penetrating PARASOUND signals and well-stratified sediments. Belonging core PS128_17 (2,270 m) is not shown.

Figure 5.3.1.6 shows a preliminary core correlation across the Eastern Bungenstock Slope area, based on magnetic susceptibility records and the lithological information derived from the visual inspection of cores PS128_14-1, 15-3, 16-4, and 17-1. Notably, the amplitude range of the magnetic susceptibility records in this area are much more pronounced (~50-max.700 Si *10-5) than further offshore (~50- max. 300 Si *10-5).

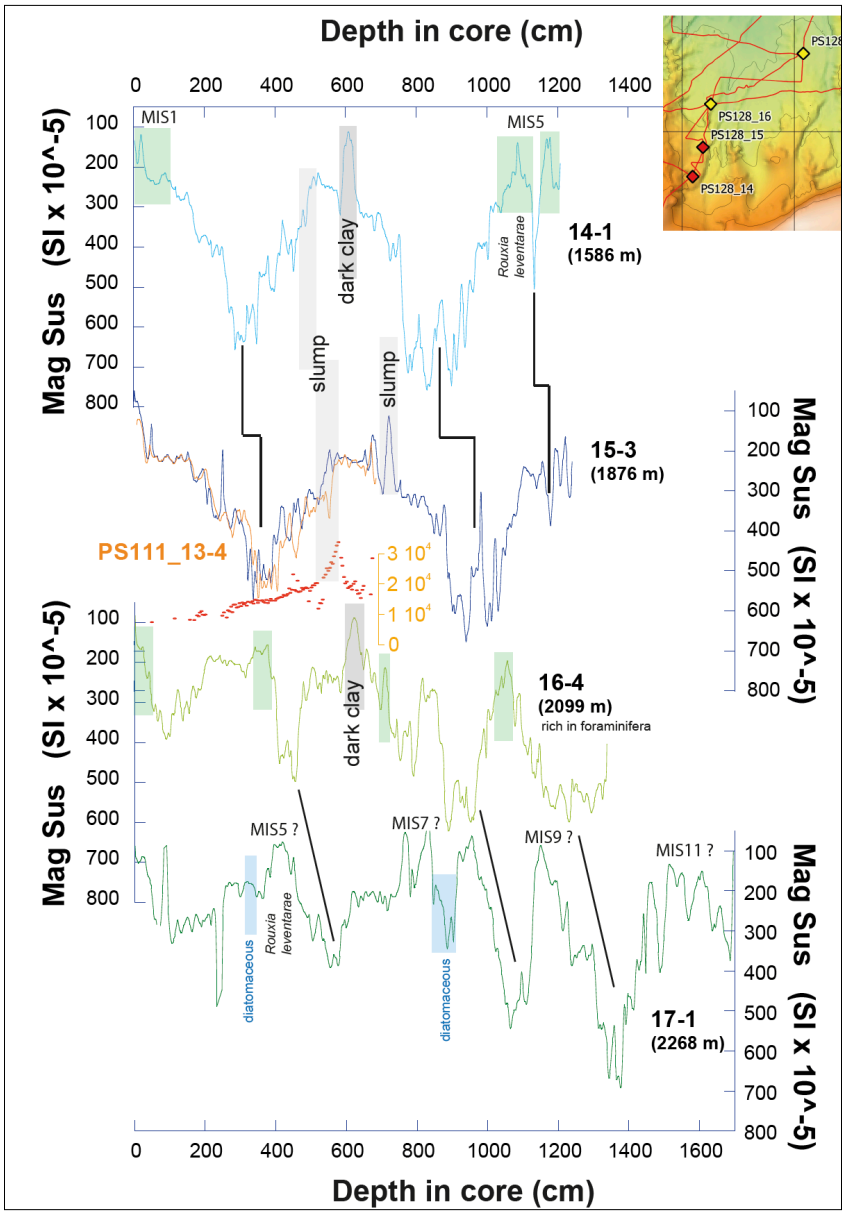

Fig. 5.3.1.6: Tentative correlation of magnetic susceptibility records from the Eastern Bungenstock Slope area, from shallow (top: PS128_14-1) to greater depth (bottom: PS128_17-1); orange = magnetic susceptibility (unpublished; Müller et al.) and radiocarbon datings (unpublished; Tiedemann, Mollenhauer et al.; y-scale in ^{14}C years BP) of closeby reference core PS111_13-4; green shading = relatively warmer climate condition (Facies-type 1); light gray shading = slumping structures identified in cores PS128_14-1 and 15-3 (c.f. lithologs in Appendix); dark gray shading = distinct layer of dark gray to black clay, low in magnetic susceptibility; blue shading = diatomaceous mud

The magnetic susceptibility records of the deep cores PS128_16-4 and 17-1 seem to be correlative, showing clear facies changes likely related to glacial/interglacial cycles over the last 9 respectively 11 marine isotope stages, and increasing sedimentation rates downslope. The correlation towards the shallow cores is still unclear. Notably, however, is the nearly one-by-one correlation of the core PS128_15-3 magnetic susceptibility record to that of adjacent reference core PS111_13-4. Also, the core PS128_16-4 magnetic susceptibility pattern is rather similar to the previously mentioned cores. The slump structures described in core PS128_15-3 and also in core PS128_14-1 may help to understand the radiocarbon-dating age reversal described in core PS111_13-4 (Tiedemann, Mollenhauer et al., unpublished data; Fig. 5.3.1.6).

Western Bungenstock Channel

In the Western Bungenstock Channel we recovered four gravity cores with the intention to reach pre-Quaternary Cenozoic sediments (Fig. 5.3.1.1.): core PS128_12-1 from 3,031 m water depth with a recovery of 4.97 m; cores PS128_13-1 and PS128_13-2 from 1,732 m water depth with a recovery of 5.72 m and 8.21 m, respectively; and core PS128_25-1 from 2,619 m water depth with a recovery of 1.83 m.

The shallow sediment core PS128_13-1 from 1,732 m water depth from the upper channel area exhibits a magnetic susceptibility record, which closely matches the core PS128_14-1 record further to the east from a similar water depth (Fig. 5.3.1.7). We therefore assume that sediment core PS128_13-1 reveals the same succession of sedimentary facies already described above, and likely includes interglacial/glacial changes. Sediment cores PS128_12-1 from 3,031 m water and PS128_25-1 from 2,619 m water depth are different, showing similar cyclic variations in magnetic susceptibility, and large excursions to high values of ~600 (Si * 10^{-5}) (which may be due to dropstones; Fig. 5.3.1.7). The sediments of both records likely contain Quaternary strata only.

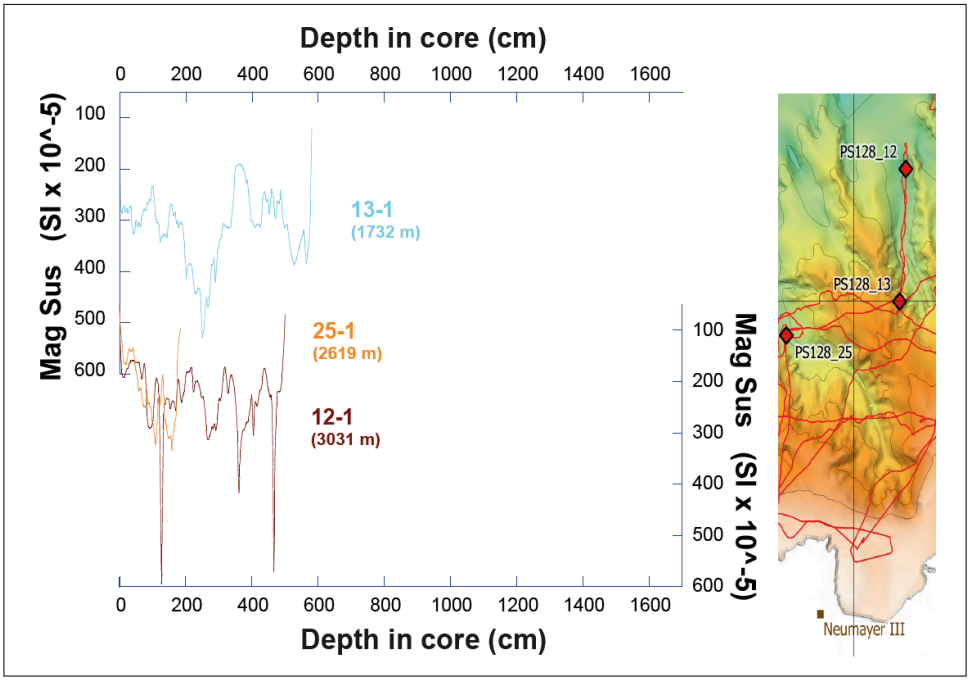

Fig. 5.3.1.7: Magnetic susceptibility records from the Western Bungenstock Channel, from shallow (top: PS128_13-1; ~1,730 m water depth) to deep (bottom: PS128_25-1; ~2,620 m water depth [orange]; PS128_12-1; ~3,030 m water depth [brown]

Paleoglaciology

A part of the PS128 marine geological program focused on investigating the narrow continental shelf offshore the Ekström Ice Shelf (EIS) to improve our understanding of past ice shelf and ice sheet processes. The seafloor beneath this ice shelf is recently under investigation for exploring its potential for future deep geological drilling (Kuhn & Gaedicke, 2014). So far, however, no reliable data exist for characterizing the extent of the East Antarctic Ice Sheet (EAIS) during past glacial maxima (Mackintosh et al., 2014), when an ice stream presumably flowed across the continental shelf reaching outer shelf areas (Smith et al., 2019; Oetting et al., 2022). This knowledge is not only necessary for defining the size of the EAIS during its past

maximum extent (Mackintosh et al., 2014) but also for constraining rates and extent of past glacial erosion that affected the completeness of geological strata present beneath EIS (see Fig. 2 in Smith et al., 2019).

During cruise PS128, we complemented already available bathymetric data (Oetting et al., 2022) between the present ice shelf edge and the continental shelf break (inset in Fig. 5.3.1.1). We were able to reveal the extension of subglacial features indicating fast flowing ice farther onto the outer continental shelf (also referred to as mega-scale glacial lineations or MSGLs). Here they get increasingly obliterated by iceberg scours but still indicate a minimum limit for grounded ice cover during its past maximum extent. In order to define a reliable time constraint for past ice-sheet coverage on this outer portion of the continental shelf offshore the EIS, we recovered two gravity cores and one giant box core from the cluster of MSGLs (PS128_4 & _ 5). On synchronously collected sediment echography data, a clear and shallow sub-bottom reflector was identified, which indicates the surface of a subglacial till, i.e., the surface of the MSGLs, that was likely penetrated by the cores. Further, a field of recessional moraines described at the eastern margin of the glacial trough (Oetting et al., 2022) was surveyed more comprehensively during our cruise to recover four more gravity cores from both their crests and the seafloor just seawards (inset in Fig. 5.3.1.1; PS128_6, _7 & _10). If those cores comprise the moraine diamicton, we hope to constrain a reliable minimum age for grounding-line retreat from that field of moraines as well. Together, those data will not only add to the yet sparse knowledge of the Last Glacial Maximum (LGM; ~26–19 calibrated kiloyears before the present) grounding-line extent along the East Antarctic margin (RAISED Consortium, 2014) but will also help characterizing past and present EIS environments for assessing its potential for a future deep drilling campaign.

Micropaleontology

Biosiliceous components

Generally, siliceous shells produced by diatoms and radiolarians found in cores from the Bungenstock plateau were poorly preserved. Remains from these two plankton groups were often absent from smear slides. When diatoms were preserved enough to estimate the assemblage, *Fragilariopsis kerguelensis* (usually most abundant near the Antarctic Polar Front (APF), *Eucampia antarctica* var. *recta* (Antarctic coastal species) and *Thalassiosira lentiginosa* (Permanent Open Ocean Zone (POOZ)) usually dominated (Fig. 5.3.1.8 a-c). For radiolarians, species from the *Antarctissa* genus (abundant south of the APF) and *Siphocampe arachnea* (cold environment species) were most often observed (Fig. 5.3.1.9 a-c). Radiolarians and diatoms were most abundant at the top of each core (*e.g.*, PS128_13-2; PS128_16-4; PS128_17-1).

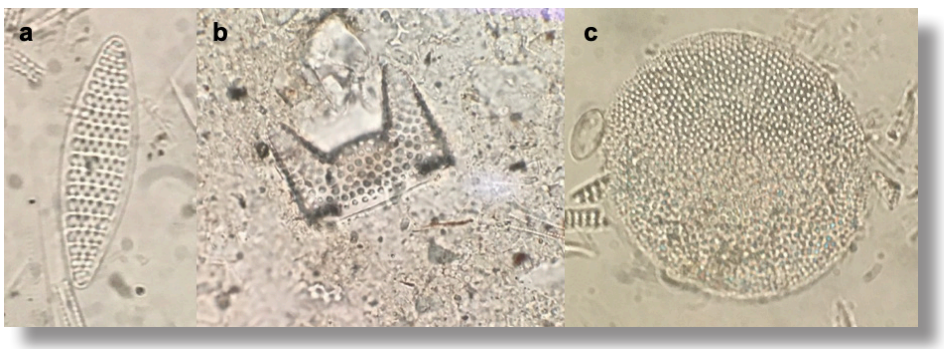

Fig. 5.3.1.8: Pictures of dominant diatom species in PS128 sediment cores a: Fragilariopsis kerguelensis; b: Eucampia antarctica; c: Thalassiosira lentiginosa.

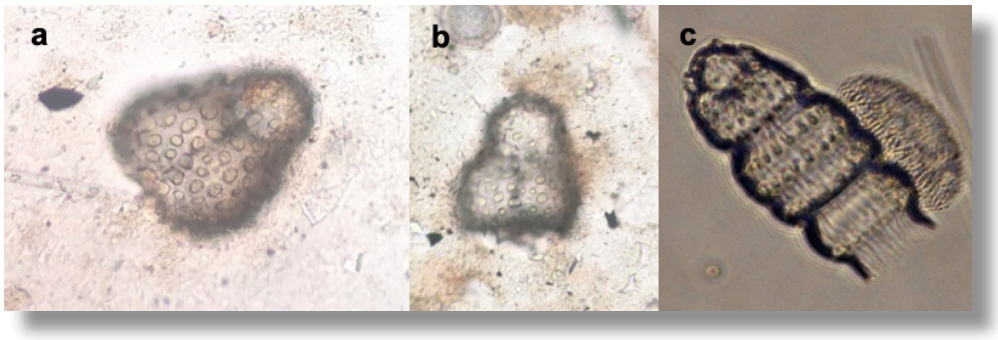

Fig. 5.3.1.9: Pictures of dominant radiolarian species in PS128 sediment cores a: Antarctissa denticulata; b: Antarctissa strelkovi; c: Siphocampe arachnea; photos A and B were taken on board. Photo C is a personal picture taken by M. Civel-Mazens.

Biogenic Calcite Components

Previous investigations of deep-sea cores form the Bungenstock Plateau have already shown that this region – opposite to the eastern study area of the expedition where silicious deposition of microfossils prevails - yields sedimentary records with relatively high abundance of calcitic microfossils. While the stratigraphy of the new cores from this area still needs to be assessed using stable C and O isotopes as well as other means the calcite assemblages in the sand-size fraction larger 63 µm is dominated by the polar planktic foraminifer *Neogloboquadrina pachyderma* with little variations in the coiling directions, i.e., of the right-coiled variant *N. incompta*. Especially in the most northern core PS128_19-3, samples from the base of the core reveal a rich fossil content of *N. pachyderma* with few or none benthic foraminifers and clastic material such as ice-rafted debris (Fig. 5.3.1.10)

It is noteworthy that all foraminifers are whitish in colour which is a definite sign for enhanced calcite dissolution due to corrosive bottom waters. It also may further indicate that sedimentation rates were relatively low at this site, which lead to a longer exposure of the shells on the seafloor surface before further burial.

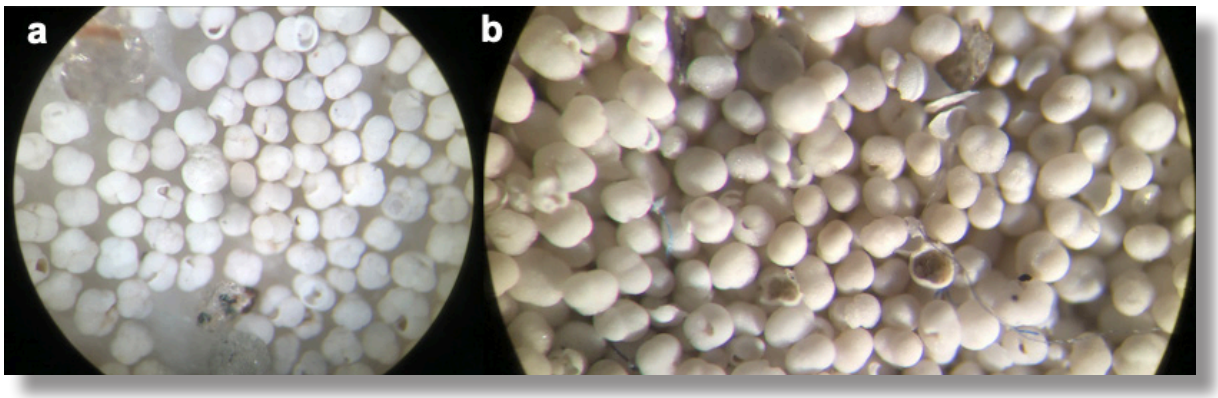

Fig. 5.3.1.10: View through a binocular microscope showing planktic foraminifer N. pachyderma in the top (A) and the base (B) of the core catcher of core PS128_19-3.

By comparison to the northern Bungenstock Plateau, where PS128_19-3 is located, sites at the southern end of the plateau yield a somewhat richer foraminiferal fauna. Near the base of core PS128_17-2, which is also dominated by *N. pachyderma* among the planktic assemblage, there were few rather small-sized specimens that appear to be *Globigerina bulloides*. These latter species might indicate an influence of the eastern flank of the Weddell Gyre bringing

warmer waters from the north nearer to the shelf margin. The benthic foraminiferal assemblage in PS128_17-2 is comprised of a number of species, among them *Cibicides* sp., *Oridorsalis umbonatus*, and *Pyrgo* sp. (Fig. 5.3.1.11). Besides these, there are several species of ostracodes altogether implying that the sample shown in Figure 5.3.1.11 reflects well ventilated bottom waters and sufficient surface water bioproductivity. The latter assumption may be additionally corroborated by the enhanced number of ice-rafted material of various types, which could be a sign of more open-water, interglacial conditions.

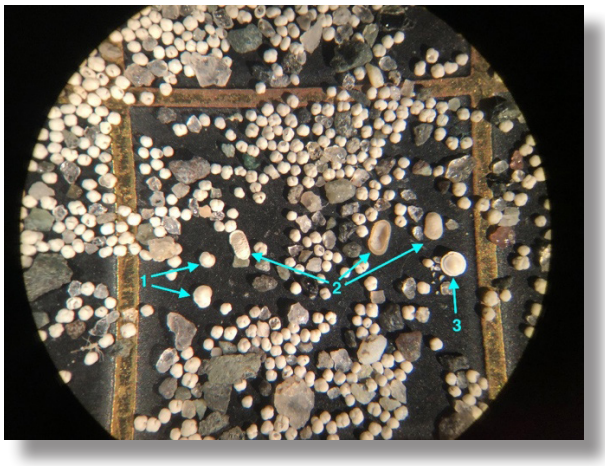

Fig. 5.3.1.11: Sand-size fraction of the bottom of core PS128_17-2 from south of Bungenstock Plateau showing species of Cibicides sp. (1), ostracodes (2) and Pyrgo sp. (3)

Provenance of terrigenous sediment fraction

Though no systematic quantification has been undertaken, visual inspection of lithogenic sand grains in smear slides and sieved samples under the microscope as well as the isolation of clasts >2 mm from samples of giant box corer PS128_4-2 point to different sources of sediment supply in the study area. Black sands with abundant augite in the heavy-mineral fraction as well as mafic clasts (Fig. 5.3.1.12) from marine sediments offshore *Neumayer* and on the Bungenstock Plateau point to nearby sediment sources from Proterozoic mafic intrusives and volcanics as well as Jurassic tholeiitic volcanics of western Dronning Maud Land (Diekmann & Kuhn, 1999). Reworking of older marine sedimentary rocks might have contributed to the terrigenous sediment fraction of sediment core PS128_23-2 from the shelf area off *Neumayer,* which yielded small glaucony pellets in the core catcher at 45 cm sediment depth (Fig. 5.3.1.13).

Fig. 5.3.1.12: Clasts sieved from giant box corer PS128_4-2; mafic massive and porphyric rock fragments of volcanic origin characterise the sample from the shelf off Neumayer.

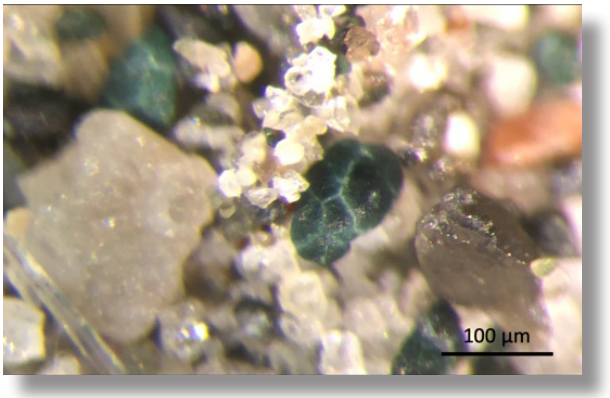

Fig. 5.3.1.13: Sieve sample from sediment core PS128_23-2, taken on the shelf off Neumayer; in addition to quartz, feldspar, and biogenic remains, greenish glaucony pellets form ubiquitous sediment particle components.

5.3.2 Continental Margin off Enderby Land and Mac. Robertson Land

Paleoceanography

Coring operations along the continental margin off Enderby Land and Mac. Robertson Land (64.3'S to 67.1'S and 48.5'E to 65.5'E) focused on the recovery of sedimentary records spanning late Pleistocene glacial-interglacial cycles and high-resolution Holocene sequences. For geographical orientation we use the terms "Daly Rise" and "Edward VIII Rise" to refer to bathymetric highs protruding from the continental margin (Fig. 5.3.2.1).

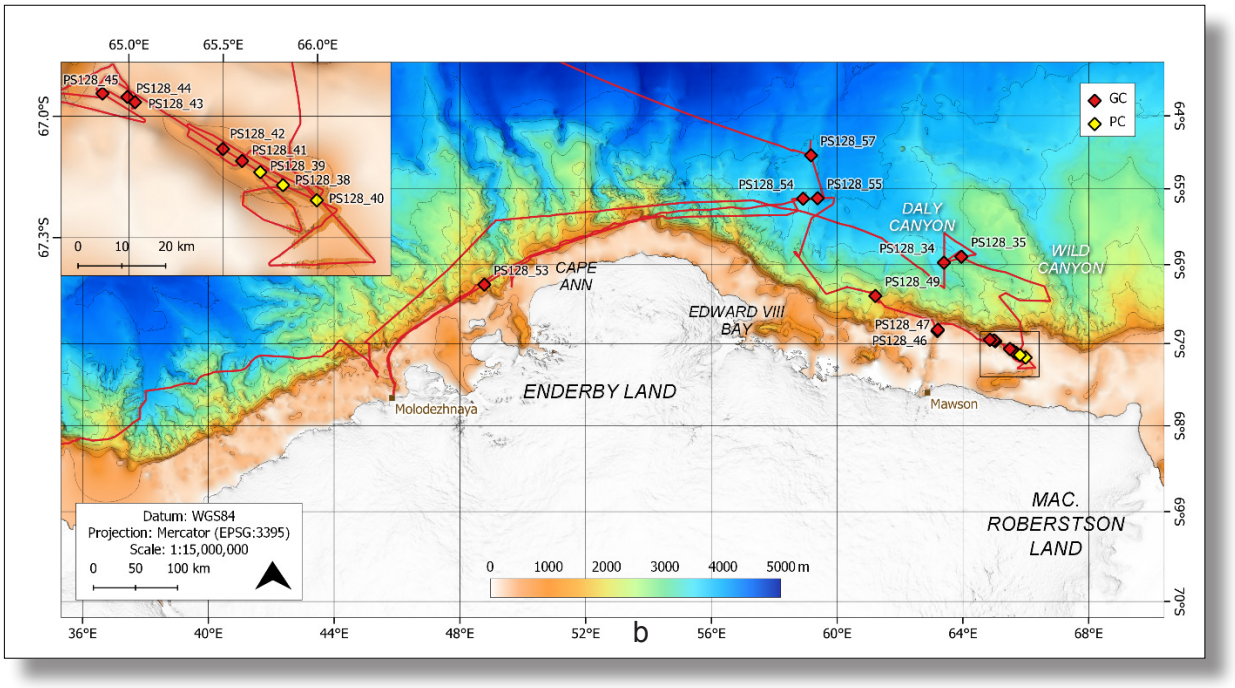

Fig. 5.3.2.1: Overview of GC and PC sites off Enderby Land and Mac. Robertson Land. The insert indicates the track for the bathymetric and sediment echography survey within Nielsen Basin with recovered sediment records (red diamonds refer to short paleoglaciologic sediment records, yellow diamonds to long paleoceanographic sites on the shelf).

At Daly Rise, two gravity cores (PS128_34-2, 13.84 m; PS128_34-3, 13.78 m; Figs. 5.3.2.1 and 5.3.2.2) were successfully recovered from a water depth of 3,090 m, while gravity core PS128_35-1 (3,289 m water depth) failed due to bending of the coring device. PS128_34-3 consists primarily of brownish gray, biosiliceous clayey silt (Appendix A.6.2) with dispersed dropstones throughout the core. Dominance of silty clay is observed between 3 and 7 m core depth. Below 8 m core depth, sediment colour changes to olive gray and more partly strongly bioturbated intervals are observed.

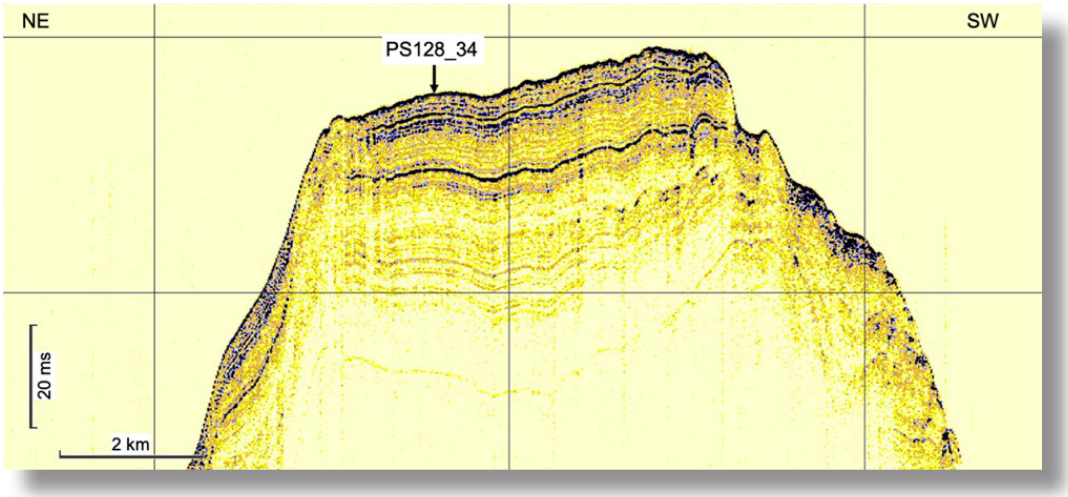

Fig. 5.3.2.2: Sediment acoustic profile of the "Daly Rise" off Mac. Robertson Land showing high penetration signals and coring site PS128_34 in well-stratified sediments

At the upper continental slope off Mac. Robertson Land, high-amplitude, low penetration PARASOUND signals revealed only thin sediment drape and coring operations were cancelled in this area.

Nielsen Basin and Iceberg Alley, two up to 1,000 m deeply incised troughs on the relatively narrow Mac. Robertson Shelf, represent high sediment accumulation basins. The PARASOUND profile of the northern part of Nielsen Basin shows very deep penetration in well-stratified sediments deposited in depressions, while low-penetration signals are observed at ridges (Fig. 5.3.2.3). Piston coring in these depressions yielded 8.59 m (PS128_39, 661 m water depth) and 23.84 m (PS128_40, 816 m water depth) sediment records, respectively. Poor recovery of 0.77 m at station PS128_38 (525 m water depth) was due to a positioning error. A suite of short gravity cores (up to 4 m recovery) to study ice sheet recession dynamics were collected at ridge structures (see below '*Paleoglaciology*').

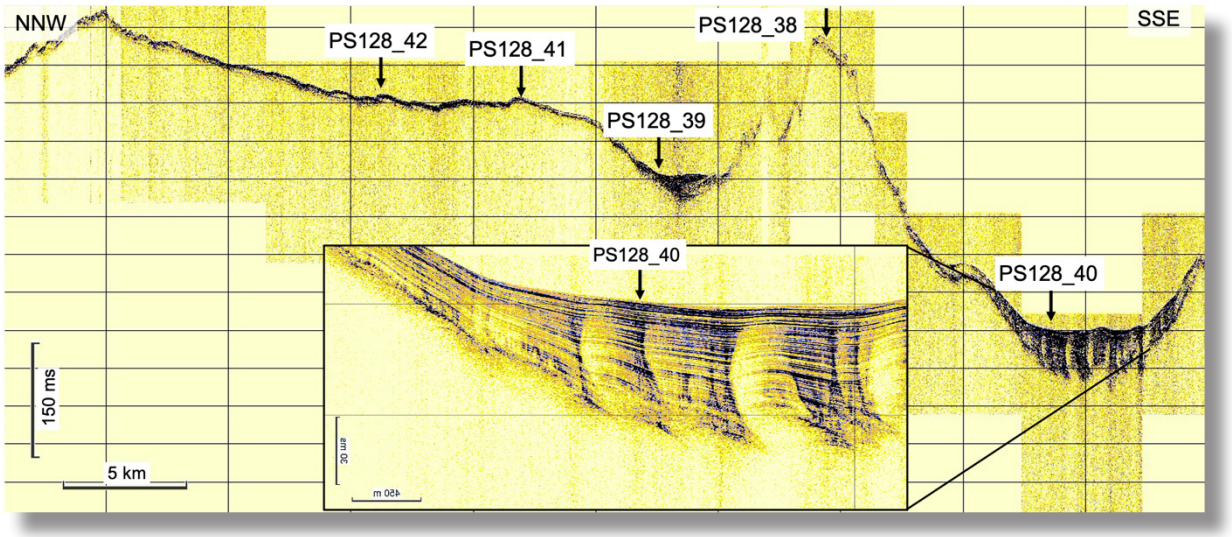

Fig. 5.3.2.3: Sediment acoustic profile of the inner Nielsen Basin, continental shelf off Mac. Robertson Land; coring stations in high-accumulation depressions (PS128_39, PS128_40) and on top of ridge structures (PS128_38, PS128_41, PS128_42)

Gravity core PS128_49 was collected at the continental slope off Mac. Robertson Land in a water depth of 2193 m (6.08 m recovery).

During transit from *Molodezhnaya Station* back into the western Cooperation Sea, a gravity core was collected at station PS128_53 at the upper continental slope off Enderby Land (1,072 m water depth; 9.17 m recovery).

At Edward VIII Rise, four gravity cores were collected at stations PS128_54 (3,457 m water depth; double coring: 13 m and 13.66 m recovery, respectively), PS128_55 (3,770 m water depth; 1.36 m recovery; bending of coring device) and PS128_57 (3,864 m water depth; 7 m recovery). PARASOUND profiles across these sites show deep-penetration in well-stratified sediments at the western and northern flank of the rise (Fig. 5.3.2.4).

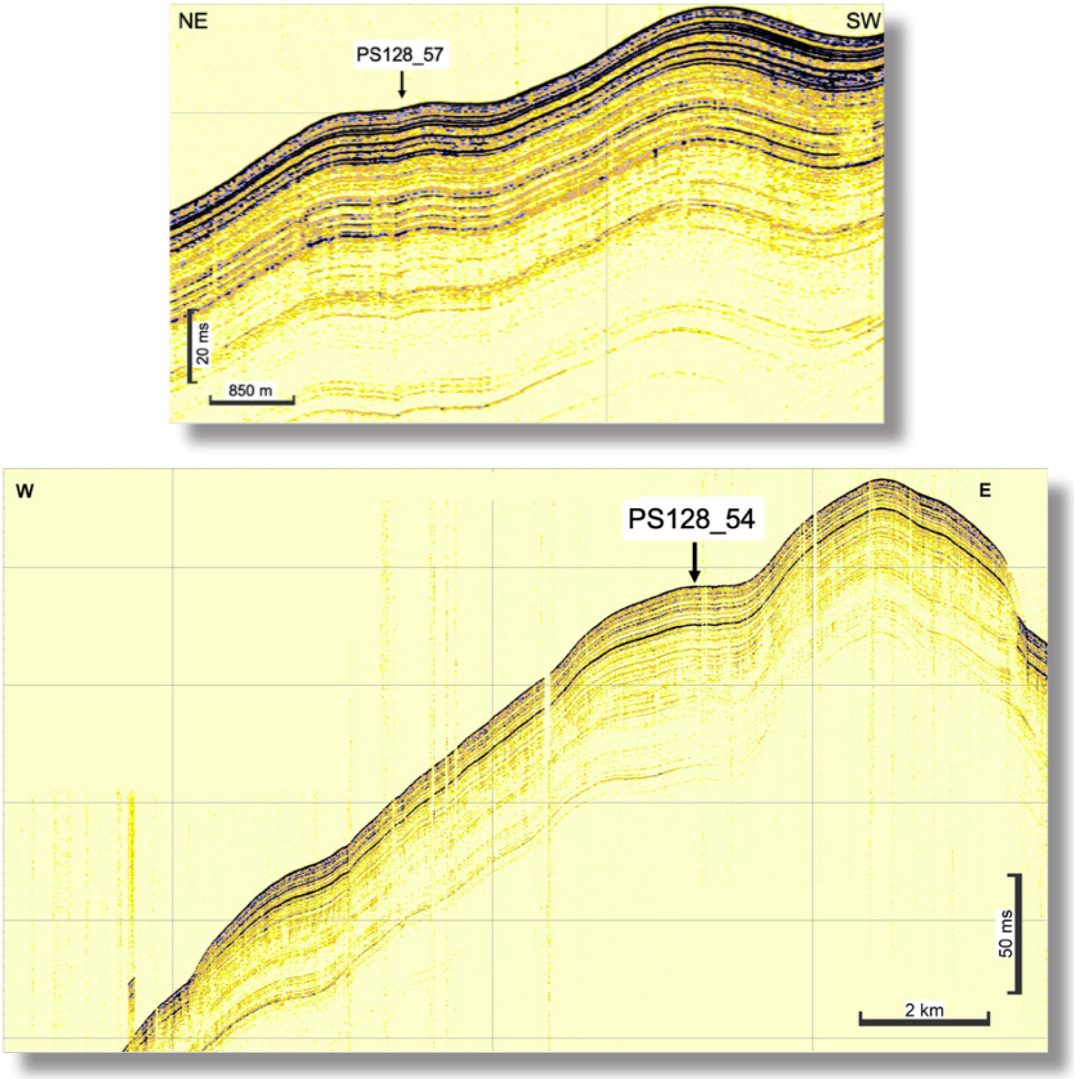

Fig. 5.3.2.4: Sediment acoustic profiles of Edward VIII Rise off Enderby Land with coring sites PS128_54 at the western flank and PS128_57 at the northern flank

PS128_54-2 revealed a more than 13 m long succession of cyclic sediments, characterized by two main end-member lithologies in transitional alternation. They consist of grayish brown biosiliceous clayey silts (Fig. 5.3.2.5) with low values of magnetic susceptibility that dominate the record. Scarce amounts of foraminifera were identified in sieve samples, but are not present

in the smear slides. The biogenic fraction consists of diatoms, radiolarians and long spikes of sponge needles. The siliciclastic fraction comprises high abundance of coarse silt. The other sediment type appears in condensed thickness (≤ 20 cm) and comprises olive gray diatom-bearing silty clay (Fig. 5.3.2.5) at high values of magnetic susceptibility. Dispersed dropstones occur rarely through the record. A 3 cm large dropstone appears at 930 cm. It consists of quarzitic red sandstone, usually found in the hinterland of Prydz Bay (Borchers et al., 2011). The sediments below 10 m core depth tend to contain higher clay and grit concentrations and include sandy layers as well as clumpy sandy mud clasts.

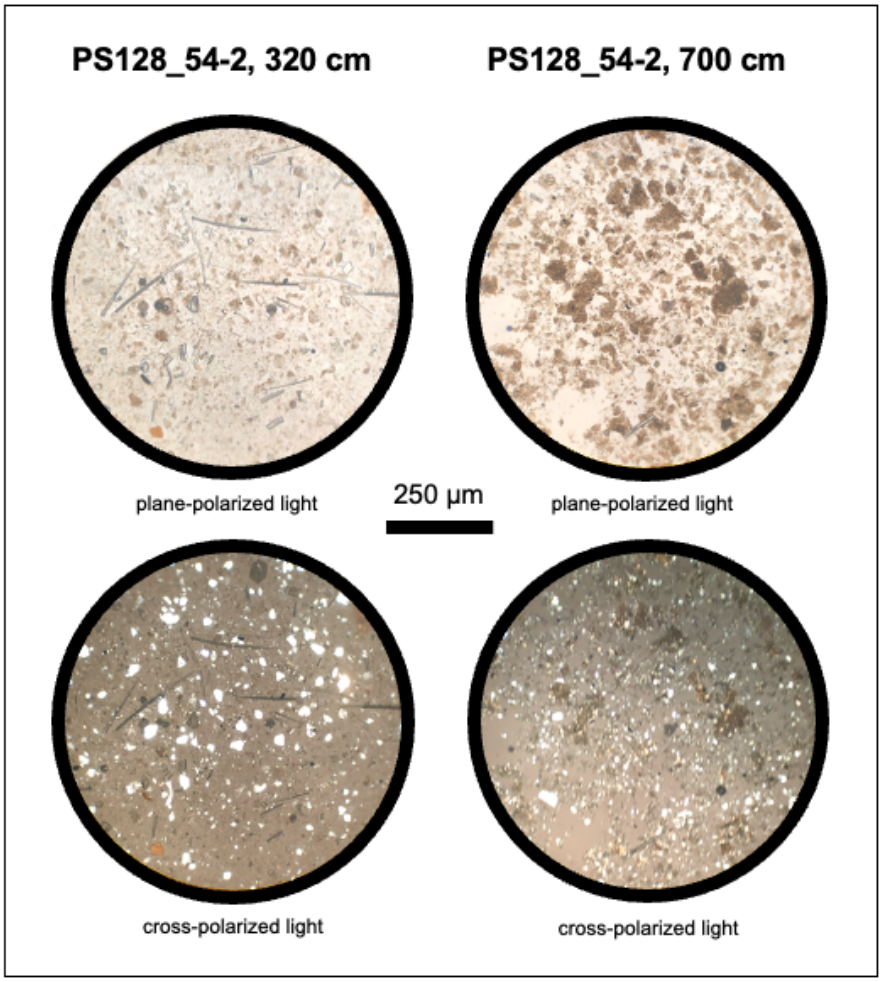

Fig. 5.3.2.5: Smear-slide photographs highlighting the two main lithologies present in sediment core PS128_54-2: biosiliceous clayey silt (left), diatom-bearing silty clay (right)

Sediment core PS128_57-1 consists of a sequence of brownish to greenish olive gray silty clay to clayey silt, which is rich in diatoms, and partly develops into typical fluffy and greenish diatomaceous oozes. Various diatom species suggest a Pleistocene age. Magnetic susceptibility values are generally low. The sequence is interrupted by several slump deposits, which consist of strongly disturbed gray to olive gray mixtures of different grain sizes, including reworked lenses of diatomaceous oozes and coal/wood fragments. With these slump deposits, the magnetic susceptibility values commonly increase. In the lowermost core meter, the sediment changes to much darker and clearly finer silty clay, with no dropstones and no bioturbation. A tentative correlation of cores PS128_54-2 and PS128_57-1 based on their magnetic susceptibility records is shown in Figure 5.3.2.6.

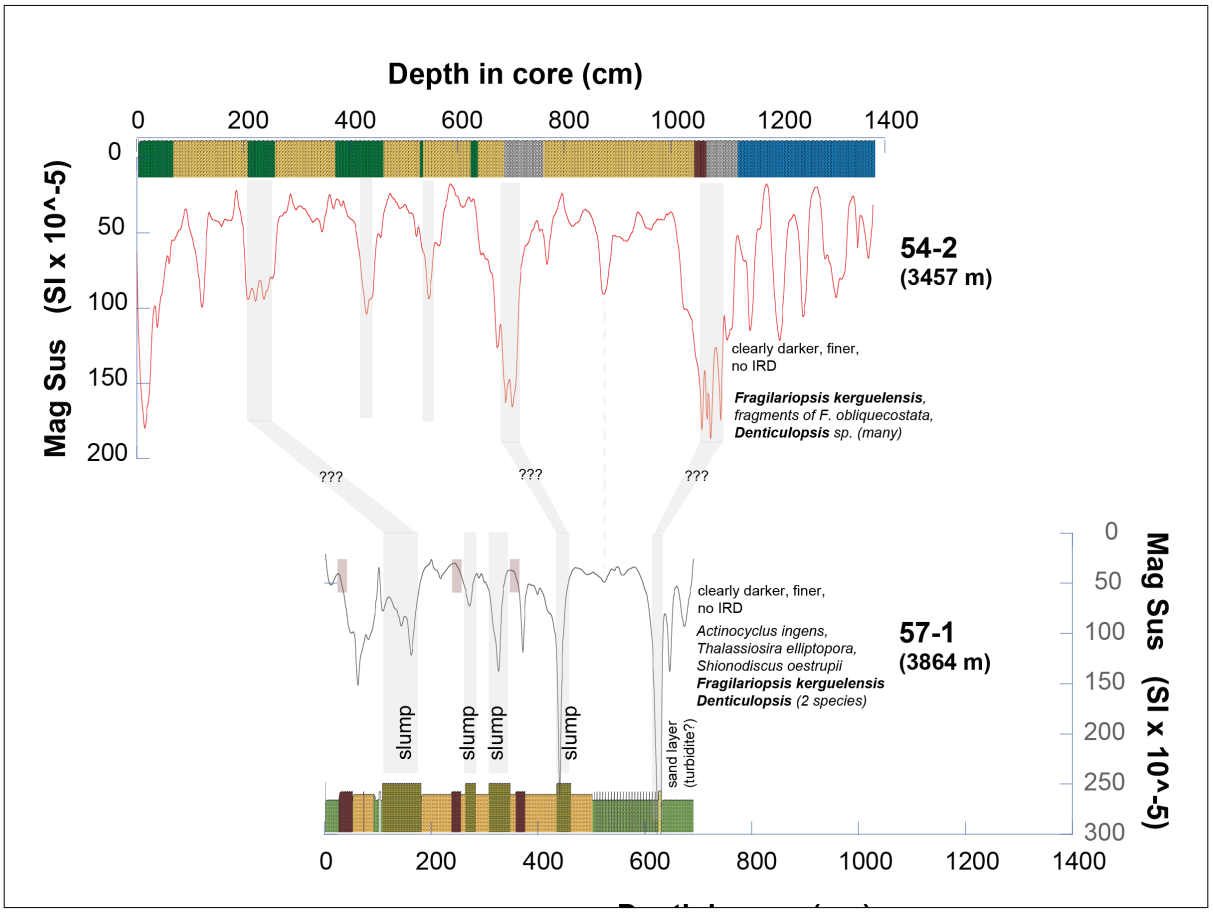

Fig. 5.3.2.6: Magnetic susceptibility records of cores PS128_54-2 and PS128_57-1 collected at Edward VIII Rise off Enderby Land

Paleoglaciology

Along the Mawson Coast (Mac. Robertson Land), our paleoglaciological studies focused on the mid- and outer shelf portions of Nielsen Basin and Iceberg Alley to study past ice-sheet dynamics on the Mac. Robertson Shelf. Those basins were suggested to be major pathways of fast-flowing ice during the last glacial period (Leventer et al., 2006; Mackintosh et al., 2011) and therefore serve as ideal indicators of past ice-sheet dynamics for a large sector of the East Antarctic margin. So far, only fragmentary bathymetric information is available from those shelf areas (Smith et al., 2021) and reliable geological constraints on initial post-LGM grounding-line retreat are lacking (Leventer et al., 2006; Mackintosh et al., 2011). Further, those authors conclude that the pattern and chronology of subsequent grounding-line retreat remains largely obscure. We therefore collected additional high-resolution bathymetric and sediment echography data along the mid and outer Nielsen Basin as well as in outer Iceberg Alley (Fig. 5.3.2.1; PS128_37). We were able to extend previous paleoglaciological knowledge from those basins (Leventer et al., 2006; Mackintosh et al., 2011) by revealing additional subglacial features indicative of past fast ice flow and episodic grounding-line retreat. Based on those detailed geophysical information, we defined locations for recovering giant box and gravity cores. In total, six short gravity cores and one giant box core were collected from the mid and outer shelf portions of Nielsen Basin (Fig. 5.3.2.1), four of which were taken from the crests of grounding-zone wedges or bedrock ridges (Fig. 5.3.2.7) since those features likely represent periods of grounding-line stabilization during general post-LGM ice-sheet retreat towards the modern grounding line. From that, we aim to constrain reliable minimum grounding-line retreat

ages for those features and provide an improved understanding of past maximum EAIS extent and subsequent retreat, which – at the same time – may serve as critical spatiotemporal benchmarks for testing and calibrating numerical ice-sheet models.

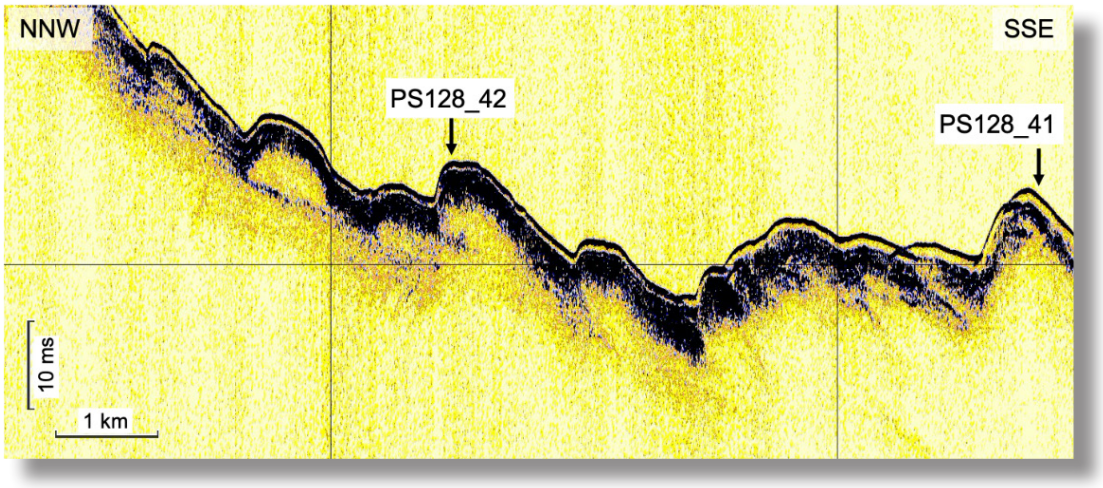

Fig. 5.3.2.7: Example for a sediment echography profile from the outer Nielsen Basin showing the prominent sub-bottom reflector likely representing the surface of a till, which was penetrated by the short gravity cores at sites PS128_41 and PS128-42

Micropaleontology

In the Cape Darnley study area, siliceous shells were generally better preserved and more abundant. Thus, species were more diverse, though the same species as in Bungenstock Plateau dominated assemblages. It was noted that more diatom species associated with sea ice were observed, probably due to the better overall conservation of their valves. Cores PS128_34-2, PS128_40-2, PS128_47-1, PS128_49-2, PS128_54-1 and PS128_57-1 had the most siliceous remains. Core PS128_40-2 had assemblages dominated by *Corethron criophilum* (Fig. 5.3.2.8a) and species from the *Chaetoceros* genus (Fig. 5.3.2.8b), as described by Stickley et al. (2005).

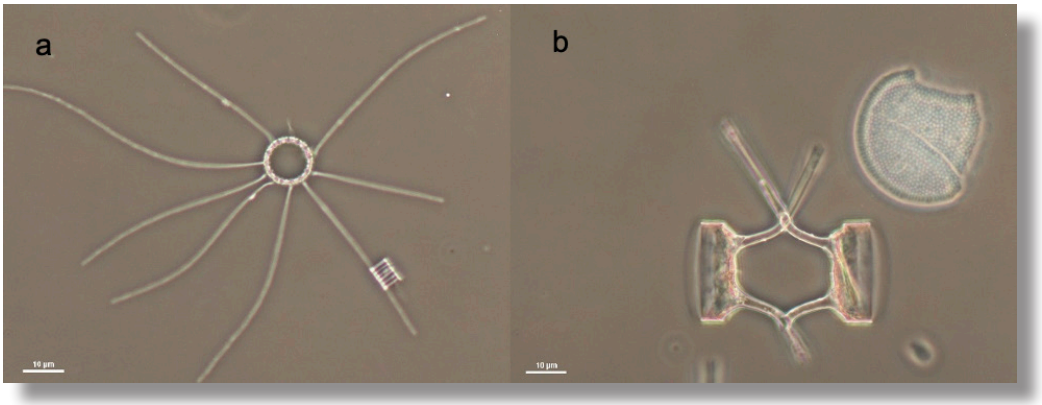

Fig. 5.3.2.8: Pictures of dominant diatom species in core PS128_40-2
a: Corethron criophilum; b: Chaetoceros dichaeta

Provenance of terrigenous sediment fraction

Samples from along and off the coast of Mac-Robertson Land are enriched in quartz, feldspar, green hornblende, orthopyroxene and especially pink garnet, indicating sediment sources in the crystalline basement rocks of East Antarctica, here from the Mawson Coast. Outcrops comprise garnet-hornblende gneisses associated with pyroxene gneisses, hypersthene-bearing charnockites and granitoids (Kuhn & Diekmann, 1999; Borchers et al., 2011). The occurrence of a dropstone of red quarzitic sandstone in sediment core PS128_54-2 from the Edward-VIII-Rise also reflects supply from Palaeozoic sandstone units that crop out in the hinterland of Prydz Bay (Borchers et al., 2011).

5.4 Data management

The entire international community involved in the planned expedition will have immediate and preferential access to the cruise report, to shipboard data and samples retrieved. The availability of expedition data and samples may remain restricted to others not directly involved in the project. After a moratorium period that protects the interests of the project partners, the scientific community will have open access to data and samples.

Environmental data will be archived, published and disseminated according to international standards by the World Data Center PANGAEA Data Publisher for Earth & Environmental Science (https://www.pangaea.de) within two years after the end of the cruise at the latest. By default, the CC-BY license will be applied.

Molecular data (DNA and RNA data) will be archived, published and disseminated within one of the repositories of the International Nucleotide Sequence Data Collaboration (INSDC, www.insdc.org) comprising of EMBL-EBI/ENA, GenBank and DDBJ).

Any other data will be submitted to an appropriate long-term archive that provides unique and stable identifiers for the datasets and allows open online access to the data.

This expedition was supported by the Helmholtz Research Programme “Changing Earth – Sustaining our Future” Topic 2 “Ocean and Cryosphere in Climate”, Subtopics 2.1 “Warming Climate” 2.2,"Variability and Extremes", 2.3 “Sea Level Change” and 2.4 "Advanced Research".

In all publications based on this expedition, the **Grant No. AWI_PS128_01** will be quoted and the following publication will be cited:

Alfred-Wegener-Institut Helmholtz-Zentrum für Polar- und Meeresforschung (2017) Polar Research and Supply Vessel *Polarstern* Operated by the Alfred-Wegener-Institute. Journal of large-scale research facilities, 3, A119. http://dx.doi.org/10.17815/jlsrf-3-163.

References

Abram NJ, et al. (2013) A review of sea ice proxy information from polarice cores. QSR 79:168–183.

Best AI & Gunn DE (1999) Calibration of marine sediment core loggers for quantitative acoustic impedance studies. Marine Geology 160:137-146.

Borchers A, et al. (2011) Mineralogy of glaciomarine sediments from the Prydz Bay-Kerguelen region: relation to modern depositional environments. Antarctic Science 23(2):164–179.

Borchers A, et al. (2016) Holocene ice dynamics and bottom-water formation associated with Cape Darnley polynya activity recorded in Burton Basin, East Antarctica. Marine Geophysical Research 37(1):49-70. https://doi.org/10.1007/s11001-015-9254-z.

Diekmann B & Kuhn G (1999): Provenance and dispersal of glacial–marine surface sediments in the Weddell Sea and adjoining areas, Antarctica: ice-rafting versus current transport. Marine Geology 158:209–231.

EPICA Community Members (2006) One-to-one coupling of glacial climate variability in Greenland and Antarctica. Nature 444:195-198.

Gersonde R, et al. (2005) Sea-surface temperature and sea ice distribution of the Southern Ocean at the EPILOG Last Glacial Maximum – A circum-Antarctic view based on siliceous microfossil records. Quaternary Science Reviews 24 (7-9):869-896.

Grobe H & Mackensen A (1992) Late Quaternary climatic cycles as recorded in sediments from the Antarctic continental margin. In J P Kennett, & D A Warkne (Eds.), The Antarctic Paleoenvironment: A Perspective on Global Change, 349–376. Washington: AGU. https://doi.org/10.1029/AR056p0349.

Gunn DE & Best AI (1998) A new automated nondestructive system for high resolution multi-sensor core logging of open sediment cores. Geo-Marine Letters 18:70-77.

Ho SL, et al. (2014) Appraisal of TEX86 and thermometries in subpolar and polar regions. Geochimica et Cosmochimica Acta 131: 213-226. https://doi.org/10.1016/j.gca.2014.01.001.

Klages J P, et al. (2016) A glacial landform assemblage from an inter-ice stream setting in the eastern Amundsen Sea Embayment, West Antarctica. Geological Society London Memoirs 46:349-352.

Klages JP, et al. (2017) Limited grounding-line advance onto the West Antarctic continental shelf in the easternmost Amundsen Sea Embayment during the last glacial period. PLOS ONE 12(7):e0181593. https://doi.org/10.1371/journal.pone.0181593.

Kuhn G & Gaedicke C (2014) A Plan for Interdisciplinary Process-Studies and Geoscientific Observations beneath the Ekström Ice Shelf (Sub-EIS-Obs). Polarforschung 84(2):99–102.

Lamping N, et al. (2021) Evaluation of lipid biomarkers as proxies for sea ice and ocean temperatures along the Antarctic continental margin. Climate of the Past. https://doi.org/10.5194/cp-2021-19.

Leventer A, et al. (2006). Marine sediment record from the East Antarctic margin reveals dynamics of ice sheet recession. GSA Today 16. https://doi.org/10.1130/GSAT01612A.1.

Mackintosh A, et al. (2011) Retreat of the East Antarctic ice sheet during the last glacial termination. Nature Geoscience 4:195-202.

Mackintosh A, et al. (2014) Retreat history of the East Antarctic Ice Sheet since the Last Glacial Maximum. Quat Sci Rev 100:10–30.

Mazzullo et al. (1988) New sediment classification scheme for the Ocean Drilling Program. In Mazzullo, J.M., and Graham, A.G. (Eds.), Handbook for shipboard sedimentologists. ODP Tech. Note, 8:45–67.

Nürnberg D et al. (2000) Paleo-sea surface temperature calculations in the equatorial east Atlantic from Mg/Ca ratios in planktic foraminifera: A comparison to sea surface temperature estimates from UK37', oxygen isotopes, and foraminiferal transfer function. Paleoceanography 15(1):124-134, https://doi.org/10.1029/1999PA000370.

Oetting A, et al. (2022) Geomorphology and shallow sub-sea floor structures underneath the Ekström Ice Shelf, Antarctica. The Cryosphere, in press.

Park E, et al. (2019) Seasonality of archaeal lipid flux and GDGT-based thermometry in sinking particles of high-latitude oceans: Fram Strait (79°N) and Antarctic Polar Front (50°S). Biogeosciences 16: 2247-2268.

Rickli J, et al. (2014) Neodymium and hafnium boundary contributions to seawater along the West Antarctic continental margin. Earth and Planetary Science Letters 394:99-110.

Smith E, et al. (2019) Detailed Seismic Bathymetry Beneath Ekström Ice Shelf, Antarctica: Implications for Glacial History and Ice-Ocean Interaction. Geophys. Res. Lett. 47. https://doi.org/10.1029/2019GL086187.

Smith J, et al. (2021) A bathymetric compilation of the Cape Darnley region, East Antarctica. Ant Sci 33: 548–559.

Stickley CE, et al. (2005) Deglacial ocean and climate seasonality in laminated diatom sediments, Mac. Robertson Shelf, Antarctica. Palaeogeography, Palaeoclimatology, Palaeoecology 227:290-310.

The RAISED Consortium (2014) A community-based geological reconstruction of Antarctic Ice Sheet deglaciation since the Last Glacial Maximum. Quat Sci Rev 100:1–9.

Vorrath ME, et al. (2019) Highly branched isoprenoids for Southern Ocean sea ice reconstructions: a pilot study from the Western Antarctic Peninsula. Biogeosciences 16: 2961-2981.

6. MARINE GEOCHEMISTRY: WATER COLUMN, BOTTOM WATER AND SEDIMENTARY POREWATER ANALYSES

Marcus Gutjahr[1], Huang Huang[2],
Frerk Pöppelmeier[3], Jinqi Xia[2], Gastón Kreps[4],
Laura Kattein[5], Gesine Mollenhauer[5]

[1]DE.GEOMAR
[2]CN.SYSU
[3]CH.UNIBE
[4]AR.UBA
[5]DE.AWI

Grant-No. AWI_PS128_05

Objectives

The Atlantic and Indian Ocean sector of the Southern Ocean (SO) is a hydrologically highly dynamic basin. It is dominated by the eastward flowing and vertically well mixed Antarctic Circumpolar Current (ACC). Its deeper portions are occupied by Antarctic Bottom Water, dominantly, but likely not exclusively, sourced from the Weddell Sea. South of the ACC, the presence of the westward flowing Antarctic Slope Current (Fahrbach et al., 1992; Williams et al., 2010) forms a thermal buffer zone around the East Antarctic Ice Sheet (EAIS) with near-freezing temperatures, preventing substantial submarine basal melting at present. The formation of new Antarctic Bottom Water (AABW) in front of the marine-based EAIS is a further important process in Antarctic waters. While the most important Antarctic Deep Water formation areas have long been known to lie in the southern Weddell and Ross Sea (e.g. Orsi et al., 1999; Purkey et al., 2018), other locations of AABW formations have been identified more recently such as the Cape Darnley region (Meijers et al., 2010; Ohshima et al., 2013; Williams et al., 2016; Williams et al., 2010). Generally speaking, AABW has warmed, declined in volume and freshened in recent decades, which likely will have consequences for the global sea level rise and heat budgets (Purkey et al., 2018). In this context, the water column work to be realised here will serve as an important assessment of the current state of regional AABW formation along the EAIS.

A major target of water column sampling during PS128 was the study of neodymium (Nd) isotope systematics within the water column. Neodymium belongs to the group of Rare Earth Elements (REE) and is systematically incorporated into continental and oceanic crust with unique isotopic signatures. Neodymium isotopes are also an increasingly employed tool to investigate the origin and flow path of water masses in the oceans today (e.g. Stichel et al., 2012) and in the past. This trace metal is supplied to the oceans through physico-chemical weathering on land and on the seafloor in shallow marine and continental rise settings. A recent modelling study reports that the relative contributions of Nd to seawater are ~60 % via boundary/benthic additions (i.e., from sediments to bottom water), ~32 % from riverine inputs, and ~9 % from partial dissolution of dust in the water column (Pöppelmeier et al., 2020). The Nd isotope signature thus reflects the isotopic signal of the material chemically weathering on land, in the water column (dust), or on the seafloor. As a consequence, water masses in contact with the ocean margin often change their isotopic composition successively along their flow path, whereas in the open ocean Nd isotopic compositions remains constant unless a parcel of water is mixed with another parcel of water with a different isotopic composition. Neodymium can therefore be categorised as behaving semi-conservative in seawater with a mean global residence time of about 690 years (Pöppelmeier et al., 2020). Earlier work by the

PIs in the southern and northwestern Weddell Sea during PS111 (2018) and PS118 (2019), as well as during PS75 in the Pacific sector of the Southern Ocean (Rickli et al., 2014) has already provided insights into the Nd isotopic and concentration behaviour in these areas, also highlighting localised hotspots of Nd addition to bottom waters on the shelf and Antarctic continental rise, most clearly resolvable along the northern Antarctic Peninsula. The work realised during PS128 will result in an extension of this new database to East Antarctic areas that are hitherto largely unsampled for this emerging geochemical isotope water mass tracer.

The oceanographic and biogeochemical work on the water column during PS128 not only investigated water mass sourcing and its consequences for the chemical composition of individual water masses, but also considered key aspects of the atmospheric and marine carbon cycle. Global climate is critically sensitive to physical and biogeochemical dynamics in the subpolar Southern Ocean, since it is where that deep, carbon-rich layers of the world ocean outcrop and exchange carbon with the atmosphere (e.g., MacGilchrist et al., 2019). It is also where that much of anthropogenic carbon is taken up by the ocean (and enhanced glacial ocean carbon storage in the deep Southern Ocean is well established (e.g., Brovkin et al., 2012). Changes in Southern Ocean carbon uptake and its export to depth are thus strongly impacting the global carbon cycle. The role of the Southern Ocean in anthropogenic carbon uptake has long been identified (Caldeira & Duffy, 2000), and it has been suspected that climate warming reduces the efficiency of this anthropogenic carbon uptake. More recently, the strength of this carbon sink has been described to have re-invigorated (Landschützer et al., 2015). The distribution of deep ocean $\Delta^{14}C$ data of dissolved inorganic carbon (DIC) is often used to illustrate the rate of deep ocean circulation, as radiocarbon is an invaluable tool to trace exchange processes in the carbon cycle and to estimate time in closed reservoirs. For instance, $\Delta^{14}C$ of DIC can be used to map the uptake of atmospheric CO_2 into the ocean, or reflect input of aged carbon from the sea floor originating, e.g., from geologic sources. Despite their usefulness, high-resolution profiles of $\Delta^{14}C$ of DIC in the water column are scarce, in particular for the Southern Ocean. The current state of knowledge is based on a large international effort, the World Ocean Circulation Experiment conducted in the early 2000s. Sampling conducted during PS128 will help extending the data base of $\Delta^{14}C$ distribution in the Southern Ocean to hitherto unsampled near-continent regions characterised by sea ice cover, which plays an important role in air-sea gas exchange processes.

The second largest carbon pool in the ocean consists of dissolved organic carbon (DOC), whose cycling is linked to the cycles of DIC and of particulate organic matter. DOC has been reported to be up to several thousand years old in deep waters, and the mechanisms of aging remain unresolved yet. It has been reported that DOC radiocarbon content decreases along with that of DIC, suggesting that transport of deep waters is the primary control of ^{14}C in DIC and DOC in the Southern Ocean (Druffel et al., 2021). As with DIC, high-resolution profiles of $DO^{14}C$ in the water column remain scarce.

Stable oxygen and carbon isotope compositions of the shells of planktic and benthic foraminifera are widely used proxies in paleoceanographic research. For example, stable isotopes of benthic foraminifera, when combined with other trace-metal based proxies like, e.g., Mg/Ca or B/Ca ratios, deliver the means to disentangle the complex signals of physical (T, S) and chemical (CO_3^{2-}, PO_4, O_2) changes of deep water masses through Earth's history. For the interpretation of the geochemical data obtained from such microfossils and the understanding of the complex mechanisms hydrographic data, chlorophyll and nutrient measurements as well as stable isotope data ($\delta^{18}O$, $\delta^{13}C$ of DIC) from the water column (surface to bottom) are needed. While these proxies and the corresponding modern seawater signatures have been studied for several decades, the study area of PS128 remains largely undersampled. Our campaign aimed at closing this gap.

In order to achieve a more comprehensive understanding of the marine Nd and carbon cycle, we also specifically targeted the ocean floor by collecting multi core water (MUC water) that contains information about the Nd isotopic composition, $DI^{14}C$ and stable isotopic signature ($\delta^{18}O$, $\delta^{13}C$ of DIC) at the ocean floor. In contrast to the standard CTD rosette seawater sampling that is usually targeting maximum depths at least five to ten meters above the seafloor, we can hence directly target ocean water at the sediment – bottom water interface, a key locality of a variety of essential trace metals and micronutrients, including Nd. The CTD and MUC water sampling work was further complemented by the extraction of local marine porewaters via slicing of multi cores in glove bags (see below) at selected sites that were obtained from the Marine Geology group (Chapter 5). Extracted porewaters will be analysed for their alkalinity, nutrient, major and trace element concentration at GEOMAR Helmholtz Centre for Ocean Research Kiel, and will also be used for planned boron and silicon isotopic work. Analyses of geochemical parameters in these water samples also comprise $DI^{14}C$ at the AWI MICADAS radiocarbon facility for comparison with equivalent analyses conducted on benthic organisms (foraminifera) that were collected life (stained with Rose Bengal, see Chapter 5). These measurements will allow further calibration and understanding of associated geochemical proxies in marine radiocarbon research.

Last but not least, the water column and benthic porewater work was further extended by the sampling of continental ice containing Antarctic rock debris that PI M. Gutjahr carried out in cooperation with the land geology group onboard PS128 (see Chapter 7).

Underway sampling of particulate organic matter from surface water/ship's seawater inlet

Particulate organic matter (POM) filtered from seawater from the ship's seawater inlet can be used for calibration of organic geochemical (biomarker) proxies for paleoenvironmental parameters. Parallel recording of environmental parameters like water temperature and salinity, sea-ice extent and weather conditions will allow an assessment of biomarker proxies for sea-surface temperatures (e.g., alkenone based $U^{K'}_{37}$ or GDGT-based TEX_{86}) and sea ice extent ($PIPSO_{25}$). Additional environmental factors that might influence the proxies performance might be identified.

Work at Sea

Conductivity, Temperature, Depth profiling

The marine geochemistry team onboard PS128 monitored the modern hydrological configuration, also including standard physical oceanographic parameters and oxygen concentrations. This is not only important for understanding the current state of SO's overturning dynamics, but will also serve as reference for any paleoceanographic reconstructions that will be realised using PS128 sediments (Chapter 5).

Water Column sampling – Instrumentation

The main instrumentation used was a SeaBird 911+ CTD (Conductivity, Temperature and Depth), with two temperature and conductivity sensors and additional oxygen, fluorescence and Beam Attenuation sensors (WET Labs), integrated in the water sampling rosette with 24 Niskin Bottles (Ocean Test Equipment Inc.) fired by an SBE32 carousel. The difference between both temperature and conductivity sensors was < 0.003, °C and mS/cm, respectively. The GPS position at any time during the profile was added to the CTD bins by means of NMEA. The raw CTD data were processed with the SeaBird Data processing software according to SeaBird recommendations. The rosette sampler was used on 17 stations along the cruise track (Tab. 6.1 and 6.2, Figs. 6.1 – 6.3). Water samples were taken with the 24 x 12 L Niskin bottles at depths chosen during the down-cast of the CTD profiler to target specific water masses.

The *Polarstern* shipboard CTD encountered problems with the oxygen sensor during PS128. Initially this device did not work at all, and after initial repairs the performance improved early during the cruise. However, it turned out that the quality of the oxygen sensor data was limited (a) usually during the downward cast and (b) the offset was pronounced in water depths below 2,000 m. The reliability of the oxygen sensor data was routinely checked via standard Winkler titration, which was carried out at all stations during PS128 (see below). Because of the rather poor performance of the oxygen sensor in deep water, for almost all water depths sampled for Nd, radiocarbon, nutrients and trace metal concentrations, Winkler titration generated oxygen concentration data were produced. Additionally, Multicore water was also sampled for its oxygen concentration (in triplicates) to compare concentrations with the deepest CTD oxygen concentration above at the same station.

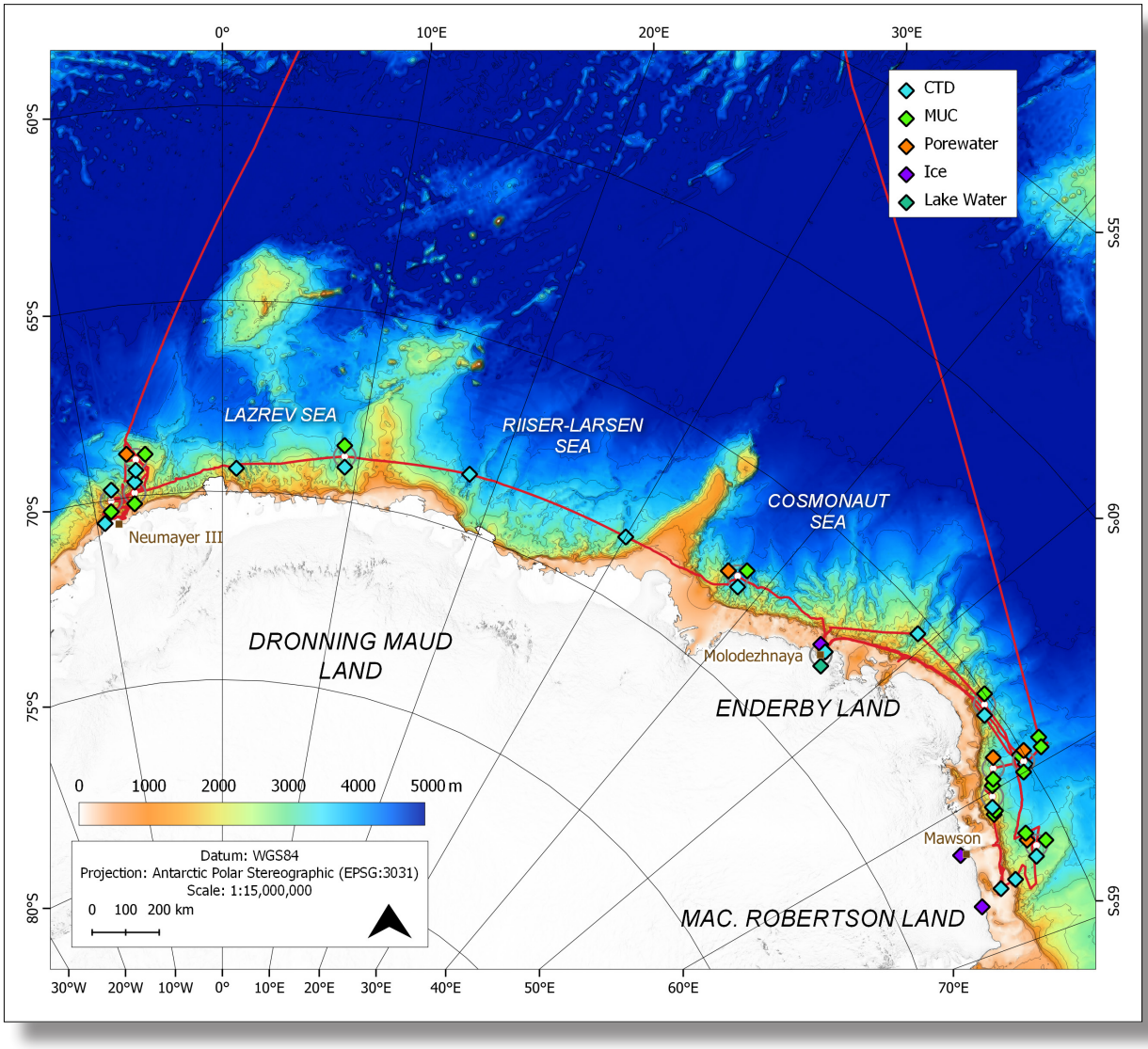

Fig. 6.1: Overview map of the East Antarctic sector visited during PS128, highlighting all stations relevant for the water column and sedimentary porewater studies; each sampling approach is depicted with a special symbol (CTD, MUC, porewater extraction from MUC, ice sampling locations (see Chapter 7) as well as a sampling location of Antarctic Lake Water (Lake Glubokoye, see Chapter 7) are also shown. (Figure: Yvonne Schulze Tenberge)

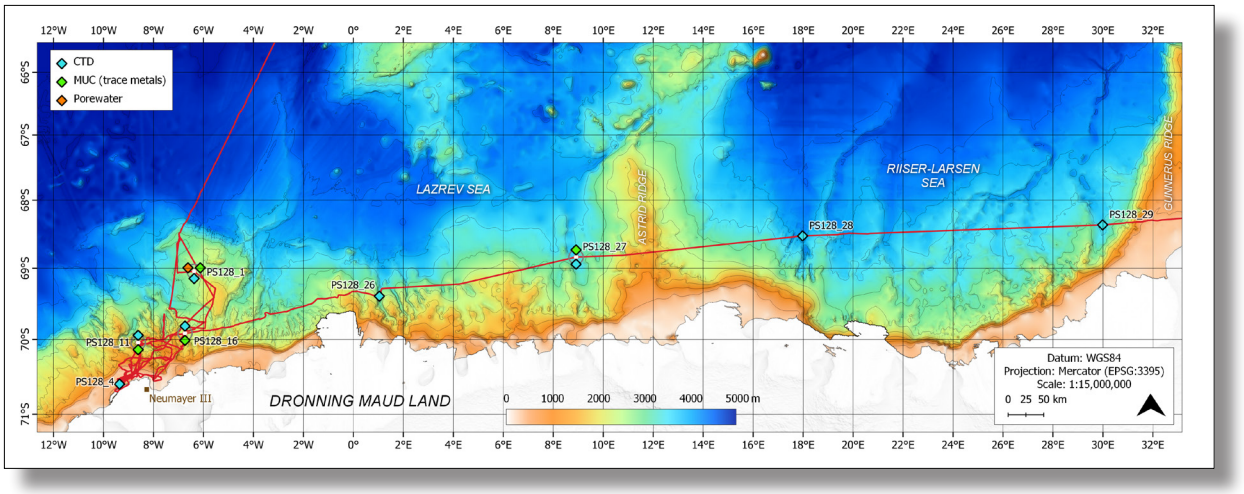

Fig. 6.2: Map of the western part of the study area visited during PS128, highlighting all stations relevant for the water column and sedimentary porewater studies, also showing station names; symbols are identical to Figure 6.1. (Figure: Yvonne Schulze Tenberge)

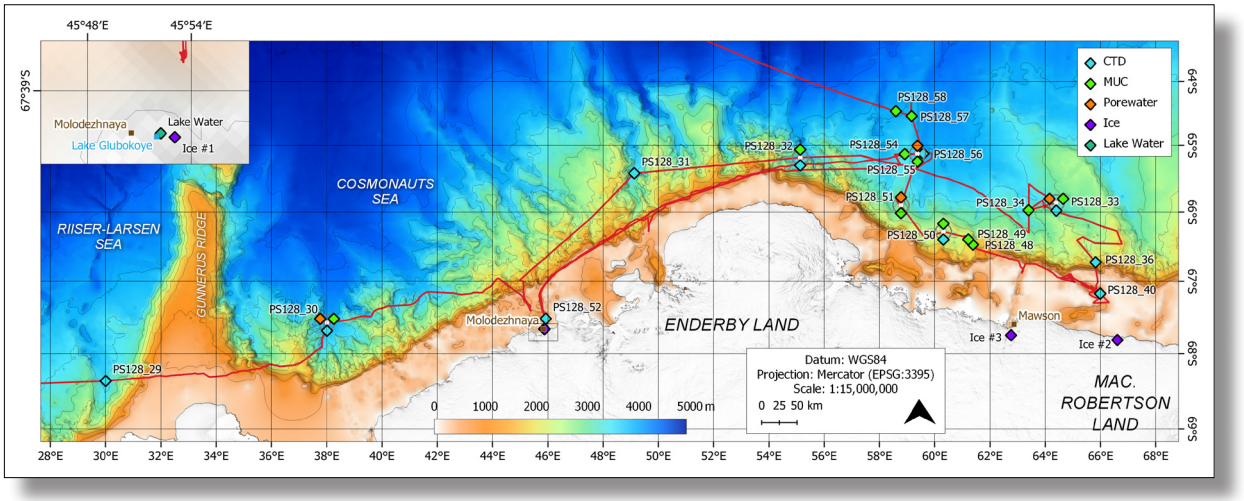

Fig. 6.3: Map of the eastern part of the study area visited during PS128, highlighting all stations relevant for the water column and sedimentary porewater studies, also showing station names; symbols are identical to Figure 6.1. Inset map shows sampling locations close to Molodezhnaya at expanded scale. (Figure: Yvonne Schulze Tenberge)

Tab. 6.1: Summary of CTD stations

Station	Date	Latitude	Longitude	Time	Water depth	Sampled depths	$DI^{14}C$		$DO^{14}C$	$\delta^{18}O$	$\delta^{13}C$	Oxygen	Nutrients	Salinity	REE + TM	εNd
				[max. depth]	[m]		[2 x 5 mL]	[500 mL]	[1 L]	[100 mL]	[50 mL]		[50 mL]			
PS128_001-3	16.01.22	69° 02.918' S	06° 22.814' W	06:17	2720	20, 250, 450, 900, 1300, 1700, 2100, 2500, 2675	x		x	x	x	x	x	x	x	x
PS128_004-1	18.01.22	70° 36.309' S	09° 21.727' W	10:56	460	10, 40, 150, 300, 454	x		x	x	x	x	x	x	x	x
PS128_011-1	19.01.22	70° 02.623' S	08° 37.000' W	12:19	2696	10, 150, 300, 520, 900, 1400, 1800, 2200, 2500, 2690	x	x	x	x	x	x	x		x	x
PS128_016-1	21.01.22	69° 54.942' S	06° 44.681' W	06:59	2096	20, 50, 130, 400, 610, 1100, 1600, 2091	x		x	x	x	x	x		x	x

Station	Date	Latitude	Longitude	Time	Water depth	Sampled depths	DI^{14}C		DO^{14}C	$\delta^{18}O$	$\delta^{13}C$	Oxygen	Nutrients	Salinity	REE + TM	εNd
				[max. depth]	[m]		[2 x 5 mL]	[500 mL]	[1 L]	[100 mL]	[50 mL]		[50 mL]			
PS128_026-1	28.01.22	69° 24.046' S	01° 02.401' E	12:28	3299	25, 150, 300, 500, 900, 1300, 1700, 2100, 2500, 2800, 3100, 3297	x			x	x	x	x	x	x	x
PS128_027-1	29.01.22	68° 50.404' S	08° 54.948' E	05:25	3571	25, 70, 150, 400, 800, 1300, 1850, 2400, 2900, 3200, 3400, 3566	x		x	x	x	x	x	x	x	x
PS128_028-1	30.01.22	68° 31.916' S	17° 59.263' E	06:31	4243	25, 80, 380, 700, 1200, 1800, 2400, 2900, 3400, 3800, 4100, 4239	x			x	x	x	x	x	x	x

Station	Date	Latitude	Longitude	Time	Water depth	Sampled depths	DI^{14}C		DO^{14}C	δ^{18}O	δ^{13}C	Oxygen	Nutrients	Salinity	REE + TM	εNd
				[max. depth]	[m]		[2 x 5 mL]	[500 mL]	[1 L]	[100 mL]	[50 mL]		[50 mL]			
PS128_029-1	31.01.22	68° 22.194' S	30° 00.005' E	09:23	3710	15, 100, 360, 550, 1000, 1500, 2000, 2500, 3000, 3250, 3500, 3646	x			x	x	x	x	x	x	x
PS128_030-1	01.02.22	67° 35.088' S	38° 00.596' E	10:36	4010	20, 140, 360, 560, 1000, 1500, 2000, 2500, 3000, 3500, 3850, 4010	x		x	x	x	x	x		x	x
PS128_031-1	03.02.22	65° 25.414' S	049° 08.062' E	08:45	3495	20, 160, 360, 550, 900, 1300, 1700, 2100, 2600, 3000, 3250, 3481	x		x	x	x	x	x		x	x

Station	Date	Latitude	Longitude	Time	Water depth	Sampled depths	DI^{14}C		DO^{14}C	δ^{18}O	δ^{13}C	Oxygen	Nutrients	Salinity	REE + TM	εNd
				[max. depth]	[m]		[2 x 5 mL]	[500 mL]	[1 L]	[100 mL]	[50 mL]		[50 mL]			
PS128_032-1	04.02.22	65° 11.187‘ S	055° 08.517‘ E	02:02	3670	20, 80, 220, 440, 800, 1125, 1600, 2100, 2600, 3100, 3500, 3660	x			x	x	x	x		x	x
PS128_033-1	07.02.22	65° 51.822‘ S	064° 24.106‘ E	02:25	3307	25, 85, 250, 430, 800, 1200, 1600, 2000, 2400, 2800, 3200, 3348	x		x	x	x	x	x		x	x
PS128_036-1	08.02.22	66° 43.799‘ S	065° 49.605‘ E	17:53	1999	25, 100, 300, 600, 700, 860, 1000, 1300, 1480, 1620, 1850, 1994	x		x	x	x	x	x		x	x

Station	Date	Latitude	Longitude	Time	Water depth	Sampled depths	DI^{14}C		DO^{14}C	δ^{18}O	δ^{13}C	Oxygen	Nutrients	Salinity	REE + TM	εNd
				[max. depth]	[m]		[2 x 5 mL]	[500 mL]	[1 L]	[100 mL]	[50 mL]		[50 mL]			
PS128_040-1	09.02.22	67° 10.379‘ S	065° 59.818‘ E	17:55	802	40, 125, 420, 600, 796	x			x	x	x	x		x	x
PS128_050-1	11.02.22	66° 17.265‘ S	060° 19.052‘ E	18:57	2805	25, 120, 290, 320, 550, 760, 1000, 1400, 1800, 2200, 2600, 2796	x			x	x	x	x		x	x
PS128_052-1	14.02.22	67° 31.399‘ S	045° 55.671‘ E	14:19	869	25, 110, 360, 585, 730, 864	x			x	x	x	x		x	x
PS128_056-1	16.02.22	65° 07.582‘ S	059° 35.353‘ E	19:48	4095	25, 220, 500, 1000, 1500, 2000, 2500, 3000, 3850, 4087	x		x *	x	x	x	x		x	x

*duplicates

Tab. 6.2: Overview of CTD / MUC / Porewater stations

Device Operation	Event Time	Event marker	Latitude	Longitude	Latitude [deg]	Longitude [deg]
PS128 stations only sampled via CTD						
PS128_4-1	18.01.22 10:56	max depth/ on ground	70° 36.309‘ S	009° 21.727‘ W	-70.605	-9.362
PS128_26-1	28.01.22 12:28	max depth/ on ground	69° 24.046‘ S	001° 02.401‘ E	-69.401	1.040
PS128_28-1	30.01.22 06:31	max depth/ on ground	68° 31.916‘ S	017° 59.263‘ E	-68.532	17.988
PS128_29-1	31.01.22 09:23	max depth/ on ground	68° 22.194‘ S	030° 00.005‘ E	-68.370	30.000
PS128_31-1	03.02.22 08:45	max depth/ on ground	65° 25.414‘ S	049° 08.062‘ E	-65.424	49.134
PS128_36-1	08.02.22 17:53	max depth/ on ground	66° 43.799‘ S	065° 49.605‘ E	-66.730	65.827
PS128_40-1	09.02.22 17:55	max depth/ on ground	67° 10.379‘ S	065° 59.818‘ E	-67.173	65.997
PS128_52-1	14.02.22 14:19	max depth/ on ground	67° 31.399‘ S	045° 55.671‘ E	-67.523	45.928
PS128_56-1	16.02.22 19:48	max depth/ on ground	65° 07.582‘ S	059° 35.353‘ E	-65.126	59.589
PS128 stations, at which both CTD and MUC water was collected						
PS128_1-3	16.01.22 06:17	max depth/ on ground	69° 02.918‘ S	006° 22.814‘ W	-69.049	-6.380
PS128_11-1	19.01.22 12:19	max depth/ on ground	70° 02.623‘ S	008° 37.000‘ W	-70.044	-8.617
PS128_16-1	21.01.22 06:59	max depth/ on ground	69° 54.942‘ S	006° 44.681‘ W	-69.916	-6.745
PS128_27-1	29.01.22 05:25	max depth/ on ground	68° 50.404‘ S	008° 54.948‘ E	-68.840	8.916
PS128_30-1	01.02.22 10:36	max depth/ on ground	67° 35.088‘ S	038° 00.596‘ E	-67.585	38.010
PS128_32-1	04.02.22 02:02	max depth/ on ground	65° 11.187‘ S	055° 08.517‘ E	-65.186	55.142
PS128_33-1	07.02.22 02:25	max depth/ on ground	65° 51.834‘ S	064° 24.099‘ E	-65.864	64.402
PS128_50-1	11.02.22 18:57	max depth/ on ground	66° 17.265‘ S	060° 19.052‘ E	-66.288	60.318
PS128 stations where both MUC water and MUC porewater were extracted						
PS128_1-4	16.01.22 08:54	max depth/ on ground	69° 02.842‘ S	006° 22.680‘ W	-69.047	-6.378
PS128_30-2	01.02.22 13:13	max depth/ on ground	67° 34.974‘ S	038° 00.574‘ E	-67.583	38.010

Device Operation	Event Time	Event marker	Latitude	Longitude	Latitude [deg]	Longitude [deg]
PS128_33-2	07.02.22 05:01	max depth/ on ground	65° 51.806‘ S	064° 24.327‘ E	-65.863	64.405
PS128_51-1	12.02.22 07:16	max depth/ on ground	65° 54.037‘ S	058° 47.143‘ E	-65.901	58.786
PS128_55-1	16.02.22 13:26	max depth/ on ground	65° 07.594‘ S	059° 22.855‘ E	-65.127	59.381
PS128 stations where only MUC water was collected (no associated CTD)						
PS128_34-1	07.02.22 10:18	max depth/ on ground	65° 58.492‘ S	063° 23.952‘ E	-65.975	63.399
PS128_48-1	11.02.22 07:43	max depth/ on ground	66° 28.661‘ S	061° 23.475‘ E	-66.478	61.391
PS128_49-1	11.02.22 10:14	max depth/ on ground	66° 24.084‘ S	061° 13.161‘ E	-66.401	61.219
PS128_54-3	16.02.22 09:48	max depth/ on ground	65° 07.965‘ S	058° 55.090‘ E	-65.133	58.918
PS128_57-2	17.02.22 07:38	max depth/ on ground	64° 32.778‘ S	059° 10.268‘ E	-64.546	59.171
PS128_58-1	17.02.22 12:02	max depth/ on ground	64° 28.299‘ S	058° 36.030‘ E	-64.472	58.601

Our sampling programme focused of the following topical groups:

Water sampling for REE, εNd

One principal aim of the water column (geo-)chemical work was the collection of a representative range of water column samples for Nd isotopic analyses. For this purpose, the content of ~1 ½ Niskin bottles was filtered directly at the rosette sampler after finalisation of sample aliquoting dedicated for other analyses (see below). Commonly 14 – 19 liters of seawater per depth could be collected for Nd isotopic analyses. Since two bottles were closed at each selected depth (i.e., 24 liters), enough seawater could be distributed for all individual approaches. Filtered seawater samples were acidified to a pH of ~2 with either concentrated HCl or concentrated HNO_3, left to equilibrate for 24 hours prior to addition of an $FeCl_3$ solution. Following another 24 hours of equilibration time, concentrated ammonia solution was added to the samples raising the seawater pH to within 8 – 9 (all reagents used are either distilled or of suprapure quality). The addition of ammonia led to precipitation of Fe from solution. Rare Earth Elements including Nd co-precipitated with this Fe. The precipitates accumulated at the bottom of each collapsible container, and the supernatant was siphoned off. Sample solutions were first transferred into 1 liter wideneck bottles, later into 50 mL centrifuge vials and centrifuged onboard to collect the seawater precipitates within the centrifuge vials. All remaining supernatant could then be discarded. In total 177 Nd isotope samples were prepared from CTD sampled depths. Samples will be further processed in the clean laboratory facilities of GEOMAR Helmholtz Centre for Ocean Research Kiel.

A similar approach was taken for bottom seawater sampled from Multicores. Here, as much water as possible was collected, usually five to ten liters, subsequently filtered in the chemistry laboratory onboard *Polarstern*, and then treated in a similar manner as the CTD seawater aliquots above. Overall, 17 MUC water samples were processed during PS128 (see Tab. 6.2).

All samples chosen for Nd isotope analyses will also be analysed for their trace element concentration. For this purpose, an extra aliquot of filtered acidified seawater was sampled in 500 mL wide-neck bottles for further analyses in Kiel. For a total of eight seawater samples, an alternative seawater sampling approach was tested, employing DGT® cationic samplers (LSNM-NP cationic metal sampler) in 1 liter wide-neck bottles for 21 days in a refrigerator. After removal from the seawater samples, DGT samplers were washed with MQ and packed in plastic bags for further processing at GEOMAR Kiel.

Discrete oxygen concentration analyses

Oxygen concentration measurements were carried out at all 17 CTD stations as well as at a total of 11 Multicore stations to (a) cross-validate the oxygen sensor derived concentrations of the CTD, and (b) to test whether oxygen concentrations determined on Multicore water can equally be determined reliably. Given that the Winkler titration results revealed substantial problems with the CTD-attached oxygen sensor, we routinely determined oxygen concentrations for each sampled water depths, thereby also generating triplicate results for two selected depths per cast. Aliquots for oxygen concentration analyses were always taken first prior to sampling for all other approaches.

Water sampling for radiocarbon analyses of DIC and DOC

Water samples for radiocarbon analyses of dissolved inorganic and organic carbon was a second focus of the campaign. Sampling depths were chosen according to water column characteristics as observed during the down-cast of the water profiling probe, and in accordance with sample depths appropriate for REE and εNd analysis. A maximum of 12 depths were sampled, with lower sampled depths numbers at shallower water depths.

Duplicate samples for radiocarbon analyses of DIC were taken at all stations and at all depths. This sampling campaign used a novel sampling approach, which requires only 5 mL of seawater to be sealed in pre-combusted gas-tight crimp-cap vials. Before sealing the crimp caps, 10 µL of a saturated $HgCl_2$ solution were added to eliminate microbial activity in the samples. Samples were stored at room temperature until analysis at the home laboratory.

At station PS128_011–1, a parallel set of 500 mL samples for radiocarbon analysis on DIC according to the method used for WOCE sampling was obtained. These samples were collected in acid-cleaned and pre-combusted 500 mL Pyrex flasks closed with a glass stopper greased with Apiezon grease. Samples were also fixed before sealing the bottles using 100 µL of saturated $HgCl_2$ solution. The glass stoppers were secured using a rubber band, flasks were placed in plastic bags and stored at room temperature until analysis, for which they will be submitted to the NOSAMS radiocarbon facility at Woods Hole Oceanographic Institution. Results will be compared with those obtained on 5 mL samples collected as described above.

Samples for radiocarbon analyses of DOC were taken at 10 stations, one of which was sampled in duplicate to enable replicate analyses (Tab. 6.1). Approximately 3 L of seawater were sampled from the Niskin bottles and stored in acid-cleaned collapsible cubitainers. 2 L of each sample were filtered over pre-combusted 25 mm glass fiber filters (GF/F, Whatman); the first 500 mL were discarded, and 1 L of filtered seawaterwas transferred into acid-cleaned 1 L brown HDPE flasks, acidified with 2 mL concentrated HCl (double-distilled) and stored at 4° C. Duplicate samples were taken from each depth at station PS128_56-1. Filters were packed in pre-combusted glass petri dishes or in Aluminium foil and frozen at –80° C.

Care was taken to avoid unnecessary contact of samples with any surfaces on board ship and containers in which the samples were stored. For example the samples in the ship's cooler were wrapped in plastic foil. This is necessary as during prior expeditions, radiocarbon tracer

work resulted in elevated (above natural) radiocarbon concentrations on some surfaces at several locations in the ship. A risk remains that the sampling programme for radiocarbon might be negatively impacted by the presence of this contamination.

Surface and deep water sampling for oxygen and carbon (of DIC) isotope and nutrient analyses

We sampled seawater from a total of 17 CTD stations with the rosette sampler deployments, for the characterisiation of modern physical ($\delta^{18}O$) and chemical (PO_4, DIC, NO_3, $\delta^{13}C$) oceanographic parameters (Tab. 6.1). The choice of stations and sampled water depth was made in accordance to the water sampling programme for REE, εNd and radiocarbon analyses. Samples for isotope and nutrient analyses were taken according to standard protocols immediately after the CTD rosette was retrieved into the hangar of *Polarstern*. Clean glass bottles with screw lids were flushed with sea water from the Niskin bottles, before fully filling the bottles bubble-free in overflow without air reservoir. From each sampled bottle depth we took the following standard series of samples: (1) one 100 mL glass bottle for oxygen isotope analysis, (2) one 50 mL glass bottle for stable carbon isotope analysis of Dissolved Inorganic Carbon ($\delta^{13}C_{DIC}$) and DIC concentrations, and (3) one 50 ml wide-necked PE plastic bottle with screw caps for phosphate and nitrate concentrations. All 50 mL samples for $\delta^{13}C_{DIC}$ were fixed with 100 µL of saturated $HgCl_2$ solution under a fume hood to stop biological activity. All glass bottles with screw caps were sealed airtight after sampling with a heated stearin/beeswax mixture to inhibit gas leakage during long-term storage. Samples were thereafter stored refrigerated in the cold rooms at +4° C (stable isotopes) or deep-frozen at –20° C (nutrients).

Multicorer water sampling

To connect water column-based data to the conditions recorded in microfossil proxy carriers within the sediment record, we sampled the bottom waters retrieved during Multicorer (MUC) deployments. Whenever possible, duplicate sample series for shore-based analyses of $\delta^{18}O$, $\delta^{13}C_{DIC}$, $DI^{14}C$ and nutrients (PO_4, NO_3) were taken from the two tubes assigned to benthic studies.

Sampling of bottom water from Multicores was carried out immediately after the MUC was back on deck (for all applications), before the tubes were retrieved from the sampling device, to minimise exposure and contamination of samples by interaction with ambient air. The sampling protocols given above for sea water stable isotope and nutrient samples were as well followed for all MUC bottom water samples.

Marine porewater extraction from Multicores

On PS128, a total of five surface sediment MUC stations were sampled for combined bottom water and sediment surface proxy analyses. These were chosen in combination with CTD stations (see Figs. 6.1 to 6.3; Tab. 6.2). Three sediment cores were used for these purposes. Two were sampled in 2 cm intervals under oxygen-free argon atmosphere in glove bags, aliquoting a small fraction for measurements of sedimentary physical properties at GEOMAR Kiel, and using the rest for porewater extraction. Per 2-centimeter interval one 50 mL centrifuge vial could be filled. These were centrifuged for 60 to 90 minutes onboard *Polarstern* prior to filtration and transfer of porewaters for (a) alkalinity, (b) nutrient and IC analyses, (c) trace metal concentration measurements, and at selected depths (d) for radiocarbon analyses. Alkalinity was measured onboard, nutrient, IC (both frozen) and trace elemental aliquots (filtered and acidified) will be analysed in Kiel.

A third Multicore at these stations was used to test the application of DGT® probes (i.e. active filter surfaces by a commercial manufacturer designed to extract 2+ and 3+ trace metals from

porewaters) in sediments. DGT® sediment probes were taken from their packing, washed with deionized water, placed within a Multicore and left to collect trace metals from the MUC for a total of 72 hours at 4° C. DGT® probes were then removed from the sediments and any attached sediment was washed off with deionized water. The DGT probes were placed in plastic bags for further processing at GEOMAR Kiel. The respective MUC was frozen and returned to the Marine Geology group. Regarding handling of the two sliced MUC sediments, one was kept for analyses at GEOMAR Kiel, while samples of the second core was also returned to the Marine Geology group after porewater extraction (in 50 mL centrifuge vials).

Underway sampling of POM from surface water

Surface water particulate organic matter was sampled during PS128 to calculate biomarkerbased proxies for environmental parameters including sea surface temperature (TEX_{86}, UK_{37}) and sea ice extend ($IPSO_{25}$). The water was obtained through an inlet in the ship's keel (~ 5 m.b.s.l.) and pumped through the internal pipeline system directly to the filtration unit, where it was passed through pre-combusted glass fibre filters (Whatman GFF, 142 mm diameter). Sampling was conducted for 1 h during transit times between stations, resulting in filtration volumes of 100–200 l. During each transect, physical parameters (water temperature and salinity) and environmental conditions (weather and sea ice conditions) were noted. A total of 50 filters were obtained from transects covering the entire geographical area of the expedition (Tab. 6.3). The filters were dried onboard for two days at 40° C and subsequently stored frozen (–20° C) until biomarker extraction, which will be conducted at AWI in Germany.

Tab. 6.3: Overview of Underway POC stations

#	Date	Latitude °S		Longitude	
		Start	End	Start	End
1	13.01.2022	59° 29.067‘	59° 39.043‘	02° 59.225‘ E	02° 51.414‘ E
2	15.01.2022	67° 12.734‘	67° 23.357‘	05° 14.599‘ W	05° 27.955‘ W
3	15.01.2022	67° 57.131‘	68° 06.135‘	06° 11.662‘ W	06° 22.953‘ W
4	17.01.2022	69° 42.489‘	69° 50.386‘	05° 54.744‘ W	05° 56.143‘ W
5	18.01.2022	70° 30.555‘	70° 32.904‘	08° 51.764‘ W	09° 03.337‘ W
6	19.01.2022	70° 04.074‘	70° 04.264‘	08° 31.956‘ W	08° 34.724‘ W
7	20.01.2022	70° 05.786‘	70° 08.203‘	07° 07.199‘ W	06° 54.041‘ W
8	22.01.2022	69° 45.561‘	69° 43.553‘	06° 02.957‘ W	06° 29.715‘ W
9	23.01.2022	68° 37.645‘	68° 48.545‘	06° 49.075‘ W	06° 32.226‘ W
10	24.01.2022	69° 27.380‘	69° 39.971‘	05° 42.200‘ W	06° 12.491‘ W
11	24.01.2022	70° 30.514‘	70° 36.232‘	08° 59.877‘ W	06° 12.491‘ W
12	25.01.2022	70° 14.621‘	70° 16.579‘	07° 31.593‘ W	09° 13.016‘ W
13	26.01.2022	70° 16.774‘	70° 11.394‘	07° 20.375‘ W	07° 25.505‘ W
14	26.01.2022	70° 10.526‘	70° 05.867‘	07° 29.822‘ W	07° 29.822‘ W
15	27.01.2022	70° 03.355‘	69° 59.970‘	08° 14.562‘ W	07° 35.091‘ W
16	28.01.2022	69° 17.315‘	69° 16.691‘	01° 16.159‘ E	01° 49.745‘ E
17	29.01.2022	68° 48.972‘	68° 46.644‘	10° 41.283‘ E	11° 44.882‘ E
18	31.01.2022	68° 21.104‘	68° 20.005‘	30° 36.065‘ E	31° 10.558‘ E
19	01.02.2022	67° 33.258‘	67° 31.077‘	38° 32.357‘ E	38° 58.612‘ E
23	05.02.2022	65° 30.651‘	65° 32.146‘	60. 32.166‘ E	60° 41.278‘ E
24	06.02.2022	65° 35.467‘	65° 38.503‘	63° 25.646‘ E	63° 35.202‘ E

#	Date	Latitude °S		Longitude	
		Start	End	Start	End
25	07.02.2022	65° 58.177‘	65° 58.498‘	63° 26.652‘ E	63° 23.955‘ E
26	08.02.2022	66° 26.476‘	66° 27.846‘	66° 45.399‘ E	66° 28.465‘ E
27	09.02.2022	67° 14.134‘	67° 06.141‘	65° 54.857‘ E	65° 41.676‘ E
28	10.02.2022	66° 54.420‘	66° 58.104‘	64° 50.205‘ E	65° 01.764‘ E
29	11.02.2022	66° 19.408‘	66° 17.908‘	60° 41.282‘ E	60° 25.719‘ E
30	12.02.2022	65° 44.729‘	65° 44.729‘	58° 54.490‘ E	59° 02.721‘ E
31	13.02.2022	65° 22.318‘	65° 23.353‘	55° 19.462‘ E	54° 45.350‘ E
32	14.02.2022	67° 26.875‘	67° 18.922‘	45° 52.271‘ E	45° 46.931‘ E
33	15.02.2022	66° 01.619‘	65° 33.651‘	49° 52.322‘ E	50° 17.506‘ E
34	16.02.2022	65° 07.518‘	64° 57.085‘	59° 35.267‘ E	59° 27.662‘ E
35	17.02.2022	64° 13.984‘	64° 04.304‘	56° 54.991‘ E	55° 51.760‘ E
36	18.02.2022	63° 04.167‘	62° 58.405‘	50° 22.408‘ E	49° 55.090‘ E
37	19.02.2022	61° 17.683‘	61° 11.136‘	43° 12.508‘ E	42° 50.040‘ E
38	19.02.2022	59° 58.915‘	59° 51.579‘	39° 04.248‘ E	38° 43.257‘ E
39	20.02.2022	58° 41.101‘	58° 33.287‘	35° 35.937‘ E	35° 16.627‘ E
40	20.02.2022	57° 53.518‘	57° 43.204‘	33° 42.224‘ E	33° 18.663‘ E
41	21.02.2022	56° 07.148‘	55° 57.690‘	29° 56.779‘ E	29° 38.424‘ E
42	22.02.2022	53° 22.100‘	53° 14.111‘	25° 47.016‘ E	25° 36.968‘ E
43	22.02.2022	52° 36.644‘	52° 36.644‘	24° 29.964‘ E	24° 14.159‘ E
44	23.02.2022	53° 37.394‘	53° 37.394‘	21° 35.060‘ E	21° 13.999‘ E
45	23.03.2022	52° 06.375‘	51° 55.151‘	19° 46.790‘ E	19° 45.638‘ E
46	24.02.2022	50° 13.316‘	49° 53.505‘	19° 35.455‘ E	19° 33.531‘ E
47	24.02.2022	48° 39.554‘	48° 24.561‘	19° 26.425‘ E	19° 25.008‘ E
48	25.02.2022	45° 30.310‘	45° 18.189‘	19° 08.996‘ E	19° 07.901‘ E
49	25.02.2022	44° 23.501‘	44° 04.038‘	19° 03.071‘ E	19° 01.379‘ E
50	26.02.2022	42° 02.979‘	41° 52.820‘	18° 51.007‘ E	18° 50.134‘ E

Preliminary results

Water column profiling

To determine which water masses are present in the CTD stations (Figs. 6.1–6.3), the neutral density (γ^n) (kg/m^3) was computed. Neutral Density is a particularly useful parameter while tracing water masses that undergo extreme pressure changes. In contrast to the isopycnals approach based on matching various potential density surfaces with a discrete set of reference pressures, Jackett & MacDougall (1997) computed a neutral density variable that is locally referenced: a well-defined function that incorporates all nonlinear terms in the equation of state for seawater, including the one arising from the pressure dependency of the thermal expansion coefficient (Orsi et al., 1999). We use the definition of Lower Circumpolar Deep Water (LCDW) as $28.1 < \gamma^n < 28.27$ kg m^3 and Antarctic Bottom Water (AABW) as $\gamma^n > 28.27$ kg m^3 (Orsi et al., 1999; Valla et al., 2018).

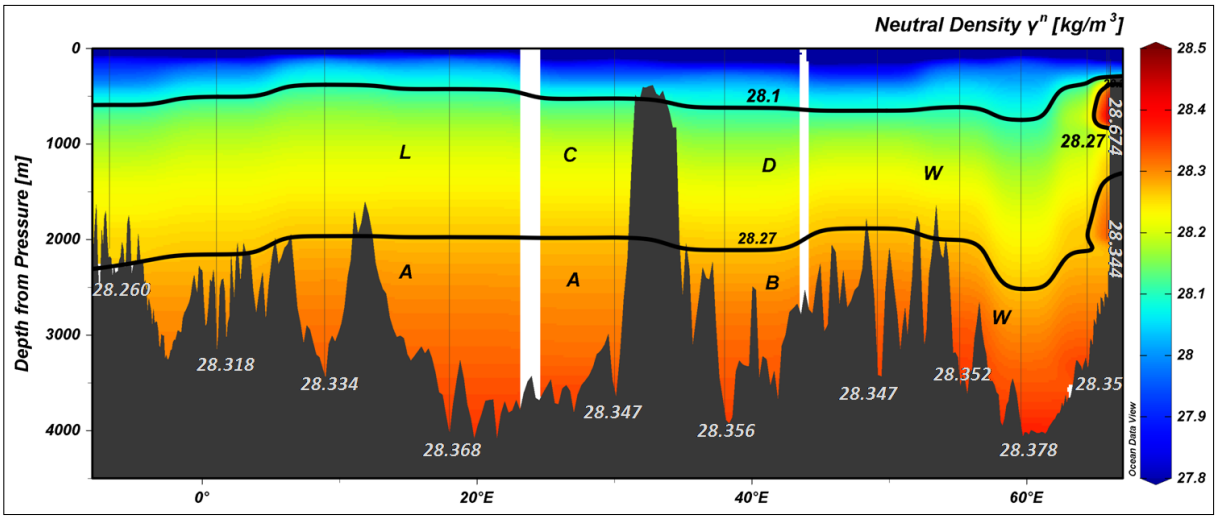

Fig. 6.4: Longitude and depth section from CTD stations during PS128. Colour bar indicates values of neutral density (γ^n) (kg/m^3). The black lines are isolines of equal γ^n for 28.1 and 28.27. Also, bottom values for γ^n are shown. Lower Circumpolar Deep Water (LCDW) and Antarctic Bottom Water (AABW) are indicated. GEBCO (6x6 minutes resolution) bathymetry is shown in dark grey.

In Figure 6.4 we present the preliminary results for a zonal section, showing the γn values with the borders for the LCDW and AABW from CTD stations during PS128 (Fig. 6.1). The bottom values are also shown to evaluate the difference between stations and depths. This could be an indication of different sources or flows from more dense shelf waters to mix and produce AABW. In Figure 6.5 we present an interpolation for sea surface temperatures (°C) in the study area observed during PS128. This surface plot shows the meridional gradient of this variable, and the difference between the more western stations relative to the ones in the east of this section under the influence not only of the Antarctica coast, also the presence of the Antarctic Circumpolar Current fronts. Further analysis will be made onshore focusing on particular stations or sections.

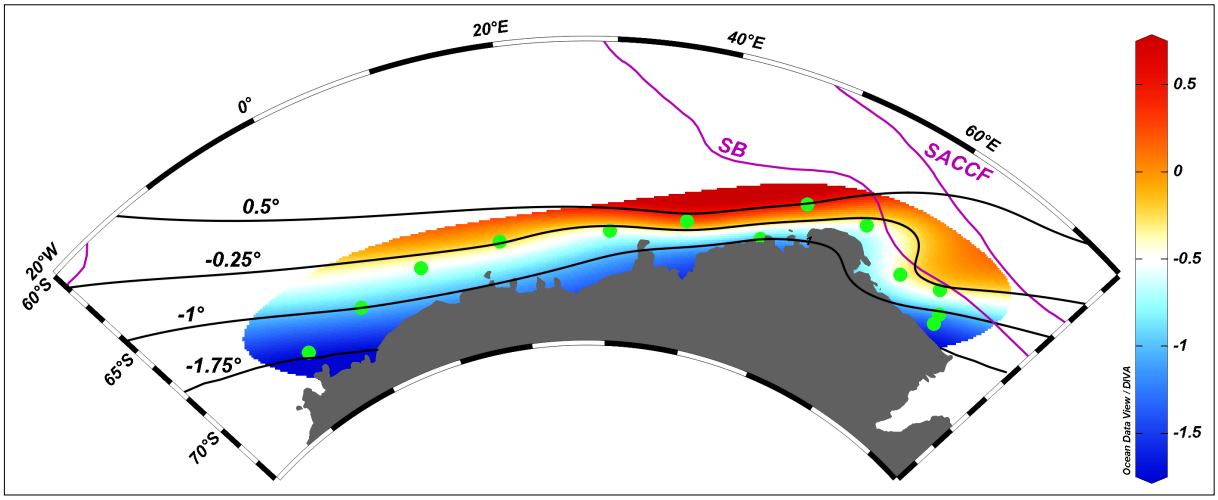

Fig. 6.5. Surface Temperature (°C) represented by the colour bar; interpolation from all CTD stations during PS128; isotherms in 0,75° C increments are represented in black curves. Antarctic Circumpolar Current (ACC) fronts are shown in purple lines (Orsi et al., 1995).
SACCF = Southern Antarctic Circumpolar Current Front; SB = Southern Boundary

REE and εNd

All planned analytical work could be carried out onboard *Polarstern*, yet all Nd isotope and trace metal concentration sub-samples will need further processing prior to mass spectrometric measurements at GEOMAR Kiel. We note that it was extremely helpful to have two MQ systems available in the chemistry lab, which significantly accelerated the required cleaning work during and after finalisation of the sampling campaign.

Oxygen and salinity

The Winkler-titrated oxygen concentration results reproduced remarkably well as evident from many triplicate results for both CTD-bottled and Multicore water samples. In total 213 Winkler titrations were carried out on CTD water samples, as well as 33 on MUC water. The MUC oxygen concentrations were almost always within error of oxygen concentrations of the lowermost CTD sample and only lower at one site with elevated surface ocean productivity. All sites in the study area are situated in areas of pronounced bottom water currents, hence the observed oxygen concentrations may indeed be realistic to generally limited oxygen depletion in bottom waters. Whether these data can be treated as reliably reflecting bottom water concentrations (i.e., not having exchanged with the water column during ascent of the MUC) will be further evaluated onshore. The CTD-derived oxygen sensor data will also be further processed with colleagues at AWI Bremerhaven, aiming to remove the spurious trends in water depths below 2,000 m. Highest oxygen concentrations in the deeper water column (below 1,500 m) were observed at the easternmost location (PS128_36-1), reflecting the presence of recently subducted newly formed AABW, most likely locally sourced from the Cape Darnley area (*cf*. Ohshima et al., 2013).

Given that only one CTD sensor worked at the first seawater station, salinity cross-calibration checks were carried out early during PS128 comparing the CTD-derived salinity data to bottled analyses of salinity using the shipboard Optimare precision salinometer in the salinometer lab. Salinity measurements were carried out at stations 1–3, 4–1, 26–1, 27–1 and 29–1 and agreed with CTD-based salinity data. Salinities obtained with both methods agreed well, making further tests unnecessary.

Radiocarbon analyses

No analytical work was planned for onboard *Polarstern*, and sample processing was restricted the minimum necessary extent (filtration of seawater to obtain DOC samples). It is necessary to avoid any unnecessary handling of samples on board in order to minimise the risk of sample contamination with above-natural radiocarbon levels derived from labelled substances used on board during previous cruises. Analyses will be carried out at AWI Bremerhaven using the radiocarbon facility MICADAS.

Data management

All marine geochemical data collected will be archived, published and disseminated according to international standards by the World Data Center PANGAEA Data Publisher for Earth & Environmental Science (https://www.pangaea.de) within two years after the end of the cruise at the latest. By default, the CC-BY license will be applied.In all publications based on this expedition, the Grant No. AWI_PS128_02 will be quoted and the following publication will be cited:

Alfred-Wegener-Institut Helmholtz-Zentrum für Polar- und Meeresforschung (2017) Polar Research and Supply Vessel POLARSTERN Operated by the Alfred-Wegener-Institute. Journal of large-scale research facilities, 3, A119. http://dx.doi.org/10.17815/jlsrf-3-163.

This expedition was supported by the Helmholtz Research Programme "Changing Earth – Sustaining our Future" Topic 2, Subtopic 2.1.

References

Brovkin V, Ganopolski A, Archer D & Munhoven G (2012) Glacial CO2 cycle as a succession of key physical and biogeochemical processes. Climate of the Past 8:251-264.

Caldeira K & Duffy PB (2000) The role of the Southern Ocean in uptake and storage of anthropogenic carbon dioxide. Science 287:620-622.

Druffel E, Griffin S, Lewis CB, Rudresh M, Garcia NG, Key RM, McNichol AP, Haukusson NE & Walker BD (2021) Dissolved Organic Radiocarbon in the Eastern Pacific and Southern Oceans. Geophysical Research Letters 48. https://doi.org/10.1029/2021GL092904.

Fahrbach E, Rohardt G & Krause G The Antarctic coastal current in the southeastern Weddell Sea. Polar Biol 12:171–182 (1992). https://doi.org/10.1007/BF00238257

Jackett DR & MacDougall TJ (1997). A neutral density variable for the world's oceans. Journal of Physical Oceanography 27:237–263.

Landschützer P, Gruber N, Haumann FA, Rödenbeck C, Bakker DCE, van Heuven S, Hoppema M, Metzl N, Sweeney C, Takahashi T, Tilbrook B & Wannikof R (2015) The reinvigoration of the Southern Ocean carbon sink. Science 349:1221-1224

MacGilchrist GA, Naveira Garabato AC, Brown PJ, Jullion L, Bacon S, Bakker DCE, Hoppema M, Meredith MP & Torres-Valdés S (2019) Reframing the carbon cycle of the subpolar Southern Ocean. Science Advances 5. https://doi.org/10.1126/sciadv.aav6410.

Meijers AJS, Klocker A, Bindoff NL, Williams GD & Marsland SJ (2010) The circulation and water masses of the Antarctic shelf and continental slope between 30 and 80° E. Deep Sea Research Part II: Topical Studies in Oceanography 57:723-737.

Ohshima K, Fukamachi Y, Williams G et al. (2013) Antarctic Bottom Water production by intense sea-ice formation in the Cape Darnley polynya. Nature Geosci 6, 235–240. https://doi.org/10.1038/ngeo1738

Orsi AH, Whitworth III T & Nowlin WD (1995) On the meridional extent and fronts of the Antarctic Circumpolar Current. Deep-Sea Research I 42(5):641–673.

Orsi AH, Johnson GC & Bullister JL (1999) Circulation, mixing, and production of Antarctic Bottom Water. Progress in Oceanography 43:55-109.

Pöppelmeier F, Gutjahr M, Blaser P, Oppo DW, Jaccard SL, Regelous M, Huang KF, Süfke F & Lippold J (2020) Water mass gradients of the mid-depth Southwest Atlantic during the past 25,000 years. Earth and Planetary Science Letters 531:115963.

Purkey SG, Smethie WM, Gebbie G, Gordon AL, Sonnerup RE, Warner MJ & Bullister JL (2018) A synoptic view of the ventilation and circulation of Antarctic Bottom Water from chlorofluorocarbons and natural tracers. Annu Rev Mar Sci 10:503-527.

Rickli J, Gutjahr M, Vance D, Fischer-Gödde M, Hillenbrand CD & Kuhn G (2014) Neodymium and hafnium boundary contributions to seawater along the West Antarctic continental margin. Earth and Planetary Science Letters 394:99-110.

Roy M, van de Flierdt T, Hemming SR & Goldstein SL (2007) 40Ar/39Ar ages of hornblende grains and bulk Sm/Nd isotopes of circum-Antarctic glacio-marine sediments: Implications for sediment provenance in the southern ocean. Chemical Geology 244:507-519.

Stichel T, Frank M, Rickli J & Haley BA (2012) The hafnium and neodymium isotope composition of seawater in the Atlantic sector of the Southern Ocean. Earth and Planetary Science Letters 317-318: 282-294.

Valla D, Piola AR, Meinen CS & Campos E (2018) Strong mixing and recirculation in the northwestern Argentine Basin. Journal of Geophysical Research: Oceans 123:4624–4648. https://doi.org/10.1029/2018JC013907

Williams GD., Nicol S, Aoki S, Meijers AJS., Bindoff NL, Iijima Y, Marsland SJ & Klocker A (2010). Surface oceanography of BROKE-West, along the Antarctic margin of the south-west Indian Ocean (30–80°E). Deep Sea Research Part II: Topical Studies in Oceanography 57:738-757. https://doi.org/10.1016/j.dsr2.2009.04.020

Williams GD, Herraiz-Borreguero L, Roquet F, Tamura T, Ohshima KI, Fukamachi Y, Fraser AD, Gao L, Chen H, McMahon CR, Harcourt R & Hindell M (2016) The suppression of Antarctic bottom water formation by melting ice shelves in Prydz Bay. Nature Communications 7:12577.

7. CONTINENTAL GEOLOGY AND GEODESY

Sonja Berg[1], Bernd Wagner[1], Ole Bennike[2], Niklas Leicher[1], Maria Kappelsberger[3], Karl Heidrich-Meisner[3], Marcus Gutjahr[4]
Not on board: Martin Melles[1], Mirko Scheinert[3], Duanne White[5]

[1]DE.UNI-Köln, [2]DK.GEUS, [3]DE.TU-Dresden, [4]DE.GEOMAR, [5]AU.UNI-Canberra

Grant-No. AWI_PS128_06

During the expedition PS128 we visited Thala Hills, an unglaciated coastal area in Enderby Land (Figs. 7.1 and 7.3). During our stay from the 02 to 14 February 2022 we collected lake sediments, glacial erratics and soil crusts (see section 7.1), conducted repeated GNSS measurements (see section 7.2) and sampled debris-rich glacier ice for provenance analysis in Thala Hills and at two other sites along the cruise track of PS128 (see section 7.3).

Field work in the Thala Hills was carried out by a joint team, with members from of the Institute of Geology and Mineralogy, University of Cologne, the Institut für Planetare Geodäsie, TU Dresden and the Geological Survey of Denmark (GEUS). The work was logistically supported by the Belarussian Antarctic Expedition (BAE), which operates the summer station *Gora Vechernyaya* in the study area.

7.1 Late Quaternary deglaciation and climate history of Thala Hills, Enderby Land

Objectives

The East Antarctic Ice Sheet (EAIS) has long been recognised as stable due to its characteristics of being mostly being grounded on bedrock lying above sea level (in contrast to the mostly marine-based West Antarctic Ice Sheet). However, in the past decade modelling approaches and field evidence have revealed that processes related to basal ice shelf melting, including intrusions of relatively warm Circumpolar Deep Water (CDW) into the ice shelf cavities, may also have a destabilising effect on some portions of the EAIS (e.g., Deconto & Pollard, 2016, Rintoul, 2018). As opposed to afflicted regions such as Wilkes Land, minimal changes or even mass-gain have been observed in Enderby Land (Rignot et al., 2019). In this respect paleoglaciological reconstructions from this part of the EAIS may provide information how far ice and bed characteristics foster ice sheet stability. The maximum ice sheet extent during the Last Glacial Maximum (LGM, 19 to 23 ka) as well as the subsequent retreat history is still largely unconstrained for Enderby Land (Bentley et al., 2014). Exposure ages of glacial erratics indicate ice sheet retreat starting in the early to mid-Holocene (ca. 9 to 5 ka) at the flanks of two outlet glaciers in Enderby Land and eastern Dronning Maud Land (White & Fink, 2014; Kawamata et al., 2020). This timing of post-glacial ice retreat differs from coastal areas in Mac. Robertson Land (easternmost working area of EASI-1), where post-LGM ice-sheet thinning occurred significantly earlier and was likely initiated by rising eustatic sea level around 14 ka (Mackintosh et al., 2011). The different timing of ice retreat points to different regional drivers of deglaciation, which may be coupled to region-specific oceanographic as well as topographic properties.

In order to better understand the drivers of ice sheet stability/instability in relation to region-specific characteristics, such as bed topography, shelf geometry and oceanographic parameters, detailed studies are needed from less-studied regions like Enderby Land.

Within the scope of expedition PS128 (EASI-1) we obtained new field data and sediment samples from Thala Hills, an unglaciated coastal area in Enderby Land (Fig. 7.1), to constrain the timing of ice sheet retreat and subsequent fluctuations in the presently un-glaciated area and to reconstruct climatic conditions following local deglaciation.

Work on land

Main working area was the western part of Thala Hills, which hosts the mothballed Russian *Molodezhnaya Station* (termed Molodezhnaya area in the following) (Fig. 7.1). Furthermore, we visited the Blisnetzov Peninsula (BLIS) (Fig. 7.1) and *Gora Vechernyaya* (Mountain Evening) (Fig. 7.5.) for lake sediment sampling and terrestrial cosmogenic nuclide (TCN) dating of glacial deposits. For the entire time on land our camp was set up in the area of *Molodezhnaya Station*, where we were based in a building provided by the BAE. Lakes and other sampling sites were reached by snowmobile and on foot, depending on the accessibility.

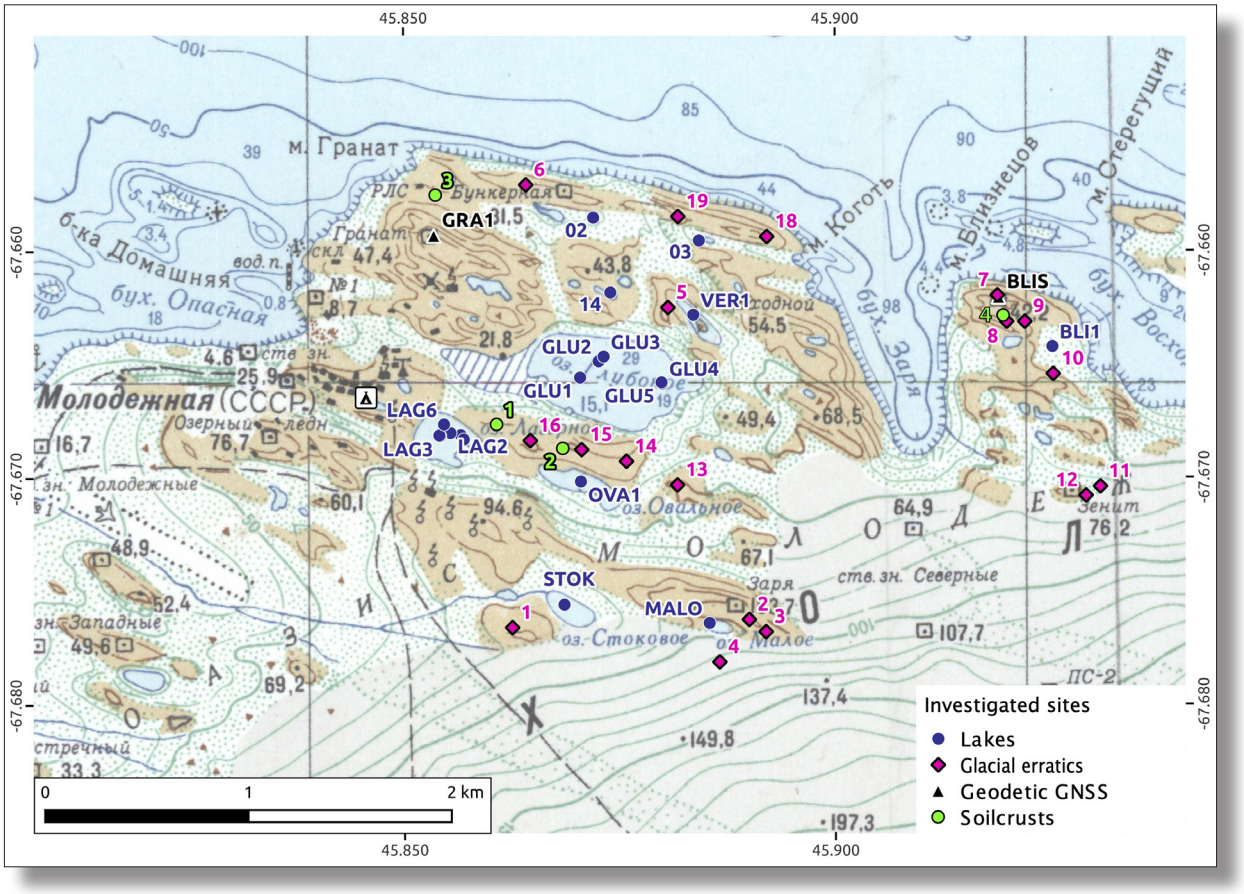

Fig. 7.1: Map of the western part of Thala Hills (Molodezhnaya area); blue dots indicate sites of lake sediment and/or water sampling, pink diamonds sites sampled for cosmogenic exposure dating, green dots sites of soil sampling, black triangles sites of geodetic GNSS measurements.

Our work was focused on lakes, which do not freeze until the ground, to obtain undisturbed sediment successions. Prior to our work on land, A. Gaidashov and E. Korzun (BAE) visited several lakes in the Molodezhnaya area in late December 2021 and late January 2022 to measure ice thickness and water depth, which allowed for a preselection of potential targets

for sediment coring. During this survey, water samples were taken and water properties were measured such as electrical conductivity (Tab. 7.1). We visited four lakes for sediment coring in the Molodezhnaya area (Lake Lagernoye, Lake Glubokoye, Lake Ovalnoye and Lake Promernoye), and one un-named lake at Blisnetzov Peninsula and Lake Niznee at *Gora Vechernyaya*. Lake ice holes were drilled using 2-stroke ice auger to access the water column for water and sediment sampling (UWITEC gravity and piston corer, Russian Peat corer). Samples for TCN dating of glacial erratics were collected along two transects from the ice sheet margin to the coast to infer the timing of ice sheet retreat.

Preliminary results

The bedrock in Thala Hills is part of the metamorphic Rayner Complex that comprises Precambrian sedimentary and igneous rocks metamorphosed under amphibolite and granulite facies conditions (Krylov & Shukolyukov, 2014). The hills in the Molodezhnaya area are mostly north to north-west trending ridges that increase in altitude inland and are bounded by the ice sheet to the south. The valleys between the ridges host several lakes at different altitudes (Fig. 7.1). The morphology to some extent reflects the strike direction of bedrock structures, which consist of changes in lithology and associated different resistance to weathering processes. During the time of our field work, snow drifts were a prominent feature in the central part of the Molodezhnaya area, covering the eastern ends of the ice-covered lakes and, presumably, accumulating parallel to the predominant direction (south, south east) of catabatic winds.

The contact between the ice sheet and land areas is quite smooth (no ice cliffs) and is mostly masked by overlying snow drifts. In the season 2021/22 large meltwater streams from the ice sheet drained into the ocean to the east and to the west of Molodezhnaya in December and the first half of January (pers. comm. Aleksei Gaidashov), but were already refrozen when we arrived in the study area in early February. These meltwater streams were deflected by the southernmost ridges of Molodezhnaya area and did not overflow into investigated lakes. During our stay snow melt on the marginal ice sheet and on land continued. Some slopes became free of snow, but most snow drift deposits seem to be multi-year features. Sea ice was closed when we arrived, but broke up within few days and completely disintegrated by mid-February.

Lakes and sediments

During our field work in Thala Hills most lakes were ice covered by multi-year lake ice, exceeding 3 m in ice thickness at most investigated lakes (Tab. 7.1). Some lakes likely form a moat (seasonal melting of lake ice along the shore) in summer, but this was refrozen by the time of our observation in February. The moat zone was represented by blue ice (smooth surface compared to the rough multi-year ice in the lakes centers) and blue colour (only few air bubbles included compared to the older ice (Fig. 7.2.). Few (likely) shallow lakes were not ice covered or started to thaw during the two weeks of our stay.

Measurement of lake water conductivities from nine lakes in the Molodezhnaya area shows that lakes closer to the coast have higher salinities than lakes closer to the ice sheet margin (Tab. 7.1). The salinity likely reflects the input of sea salt (either direct aeolian input from sea spray or surficial run-off from the surrounding bedrock) and input of meltwater from seasonal snow and ice sheet melt.

We selected six lakes, which were not frozen until the ground, for sediment coring. We found that post-glacial sedimentation in all lakes is dominated by biogenic sedimentation, which is reflected in centimeter to multi-decimeter thick deposits of microbial/algae mats that overlay clastic sediments or bedrock.

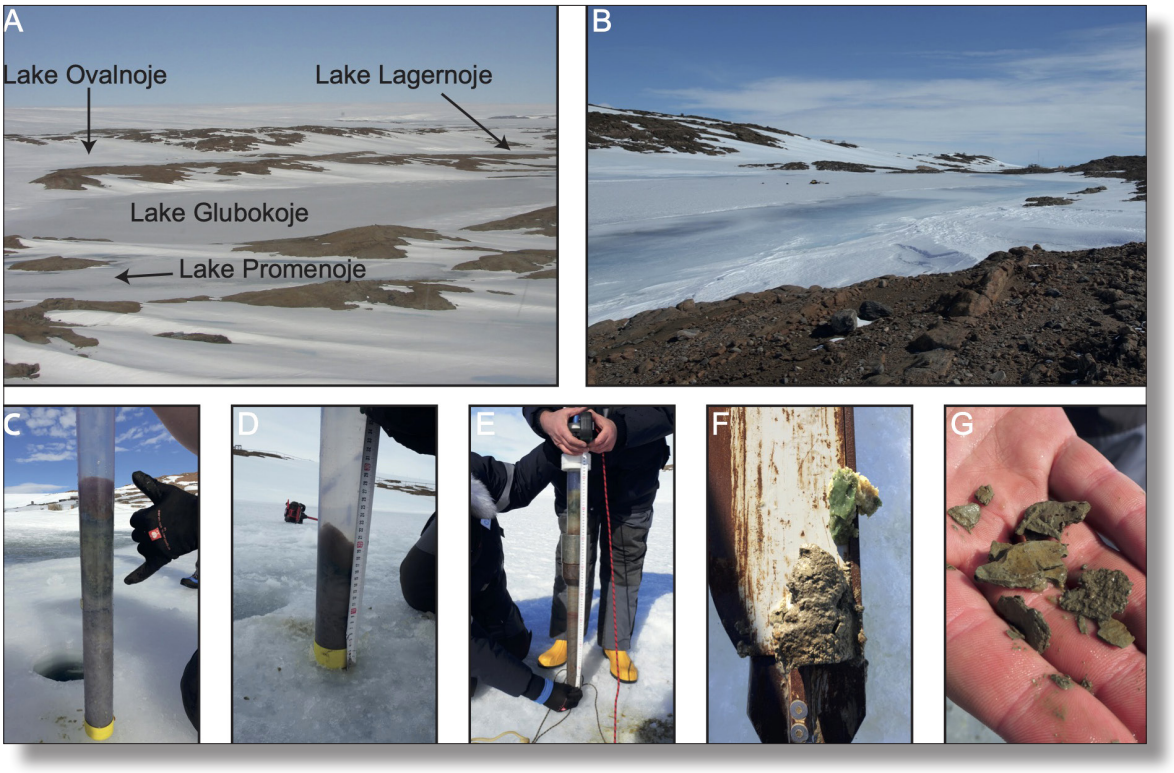

Fig. 7.2: Selected lakes and sediment samples from lakes in the Thala Hills: A) Overview of studied lakes Glubokoye, Promenoye, Ovalnoye and Lagernoye in Molodezhnaya; B) Blue lake ice indicates moat formation at Lake Ovalnoye in summer. C) Core NIZ22_6 from Lake Niznee D) Core LAG22_1 from Lake Lagernoye. E) Core OVA22_2 from Lake Ovalnoye F) Russian peat corer sample LAG22_4 G) Solidified sediment chips from LAG22_3

Lake Lagernoye

Lake Lagernoye is located directly to the East of *Molodezhnaya Station* and served as its drinking water reservoir. The lake has an extent of about 320 m x 190 m with a relatively even bathymetry with a water depth of 4.1 m and a conductivity of approximately 63 µS/cm. A sill in the NE of the lake may allow for an overflow into Lake Glubokoye at higher lake levels. Sediment sampling at all six investigated sites indicate a heterogeneous distribution of algae mats and sediments varying in thickness between c. 1 and 20 cm (Fig. 7.2). Solidified clastic sediment chips were recovered at station LAG_6 (LAG22_3), whereas elsewhere no sediments (LAG-5) or only algae mats were cored with the gravity corer. A Russian peat corer was subsequently used to increase penetration capabilities, but penetration was stopped by bedrock at all sites few cm below the algae mats (Fig. 7.2.F) or confirmed the lack of any sediments. Recovered clastic sediments were poorly sorted and of angular shape, similarly to the weathering products identified in the surrounding hills.

Lake Ovalonoye

Lake Ovalonoye is located to the E of Lake Lagernoye and has a length of 460 m and a width of 140 m. The water depth was determined to 8.4 m and a mean conductivity of 48 µS/cm was measured (Tab. 7.1). The lake has an overflow to Lake Glubokye towards its SE end, which was not active during the observation period. The blueish lake ice at the margin of the lake indicates a potential moat and thus marginal thawing during the summer season (Fig. 7.2.B). At site OVA 1, three gravity corer deployments revealed up to 70 cm thick algae mats underlain by ca. 8 cm of clastic sediment, which was recovered by Russian Peat Corer. Similar to Lake Lagernoye, a deeper penetration was hampered by the bedrock.

Tab. 7.1: Lakes surveyed for lake ice thickness, water depth, lake water conductivity and sediment thickness

Site	Longitude	Latitude	Altitude [m asl]	Ice thickness [m]	Water depth [m]	Water conductivity [µS/cm]	Sediment thickness [cm]
Lake Glubokoye	S67°39‘53.5“	E045°52‘21.3“	12	3.0	22.4-32.4	11-39	10-90
Lake Lagernoye	S67°40‘5.28“	E045°51‘14.75“	21	3.1	4.1	*57-70	0-20
Lake Ovalonoye	S67°40’12.64”	E045°52’13.8”	29	3.8	8.4	*48	70
Lake Promenoye	S67°39’46.2”	E045°53’00.8”	33	3.1	5.5	*102	10
Lake Blisnetzov	S67°39‘51.25“	E045°55‘30.7“	> 20	2.8	7.2	-	< 2
Lake Niznee	S67°39‘22.82“	E046°9‘31.26“	31	0.2- >1m	4.2	50	95-130
*Lake Stokovoye	S67°40‘30.36“	E045°51‘54.97“	78	>4	-	9-69	n.d.
*Lake Maloye	S67°40‘35.11“	E045°53‘7.44“	100	>4	-	16	n.d.
*Lake 14	S67°39‘37.33“	E045°52‘52.07“	> 30	>4	-	71	n.d.
*Lake 03	S67°39‘34.42“	E045°53‘3.23“	18	>4	-	752	n.d.
*Lake 02	S67°39‘30.78“	E045°52‘43.43“	30	>4	-	369	n.d.

** By the time of the observations on the 21.12.2012 and 22.01.2022 the lake ice thickness exceeded 4 m and the underlying water column could not be accessed. Water samples were taken from water inside the ice hole.*

Lake Glubokoye

Lake Glubokoye is located in the center of the Molodezhnaya area, between the coast and the ice sheet of the western Thala Hills. It is the largest and deepest lake of the area, with an extent of 1,000 x 500 m and a water depth between 20 and 33 m, which is deepening towards the NE. Lake level changes of 7 – 8 m have been reported to occur every 7 – 10 years (Sharov et al. 2015, A. Gaidashov, pers. comm.) and may have caused formation of a snow cliff observed on the eastern end of the lake. By the time of our fieldwork the lake level was well below the outflow on the north-western side of the lake. The hydrological parameters of the lake were investigated in two water profiles with a 5 m resolution at station GLU1 and GLU6. The temperature rises from 0.5° C directly below the lake ice to c. 4° C close the lake bottom, and conductivity ranges from 11 µS/cm directly below the ice to 39 µS/cm in the bottom water. Water samples were taken for lab-based analyses of nutrient, radiocarbon and trace metal concentrations. At five stations the lake was investigated for its sedimentary infill using a UWITEC gravity corer at all sites (Fig. 7.1). The recovered sediment thicknesses vary between 10 and 90 cm, with the highest sediment recovery in the deep NE area of the lake. At the deepest station GLU6, a UWITEC piston corer was used. Recovery of the piston corer was similar to the recovery of the gravity cores. Penetration was hampered either by coarse-grained sediments (pebbles) or bedrock lying directly below the algae mats.

Tab 7.2: List of sediment cores/samples obtained from Lakes in Thala Hills. Coring devices used were gravity corer (GC), piston corer (PC), Russian Peat Corer (RPC)

Lake/Station ID	Latitude (South) [dms]	Longitude (East) [dms]	Sample ID	Coring device	Core lengths [cm]
Lake Glubokoye					
GLU2	67°39‘53.5“	45°52‘21.3“	GLU22_1	GC	10
GLU3	67°39‘ 52.81“	45° 52‘ 23.38“	GLU22_2	GC	20
GLU4	67°39’57.1”	45° 52’47.7”	GLU22_4	GC	76
GLU4	67°39’57.1”	45° 52’47.7”	GLU22_5	GC	93
GLU4	67°39’57.1”	45° 52’47.7”	GLU22_6	GC	77
GLU6	67°39‘ 56.92“	45°52‘47.52“	GLU22_7	GC	66
GLU6	67°39‘ 56.92“	45°52‘47.52“	GLU22_8	PC	56
Lake Ovalonoye					
OVA1	67° 40’12.6”	45° 52’13.8”	OVA22_1	GC	-
	67° 40’12.6”	45° 52’13.8”	OVA22_2	GC	70
	67° 40’12.6”	45° 52’13.8”	OVA22_3	GC	0
	67° 40’12.6”	45° 52’13.8”	OVA22_4	RPC	basal sediments
Lake Promenoye					
VER1	67° 39’46.2”	45° 53’00.8”	VER22_1	GC	< 2
	67° 39’46.2”	45° 53’00.8”	VER22_2	GC	10
Lake Lagernoye					
LAG3	67°40‘ 5.38“	45°51‘ 15.13“	LAG22_1	GC	20
LAG3	67°40‘ 5.38“	45°51‘ 15.13“	LAG22_2	GC	22
LAG6	67°40‘ 3.53“	45°51‘ 16.7“	LAG22_3	GC	10
LAG1	67°40‘5.24“	45° 51‘ 23.69“	LAG22_7	RPC	basal sediments
LAG2	67°40‘4.9“	45° 51‘ 19.39“	LAG22_8	RPC	basal sediments
LAG3	67°40‘5.38“	45° 51‘ 15.13“	LAG22_5	RPC	basal sediments
LAG4	67°40‘5.28“	45° 51‘ 14.75“	LAG22_4	RPC	basal sediments
	67°40‘3.53“	45°51‘16.7“	LAG_22_6	RPC	basal sediments
Lake Niznee					
	67°39‘30.78“	45°52‘43.43“	NIZ_22_1	-	150
	67°39‘30.78“	45°52‘43.43“	NIZ_22_2	-	135
	67°39‘22.82“	46°9‘31.26“	NIZ_22_3	GC	42
	67°39‘22.82“	46°9‘31.26“	NIZ_22_4	GC	97.5
	67°39‘22.82“	46°9‘31.26“	NIZ_22_5	GC	64.5
	67°39‘22.82“	46°9‘31.26“	NIZ_22_6	GC	

All sediment cores (six gravity cores, one piston core) recovered from Lake Glubokoye are composed of water rich microbial/algae mats, which show layering of variable colour (white, green, red), consistency and thickness. Below the algae mats a several centimeter thin layer of clastic sediments was found at sites in the NE, most likely representing the initial sedimentation of lake formation after the ice retreat.

Lake Promenoye

Lake Promenoye is located on a seaward ridge close to Lake Glubokoye and is 330 m long and 100 m wide. The lake has a central bedrock island and a water depth of 5.5 m, measured at station VER1 to the north of the island. The relatively high water conductivity of 102 µS/cm is most likely related to its closer vicinity to the sea compared to the other lakes. The thickness of algae mats at station VER1 is about 10 cm. The algae mats were dark greenish and fluffy in the surface layers and consisted of whitish and stiff at the bottom. We did not recover clastic sediments at the base of the algae mats, which likely initially formed directly on bedrock.

Lake Blisnetzov

Lake Blisnetzov is located on the Blisnetzov Peninsula east of Molodezhnaya and is a ca. 150 x 40 m large lake, with a water depth of about 7.2 m at site BLI1. The lake is likely fed by meltwater from the snow-covered slopes surrounding the lake. Sediment infill at the investigated site BLI1 is less than 2 cm and also consists of algae mats, similar to the other investigated lakes.

Lake Niznee

Lake Niznee is located in the eastern part of Thala Hills (*Gora Vechernyaya*) in the vicinity of the Belarussian station. The lake consists of two basins with an overall dimension of 190 x 110 m. The basins are separated by snow drift deposits of up to 5 m in thickness (A. Gaidashov, pers. comm.). By the time of our visit the lake was ice covered, but ice thickness was only c. 20 cm at the coring site in the central part of the northern basin, which had a water depth of 4.2 m. The conductivity of the lake is c. 50 µS/cm. At site NIZ1 four gravity cores were retrieved from two ice holes, recovering 40 – 95 cm of algae mats superposing clastic sediments at the bottom. In addition, two up to 150 cm long, sediment cores from Lake Niznee were sampled by the Belarussian collaboration partners (NIZ_22_1 and NIZ_22_2).

Sampling of glacial erratics

In the eastern part of Molodezhnaya many buildings, roads and other remnant constructions (posts, wires, pipes etc.) indicate intensive human activities, which may also have included displacement of surficial sediments. Therefore, sampling of glacial erratics was avoided in the vicinity of the *Molodezhnaya Station* and at sites of obvious constructions due to possible anthropogenic reworking. Depending on the availability of suitable samples, we either collected whole rocks or chipped off the surface of large boulders. If possible, we also sampled the underlying bedrock to take into account site specific effects such as erosion rates and inheritance. We sampled a total of 19 sites, most of them in Molodezhnaya and Blisnetzov and one site at Gora Vechernaya (Fig. 7.1 and Tab. 7.3).

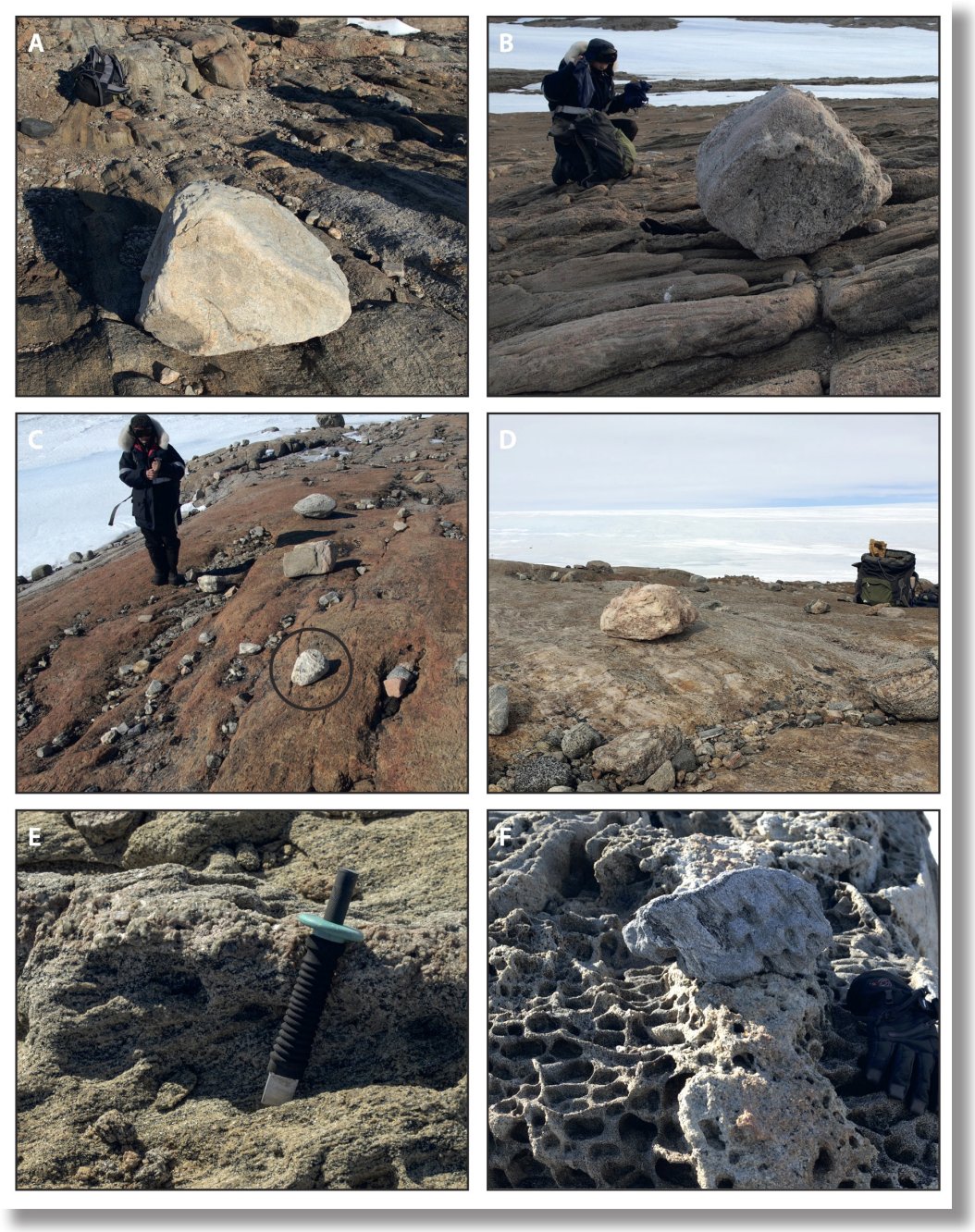

Fig. 7.3: Selected cosmogenic nuclide sampling sites:
A) Boulder at site COSMO14 on moderately weathered bedrock B) Boulder at site COSMO06 on intensively weathered bedrock C) Small boulder at site COSMO12 on relatively fresh bedrock surface D) Boulder at site Cosmo01 close to the present-day ice sheet margin
E) Differential weathering at site COSMO10: Quartz vein protruding from surrounding bedrock
F) Site COSMO07: erratic with tafoni-type of weathering close to the coast.

The glacial erratics were abundant in most parts of Thala Hills. Only at the eastern-most ridges at the coast of Molodezhnaya (sites 18 and 19) no glacial erratics were found, which may be due to extensive weathering and disintegration of erratics in this area. Glacial erratics as well as the underlying bedrock showed a distinct gradient in weathering, with least weathered material in proximity to the present-day ice sheet margin and intensive weathering features (such as tafoni-type and differential weathering) towards the sea-ward side (Fig. 7.3). This

may reflect a step-wise ice sheet retreat across the area, but could also be a result of more intensive weathering in areas affected by sea spray. Further analyses will provide information on the age of glacial deposits and result in a first comprehensive deglaciation history of the area.

Tab 7.3: Sites sampled for glacial erratics; at most sites replicate sampling of erratics and sampling of bedrock could be conducted. See Figure 7.1 for locations of sampling sites.

Site ID	Latitude (South) [dms]	Longitude (East) [dms]	Elevation (approximate) [m asl]
COSMO01	67° 40‘ 35.796“	45° 51‘45.144“	90
COSMO02	67° 40‘ 34.572“	45° 53‘ 24“	108
COSMO03	67° 40‘ 36.516“	45° 53‘ 31.02“	105
COSMO04	67° 40‘ 41.304“	45° 53‘11.652“	116
COSMO05	67° 39‘ 45.036“	45° 52‘50.268“	47
COSMO06	67° 39‘ 25.53“	45° 51‘ 51.01“	22
COSMO07	67° 39‘ 43.13“	45° 55‘ 7.75“	33
COSMO08	67° 39‘ 47.3“	45° 55‘ 11.63“	33
COSMO09	67° 39‘ 47.31“	45° 55‘ 19.18“	9
COSMO10	67° 39‘ 55.59“	45° 55‘ 31.03“	33
COSMO11	67° 40‘ 13.46“	45° 55‘ 50.7“	56
COSMO12	67° 40‘ 14.9“	45° 55‘ 44.73“	59
COSMO13	67° 40‘ 13.21“	45° 52‘ 54.12“	51
COSMO14	67° 40‘ 9.43“	45° 52‘ 32.83“	39
COSMO15	67° 40‘ 7.57“	45° 52‘ 14.13“	41
COSMO16	67° 40‘ 6.12“	45° 51‘ 52.72“	41
COSMO17	67° 39‘ 19.39“	46° 9‘ 36.34“	40
COSMO18	67° 39‘ 33.81“	45° 53‘ 31.53“	14
COSMO19	67° 39‘ 30.6“	45° 52‘ 54.46“	20

Sampling of soil crusts

Biological soil crusts and their biodiversity were not widely investigated in terrestrial areas of Enderby Land so far. We collected samples of biological soil crusts for biodiversity studies in collaboration with Karin Glaser (University of Rostock). The samples obtained from Thala Hills will be used to characterise the microbial networks and functionality in these unique ecosystems. The results will provide a baseline for the current state of microbial diversity, which is needed to document environmental changes on the microbial level.

At many sites in Thala Hills, where the ground was free of snow cover and consisted of loose sediment, the surface was colonised by soil crusts and mosses. Samples for the analysis of species assemblages in these biological soil crusts were taken at four sites in Molodezhnaya and Blisnetzov Peninsula (Fig. 7.4).

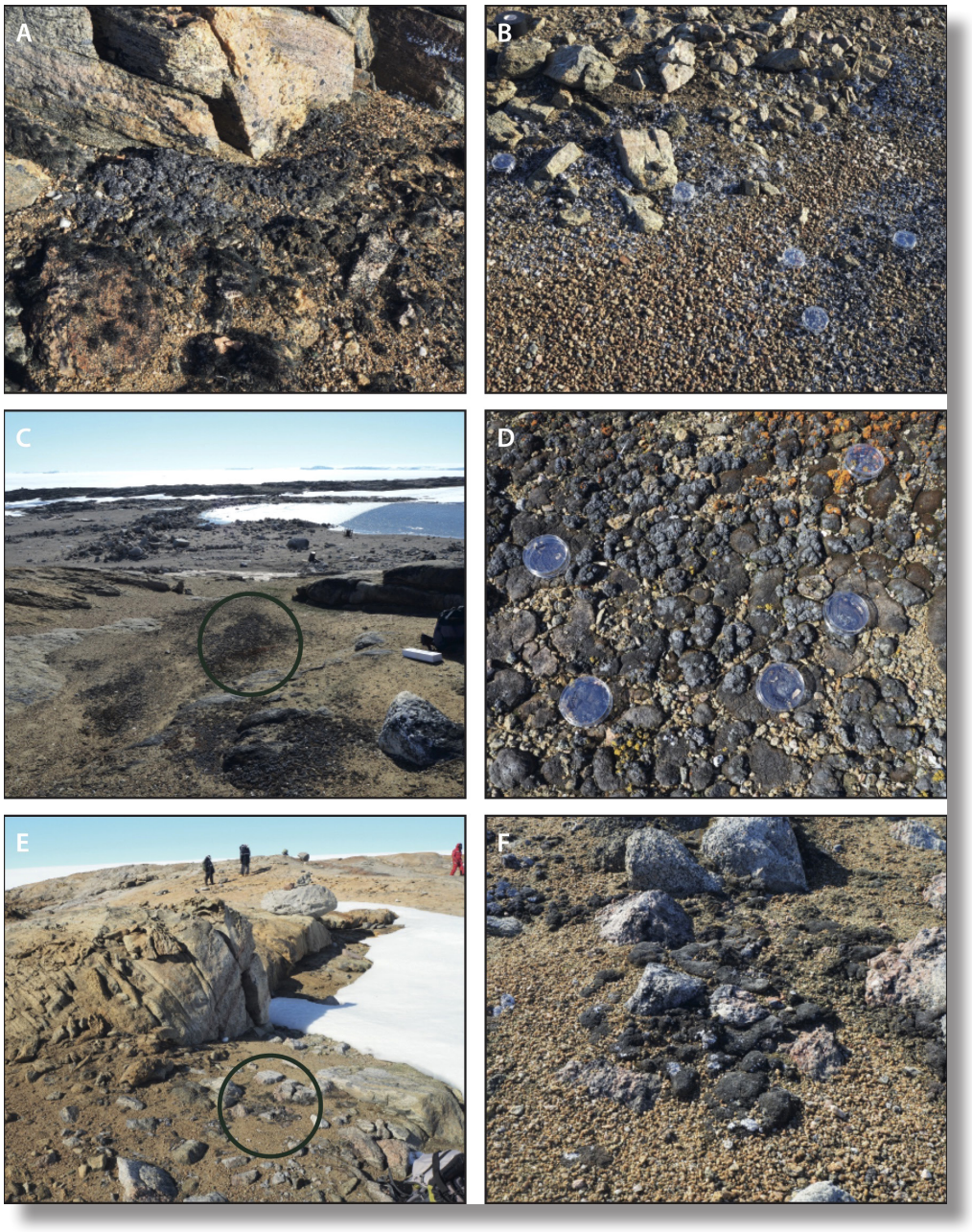

Fig. 7.4: A) Sampling site BIO1 in Molodezhnaya B) Petri dishes indicate the position of the five replicates taken at site BIO2. For scale: Petri dishes have a diameter of 4.5 cm C) Sampling site BIO3 located on a slope close to the coast D) Sampling site BIO3, close-up with position of replicates E) and F) sampling site BIO4 on Blisnetzov Peninsula; see Figure 7.1 for map with sampling locations.

We sampled sites, which were most likely not influenced by anthropogenic activities of the station (e.g., by input of nutrients due to burning of waste or physical disturbance by vehicle tracks). The soil crusts were sampled with petri dishes of 4.5 cm in diameter. At each site five replicates were collected to provide material that is representative for each site. The first site BIO1 was located at the ridge between the lakes Lagernoye and Glubokoye (Fig. 7.1). By the time of sampling the area was very dry, with no snow field that may provide meltwater runoff (Fig. 7.4). The second site BIO2 was located on the ridge between the lakes Ovalonoye and Glubokoye in a small depression (Fig. 7.1.). As for site BIO1 the area was dry with no direct input of meltwater by the time of sampling. Site BIO3 was located on a slope towards the sea.

Bird remains (feathers and guano) in the area could be a source of nutrients to the soil crusts, although no direct run-off of water was observed (Fig. 7.4). The fourth sample BIO4 was taken at Blisnetzov Peninsula, at a site close to a snow field (Fig. 7.4).

Tab 7.4: Coordinates of the four sites sampled for biological soil crusts in Thala Hills. See map in Figure 7.1 for location of sampling site.

ID	Date of sampling	Latitude (South) [dms]	Longitude (East) [dms]	Elevation (approx.) [m]
BIO1	07.02.2022	67°40‘3.54“	45°51‘38.63“	46
BIO2	07.02.2022	67°40‘7.36“	45°52‘6.24“	43
BIO3	08.02.2022	67°39‘27.12“	45°51‘13.26“	13
BIO4	10.02.2022	67°39‘46.32“	45°55‘10.14“	22

7.2 Interaction between mass changes of the Antarctic ice sheet and solid Earth in East Antarctica

Objectives

The past and current evolution of the Antarctic Ice Sheet is one of the most important topics regarding climate change and global sea-level rise. In this respect, the Ice Sheet Mass Balance Intercomparison Exercise (IMBIE) (Shepherd et al. 2019) still reveals remarkable differences between the three main satellite-based methods to infer the Antarctic ice-mass balance. Among the regional estimates, those for the East Antarctic Ice Sheet (EAIS) are least certain as reflected by the largest average per-epoch standard deviation of individual solutions of ±37 Gt/a and the uncertainty of ±46 Gt/a for the average 25-year mass trend yielding a gain of 5 Gt/a (Shepherd et al. 2019). Regarding the gravimetric method, it has still to be emphasised that glacial-isostatic adjustment (GIA) “remains poorly constrained” (ibid.), although the GIA mass effect makes up about 50 % of the Antarctic-wide ice-mass balance. In contrast, the GIA effect plays a negligible role in the geometric and input/output method.

Past developments and aspects of future research with respect to GIA were discussed by Whitehouse (2018) while Whitehouse et al. (2019) reviewed recent GIA models for Antarctica. There is still a high variance of modelled GIA-induced vertical displacement rates regarding both, their spatial pattern and magnitude. This variance can be partially explained by the different methodology underlain the GIA modelling which can be categorised as either forward models (using either 1D or 3D–rheology), coupled GIA-ice sheet models, or models based on data inversion (Whitehouse et al., 2019). Caron et al. (2018) developed a global GIA model based on a stochastic approach in a Bayesian framework adopting a varying 1D-rheology and an ice-load history. The model runs are constrained by relative sea-level (RSL) data and vertical deformation rates derived from GNSS sites in Europe, North America and Antarctica. Caron et al. (2018) yields agreement to GNSS-inferred results also in regions where GNSS data were not included in their modelling, e.g. in north-east Greenland (Kappelsberger et al., 2021). Thus, developments in the theoretical basis of GIA modelling refer to different aspects of rheology and time scales involved in the deformation of the solid Earth. However, it has to be emphasised that geodetic GNSS measurements at specially marked bedrock points provide most valuable observational evidence to constrain the GIA modelling since they are capable to infer coordinate changes with an accuracy at the level of mm/a.

Dronning Maud Land (DML) and Enderby Land are areas where vertical deformation rates caused by GIA are expected to be relatively small. The only method to directly measure GIA is given by performing geodetic GNSS measurements on bedrock. For this, the group of TU

Dresden initiated campaign-style geodetic GNSS measurements in DML in 1995, and in Enderby Land in 2006. These GNSS sites are situated in the mountain ranges that run parallel to the coast about 100 to 200 km inland as well as in coastal areas like Oasis Molodezhnaya (Thala Hills). Carrying out repeated GNSS measurements we are able to cover time spans of about 15 years. We expect to determine the vertical deformation rate with an accuracy of down to a few mm/a. Thus, the GNSS-inferred vertical deformation rates will serve as constraints for an improved GIA determination.

Work on land

We carried out repeated GNSS measurements at three points already marked in bedrock (Fig. 7.5, Tab. 7.4). The GNSS site ABE1 (Fig. 7.6.A), located at *Gora Vechernyaya*, was reached on the first day of the campaign (2 February) by means of the first helicopter flight. On the following two days the GNSS site GRA1 (Fig. 7.6.B), which is closest to the Oasis Molodeshnaya, and the GNSS site BLIS (Fig. 7.6.C, D), located at the Blisnetzov Peninsula, were set up.

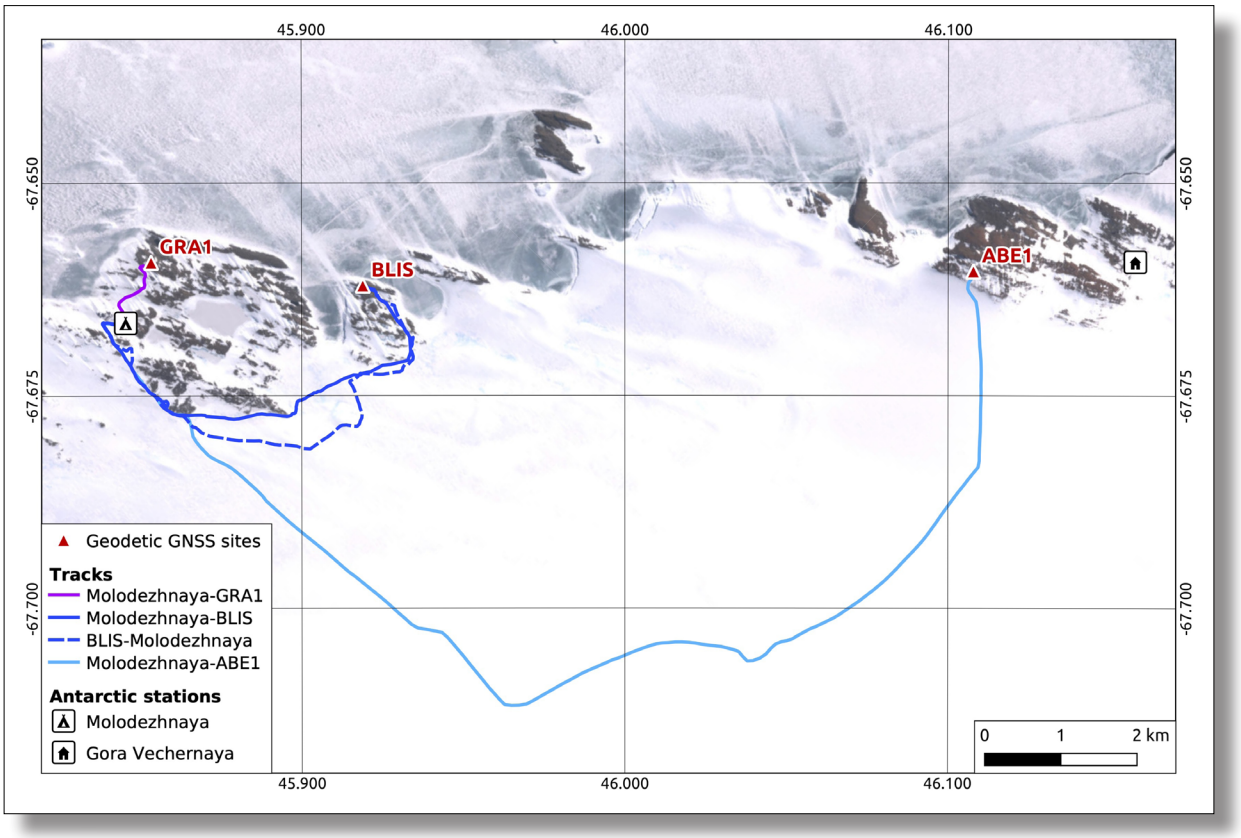

Fig. 7.5: Overview map of the area of investigation showing the re-observed GNSS sites (black/red triangles). The routes taken by snowmobile from the accommodation at Molodezhnaya to the sites GRA1, BLIS and ABE1 are shown in solid lines. The return route from BLIS (dashed line) was changed due to blue ice spots on the outward journey. The Sentinel-2 satellite scene from 29 January 2022 served as map background.

Tab. 7.5: Re-observed, geodetic GNSS sites

Site	Location	Latitude (South) [°]	Longitude (East) [°]
ABE1	Abendberg	67.6604	46.1078
BLIS	Blisnetzow	67.6621	45.9189
GRA1	Granat	67.6593	45.8535

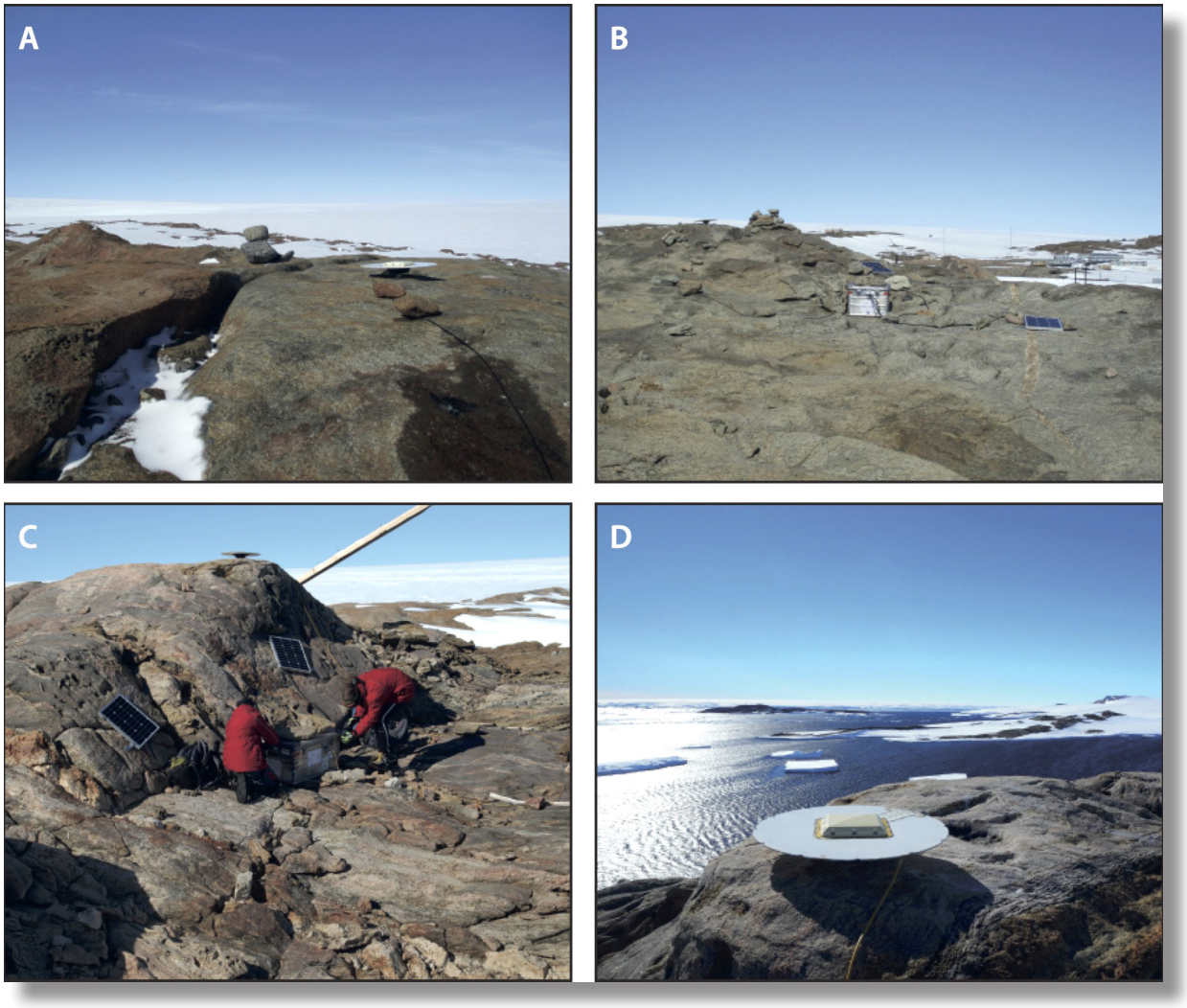

Fig. 7.6: A) Antenna at the GNSS site ABE1 with the ice sheet in the background B) Mounted GNSS site GRA1 consisting of a GNSS antenna, a GNSS receiver and power supply realised by solar panels and battery; the GNSS receiver and the battery are stored in an aluminium box. In the background buildings of the station Molodezhnaya are visible. C) Check-up of the GNSS site BLIS. D) Antenna at the GNSS site BLIS with view towards Gora Vechernyaya

During the observation period, the equipment and the devices at each GNSS site were checked once. Except for the installation of ABE1 a snowmobile was used to reach the sites. For the sites BLIS and ABE1 the transportation by snowmobile was essential because of the distance of 7 km and 18 km, respectively (Fig. 7.5). For that reason, good weather conditions and good

visibility were required to visit the sites. We unmounted BLIS and ABE1 on 11 February since the weather forecast for the following two days was very bad (strong winds and low visibility). We received strong logistical support from BAE especially for the transportation and works in the area of *Gora Vechernyaya* (site ABE1). The site GRA1 was retrieved on 13 February. All observation periods are visualised in Table 7.6.

Preliminary results

The newly acquired data will be analysed after the expedition has been terminated by means of a so-called post-processing with the Bernese GNSS software. Previous site occupations took place during the period 2006 to 2013. Incorporating the GNSS observations of the present field campaign allows the time base for deriving deformation rates to be decisively extended (to over 15 years) which will also help to improve their accuracy.

Tab. 7.6: Observation periods of the GNSS sites

Date	February											
ID	02	03	04	05	06	07	08	09	10	11	12	13
ABE1												
BLIS												
GRA1												

Dark blue: full 24 h recordings; light blue: less than 24 h data

7.3 Sampling of dirty ice

Objectives

A further objective of the shore-based research targets was the collection of basal continental ice containing enclosed sediment. This objective serves to better constrain isotope geochemical signatures of crustal sequences along the East Antarctic continental margin. First, it is important to obtain regional crustal isotope geochemical information for comparison with sedimentary isotope geochemical signatures collected offshore on the Antarctic shelf or continental rise. Second, we are interested in regional-scale glacial weathering dynamics in East Antarctica. Under non-glacial climatic conditions exposed crustal rocks undergo chemical and physical weathering during which primary mineral phases are partially dissolved and transported towards the oceans within streams and rivers. In Antarctica, this situation is very different: crustal rock sequences are mainly only physically eroded prior to transfer into shelf and deep water sedimentary depocenters. Even more, continental rocks experience extreme glacial grinding, with substantial consequences for the solubility of finer grained rock debris in Southern Ocean seawater. During this process, previous studies have found that certain accessory mineral phases are weathered very efficiently, whilst others are more inert against glacial weathering (Gutjahr et al., 2014; Dausmann et al., 2019; Süfke et al., 2019). As a result, we need to assess whether trace metal isotope signatures released from such glacial debris (that is quantitatively captured within the enclosing ice) indeed matches bulk rock isotopic signatures. Isotope geochemists refer to this process as incongruent weathering. Elemental and isotopic data retrieved from this work will also help to better understand particulate, adsorbed, as well as dissolved porewater Nd and Pb isotopic signatures from sediments that were collected during PS128.

Along the cruise track of PS128, selected unglaciated coastal sites in Enderby Land were visited for sampling of continental ice with enclosed debris for the Nd and Pb isotopic geochemical investigations. Individual blocks of maximum 20 kg were cut out from basal ice sequence using an ice saw, a hammer and chisel. Samples were wrapped in cling film and will be taken back to the clean laboratories at GEOMAR Kiel for further processing.

The Nd and Pb isotopic data will provide crucial boundary parameters for the marine geology as well as marine geochemical investigations.

Work on land

Three sites were visited in total for the collection of dirty ice (Fig. 6.1, 6.3; Tab. 7.7). The first location was targeted by the geology team based in Molodezhnaya area, while the other two locations were selected by Marcus Gutjahr during helicopter flights near Nunataks. Ideal locations could be located during each flight, and the sampling was very successful. At ice station #2, one layer of moraine material could be sampled within otherwise sediment-free glacial ice (Fig. 7.7).

Fig. 7.7: Discrete dirty ice layer near Neill Peak (67° 49.27' S, 066° 37.39' E) sampled on 9 February 2022; width of the sediment-containing ice layer is approximately 30 cm. The ice above and below did not contain sediment fragments.

At sampling location ice #2, ideal conditions for sampling could be found (Fig. 7.8). Clearly distinguishable ice layers with abundant sediment (Figs. 7.8, 7.9) could be sampled and a total of nine smaller and larger blocks of ice were recovered weighing within 1 to 15 kg. All specimens were wrapped in cling film and will be further processed at the clean laboratory facilities of GEOMAR Kiel.

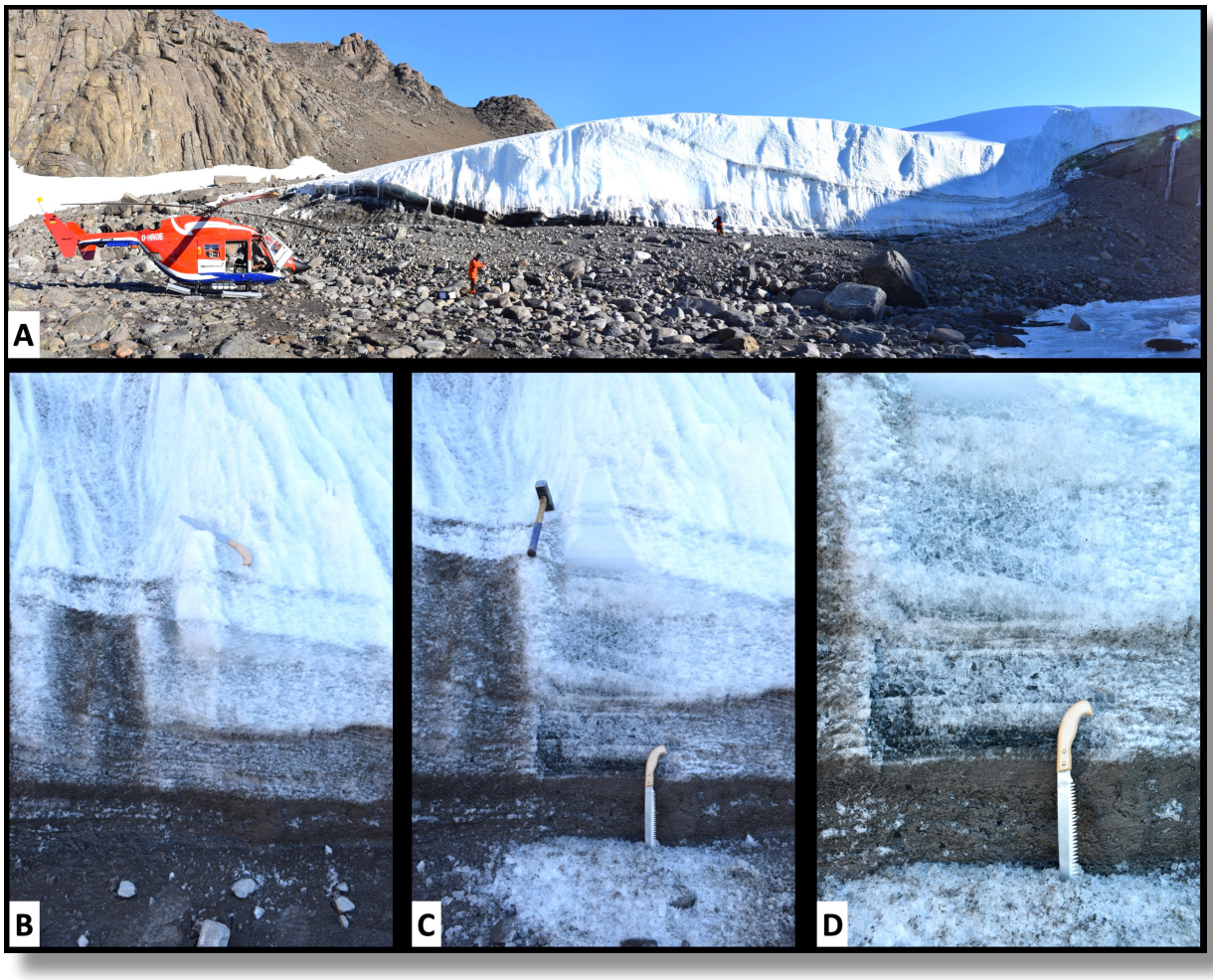

Fig. 7.8: A) Glacier tongue reaching into a dry valley at Painted Peak (near the Australian Mawson Station) (67° 45.47' S, 062° 46.25' E); the site was visited on 10 February 2022 for dirty ice sampling. B) Surface section at glacier front, note the clearly distinguishable increase in enclosed sediment content closer to the bottom of the glacier; C) and D) Photos of the same sections after removal of the previously exposed and partially melted surface layer

Fig. 7.9: Images of two dirty ice layers sampled at the glacier tongue near Painted Peak

Tab. 7.7: Coordinates and location names of three dirty ice sampling stations targeted during PS128

Site	Location	Date of sampling	Latitude (South) [°]	Longitude (East) [°]
Ice #1	Near *Molodezhnaya*	06.02.22	67°40'41.3"	045°53'11.7"
Ice #2	Neill Peak	09.02.22	67° 49.27' S	066° 37.39' E
Ice #3	Painted Peak (near *Mawson*)	10.02.22	67° 45.47' S	062° 46.25' E

Preliminary results

Isotope geochemical results of the dirty ice sampling can only be generated in Kiel. The sampled pieces are ideal for the study of both objectives, (a) assessing the local geological Nd and Pb isotope composition of continental crust in the area, and (b) quantifying the degree of incongruent weathering of glacially eroded continental crust. The local continental crust consists of Precambrian high-grade metamorphic rocks (amphibolites, migmatites, garnet schists), which are ideal candidates for such petrographic studies because of the presence of various accessory mineral phases enriched in U/Th, as well as the very old formation age of these rocks.

Data Management

Environmental data will be archived, published and disseminated according to international standards by the World Data Center PANGAEA Data Publisher for Earth & Environmental Science (https://www.pangaea.de) within two years after the end of the cruise. By default, the CC-BY license will be applied.

The geodetic GPS data will be stored within the frame of the SCAR GPS Database which is maintained at TU Dresden. The long-term preservation of the data will be maintained also through the close cooperation within the SCAR Scientific Program INSTANT (Instabilities and Thresholds of Antarctica). A common structure of the data holdings is ensured through the application of the same scientific software package utilised to analyse geodetic GNSS measurements at TU Dresden (i.e., the Bernese GPS Software). Further products and resulting models will be archived in the PANGEA database at AWI.

This work was supported by the Deutsche Forschungsgemeinschaft (DFG) in the framework of the priority program SPP 1158 "Antarctic Research with comparative investigations in Arctic ice areas" by the following grant BE 4764/6-1 an contributes to the Helmholtz Research Programme "Changing Earth – Sustaining our Future" Topic 2, Subtopics 2.1, 2.2, 2.3, and 2.4.

In all publications based on this expedition, the **Grant No. AWI_PS128_06** will be quoted and the following publication will be cited:

Alfred-Wegener-Institut Helmholtz-Zentrum für Polar- und Meeresforschung (2017) Polar Research and Supply Vessel /Polarstern/ Operated by the Alfred-Wegener-Institute. Journal of large-scale research facilities, 3, A119. http://dx.doi.org/10.17815/jlsrf-3-163.

References

Bentley M, et al. (2014) A community-based geological reconstruction of Antarctic Ice Sheet deglaciation since the Last Glacial Maximum. Quaternary Science Reviews 100, 1-9.

Caron L, Ivins ER, Larour E, Adhikari S, Nilsson J, Blewitt G (2018) GIA model statistics for GRACE hydrology, cryosphere, and ocean science. Geophysical Research Letters 45:2203–2212. https://doi.org/10.1002/2017GL076644

Dausmann V, Gutjahr M, et al. (2019) Experimental evidence for mineral-controlled release of radiogenic Nd, Hf and Pb isotopes from granitic rocks during progressive chemical weathering. Chemical Geology 507:64-84.

DeConto RM, Pollard D (2016) Contribution of Antarctica to past and future sea-level rise. Nature 531:591–597.

Gutjahr M, et al. (2014) Peak Last Glacial weathering intensity on the North American continent recorded by the authigenic Hf isotope composition of North Atlantic deep-sea sediments. Quaternary Science Reviews 99:97-111.

Kappelsberger MT, Strößenreuther U, Scheinert M, Horwath M, Groh A, Knöfel C, Lunz S, Khan SA (2021) Validating surface-deformation predictions in north-east Greenland using refined estimates of contemporary ice-mass change and densified GNSS measurements. J. Geophys. Res. Earth Surf. https://doi.org/10.1029/2020JF005860.

Kawamata M, et al. (2020). Abrupt Holocene ice-sheet thinning along the southern Soya Coast, Lützow-Holm Bay, East Antarctica, revealed by glacial geomorphology and surface exposure dating. Quaternary Science Reviews 24. https://doi.org/10.1016/j.quascirev.2020.106540

Krylov DP, Shukolyukov YA (2014) Xe_s–Xe_n Thermochronology of the Rayner Metamorphic Complex, Enderby Land (East Antarctica, Molodezhnaya Station Area). Petrology 5:438-449.

Mackintosh A, et al. (2011) Retreat of the East Antarctic ice sheet during the last glacial termination. Nature Geoscience 4:195-202.

Rignot E, et al. (2019) Four decades of Antarctic ice sheet mass balance from 1979-2017. PNAS 116:1095-1103. https://doi.org/10.1073/pnas.1812883116

Rintoul SR (2018) The global influence of localized dynamics in the Southern Ocean. Nature 558:209–218.

Sharov A, Berezina N, Tolstikov A (2015) Life under ice in the perennial ice-covered Lake Gubokoe in Summer (East Antarctica). Lakes and Reservoirs: Research and Management 20:120-127.

Shepherd A, Gilbert L, Muir AS, Konrad H, McMillan M, Slater T, et al. (2019) Trends in Antarctic Ice Sheet elevation and mass. Geophysical Reserach Letters 46:8174–8183. https://doi.org/10.1029/2019GL082182

Süfke F, Gutjahr M, et al. (2019) Early-stage weathering systematics of Pb and Nd isotopes derived from a high-Alpine Holocene lake sediment record. Chemical Geology 507:42-53.

White D, Fink D (2014) Late Quaternary glacial history constrains glacio-isostatic rebound in Enderby Land, East Antarctica, Journal of Geophysical Research Earth Surface 119:401-413.

Whitehouse PL (2018) Glacial isostatic adjustment modelling: historical perspectives, recent advances, and future directions. Earth Syst. Dynam. 6:401–429. https://doi.org/10.5194/esurf-6-401-2018

Whitehouse PL, Gomez N, King MA, Wiens DA (2019) Solid Earth change and the evolution of the Antarctic Ice Sheet. Nature Communications 10. https://doi.org/10.1038/s41467-018-08068-y

APPENDIX

A.1 TEILNEHMENDE INSTITUTE / PARTICIPATING INSTITUTES

A.2 FAHRTTEILNEHMER:INNEN / CRUISE PARTICIPANTS

A.3 SCHIFFSBESATZUNG / SHIP'S CREW

A.4 STATIONSLISTE / STATION LIST PS128

A.5 PARASOUND DATA

A.5.1 Parasound Log PS128

A.5.2 Parasound Station Profiles PS128

A.5.3 Parasound File List PS128

A.6 MARINE GEOLOGY

A.6.1 Core Images PS128

A.6.2 Litho Logs PS128

A.6.3 Smear Slide Analyses PS128

A.6.4 Coarse Fraction Analyses PS128

A.1 TEILNEHMENDE INSTITUTE / PARTICIPATING INSTITUTES

Affiliation	Address
AR.MARYBIO	Marybio Foundation Alvares Thomas 3550, 3° A CP1431 Buenos Aires Argentina
AR.UBA	Universidad Buenos Aires Ayacucho 1245 Ciudad Universitaria C1111AA Buenos Aires Argentina
AT.UIBK.AC	Universität Innsbruck Innrain 52 6020 Innsbruck Austria
AU.ANU.EDU	Research School of Earth Science The Australian National University 1 Mills Road, Acton 2601 Canberra Australia
AU.GA.GOV	Geoscience Australia GPO Box 378 Canberra ACT 2601 Australia
AU.UQ.EDU.SEES	School of Earth and Environmental Sciences University of Queensland St Lucia 4072, Queensland Australia
CH.UNIBE	Universität Bern Sidlerstrasse 5 3012 Bern Switzerland
CN.SYSU	Sun Yat-sen University Hailin Rd 519082 Zhuhai China
DE.AWI	Alfred-Wegener-Institut Helmholtz-Zentrum für Polar- und Meeresforschung Am Handelshafen 12 27570 Bremerhaven Germany

Affiliation	Address
DE.BGR	Bundesanstalt für Geowissenschaften und Rohstoffe Stilleweg 2 30655 Hannover Germany
DE.DWD	Deutscher Wetterdienst Geschäftsbereich Wettervorhersage Seeschifffahrtsberatung Bernhard-Nocht-Straße 76 20359 Hamburg Germany
DE.GEOMAR	GEOMAR Helmholtz-Zentrum für Ozeanforschung Wischhofstraße 1-3 24148 Kiel Germany
DE.HeliService	Heli-Service International GmbH Gorch-Fock-Straße 105 26721 Emden Germany
DE.TU-DRESDEN	Technische Universität Dresden Helmholtzstraße 10 01069 Dresden Germany
DE.UNI-Bremen	Universität Bremen Klagenfurter Straße 2-4 28359 Bremen Germany
DE.UNI-GREIFSWALD	Universität Greifswald Domstrasse 11 17489 Greifswald Germany
DE.UNI-KÖLN	Universität Köln Zuelpicherstr. 49 50674 Köln Germany
DK.GEUS	Geological Survey of Denmark and Greenland Oester Voldgade 10 1350 Copenhagen Denmark

Affiliation	Address
JP.KOCHI-U.AC	Kochi University Kochi Core Center 200 Monobe-otsu 783-8502 Nankoku Japan
NZ.GNS.CRI	GNS Science 1 Fairway Drive, Avalon 5010 PO Box 30-368 Lower Hutt 5040 New Zealand
UK.BAS	British Antarctic Survey High Cross, Madingley Road Cambridge, CB3 0ET United Kingdom
UK.UNI- SOUTHAMPTON-SOE	University of Southampton School of Ocean and Earth Science University Road Southampton, SO17 1BJ United Kingdom

A.2 FAHRTTEILNEHMER:INNEN / CRUISE PARTICIPANTS

Name/ Last name	Vorname/ First name	Institut/ Institute	Beruf/ Profession	Fachrichtung/ Discipline
Arney	Thomas	UK.UNI-SOUTHAMPTON	PhD Student	Marine Geology
Bauch	Henning	DE.AWI	Scientist	Marine Geology
Bennike	Ole	DK.GEUS	Scientist	Geology
Berg	Sonja	DE.UNI-Köln	Scientist	Geology
Cammareri	Alejandro	AR.MARYBIO	Scientist	MMO
Civel-Mazens	Matthieu	JP.KOCHI-U.AC	Scientist	Micropaleontology
Daub	Pascal	DE.AWI	Technician	Marine Geology
Diekmann	Bernhard	DE.AWI	Scientist	Marine Geology
Diekstall	Denise	DE.AWI	Technician	Glaciology
Eifried	Markus	DE.DWD	Scientist	Meteorology
Fuchs	Lea Tabea Antonia	DE.UNI-Bremen	Student	Geosciences
Gaedicke	Christoph	DE.BGR	Scientist	Geophysics
Gießler	Maybrit	DE.AWI	Student	Geophysics
Gohl	Karsten	DE.AWI	Scientist	Geophysics
Gutjahr	Marcus	DE.GEOMAR	Scientist	Geochemisty
Hamann	Jakob	DE.AWI	Student	Geophysics
Heidrich-Meisner	Karl	DE.TU-Dresden	Student	Geodesy
Herr	Niclas	DE.Heliservice	Pilot	Aviation
Huang	Huang	CN.SYSU	Scientist	Chemistry
Ivanova	Alina	DE.UNI-Bremen	Student	Geology
Jager	Harold	DE.Heliservice	Pilot	Aviation
Jinqi	Xia	CN.SYSU	Student	Oceanography
Kappelsberger	Maria Theresia	DE.TU-Dresden	PhD Student	Geodesy
Kattein	Laura	DE.UNI-Bremen	PhD Student	Geosciences
Khoo	Wee Wei	DE.AWI	PhD Student	Marine Geology
Klages	Johann	DE.AWI	Scientist	Marine Geology
Kreps	Gastón	AR.UBA DE.AWI	Scientist	Oceanography
Leicher	Niklas	DE.UNI-Köln	Scientist	Geology
Lembke-Jene	Lester	DE.AWI	Scientist	Marine Geology
Lensch	Norbert	DE.AWI	Technician	Marine Geology
Mollenhauer	Gesine	DE.AWI	Scientist	Geochemistry
Müller	Juliane	DE.AWI	Scientist	Marine Geology
Nürnberg	Dirk	GEOMAR	Scientist	Marine Geology
Nürnberg	Ebbe	DE.UNI-GREIFSWALD	Student	Biology

Name/ Last name	**Vorname/ First name**	**Institut/ Institute**	**Beruf/ Profession**	**Fachrichtung/ Discipline**
Pinho	Tainã	DE.AWI	PhD Student	Marine Geology
Pfeiffer	Adalbert	DE.AWI	Technician	Geophysics
Pöppelmeier	Frerk	CH.UNIBE	Scientist	Oceanography
Preckel	Hinner	DE.UNI-Bremen	Student	Geography
Rigalleau	Vincent	DE.AWI	PhD Student	Marine Geology
Rohleder	Christian	DE.DWD	Scientist	Meteorology
Salazar	Juan	AR.MARYBIO	Scientist	MMO
Santos	Victor	DE.Heliservice	Technician	Aviation
Schönborn	Lisa	DE.AWI	Technician	Marine Geology
Schulze-Tenberge	Yvonne	DE.AWI	Scientist	Bathymetry
Schumacher	Valéa	DE.AWI	Technician	Marine Geology
Sonnemann	Patricia	AT.UIBK.AC	Student	Geology
Szczepan	Bartek	DE.Heliservice	Technician	Aviation
Tiedemann	Ralf	DE.AWI	Scientist	Marine Geology
Unland	Ellen	DE.AWI	Student	Geophysics
Wagner	Bernd	DE.UNI-Köln	Scientist	Geology
Weigelt	Estella	DE.AWI	Scientist	Geophysics
Witte	Marlena	DE.AWI	Online Editor	Communication and Media

A.3 SCHIFFSBESATZUNG / SHIP'S CREW

No.	Nachname	Vorname	Position
1	Langhinrichs	Moritz	Master
2	Spielke	Steffen	Chiefmate
3	Strauß	Erik	2nd Mate Cargo
4	Ziemann	Olaf	Chief
5	Peine	Lutz	2nd Mate
6	Hering	Igor	2nd Mate
7	Römer	Mario	Ships Doc
8	Ehrke	Tom	2nd. Eng
9	Krinfeld	Oleksandr	2nd. Eng
10	Rusch	Torben	2nd. Eng
11	Hofmann	Jörg	Chief ELO
12	Pommerencke	Bernd	ELO
13	Krüger	Lars	ELO
14	Schwedka	Thorsten	ELO
15	Pliet	Johannes	SYS
16	Plehn	Markus	Storek.
17	Brück	Sebastian	Bosun
18	Lello	Ants	Carpen.
19	Klee	Philipp	MP Rat.
20	Buchholz	Joscha	MP Rat.
21	Fölster	Michael	MP Rat.
22	Schade	Tom	MP Rat.
23	Decker	Jens	MP Rat.
24	Weiß	Daniel	MP Rat.
25	Möller	Falko	MP Rat.
26	Lutz	Johannes	MP Rat.
27	Niebuhr	Tim	MP Rat.
28	Arnold-Becker	André	MP Rat. Motor
29	Hansen	Jan Nils	MP Rat. Motor
30	Clasen	Nils	MP Rat. Motor

No.	Nachname	Vorname	Position
31	Teichert	Uwe	MP Rat. Motor
32	Thiele	Linus	MP Rat. Motor
33	Schnieder	Sven	Cook
34	Matter	Sebastian	Cooksm.
35	Hermann	Philipp	Cooksm.
36	Wartenberg	Irina	Chief Stew.
37	Ilk	Romy	Nurse
38	Witusch	Petra	2nd Stew.
39	Zarend	Christian	2nd Stew.
40	Shi	Wubo	2nd Stew.
41	Chen	Quan Lun	2nd Stew.
42	Winkler	Maria	2nd Stew.
43	Hu	Guo Yong	Laundrym.

A.4 STATIONSLISTE / STATION LIST PS128

Tab. A.4: Station list of expedition PS128 from Cape Town to Cape Town; the list details the action log for all stations along the cruise track.

See https://www.pangaea.de/expeditions/events/PS128 to display the station (event) list for expedition PS128.
This version contains Uniform Resource Identifiers for all sensors listed under https://sensor.awi.de.
See https://www.awi.de/en/about-us/service/computing-centre/data-flow-framework.html for further information about AWI's data flow framework from sensor observations to archives (O2A).

Event label	Optional label	Date/Time	Latitude	Longitude	Depth [m]	Gear	Action	Comment [*]
PS128-track		2022-01-06T00:00:00	-33.90680	18.43370		CT	Station start	Cape Town - Cape Town
PS128-track		2022-01-06T00:00:00	-33.90680	18.43370		CT	Station end	Cape Town - Cape Town
PS128_0_Underway-29		2022-01-06T04:00:00	-33.90978	18.43587		SWEAS	Station start	
PS128_0_Underway-29		2022-01-06T04:00:00	-38.01857	18.52014	4702.4	SWEAS	Station end	
PS128_0_Underway-1		2022-01-07T07:51:17	-36.20467	17.14537		ADCP	Station start	
PS128_0_Underway-1		2022-01-07T07:51:17	-38.01857	18.52014	4702.4	ADCP	Station end	
PS128_0_Underway-23		2022-01-07T08:31:56	-36.31740	17.08985		TSG	Station start	
PS128_0_Underway-23		2022-01-07T08:31:56	-52.62412	7.90073	3595.1	TSG	Station end	
PS128_0_Underway-24		2022-01-07T08:32:31	-36.31900	17.08907		TSG	Station start	

Event label	Optional label	Date/Time	Latitude	Longitude	Depth [m]	Gear	Action	Comment [*]
PS128_0_Underway-24		2022-01-07T08:32:31	-52.62501	7.90017	3597.8	TSG	Station end	
PS128_0_Underway-11		2022-01-07T08:34:03	-36.32335	17.08691		MAG	Station start	
PS128_0_Underway-11		2022-01-07T08:34:03	-52.61939	7.90380	3568.3	MAG	Station end	
PS128_0_Underway-22		2022-01-07T11:26:20	-36.78188	16.85984		SNDVELPR	Station start	
PS128_0_Underway-22		2022-01-07T11:26:20	-38.01857	18.52014	4702.4	SNDVELPR	Station end	
PS128_0_Underway-7		2022-01-07T11:56:43	-36.86419	16.81898		FBOX	Station start	
PS128_0_Underway-7		2022-01-07T11:56:43	-52.55763	7.94435	3731.4	FBOX	Station end	
PS128_0_Underway-18		2022-01-07T11:58:55	-36.87020	16.81592		pCO2	Station start	
PS128_0_Underway-18		2022-01-07T11:58:55	-38.01857	18.52014	4702.4	pCO2	Station end	
PS128_0_Underway-17		2022-01-07T11:59:33	-36.87187	16.81506		pCO2	Station start	
PS128_0_Underway-17		2022-01-07T11:59:33	-38.01857	18.52014	4702.4	pCO2	Station end	
PS128_0_Underway-13		2022-01-07T16:41:30	-37.65674	16.42279	4613	MBES	Station start	
PS128_0_Underway-13		2022-01-07T16:41:30	-38.01857	18.52014	4702.4	MBES	Station end	
PS128_0_Underway-20		2022-01-08T06:43:27	-39.89768	15.27904	4837.3	PS	Station start	

Event label	Optional label	Date/Time	Latitude	Longitude	Depth [m]	Gear	Action	Comment [*]
PS128_0_Underway-20		2022-01-08T06:43:27	-38.01857	18.52014	4702.4	PS	Station end	
PS128_0_Underway-6		2022-01-09T07:35:05	-43.90828	13.13334	4999.1	MYON	Station start	
PS128_0_Underway-6		2022-01-09T07:35:05	-52.61448	7.90710	3544.2	MYON	Station end	
PS128_0_Underway-14		2022-01-09T07:36:05	-43.91098	13.13184	4946.5	NEUMON	Station start	
PS128_0_Underway-14		2022-01-09T07:36:05	-52.61612	7.90604	3542.7	NEUMON	Station end	
PS128_0_Underway-12		2022-01-13T05:59:11	-59.19006	3.21745	5413.6	GRAV	Station start	
PS128_0_Underway-12		2022-01-13T05:59:11	-52.61722	7.90527	3561.7	GRAV	Station end	
PS128_1-1		2022-01-16T02:26:00	-69.04722	-6.37779	2675.7	CTD-RO	max depth	
PS128_1-2		2022-01-16T04:17:46	-69.04704	-6.37736		MUC	max depth	
PS128_1-3		2022-01-16T06:17:36	-69.04864	-6.38024	2713.4	CTD-RO	max depth	
PS128_1-4		2022-01-16T08:54:27	-69.04737	-6.37800	2712.1	MUC	max depth	
PS128_1-5		2022-01-16T13:21:35	-69.04852	-6.38428	2711	GC	max depth	
PS128_1-6		2022-01-16T15:28:39	-69.04731	-6.37811	2711.9	GC	max depth	
PS128_2-2		2022-01-16T23:17:20	-69.41163	-5.58965	1868.6	GC	max depth	

Event label	Optional label	Date/Time	Latitude	Longitude	Depth [m]	Gear	Action	Comment [*]
PS128_2-3		2022-01-17T00:54:00	-69.41169	-5.58741	1868	GC	max depth	
PS128_2-4		2022-01-17T02:58:44	-69.41123	-5.59041	1869.3	MUC	max depth	
PS128_3-1		2022-01-17T21:57:55	-70.48049	-8.81318	404.2	MBES	Station start	
PS128_3-1		2022-01-17T21:57:55	-70.60567	-9.36069		MBES	Station end	
PS128_4-1		2022-01-18T10:56:08	-70.60515	-9.36211		CTD-RO	max depth	
PS128_4-2		2022-01-18T11:39:19	-70.60483	-9.36394	465.8	GKG	max depth	
PS128_4-3		2022-01-18T13:13:51	-70.60466	-9.36298	465.7	GC	max depth	
PS128_4-4		2022-01-18T13:58:00	-70.60435	-9.36232	465.6	GC	max depth	
PS128_5-1		2022-01-18T15:11:00	-70.55023	-9.34361	390.3	GC	max depth	
PS128_6-1		2022-01-18T17:37:21	-70.50186	-8.86473	428.6	GC	max depth	
PS128_6-2		2022-01-18T18:25:20	-70.50220	-8.86523	427.1	GKG	max depth	
PS128_7-1		2022-01-18T19:41:51	-70.48347	-8.85962	442.9	GC	max depth	
PS128_8-1		2022-01-18T20:24:14	-70.48539	-8.89034	448.5	GC	max depth	
PS128_9-1		2022-01-18T21:09:14	-70.48932	-8.97237	433.9	GC	max depth	

Event label	Optional label	Date/Time	Latitude	Longitude	Depth [m]	Gear	Action	Comment [*]
PS128_9-2		2022-01-18T21:47:39	-70.48927	-8.97331	433.9	GKG	max depth	
PS128_10-1		2022-01-18T22:49:55	-70.46503	-8.85489	434.3	GC	max depth	
PS128_11-1		2022-01-19T12:19:13	-70.04372	-8.61667	2690.3	CTD-RO	max depth	
PS128_11-2		2022-01-19T14:37:25	-70.04816	-8.61656	2716.4	MUC	max depth	
PS128_12-1		2022-01-20T03:14:25	-69.70863	-7.57420	3066.1	GC	max depth	
PS128_13-1		2022-01-20T07:52:58	-70.00140	-7.62892	1578.5	GC	max depth	
PS128_13-2		2022-01-20T10:09:44	-70.00130	-7.62849	1577.4	GC	max depth	
PS128_14-1		2022-01-20T15:34:22	-70.13639	-6.90271	1612	GC	max depth	
PS128_14-2		2022-01-20T17:46:01	-70.13692	-6.90209	1612.6	GC	max depth	
PS128_14-3		2022-01-20T19:27:48	-70.13690	-6.90175	1612.4	MUC	max depth	
PS128_15-1		2022-01-20T21:59:53	-70.04780	-6.81228	1907.2	MUC	max depth	
PS128_15-2		2022-01-21T00:16:04	-70.04802	-6.81212	1906.4	GC	max depth	
PS128_15-3		2022-01-21T03:03:34	-70.04777	-6.81206	1906.9	GC	max depth	
PS128_16-1		2022-01-21T06:59:09	-69.91570	-6.74468	2136.3	CTD-RO	max depth	

Event label	Optional label	Date/Time	Latitude	Longitude	Depth [m]	Gear	Action	Comment [*]
PS128_16-2		2022-01-21T08:36:36	-69.91619	-6.74539	2135.7	MUC	max depth	
PS128_16-3		2022-01-21T14:56:50	-69.91576	-6.74318	2134.9	PC	max depth	
PS128_16-4		2022-01-21T20:36:54	-69.91600	-6.74294	2135.9	PC	max depth	
PS128_17-1		2022-01-22T02:55:28	-69.76034	-5.92014	2305	PC	max depth	
PS128_17-2		2022-01-22T07:31:01	-69.75869	-5.91346	2310.5	PC	max depth	
PS128_17-3		2022-01-22T10:38:03	-69.75989	-5.92206	2304.6	MUC	max depth	
PS128_18-1		2022-01-22T15:01:00	-69.67108	-7.08800	2494.3	SEISREFL	Station start	
PS128_18-1		2022-01-22T15:01:00	-69.57624	-7.37015	2393.3	SEISREFL	Station end	
PS128_19-1		2022-01-23T02:04:26	-68.53115	-6.96619	2956.4	MUC	max depth	
PS128_19-2		2022-01-23T06:39:31	-68.53146	-6.96490	2956.6	PC	max depth	
PS128_19-3		2022-01-23T10:55:17	-68.53128	-6.96673	2956.3	PC	max depth	
PS128_20-1		2022-01-23T19:39:14	-69.41145	-5.58876	1868.7	PC	max depth	
PS128_20-2		2022-01-24T02:12:59	-69.41151	-5.58893	1868.2	BC	max depth	
PS128_21-1		2022-01-24T19:33:30	-70.69077	-9.40704	553.9	SEISREFR	Station start	Station was cancelled early due to the ice conditions

Event label	Optional label	Date/Time	Latitude	Longitude	Depth [m]	Gear	Action	Comment [*]
PS128_21-1		2022-01-24T19:33:30	-70.36210	-9.37881		SEISREFR	Station end	Station was cancelled early due to the ice conditions
PS128_22-1		2022-01-25T12:40:26	-70.25619	-8.02951	1470.7	SEISREFL	Station start	
PS128_22-1		2022-01-25T12:40:26	-70.50840	-8.94395	439	SEISREFL	Station end	
PS128_23-1		2022-01-27T03:20:22	-70.45613	-9.12041		GC	max depth	
PS128_23-2		2022-01-27T03:52:21	-70.45610	-9.12049		GC	max depth	
PS128_24-1		2022-01-27T04:33:28	-70.45914	-9.13638		GC	max depth	
PS128_25-1		2022-01-27T10:46:38	-70.07548	-8.55167	2658.2	GC	max depth	
PS128_26-1		2022-01-28T12:28:08	-69.40076	1.04002	3339.7	CTD-RO	max depth	
PS128_27-1		2022-01-29T05:25:25	-68.84007	8.91581	3495.4	CTD-RO	max depth	
PS128_27-2		2022-01-29T08:07:50	-68.84031	8.91665	3494.8	MUC	max depth	
PS128_28-1		2022-01-30T06:31:30	-68.53193	17.98772	4138.8	CTD-RO	max depth	
PS128_29-1		2022-01-31T09:23:18	-68.36990	30.00009	3572.7	CTD-RO	max depth	
PS128_30-1		2022-02-01T10:36:56	-67.58480	38.00994	3915.3	CTD-RO	max depth	
PS128_30-2		2022-02-01T13:13:40	-67.58291	38.00957	3918	MUC	max depth	

Event label	Optional label	Date/Time	Latitude	Longitude	Depth [m]	Gear	Action	Comment [*]
PS128_31-1		2022-02-03T08:45:31	-65.42357	49.13436	3419.2	CTD-RO	max depth	
PS128_32-1		2022-02-04T02:02:15	-65.18645	55.14196	3586.2	CTD-RO	max depth	
PS128_32-2		2022-02-04T04:36:11	-65.18489	55.13825	3586.2	MUC	max depth	
PS128_33-1		2022-02-07T02:25:06	-65.86389	64.40165	3296.9	CTD-RO	max depth	
PS128_33-2		2022-02-07T05:01:53	-65.86344	64.40544	3276.3	MUC	max depth	
PS128_34-1		2022-02-07T10:18:51	-65.97486	63.39921	3025.2	MUC	max depth	
PS128_34-2		2022-02-07T12:58:59	-65.97533	63.39995	3024.5	GC	max depth	
PS128_34-3		2022-02-07T15:55:37	-65.97514	63.40100	3023.9	GC	max depth	
PS128_35-1		2022-02-07T22:37:20	-65.89682	63.95677		GC	max depth	
PS128_36-1		2022-02-08T17:53:41	-66.72999	65.82675	1963.9	CTD-RO	max depth	
PS128_37-1		2022-02-08T22:55:54	-67.30042	66.30386	294	PS	Station start	
PS128_37-1		2022-02-08T22:55:54	-67.02160	65.31007	514.3	PS	Station end	
PS128_37-2		2022-02-08T22:55:54	-67.30042	66.30386	294	MBES	Station start	
PS128_37-2		2022-02-08T22:55:54	-67.02160	65.31007	514.3	MBES	Station end	

Event label	Optional label	Date/Time	Latitude	Longitude	Depth [m]	Gear	Action	Comment [*]
PS128_38-1		2022-02-09T08:35:12	-67.14228	65.81793	518.3	MUC	max depth	
PS128_38-2		2022-02-09T10:00:57	-67.14229	65.81721	517.8	PC	max depth	
PS128_39-1		2022-02-09T15:00:48	-67.11582	65.69609	647.2	PC	max depth	
PS128_40-1		2022-02-09T17:55:08	-67.17298	65.99697	796.2	CTD-RO	max depth	
PS128_40-2		2022-02-09T19:09:48	-67.17338	65.99683	797.2	PC	max depth	
PS128_40-3		2022-02-09T21:10:17	-67.17339	65.99756	796.8	MUC	max depth	
PS128_41-1		2022-02-09T23:20:18	-67.09232	65.60000		GC	max depth	
PS128_42-1		2022-02-10T00:23:09	-67.06775	65.49834		GC	max depth	
PS128_43-1		2022-02-10T09:53:28	-66.97088	65.03181	393	GC	max depth	
PS128_44-1		2022-02-10T11:00:39	-66.96009	64.99006	402	GC	max depth	
PS128_44-2		2022-02-10T11:51:22	-66.95982	64.99172	400	GKG	max depth	
PS128_45-1		2022-02-10T13:01:34	-66.95273	64.85897	357	GC	max depth	
PS128_46-1		2022-02-10T20:44:15	-66.84359	63.18823	376	GC	max depth	
PS128_47-1		2022-02-10T21:34:36	-66.82860	63.20808	392	GC	max depth	
PS128_48-1		2022-02-11T07:43:02	-66.47768	61.39125	1569.7	MUC	max depth	

Event label	Optional label	Date/Time	Latitude	Longitude	Depth [m]	Gear	Action	Comment [*]
PS128_49-1		2022-02-11T10:14:08	-66.40140	61.21935	2154.1	MUC	max depth	
PS128_49-2		2022-02-11T12:26:03	-66.40086	61.21712	2157.3	GC	max depth	
PS128_50-1		2022-02-11T18:57:28	-66.28774	60.31754	2756	CTD-RO	max depth	
PS128_50-2		2022-02-11T20:59:13	-66.28778	60.31754	2755.5	MUC	max depth	
PS128_51-1		2022-02-12T07:16:16	-65.90061	58.78572	2724.4	MUC	max depth	
PS128_52-1		2022-02-14T14:19:14	-67.52332	45.92785	800	CTD-RO	max depth	
PS128_53-1		2022-02-15T02:50:43	-66.25696	48.77769	1060.7	GC	max depth	
PS128_54-1		2022-02-16T04:39:34	-65.13298	58.91806	3377.8	GC	max depth	
PS128_54-2		2022-02-16T07:12:45	-65.13291	58.91856	3377.2	GC	max depth	
PS128_54-3		2022-02-16T09:48:36	-65.13274	58.91817	3377.6	MUC	max depth	
PS128_55-1		2022-02-16T13:26:25	-65.12657	59.38092	3677.7	MUC	max depth	
PS128_55-2		2022-02-16T16:11:49	-65.12671	59.38095	3678.1	GC	max depth	
PS128_56-1		2022-02-16T19:48:23	-65.12636	59.58921	3991.7	CTD-RO	max depth	
PS128_57-1		2022-02-17T05:14:32	-64.54672	59.17056	3770.5	GC	max depth	

Event label	Optional label	Date/Time	Latitude	Longitude	Depth [m]	Gear	Action	Comment [*]
PS128_57-2		2022-02-17T07:38:27	-64.54630	59.17113	3770.8	MUC	max depth	
PS128_58-1		2022-02-17T12:02:15	-64.47165	58.60050	3926.4	MUC	max depth	

** Comments are limited to 130 characters. See https://www.pangaea.de/expeditions/events/PS128 to show full comments in conjunction with the station (event) list for expedition PS128*

Abbreviation	Method/Device
ADCP	Acoustic Doppler Current Profiler
BC	Box corer
CT	Underway cruise track measurements
CTD-RO	CTD/Rosette
FBOX	FerryBox
GC	Gravity corer
GKG	Giant box corer
GRAV	Gravimetry
MAG	Magnetometer
MBES	Multibeam echosounder
MUC	MultiCorer
MYON	DESY Myon Detector
NEUMON	Neutron monitor
PC	Piston corer
PS	ParaSound
SEISREFL	Seismic reflection profile
SEISREFR	Seismic refraction profile
SNDVELPR	Sound velocity probe
SWEAS	Ship Weather Station
TSG	Thermosalinograph
pCO2	pCO2 sensor

A.5 PARASOUND DATA

A.5.1 Parasound Log Sheet PS128

A.5.2 Parasound Station Profiles PS128

A.5.3 Parasound File List PS128

A.5.1 Parasound Log Sheet PS128

Tab. A.5.1: Parasound log of expedition PS128 from Cape Town to Cape Town; the list details the parasound operation

Year	**Month**	**Day**	**Time UTC**	**Station**	**Action** (e.g. “Start; Stop...”) **–and Reason** (e.g. „Station reached; Whale Stop;...“)	**Ob-server**	**Modus** (Single Pulse or QED)	**Puls rate waiting time**	**Frequencies** PHF / SLF	**System Depth Source**	**Comments**
2022	Jan.	7	14:43	n/a	Start Parasound for PS128	ew	Single Pulse	0 s	20 kHz / 4 kHZ	Hydro PHF	Lon: 37.34°E Lat: -16.58°S, Speed ~10 Kn, Depth ~ 4500 m, Storage Disk Fill: 41%
		7	14:49			ew		0 s		Cntr.Para. PHF	
		8	07:40			ew		0 s		„	LowPass in SLF-Window
		8	09:35			ew		0 s		„	Malvinas(Falkland) AgulhasRidgeFragment
		8	11:20			ew		0 s		„	Ridge edge, steep slope = poor signal
		8	12:08			ew		0 s		Hydro PHF	steep slope, depth lost
		8	13:26			ew		0 s		Cntr.Para. PHF	
		8	17:29			ew		0 s		Hydro PHF	Automatic depth control 20%
		9	~04:40			ew		0 s		Cntr.Para. PHF	no SLF Depth, SLF window restarted, values ok
		9	05:46			ew		0 s			Automatic depth control 5%

Year	Month	Day	Time UTC	Station	**Action** (e.g. “Start; Stop...”) **–and Reason** (e.g. „Station reached; Whale Stop;...“)	Ob-server	**Modus** (Single Pulse or QED)	Puls rate waiting time	**Frequencies** PHF / SLF	System Depth Source	Comments
		9	14:20		Stop Parasound , poor signals, wrong depths	ew		0 s			depth differences between PHF and SLF, noisy signal
		9	14:30		Start Sounding	ew		0 s		Hydro PHF	
		11	13:25		Stop Sounding, EEZ Bouvet Island	ew		0 s			
		12	21:18		Start Sounding, out off EEZ Bouvet Island	ew		0 s		Cntr.Para. PHF	Automatic depth control 5%
2022	Jan.	13	11:00	n/a	Start oportunistic whale watch reaching 60 °S	ew		0 s			reaching 60 °S
2022	Jan.	13	11:00	n/a	Start with MMO-watches because passing Lat. 60° S and entering area of Antarctic Treaty System.	ew		0s			Start of MMO-watches because south of 60°S, and entering area of Antarctic Treaty System. MMO opportunistic during moving, MMO-watch continous during stations. System settings: Frequencies: PHF/ SLF=20kHz/4kHz Pulse Rate waiting time: 0 s on moving, 10 s during stations
		13	16:00	n/a	Stop recording, Storage window disarranged	ew					SLF window got stucked, no reaction
			16:03	n/a	Start recording, storage window ok	ew					PHF and SLF window opened
	Jan.	15	17:14	n/a	Stop sounding because of whale approach. But whale >100 m away	bd	off	off			Stop sounding after call from oportunistic observations. But whale > 100m away
		15	17:38	n/a	Start sounding after whale retreat , after 15 min. Whale watch minimum	bd	Single Pulse	0 s	20 kHz / 4 kHZ	Hydro PHF	

Year	Month	Day	Time UTC	Station	**Action** (e.g. “Start; Stop...”) **–and Reason** (e.g. „Station reached; Whale Stop;...“)	Ob-server	**Modus** (Single Pulse or QED)	Puls rate waiting time	**Frequencies** PHF / SLF	System Depth Source	Comments
	Jan.	16	02:37	PS128/001	Reduced ping rate (10s) when Station reached for exact positioning for sampling with whale watch during station	ew	Single Pulse	10 s	20 kHz / 4 kHZ	Ctr. Paras. PHF	Lon: -6.042°W Lat: -69.048°S Station PS128/001
	Jan.	16	17:27	PS128/001	Resume sounding with noraml ping rate after station end; after Whale watch during whole station time	ew	Single Pulse	0	20 kHz / 4 kHZ	Ctr. Paras. PHF	Station end of PS128/001
	Jan.	18	10:40	PS128_4	Reduced ping rate (10s) when Station reached for exact positioning for sampling; with whale watch during station	jh	Single Pulse	10 s	20 kHz / 4 kHZ	Ctr. Paras. PHF	Long approach until final confirmation of start position of Station PS128_4-1. Lon: -9.362429°, Lat: -70.605108°, 462m
	Jan.	18	13:31		Resume sounding with normal ping rate after station end; after whale watch during whole station time	jh	Single Pulse	0	20 kHz / 4 kHZ	Ctr. Paras. PHF	End of station work PS128_4
	Jan.	18	13:36	PS128_4	Reduced ping rate (10s), because of return to station PS128_4, and resampling at station	ew	Single Pulse	10 s	20 kHz / 4 kHZ	Ctr. Paras. PHF	Reduced ping rate (10s) because of return to station PS128_4, because corer was empty, resamping of PS128_4 (PS128_4-4)
	Jan.	18	14:24		Resume sounding with normal ping rate after station end; after whale watch during whole station time	ew	Single Pulse	0	20 kHz / 4 kHZ	Ctr. Paras. PHF	End of station work PS128_4
	Jan.	18	15:05	PS128_5	Reduced ping rate (10s) when Station reached for exact positioning for sampling; with whale watch during station	ew	Single Pulse	10s	20 kHz / 4 kHZ	Ctr. Paras. PHF	Start of Station PS128_5-1. Lon: -9.343524°, Lat: -70.550329° , 389m No message of bridge when station exactly was reached

Year	Month	Day	Time UTC	Station	**Action** (e.g. “Start; Stop...”) **–and Reason** (e.g. „Station reached; Whale Stop;...“)	Ob-server	**Modus** (Single Pulse or QED)	Puls rate waiting time	**Frequencies** PHF / SLF	System Depth Source	Comments
	Jan.	18	15:39		Resume sounding with normal ping rate after station end; after whale watch during whole station time	ew	Single Pulse	0	20 kHz / 4 kHZ	Ctr. Paras. PHF	End of station work PS128_5
	Jan.	18	17:23	PS128_6	Reduced ping rate (10s) when Station reached for exact positioning for sampling; with whale watch during station	ew	Single Pulse	10 s	20 kHz / 4 kHZ	Ctr. Paras. PHF	Start of Station PS128_6 at 17:29 Lon: -8.863863°, Lat: -70.501763°, 428m
	Jan.	18	19:07		Resume sounding with normal ping rate after station end; after whale watch during whole station time	cg	Single Pulse	0	20 kHz / 4 kHZ	Ctr. Paras. PHF	End of station work PS128_6
	Jan.	18	19:20	PS128_7	Reduced ping rate (10s) when Station reached for exact positioning for sampling; with whale watch during station	cg	Single Pulse	10 s	20 kHz / 4 kHZ	Ctr. Paras. PHF	Start of Station PS128_7 at 19:32 Lon: -8.860106°, Lat: 70.483538, 446m
	Jan.	18	19:58		Resume sounding with normal ping rate after station end; after whale watch during whole station time	cg	Single Pulse	0	20 kHz / 4 kHZ	Ctr. Paras. PHF	End of station work PS128_7
	Jan.	18	20:10	PS128_8	Normal ping rate still to approach station slowly for exact positioning for sampling; with whale watch during station	cg	Single Pulse	0	20 kHz / 4 kHZ	Ctr. Paras. PHF	Official Start of Station PS128_8 at 20:10 Lon: -8.890111, Lat: -70.485959, 447m. But pinging was continued with normal rate until 20:13 to locate exact position for sampling PS128_8.

Year	Month	Day	Time UTC	Station	**Action** (e.g. "Start; Stop...") **–and Reason** (e.g. „Station reached; Whale Stop:...")	Ob-server	**Modus** (Single Pulse or QED)	**Puls rate waiting time**	**Frequencies** PHF / SLF	**System Depth Source**	**Comments**
	Jan.	18	20:13	PS128_8	Reduced ping rate (10s) when Station reached for exact positioning for sampling; with whale watch during station	cg	Single Pulse	10 s	20 kHz / 4 kHZ	Ctr. Paras. PHF	Start of Station PS128_8 Lon: -8.890111, Lat: -70.485959, 447m, Long approach until final confirmation of start position of Station PS128_8
	Jan.	18	20:43		Resume sounding with normal ping rate after station end; after whale watch during whole station time	cg	Single Pulse	0	20 kHz / 4 kHZ	Ctr. Paras. PHF	End of station work PS128_8
	Jan.	18	20:57	PS128_9	Normal ping rate to approach station slowly for exact positioning for sampling; with whale watch during station	cg	Single Pulse	0	20 kHz / 4 kHZ	Ctr. Paras. PHF	Official start of Station PS128_9 at20:57 Lon: -8.970549°, Lat: -70.489517°, 434m. But pinging was continued with normal rate until 21:03 to locate exact position for sampling PS128_9
	Jan.	18	21:03	PS128_9	Reduced ping rate (10s) when Station reached for exact positioning for sampling; with whale watch during station	cg	Single Pulse	10 s	20 kHz / 4 kHZ	Ctr. Paras. PHF	Start of Station PS128_9 Lon: -8.970549°, Lat: -70.489517°, 434m. Long approach until final confirmation of start position of Station PS128_8
	Jan.	18	22:01		Resume sounding with normal ping rate after station end; after whale watch during whole station time	jh	Single Pulse	0	20 kHz / 4 kHZ	Ctr. Paras. PHF	End of station work PS128_9
	Jan.	18	22:40	PS128_10	Reduced ping rate (10s) when Station reached for exact positioning for sampling; with whale watch during station	jh	Single Pulse	10 s	20 kHz / 4 kHZ	Ctr. Paras. PHF	Start of station work PS128_10 Lon: -8.851526, Lat: -70.464220, 426m

Year	Month	Day	Time UTC	Station	**Action** (e.g. “Start; Stop...”) **–and Reason** (e.g. „Station reached; Whale Stop;...“)	Ob-server	**Modus** (Single Pulse or QED)	Puls rate waiting time	**Frequencies** PHF / SLF	System Depth Source	Comments
	Jan.	18	23:10		Resume sounding with normal ping rate after station end; after whale watch during whole station time	jh	Single Pulse	0	20 kHz / 4 kHZ	Ctr. Paras. PHF	End of station work PS128_10
	Jan.	18	23:10		Start bathymetric and sediment sounding survey	jh	Single Pulse	0	20 kHz / 4 kHZ	Ctr. Paras. PHF	
	Jan.	19	03:45	n/a		ew					heavy ice, poor reflections, depth lost
		19	03:59	n/a	reset depth, first manual, later ext. Hydro PHF	ew				Manual and Hydro PHF	depth lost, heavy ice, poor signal
		19	04:02	n/a	Rammfahrt, back and forth , with whale watch all time	ew					stuck in ice = Rammfahrt (back and forth)
	Jan.	19	06:19		Reduced ping rate (10s), Stop moving, test of crane, with whale watch	cg	Single Pulse	10 s	20 kHz / 4 kHZ	Hydro PHF	
			07:24		Resume sounding , moving again after service stop, with whale watch all time	cg	Single Pulse	0	20 kHz / 4 kHZ	Hydro PHF	
			07:40		Rammfahrt, back and forth, with whale watch all time	ew	Single Pulse	0	20 kHz / 4 kHZ	Hydro PHF	
			08:11			ew	Single Pulse	0	20 kHz / 4 kHZ	Hydro PHF	passing Canyon Deep at -8.5673° , -70.0752°, at 08:11
	Jan.	19	08:36		Stop sounding and logging, because of seals in water, message of MMO	ew	off	off	off	Hydro PHF	Opportunistic sighting of seals by MMO
			08:52		Start sounding and logging after seals retreat , after Whale watch all times, message of MMO	ew	Single Pulse	0	20 kHz / 4 kHZ	Hydro PHF	

Year	Month	Day	Time UTC	Station	**Action** (e.g. "Start; Stop...") **–and Reason** (e.g. „Station reached; Whale Stop;...")	Ob-server	**Modus** (Single Pulse or QED)	Puls rate waiting time	**Frequencies** PHF / SLF	System Depth Source	Comments
	Jan.	19	11:12	PS128_11	Reduced ping rate (10s) when Station reached for exact positioning for sampling; with whale watch during station	jh	Single Pulse	10 s	20 kHz / 4 kHZ	Ctr. Paras. PHF	Start of station work PS128_11 at 11:19 Lon: - 8.617741°, Lat: -70.043582°, 2688 m
			15:57		Resume sounding with normal ping rate after station end; after whale watch during whole station time	ew	Single Pulse	0	20 kHz / 4 kHZ	Hydro PHF	End of station work PS128_11
	Jan.	19	20:22	Start part 1	Parasound/Hydrosweep profile on MCS line 5604; part 1	cg	Single Pulse	0	20 kHz / 4 kHZ	Hydro PHF	Start: 7°37.946‘ W; 70°01.288‘ S
			20:35	End part1	Parasound/Hydrosweep profile on MCS line 5604; part 1	cg	Single Pulse	0	20 kHz / 4 kHZ	Hydro PHF	End: 7°37.587‘ W; 69°59.669‘ S; Wassertiefe: 1745 m
		19	21:46	Start part 2	Parasound/Hydrosweep profile on MCS line 5604; part 2	cg	Single Pulse	0	20 kHz / 4 kHZ	Hydro PHF	Start: 7°35.249‘ W; 69°49.545‘ S; Wassertiefe: 2780 m
			22:37	End part 2	Parasound/Hydrosweep profile on MCS line 5604; part 2	cg	Single Pulse	0	20 kHz / 4 kHZ	Hydro PHF	End: 7°34.344‘ W; 69°45.764‘ S; 2882 m
	Jan.	19		Start part 3	Parasound/Hydrosweep profile on MCS line 5604; part 3	jh	Single Pulse	0	20 kHz / 4 kHZ	Hydro PHF	Start: 7°32.268‘ W; 69°36.341‘ S; m
				End part 3	Parasound/Hydrosweep profile on MCS line 5604; part 3	jh	Single Pulse	0	20 kHz / 4 kHZ	Hydro PHF	End: 7°32.579‘ W; 69°37.519‘ S; m
	Jan.	19	23:58		Stop sounding and logging, because of complete signal loss, probably due to heavy ice (~15s)	jh/ew	Single Pulse	0	20 kHz / 4 kHZ	Hydro PHF	
	Jan.	19	23:59		Resume sounding after quick pause (~15s)	jh/ew	Single Pulse	0	20 kHz / 4 kHZ	Hydro PHF	

Year	Month	Day	Time UTC	Station	**Action** (e.g. “Start; Stop...”) **–and Reason** (e.g. „Station reached; Whale Stop;...“)	Ob-server	**Modus** (Single Pulse or QED)	**Puls rate waiting time**	**Frequencies** PHF / SLF	**System Depth Source**	**Comments**
	Jan.	20	01:57		Reduced ping rate (10s); during approach to Station for exact positioning for sampling; with whale watch	jh/ew	Single Pulse	10 s	20 kHz / 4 kHZ	Ctr. Paras. PHF	Slow approach to Station PS128_12 due to heavy ice
	Jan.	20	02:35	PS128_12	Reduced ping rate (10 s) when Station reached for exact positioning for sampling; with whale watch during station	ew	Single Pulse	10 s	20 kHz / 4 kHZ	Ctr. Paras. PHF	Official start of station PS128_12 at 02:35 Lon: -7.573751°, Lat: -69.708690, 3068m
	Jan.	20	04:20		Resume sounding with normal ping rate after station end; after whale watch during whole station time	ew	Single Pulse	0	20 kHz / 4 kHZ	Hydro PHF	End of station work PS128_12
	Jan.	20	06:33		Reduced ping rate (10 s); approach to Station PS128_13 for exact positioning for sampling; with whale watch during station	cg	Single Pulse	10 s	20 kHz / 4 kHZ	Ctr. Paras. PHF	Slow approach to station PS128_13 due to heavy ice
	Jan.	20	07:06	PS128_13	Reduced ping rate (10 s); approach Station for exact positioning for sampling; with whale watch during station	cg	Single Pulse	10 s	20 kHz / 4 kHZ	Ctr. Paras. PHF	Start of station work PS128_13, Lon:-7.629235°, Lat:-70.001298°, 1577m
	Jan.	20	12:18		Resume sounding with normal ping rate after station end; after whale watch during whole station time	jh	Single Pulse	0	20 kHz / 4 kHZ	Hydro PHF	End of station work PS128_13

Year	Month	Day	Time UTC	Station	**Action** (e.g. “Start; Stop...”) **–and Reason** (e.g. „Station reached; Whale Stop;...“)	Ob-server	**Modus** (Single Pulse or QED)	Puls rate waiting time	**Frequencies** PHF / SLF	System Depth Source	Comments
	Jan.	20	14:44		Reduced ping rate (10s); approach to Station PS128_13 for exact positioning for sampling; with whale watch during station	ew	Single Pulse	10 s	20 kHz / 4 kHZ	Ctr. Paras. PHF	Slow approach to station PS128_14 due to ice
	Jan.	20	14:48	PS128_14	Reduced ping rate (10s); approach Station for exact positioning for sampling; with whale watch during station	ew	Single Pulse	10 s	20 kHz / 4 kHZ	Ctr. Paras. PHF	Start of station work PS128_14, Lon: -6.897941°, Lat: -70.136168, 1586 m
	Jan.	20	17:01		Stop sounding and logging, because of seal approach during station.	ew	off	off			Stop after telefone call of MMO , because of seal approach.
	Jan.	20	17:22		Start sounding and logging after seal retreat, after 15 min. MMO watch minimum	ew	Single Pulse	10 s	20 kHz / 4 kHZ	Ctr. Paras. PHF	no seal observed for at least 15 Min. around the station
	Jan.	20	20:18		Resume sounding with normal ping rate after station end; after whale watch during whole station time	cg	Single Pulse	0	20 kHz / 4 kHZ	Hydro PHF	End of station work PS128_14
	Jan.	20	21:15 21:16	PS128_15	Reduced ping rate (10 s); approach Station for exact positioning for sampling; with whale watch during station	cg	Single Pulse	10 s	20 kHz / 4 kHZ	Ctr. Paras. PHF	Start of station work PS128_15, 21:16 Lon: -6.813041°, Lat: -70.047672°, 1875 m
	Jan.	20	23:15		Stop sounding and logging, because of seal approach during station.	jh	off	off			Stop after telefone call of MMO , because of seal approach.

Year	Month	Day	Time UTC	Station	**Action** (e.g. "Start; Stop...") **–and Reason** (e.g. „Station reached; Whale Stop;...")	Ob-server	**Modus** (Single Pulse or QED)	Puls rate waiting time	**Frequencies** PHF / SLF	System Depth Source	Comments
	Jan.	20	23:33		Start sounding and logging after seal retreat, after 15 min. MMO watch minimum	jh	Single Pulse	10 s	20 kHz / 4 kHZ	Ctr. Paras. PHF	no seal observed for at least 15 Min. around the station
	Jan.	21	05:00		Resume sounding with normal ping rate after station end; after whale watch during whole station time	ew	Single Pulse	0	20 kHz / 4 kHZ	Ctr. Paras. PHF	End of station work PS128_15
	Jan.	21	06:08	PS128_16	Reduced ping rate (10s); approach Station for exact positioning for sampling; with whale watch during station	cg	Single Pulse	10 s	20 kHz / 4 kHZ	Ctr. Paras. PHF	Start of station work PS128_16, Lon: -6.745028°, Lat: -69.916510°, 2135m
	Jan.	21	21:57		Resume sounding with normal ping rate after station end; after whale watch during whole station time	cg	Single Pulse	0	20 kHz / 4 kHZ	Ctr. Paras. PHF	End of station work PS128_16
	Jan.	22	01:13	PS128_17	Reduced ping rate (10s); very slow approach to Station for exact positioning for sampling; with whale watch during station	jh	Single Pulse	10 s	20 kHz / 4 kHZ	Ctr. Paras. PHF	Very slow approach to final Station location, Start of station work PS128_17, at 01:43, Lon: -5.920082°, Lat: -69.760823°, 2305 m
	Jan.	22	11:27		Resume sounding with normal ping rate after station end; after whale watch during whole station time	jh	Single Pulse	0	20 kHz / 4 kHZ	Ctr. Paras. PHF	End of station work PS128_17

Year	Month	Day	Time UTC	Station	**Action** (e.g. “Start; Stop...”) **–and Reason** (e.g. „Station reached; Whale Stop;...“)	Ob-server	**Modus** (Single Pulse or QED)	Puls rate waiting time	**Frequencies** PHF / SLF	System Depth Source	Comments
	Jan.	22	12:43		Stop sounding and logging, because of whale approach < 100m .	jh	off	off			Stop after telefone call of MMO, because of whale approach closer than 100 m, Opportunistic sighting
	Jan.	22	12:59		Start sounding and logging after whale retreat , after 15 min. MMO watch minimum	jh	Single Pulse	0	20 kHz / 4 kHZ	Ctr. Paras. PHF	no whale observed for at least 15 Min. around the station
	Jan.	22	15:01	PS128_18	Continued sounding and logging during seismic test	ew	Single Pulse	0	20 kHz / 4 kHZ	Ctr. Paras. PHF	Seismik-Test PS128_18, 15:01-18:05 with special MMO during all the time
	Jan.	23	00:56	PS128_19	Reduced ping rate (10s); approach Station for exact positioning for sampling; with whale watch during station	jh	Single Pulse	10 s	20 kHz / 4 kHZ	Ctr. Paras. PHF	Start of station work PS128_19 at 01:03, Lon: -6.970819°, Lat: -68.532743°, 2956m
	Jan.	23	12:25		Resume sounding with normal ping rate after station end; after whale watch during whole station time	jh	Single Pulse	0	20 kHz / 4 kHZ	Ctr. Paras. PHF	End of station work PS128_19
	Jan.	23	18:20	PS128_20	Reduced ping rate (10s); approach Station for exact positioning for sampling; with whale watch during station	cg	Single Pulse	10 s	20 kHz / 4 kHZ	Ctr. Paras. PHF	Start of station work PS128_20 at 18:30, Lon: -5.588730°, Lat: -69.413031°, 1867 m
	Jan	24	05:19		Resume sounding with normal ping rate after station end; after whale watch during whole station time	ew	Single Pulse	0	20 kHz / 4 kHZ	Ctr. Paras. PHF	End of station work PS128_20

Year	Month	Day	Time UTC	Station	**Action** (e.g. “Start; Stop...”) **–and Reason** (e.g. „Station reached; Whale Stop;...“)	Ob-server	**Modus** (Single Pulse or QED)	Puls rate waiting time	**Frequencies** PHF / SLF	System Depth Source	Comments
	Jan	25	15:40	PS128_21	Continued sounding with normal ping rate during seismc survey, with whale watch during whole survey	ew	Single Pulse	0	20 kHz / 4 kHZ	Ctr. Paras. PHF	start seismic survey, seismic profile 20220105, Lon: -8° 12.361´W, Lat: -70° 18.022S, WD = 980 m
	Jan.	25	03:36		Reduced ping rate (10s); very slow ship speed , with whale watch during whole time	ew	Single Pulse	10s	20 kHz / 4 kHZ	Ctr. Paras. PHF	Reduced ping rate (10s), ship slowed down < 1Kn , because of problems with seismic.
	Jan.	25	03:41		Resume sounding with normal ping rate ship moves slowely on, with whale watch during whole time	ew	Single Pulse	0	20 kHz / 4 kHZ	Ctr. Paras. PHF	Resume sounding with normal ping rate , ship moves slowely on, and than speeds up again > 5Kn
	Jan.	27	00:11	PS128_22	Continued sounding with normal ping rate during seismc survey, with whale watch during whole survey	ew	Single Pulse	0	20 kHz / 4 kHZ	Ctr. Paras. PHF	end seismic survey, seismic profile 20220116, Lon: -8° 39.326’W, Lat: -70° 29.258’S ,WD = 205 m
	Jan.	27	03:08	PS128_23	Reduced ping rate (10s); slow approach Station for exact positioning for sampling; with whale watch during station	ew	Single Pulse	10 s	20 kHz / 4 kHZ	Ctr. Paras. PHF	Start of station work PS128_23 at 03:09, Lon: -9.119893°, Lat: -70.455736°, 356m
	Jan.	27	04:11		Resume sounding with normal ping rate after station end; after whale watch during whole station time	ew	Single Pulse	0	20 kHz / 4 kHZ	Ctr. Paras. PHF	End of station work PS128_23
	Jan.	27	04:23	PS128_24	Reduced ping rate (10s); slow approach Station for exact positioning for sampling; with whale watch during station	ew	Single Pulse	10 s	20 kHz / 4 kHZ	Ctr. Paras. PHF	Start of station work PS128_24 at 04:27, Lon: -5.588730°, Lat: -69.413031°, 1867m

Year	Month	Day	Time UTC	Station	**Action** (e.g. “Start; Stop...”) **–and Reason** (e.g. „Station reached; Whale Stop;...“)	Ob-server	**Modus** (Single Pulse or QED)	Puls rate waiting time	**Frequencies** PHF / SLF	System Depth Source	Comments
	Jan.	27	04:47		Resume sounding with normal ping rate after station end; after whale watch during whole station time	ew	Single Pulse	0	20 kHz / 4 kHZ	Ctr. Paras. PHF	End of station work PS128_24
	Jan.	27	07:57	PS128_25	Reduced ping rate (10s); slow approach Station for exact positioning for sampling; with whale watch during station	cg	Single Pulse	10 s	20 kHz / 4 kHZ	Ctr. Paras. PHF	Start of station work PS128_25 at 08:00, Lon: -8.552672°, Lat: -70.074978°, 2619m
	Jan.	27	12:04		Resume sounding with normal ping rate after station end; after whale watch during whole station time	jh	Single Pulse	0	20 kHz / 4 kHZ	Ctr. Paras. PHF	End of station work PS128_25
	Jan.	28	11:16	PS128_26	Reduced ping rate (10s); slow approach Station for exact positioning for sampling; with whale watch during station	jh	Single Pulse	10	20 kHz / 4 kHZ	Ctr. Paras. PHF	Start of station work PS128_26, Lon: 1.035782°E , Lat: -69.401338°S, 3300m
	Jan.	28	13:50		Resume sounding with normal ping rate after station end; after whale watch during whole station time	ew	Single Pulse	0	20 kHz / 4 kHZ	Ctr. Paras. PHF	End of station work PS128_26
	Jan.	28	14:39		QED, 2Pulse, Test	ew	QED	2Pulse	20 kHz / 4 kHZ	Ctr. Paras. PHF	WD:~ 3000m, test, ship speed > 10-12 Kn, rough topography
	Jan.	28	16:12		QED, 4Pulse, Test	ew	QED	4Pulse	20 kHz / 4 kHZ	Ctr. Paras. PHF	WD:~ 3000m, test, ship speed > 10-12 Kn, rough topography
	Jan.	28	17:49		Single Pulse	ew	Single Pulse	0	20 kHz / 4 kHZ	Ctr. Paras. PHF	End of Test
	Jan.	29	02:14		QED, 4Pulse	ew	QED	4Pulse	20 kHz / 4 kHZ	Ctr. Paras. PHF	WD:~ 3000m, test, ship speed > 10-12 Kn, rough topography

Year	Month	Day	Time UTC	Station	**Action** (e.g. "Start; Stop...") **–and Reason** (e.g. „Station reached; Whale Stop:...")	Ob-server	**Modus** (Single Pulse or QED)	**Puls rate waiting time**	**Frequencies** PHF / SLF	**System Depth Source**	**Comments**
	Jan.	29	04:07	PS128_27	Reduced ping rate (10s); slow approach Station for exact positioning for sampling; with whale watch during station	ew	Single Pulse	10s	20 kHz / 4 kHZ	Ctr. Paras. PHF	Start of station work PS128_27, Lon: 8.913578°E , Lat: -68.838910 °S, 3577m
	Jan.	29	06:37		Stop sounding and logging, because on station with even seafloor and subsurface .	cg	off	off			Station PS128_27; Stop sounding and logging, because on station with an even seafloor and subsurface . So no detailed sounding necessary.
	Jan.	29	09:21		Resume sounding with reduced ping rate after station end; after 15 min. whale watch minimum	cg	Single Pulse	10s	20 kHz / 4 kHZ	Ctr. Paras. PHF	End of station work PS128_27; soft start wait time 10 s
	Jan.	29	09:28		Resume sounding with normal ping rate after soft start with reduced ping rate	cg	Single Pulse	0	20 kHz / 4 kHZ	Ctr. Paras. PHF	normal ping rate after soft start; wait time 0 s
	Jan.	29	15:08		QED, 2Pulse, transit	ew	QED	2Pulse	20 kHz / 4 kHZ	Ctr. Paras. PHF	WD:~ 1500m, transit, ship speed > 10-12 Kn, rough topography
	Jan.	30	01:56		QED, 4Pulse, transit	ew	QED	4Pulse	20 kHz / 4 kHZ	Ctr. Paras. PHF	WD:~ 3500m, transit, ship speed > 10-12 Kn, rough topography
	Jan.	30	02:17		QED, 2Pulse, transit	ew	QED	2Pulse	20 kHz / 4 kHZ	Ctr. Paras. PHF	WD:~ 3500m, transit, ship speed >10-12Kn, rough, hard topography, 4Pulses = image noisy Bild "verschneit"
	Jan.	30	04:56	PS128_28	Stop sounding and logging, because on CTD station without penetration.	ew	off	off			Station PS128_28; Stop sounding and logging, because on CTD station without penetration . So no detailed sounding necessary.

Year	Month	Day	Time UTC	Station	**Action** (e.g. “Start; Stop...”) **–and Reason** (e.g. „Station reached; Whale Stop;...“)	Ob-server	**Modus** (Single Pulse or QED)	Puls rate waiting time	**Frequencies** PHF / SLF	System Depth Source	Comments
	Jan.	30	08:11		Resume sounding with reduced ping rate after station end; after 15 min. whale watch minimum	cg	QED	10s	20 kHz / 4 kHZ	Ctr. Paras. PHF	End of station work PS128_28; soft start wait time 10 s
	Jan.	30	08:18		Resume sounding with normal ping rate after soft start with reduced ping rate	cg	QED	2Pulse	20 kHz / 4 kHZ	Ctr. Paras. PHF	normal ping rate after soft start; wait time 0 s
	Jan.	31	07:59	PS128_29	Stop sounding and logging, because on CTD station without penetration.	cg	off	off			Station PS128_29; Stop sounding and logging, because on CTD station without penetration . So no detailed sounding necessary.
	Jan.	31	10:55		Resume sounding with reduced ping rate after station end; after 15 min. whale watch minimum	jh	QED	10s	20 kHz / 4 kHZ	Ctr. Paras. PHF	End of station work PS128_29; soft start wait time 10 s
	Jan.	31	11:00		Resume sounding with normal ping rate after soft start with reduced ping rate	jh	QED	2Pulse	20 kHz / 4 kHZ	Ctr. Paras. PHF	normal ping rate after soft start; wait time 0 s
	Jan.	31	13:02		Change to Single Pulse	jh	Single Pulse	0	20 kHz / 4 kHZ	Ctr. Paras. PHF	High speed through ice, and up onto the shelf
2022	Feb.	1	03:52		Sounding and logging for survey of bathymetry and sediment echolot	ew	Single Pulse	0	20 kHz / 4 kHZ	Ctr. Paras. PHF	Gulli-Profilfahrt, 5 Kn über Grund, viel Eisbedeckung = viele Tiefensprünge
	Feb.	1	05:17		Normal sounding and logging after survey	ew	Single Pulse	0	20 kHz / 4 kHZ	Ctr. Paras. PHF	Ende der detaillierten Gulli-Profilfahrt, Fahrt > 12 Kn

Year	Month	Day	Time UTC	Station	**Action** (e.g. “Start; Stop...”) **–and Reason** (e.g. „Station reached; Whale Stop;...“)	Ob-server	**Modus** (Single Pulse or QED)	Puls rate waiting time	**Frequencies** PHF / SLF	System Depth Source	**Comments**
	Feb.	1	09:11	PS128_30	Stop sounding and logging, because on station with even seafloor and subsurface .	cg	off	off			Station PS128_30; 09:16, WD = 3914m. Lat: -67.584846°S, Lon: 38.007862° E Stop sounding and logging, because on station with an even seafloor and subsurface , sounding not necessary.
	Feb.	1	08:55-15:03		Parasound "frozen" with wrong water depth during whole station time		off	off			Parasound jumped to wrong waterdepth (Parasound: 1050m=wrong, Fishlot3920m=true). Wrong parasound depth during whole station time, likely due to ice just at the moment sounding was stopped. Comment :ew
	Feb.	1	15:03		Resume sounding with reduced ping rate after station end; after 15 min. whale watch minimum	ew	Single Pulse	10s	20 kHz / 4 kHZ	Ctr. Paras. PHF	End of station work PS128_30; soft start wait time 10 s, jump back of WD = 4067m = ok again
	Feb.	1	15:10		Resume sounding with normal ping rate after soft start with reduced ping rate	ew	Single Pulse	0	20 kHz / 4 kHZ	Ctr. Paras. PHF	normal ping rate after soft start; wait time 0 s
	Feb.	1	16:01		System Depth source to Hydro PHF, automatic 20%, high speed >> 10 Kn	ew	Single Pulse	0	20 kHz / 4 kHZ	Hydro PHF	speed > 14 Kn

Year	Month	Day	Time UTC	Station	**Action** (e.g. "Start; Stop...") **–and Reason** (e.g. „Station reached; Whale Stop:...")	Ob-server	**Modus** (Single Pulse or QED)	**Puls rate waiting time**	**Frequencies** PHF / SLF	**System Depth Source**	**Comments**
	Feb.	2	~ 7:00		Manual depth control because of unstable depth values	ew	Single Pulse	0	20 kHz / 4 kHZ	Combined Ctr. Paras. PHF, Hydro PHF, and NAVlot as base	Manual depth control because of jumping depth values. Additional attension on hardly known shelf region with shallow water depths (< 600m), heavy ice and various ship speed (3-9 Kn).
	Feb.	2	10:37		Stopp sounding and logging, because ship stopped for some hours	jh	off	off			Stopp sounding and logging after information from bridge that ship will stay for safety and rescue training
	Feb.	2	14:40								Call from bridge to prepare for profiling, activation of MMO
	Feb.	2	15:10		Resume sounding with reduced ping rate after station end; after 15 min. whale watch minimum	ew	Single Pulse	10s	20 kHz / 4 kHZ	Ctr. Paras. PHF	End of stopp for savety drill
	Feb.	2	15:15		Resume sounding with normal ping rate after soft start with reduced ping rate	ew	Single Pulse	0	20 kHz / 4 kHZ	Ctr. Paras. PHF	normal ping rate after soft start; wait time 0 s
	Feb.	3	03:00		System Depth source to Hydro PHF, automatic 20%, high speed >> 10 Kn	ew	Single Pulse	0	20 kHz / 4 kHZ	Hydro PHF	ship speed >> 10 Kn

Year	Month	Day	Time UTC	Station	**Action** (e.g. “Start; Stop...”) **–and Reason** (e.g. „Station reached; Whale Stop;...“)	Ob-server	**Modus** (Single Pulse or QED)	Puls rate waiting time	**Frequencies** PHF / SLF	System Depth Source	Comments
	Feb.	3	07:26	PS128_31	Stop sounding and logging, because on station for CTD only .	ew	off	off			Start Station PS128_31, WD = 3582 m. Lat:-65.423042°S, Lon: 49.136241° E Stop sounding because CTD only. WD-values at station start: 3420m (Fishlot), 3550 m (Parasound), but CTD actually reached down to 3582 m!
	Feb.	3	10:08		Resume sounding with reduced ping rate after station end; after 15 min. whale watch minimum	jh	Single Pulse	10s	20 kHz / 4 kHZ	Hydro PHF	End of Station work PS128_31; soft start wait time 10 s
	Feb.	3	10:14		Resume sounding with normal ping rate after soft start with reduced ping rate	jh	Single Pulse	0	20 kHz / 4 kHZ	Hydro PHF	normal ping rate after soft start; wait time 0 s
	Feb.	3	13:27		Stop sounding and logging, because of whale approach < 100m .	jh	off	off			Stop after telefone call of MMO , because of whale approach closer than100m, Opportunistic sighting
	Feb.	3	14:01		Softstart: Resume sounding with reduced ping rate after whale retreat; after 15 min. whale watch minimum	ew	Single Pulse	10s	20 kHz / 4 kHZ	Hydro PHF	Call of MMO, whale retreat, and no whales sighted for at least 15 min.
	Feb.	3	14:06		Resume sounding with normal ping rate after soft start with reduced ping rate	ew	Single Pulse	0	20 kHz / 4 kHZ	Hydro PHF	normal ping rate after soft start; wait time 0 s
	Feb.	4	00:35	PS128_32	Stop sounding and logging, because on station.	jh	off	off			Start Station PS128_32, WD (Fishlot) =3586 m, Lat: -65.185118°S, Lon: 55.137033°E.

Year	Month	Day	Time UTC	Station	**Action** (e.g. "Start; Stop...") **–and Reason** (e.g. „Station reached; Whale Stop:...")	Ob-server	**Modus** (Single Pulse or QED)	**Puls rate waiting time**	**Frequencies** PHF / SLF	**System Depth Source**	**Comments**
	Feb.	4	05:55		Resume sounding with reduced ping rate after station end; after 15 min. whale watch minimum	cg	Single Pulse	10s	20 kHz / 4 kHZ	Hydro PHF	End of station work PS128_32; soft start wait time 10 s
	Feb.	4	06:02		Resume sounding with normal ping rate after soft start with reduced ping rate	cg	Single Pulse	0	20 kHz / 4 kHZ	Hydro PHF	normal ping rate after soft start; wait time 0 s
	Feb.	4	08:18		QED, 2Pulse, transit	ew	QED	2Pulse	20 kHz / 4 kHZ	manual	WD:~ 3500m, transit, ship speed ~ 10 Kn, rough, hard topography
	Feb.	4	08:24		back to single Pulse, strong topographiy and heavy sea	ew	Single Pulse	0	20 kHz / 4 kHZ	manual	
	Feb.	5	02:00		heavy sea	ew	Single Pulse	0	20 kHz / 4 kHZ	automatic 5%	WD:~ 3500m, heavy sea
	Feb.	6	02:00		heavy sea	ew	Single Pulse	0	20 kHz / 4 kHZ	automatic 5%	WD:~ 3500m, heavy sea
	Feb.	6	18:27		Stop sounding and logging, waiting for better wheather for station work	cg	off	off			
	Feb.	7	01:14		Still no sounding and logging, Start Station PS128_33	cg	off	off			Start Station PS128_33, WD(Fishl)=3283m Lat: -65.863037°S, Lon: 64.398677°E.
	Feb.	7	06:31		Softstart: Resume sounding with reduced ping rate after whale retreat; after 15 min. whale watch minimum	cg	Single Pulse	10s	20 kHz / 4 kHZ	Ctr. Paras. PHF,	End of station work PS128_33; soft start wait time 10 s
	Feb.	7	06:38		Resume sounding with normal ping rate after soft start with reduced ping rate	cg	Single Pulse	0	20 kHz / 4 kHZ	Ctr. Paras. PHF,	normal ping rate after soft start; wait time 0 s

Year	Month	Day	Time UTC	Station	**Action** (e.g. “Start; Stop...”) **–and Reason** (e.g. „Station reached; Whale Stop;...“)	Ob-server	**Modus** (Single Pulse or QED)	Puls rate waiting time	**Frequencies** PHF / SLF	System Depth Source	Comments
	Feb.	7	09:20	PS128_34	Reduced ping rate (10s); slow approach to Station, continued sounding for exact positioning for sampling; with whale watch during all station work	ew	Single Pulse	10	20 kHz / 4 kHZ	Ctr. Paras. PHF	Start of station work PS128_34, Lon: 63.398880°E , Lat: -65.974846 °S, WD (Fishlot) = 3024 m, Paras. = 3140m, Hydro. 3093m
	Feb.	7	18:05		Resume sounding with normal ping rate after station end; after whale watch during whole station time	cg	Single Pulse	0	20 kHz / 4 kHZ	Ctr. Paras. PHF	End of station work PS128_234
	Feb.	7	21:09	PS128_35	Reduced ping rate (10s); slow approach to station, continued sounding for exact positioning for sampling; no whale watch possible due to darkness, heavy sea and low visibility	cg	Single Pulse	10s	20 kHz / 4 kHZ	Ctr. Paras. PHF	Start of station work PS128_35, Lon:63.955646°E , Lat: -65.896642 °S, WD (Fishlot) = 3160
	Feb.	8	00:35		Resume sounding with normal ping rate after soft start with reduced ping rate	jh	Single Pulse	0	20 kHz / 4 kHZ	Ctr. Paras. PHF	End of station work PS128_35
	Feb.	8	07:20	Parasound survey	Start Parasound survey	ew	Single Pulse	0	20 kHz / 4 kHZ	Manual	Start of Parasound survey , Lon: 66.60005°E, Lat: -66.28039°S, WD=2160m (Paras), 2110m (Hydro)
	Feb.	8	09:00		Continue sounding for Parasound survey, change course to new WP	ew	Single Pulse	0	20 kHz / 4 kHZ	Manual	Continue sounding for Parasound survey, change course to new WP, WD= 1894 m (Hydro), 1975 m (Paras)

Year	Month	Day	Time UTC	Station	**Action** (e.g. "Start; Stop...") **–and Reason** (e.g. „Station reached; Whale Stop;...")	Ob-server	**Modus** (Single Pulse or QED)	**Puls rate waiting time**	**Frequencies** PHF / SLF	**System Depth Source**	**Comments**
	Feb.	8	17:02	PS128_36	Stop sounding and logging, because on station with CTD only	ew	off	off			Start of station work PS128_36, Lon: 65.826429°E , Lat: -66.730078°S, WD (Fishlot) = 1970 m, Paras. = 2040m, Hydro. 2001m
	Feb.	8	18:51		Reduced ping rate (10s); soft start after station; no whale watch possible due to darkness and low visibility, but sounding necessary due to unknown and shallow shelf	cg	Single Pulse	10s	20 kHz / 4 kHZ	Ctr. Paras. PHF	End of station work PS128_36, promt sounding start necessary because in unknown but very shallow shelf-region (WD=95m only)
	Feb.	8	18:58		Resume sounding with normal ping rate after soft start with reduced ping rate	cg	Single Pulse	0	20 kHz / 4 kHZ	Ctr. Paras. PHF	
	Feb.	8	22:55	PS128_37	Sounding and logging for survey of bathymetry and sediment echolot	ew	Single Pulse	0	20 kHz / 4 kHZ	Ctr. Paras. PHF	Start of bathymetry and sediment echolot survey, continous sounding and logging on very shallow shelf, speed ~5-6 Kn. Lon: 66.303861°E, Lat: -67.300424°S, WD=294m
	Feb.	9	06:28		End of special survey for bathymetry and echosounding; ongoing sounding and logging	cg	Single Pulse	0	20 kHz / 4 kHZ	Ctr. Paras. PHF	End of survey PS128_37, Lon: 65.310067°E, Lat:-67.021598°S, WD=514m, change of course and increase of speed during transit to next station

Year	Month	Day	Time UTC	Station	**Action** (e.g. “Start; Stop...”) **–and Reason** (e.g. „Station reached; Whale Stop;...“)	Ob-server	**Modus** (Single Pulse or QED)	Puls rate waiting time	**Frequencies** PHF / SLF	System Depth Source	Comments
	Feb.	9	08:18	PS128_38	Reduced ping rate (10s); slow approach to Station, continued sounding for exact positioning for sampling; with whale watch during all station work	ew	Single Pulse	10	20 kHz / 4 kHZ	Ctr. Paras. PHF	Start of station work PS128_38, Lon: 65.817024°E , Lat: -67.142642 °S, WD (Fishlot) = 514 m, Paras. = 547m, Hydro. 524m
	Feb.	9	11:01		Resume sounding with normal ping rate after station end; after whale watch during whole station time	jh	Single Pulse	0	20 kHz / 4 kHZ	Ctr. Paras. PHF	End of station work PS128_38
	Feb.	9	14:01	PS128_39	Reduced ping rate (10s); slow approach to Station, continued sounding for exact positioning for sampling; with whale watch during all station work	jh	Single Pulse	10	20 kHz / 4 kHZ	Ctr. Paras. PHF	Start of station work PS128_39, Lon: 65.694737°E , Lat: -67.115734 °S, WD (Fishlot) = 647 m, Paras. = 685m, Hydro=661 m
	Feb.	9	16:26		Resume sounding with normal ping rate after station end; after whale watch during whole station time	ew	Single Pulse	0	20 kHz / 4 kHZ	Ctr. Paras. PHF	End of station work PS128_39
	Feb.	9	17:30	PS128_40	Reduced ping rate (10s); slow approach to station, continued sounding for exact positioning for sampling; no whale watch possible due to darkness	ew	Single Pulse	10	20 kHz / 4 kHZ	Ctr. Paras. PHF	Start of station work PS128_40, Lon: 65.993619°E , Lat: -67.172171 °S, WD (Fishlot) = 816 m, Paras. = 848m, Hydro. --m
	Feb.	9	21:36		Resume sounding with normal ping rate after station end	cg	Single Pulse	0	20 kHz / 4 kHZ	Ctr. Paras. PHF	End of station work PS128_40

Year	Month	Day	Time UTC	Station	**Action** (e.g. “Start; Stop...”) **–and Reason** (e.g. „Station reached; Whale Stop;...“)	Ob-server	**Modus** (Single Pulse or QED)	Puls rate waiting time	**Frequencies** PHF / SLF	System Depth Source	Comments
	Feb.	9	23:03	PS128_41	Reduced ping rate (10s); slow approach to Station, continued sounding for exact positioning for samplingafter; whale watch during whole station time	jh	Single Pulse	10	20 kHz / 4 kHZ	Ctr. Paras. PHF	Start of station work PS128_40, Lon: 65.598867°E , Lat: -67.091858 °S, WD (Fishlot) = 550 m, Paras. = --m, Hydro. --m
	Feb.	9	23:39		Resume sounding with normal ping rate after station end	jh	Single Pulse	0	20 kHz / 4 kHZ	Ctr. Paras. PHF	End of station work PS128_41
	Feb.	10	00:11	PS128_42	Reduced ping rate (10s); slow approach to Station, continued sounding for exact positioning for sampling; with whale watch during all station work	jh	Single Pulse	10	20 kHz / 4 kHZ	Ctr. Paras. PHF	Start of station work PS128_42, Lon: 65.497155°E , Lat:-67.067495 °S, WD (Fishlot) = 581 m, Paras. = 591 m, Hydro. --m
	Feb.	10	00:45		Resume sounding with normal ping rate after station end	jh	Single Pulse	0	20 kHz / 4 kHZ	Ctr. Paras. PHF	End of station work PS128_42
	Feb.	10	00:45		Sounding and logging for survey of bathymetry and sediment echolot	ew	Single Pulse	0	20 kHz / 4 kHZ	Ctr. Paras. PHF	Start of bathymetry and sediment echolot survey, continous sounding and logging on very shallow shelf, speed ~5-6 Kn. Lon:65.497913°E, Lat: -67.067806°S, WD=580m
	Feb.	10	08:58		Continue of sounding and logging. End of survey of bathymetry and sediment echolot.	ew	Single Pulse	0	20 kHz / 4 kHZ	Ctr. Paras. PHF	End of bathymetrie and parasound survey, ~ Lon: 64° 55.3'E, Lat: 66° 53.7' S, WD (Hydro) = 312 m , Paras = 328m

Year	Month	Day	Time UTC	Station	**Action** (e.g. "Start; Stop...") **–and Reason** (e.g. „Station reached; Whale Stop:...")	Ob-server	**Modus** (Single Pulse or QED)	**Puls rate waiting time**	**Frequencies** PHF / SLF	**System Depth Source**	**Comments**
	Feb.	10	09:42	PS128_43	Reduced ping rate (10s); slow approach to Station, continued sounding for exact positioning for sampling; with whale watch during all station work	ew	Single Pulse	10	20 kHz / 4 kHZ	Ctr. Paras. PHF	Start of station work PS128_43, Lon: 65.031605°E , Lat: -66.970524 °S, WD = 391
	Feb.	10	10:10		Resume sounding with normal ping rate after station end	jh	Single Pulse	0	20 kHz / 4 kHZ	Ctr. Paras. PHF	End of station work PS128_43
	Feb.	10	10:47	PS128_44	Reduced ping rate (10s); slow approach to Station, continued sounding for exact positioning for sampling; with whale watch during all station work	jh	Single Pulse	10	20 kHz / 4 kHZ	Ctr. Paras. PHF	Start of station work PS128_44, Lon:64.991464°E , Lat:-66.960064 °S, WD =403
	Feb.	10	12:12		Resume sounding with normal ping rate after station end	jh	Single Pulse	0	20 kHz / 4 kHZ	Ctr. Paras. PHF	End of station work PS128_44
	Feb.	10	12:48	PS128_45	Reduced ping rate (10s); slow approach to Station, continued sounding for exact positioning for sampling; with whale watch during all station work	jh	Single Pulse	10	20 kHz / 4 kHZ	Ctr. Paras. PHF	Start of station work PS128_45, Lon: 64.857773°E , Lat: -66.952607 °S, WD = 385
	Feb.	10	13:24		Resume sounding with normal ping rate after station end	jh	Single Pulse	0	20 kHz / 4 kHZ	Ctr. Paras. PHF	End of station work PS128_45
	Feb.	10	20:16	PS128_46	Reduced ping rate (10s); slow approach to station, continued sounding for exact positioning for sampling; no whale watch possible due to darkness	cg	Single Pulse	10	20 kHz / 4 kHZ	Ctr. Paras. PHF	Start of station work PS128_46, Lon: 63.188769°E , Lat: -66.843023 °S, WD = 377, Ausnahmegenehmigung (§17,Abs.2 Satz 1 AUG, V.)3.))

Year	Month	Day	Time UTC	Station	**Action** (e.g. “Start; Stop...”) **– and Reason** (e.g. „Station reached; Whale Stop;...“)	Ob-server	**Modus** (Single Pulse or QED)	Puls rate waiting time	**Frequencies** PHF / SLF	System Depth Source	Comments
	Feb.	10	21:07		Resume sounding with normal ping rate after station end	cg	Single Pulse	0	20 kHz / 4 kHZ	Ctr. Paras. PHF	End of station work PS128_46
	Feb.	10	21:19	PS128_47	Reduced ping rate (10s); slow approach to station, continued sounding for exact positioning for sampling; no whale watch possible due to darkness	cg	Single Pulse	10	20 kHz / 4 kHZ	Ctr. Paras. PHF	Start of station work PS128_47, Lon: 63.208385°E , Lat: -66.828251 °S, WD = 390, Ausnahmegenehmigung (§17,Abs.2 Satz 1 AUG, V.)3.))
	Feb.	10	21:51		Resume sounding with normal ping rate after station end	cg	Single Pulse	0	20 kHz / 4 kHZ	Ctr. Paras. PHF	End of station work PS128_47
	Feb.	11	02:54		Start Parasound survey	ew	Single Pulse	0	20 kHz / 4 kHZ	Ctr. Paras. PHF	Start HS/PS-Survey at 03:00 Lon: 61.51864°E, Lat: -66.53495°S
	Feb.	11	05:36		Turn course of Parasound survey	ew	Single Pulse	0	20 kHz / 4 kHZ	Ctr. Paras. PHF	Turn back for coring to position Lat: -66° 28.668'S, Lon: 61° 23.415'E (was at 03:46UTC)
	Feb.	11	06:58	PS128_48	Reduced ping rate (10s); slow approach to Station, continued sounding for exact positioning for sampling; with whale watch during all station work	cg	Single Pulse	10	20 kHz / 4 kHZ	Ctr. Paras. PHF	Start of station work PS128_48, Lon:61.391055°E , Lat:-66.477115 °S, WD = 1571m
	Feb.	11	08:47		Resume sounding with normal ping rate after station end	ew	Single Pulse	0	20 kHz / 4 kHZ	Ctr. Paras. PHF	End of station work PS128_48

Year	Month	Day	Time UTC	Station	**Action** (e.g. "Start; Stop...") **– and Reason** (e.g. „Station reached; Whale Stop;...")	Ob-server	**Modus** (Single Pulse or QED)	Puls rate waiting time	**Frequencies** PHF / SLF	System Depth Source	Comments
	Feb.	11	09:35	PS128_49	Reduced ping rate (10s); slow approach to Station, continued sounding for exact positioning for sampling; with whale watch during all station work	ew	Single Pulse	10	20 kHz / 4 kHZ	Ctr. Paras. PHF	Start of station work PS128_49, Lon:61.216545°E , Lat:-66.401271 °S, WD = 2193
	Feb.	11	10:26		Stop sounding and logging, because of whale approach < 100m .	jh	off	off			Stop after telefone call of MMO , because of whale approach closer than100m.
	Feb.	11	10:42		Resume sounding with reduced ping rate after whale retreat; after 15 min. whale watch minimum	jh	Single Pulse	10	20 kHz / 4 kHZ	Ctr. Paras. PHF	Call of MMO, whale retreat, and no whales sighted for at least 15 min.
	Feb.	11	13:44		Resume sounding with normal ping rate after station end	jh	Single Pulse	0	20 kHz / 4 kHZ	Ctr. Paras. PHF	End of station work PS128_49 at 13:09, but long time to save equipment until steaming on
	Feb.	11	14:43		Sounding and logging for survey of bathymetry and sediment echolot	ew	Single Pulse	0	20 kHz / 4 kHZ	Ctr. Paras. PHF	Start of bathymetry and sediment echolot survey, continous sounding and logging , speed ~5-6 Kn, WD=2 500m
	Feb.	11	17:53	PS128_50	Reduced ping rate (10s); slow approach to station, continued sounding for exact positioning for sampling; no whale watch possible due to darkness	ew	Single Pulse	10	20 kHz / 4 kHZ	Ctr. Paras. PHF	Start of station work PS128_49, Lon: 60.316343°E , Lat:-66.288943 °S, WD =2817m, Ausnahmegenehmigung (§17,Abs.2 Satz 1 AUG, V.)3.))
	Feb.	11	21:56		Resume sounding with normal ping rate after station end	cg	Single Pulse	0	20 kHz / 4 kHZ	Ctr. Paras. PHF	End of station work PS128_50

Year	Month	Day	Time UTC	Station	**Action** (e.g. “Start; Stop...”) **–and Reason** (e.g. „Station reached; Whale Stop;...“)	Ob-server	**Modus** (Single Pulse or QED)	Puls rate waiting time	**Frequencies** PHF / SLF	System Depth Source	Comments
	Feb.	12	04:03		Sounding and logging for survey of bathymetry and sediment echolot	ew	Single Pulse	0	20 kHz / 4 kHZ	Ctr. Paras. PHF	Start of bathymetry and sediment echolot survey, continous sounding and logging , speed ~5-6 Kn, WD=2630m Lon: 58°50,7'E, Lat:-65°56.34°S,
	Feb.	12	05:30		turn back to 04:32 position for sampling	ew	Single Pulse	0	20 kHz / 4 kHZ	Ctr. Paras. PHF	
	Feb.	12	06:24	PS128_51	Reduced ping rate (10s); slow approach to Station, continued sounding for exact positioning for sampling; with whale watch during all station work	cg	Single Pulse	10	20 kHz / 4 kHZ	Ctr. Paras. PHF	Start of station work PS128_51, Lon: 58.784315°E , Lat: -65.901227°S, WD = 2724 m
	Feb.	12	09:08		Resume sounding with normal ping rate after station stop, with whale watch during all station work	ew	Single Pulse	0	20 kHz / 4 kHZ	Ctr. Paras. PHF	Station work at PS128_51 cancelled because of rough sea
	Feb.	13	07:40		Continuous sounding and logging during fast return to Molodezhnaya		Single Pulse	0	20 kHz / 4 kHZ	Ctr. Paras. PHF	Fast return to Molodezhnaya (12-14Kn) along shelf edge = rough topography = poor signal quality
	Feb.	13	14:44		Stop sounding and logging, because of whale approach < 100m	ew	off	off			Stop sounding and logging, because of whale approach. Call from MMO, Opportunistic sighting
	Feb.	13	14:59		Resume sounding and logging with normal ping rate after whale retreat	ew	Single Pulse	0	20 kHz / 4 kHZ	Ctr. Paras. PHF	Resume sounding with normal ping rate, no whale was sighted for at least 15 min., information from bridge

Year	Month	Day	Time UTC	Station	**Action** (e.g. “Start; Stop...”) **–and Reason** (e.g. „Station reached; Whale Stop;...“)	Ob-server	**Modus** (Single Pulse or QED)	**Puls rate waiting time**	**Frequencies** PHF / SLF	**System Depth Source**	**Comments**
	Feb.	13	15:50		Stop sounding and logging, because of whale approach < 100m	ew	off	off			Stop sounding and logging, because of whale approach. Call from MMO, Opportunistic sighting
	Feb.	13	16:05		Resume sounding and logging with normal ping rate after whale retreat	ew	Single Pulse	0	20 kHz / 4 kHZ	Ctr. Paras. PHF	Resume sounding with normal ping rate, no whale was sighted for at least 15 min., information from bridge
	Feb.	14	02:30			ew	Single Pulse	0	20 kHz / 4 kHZ	Ctr. Paras. PHF	Reaching shelf edge off Molodezhnaya WD < 500m
	Feb.	14	07:37		Stop sounding and logging, approaching off Molodezhnaya, flight operations	cg	off	off			
	Feb.	14	12:57		Resume sounding with reduced ping rate (sofstart) after leaving Molodezhnaya; after 15 min. whale watch minimum	ew	Single Pulse	10	20 kHz / 4 kHZ	Ctr. Paras. PHF	Resume sounding with normal ping rate, no whale was sighted for at least 15 min., information from bridge, MMO
	Feb.	14	13:05		Resume sounding and logging with normal ping rate after leaving Molodezhnaya, after 15. min whale whatch minimum	ew	Single Pulse	0	20 kHz / 4 kHZ	Ctr. Paras. PHF	Resume sounding with normal ping rate (wait time = 0),
	Feb.	14	13:50	PS128_52	Reduced ping rate (10s); slow approach to Station, continued sounding for exact positioning for sampling; with whale watch during all station work	ew	Single Pulse	10	20 kHz / 4 kHZ	Ctr. Paras. PHF	Start of station work PS128_52, Lon: 45.927384°E , Lat: -67.523105°S, WD = 697 m

Year	Month	Day	Time UTC	Station	**Action** (e.g. "Start; Stop...") **–and Reason** (e.g. „Station reached; Whale Stop:...")	Ob-server	**Modus** (Single Pulse or QED)	**Puls rate waiting time**	**Frequencies** PHF / SLF	**System Depth Source**	**Comments**
	Feb.	14	14:47		Resume sounding with normal ping rate after station end,with whale watch during all station work	jh	Single Pulse	0	20 kHz / 4 kHZ	Ctr. Paras. PHF	End of station work PS128_52
	Feb.	15	01:58	PS128_53	Reduced ping rate (10s); slow approach to Station, continued sounding for exact positioning for sampling; with whale watch during all station work	ew	Single Pulse	10	20 kHz / 4 kHZ	Ctr. Paras. PHF	Start of station work PS128_53, Lon: 48.779406°E , Lat:-66.257502°S, WD = 1072 m
	Feb.	15	03:34		Resume sounding with normal ping rate after station end,with whale watch during all station work	ew	Single Pulse	0	20 kHz / 4 kHZ	Ctr. Paras. PHF	End of station work PS128_53
			05:54		Kursänderung um japanischen Eisbrecher zu treffen						
	Feb.	15	15:00		Stop sounding and logging, because of whale approach < 100m	ew	off	off			Stop sounding and logging, because of whale approach. Call from bridge, opportunistic sighting
	Feb.	15	15:15		Resume sounding and logging with normal ping rate after whale retreat	ew	Single Pulse	0	20 kHz / 4 kHZ	Hydro PHF	Resume sounding with normal ping rate, no whale was sighted for at least 15 min., information from bridge
	Feb.	15	15:27		Stop sounding and logging, because of whale approach < 100m	ew	off	off			Stop sounding and logging, because of whale approach. Call from bridge, opportunistic sighting

Year	Month	Day	Time UTC	Station	**Action** (e.g. “Start; Stop...”) **–and Reason** (e.g. „Station reached; Whale Stop;...“)	Ob-server	**Modus** (Single Pulse or QED)	Puls rate waiting time	**Frequencies** PHF / SLF	System Depth Source	Comments
	Feb.	15	15:51		Resume sounding and logging with normal ping rate after whale retreat	ew	Single Pulse	0	20 kHz / 4 kHZ	Hydro PHF	Resume sounding with normal ping rate, no whale was sighted for at least 15 min., information from bridge
	Feb.	16	03:32	PS128_54	Reduced ping rate (10s); slow approach to Station, continued sounding for exact positioning for sampling; with whale watch during all station work	ew	Single Pulse	10	20 kHz / 4 kHZ	Ctr. Paras. PHF	Start of station work PS128_54 at 03:30, but call from bridge to reduce ping rate at 03:32, WD = 3456 m Lon: 58.920861°E , Lat:-65.132182°S
	Feb.	16	04:54		Stop sounding and logging, because of whale approach < 100m	ew	off	off			Stop sounding and logging, because of whale approach. Call from MMO
	Feb.	16	10:56		Resume sounding with reduced ping rate after station end; after 15 min. whale watch minimum	jh	Single Pulse	10	20 kHz / 4 kHZ	Ctr. Paras. PHF	End of station work PS128_54; soft start wait time 10 s
	Feb.	16	11:02		Resume sounding with normal ping rate after soft start with reduced ping rate	jh	Single Pulse	0	20 kHz / 4 kHZ	Ctr. Paras. PHF	normal ping rate after soft start; wait time 0 s
	Feb.	16	11:20	PS128_55	Reduced ping rate (10s); slow approach to Station, continued sounding for exact positioning for sampling; with whale watch during all station work	jh	Single Pulse	10	20 kHz / 4 kHZ	Ctr. Paras. PHF	Start of station work PS128_55, Lon: 59.378648°E, Lat: -65.125787°S WD = 3677 m
	Feb.	16	17:38		Resume sounding with normal ping rate after station end,with whale watch during all station work	ew	Single Pulse	0	20 kHz / 4 kHZ	Ctr. Paras. PHF	End of station work PS128_55

Year	Month	Day	Time UTC	Station	**Action** (e.g. "Start; Stop...") **–and Reason** (e.g. „Station reached; Whale Stop;...")	Ob-server	**Modus** (Single Pulse or QED)	**Puls rate waiting time**	**Frequencies** PHF / SLF	**System Depth Source**	**Comments**
	Feb.	16	18:18	PS128_56	Reduced ping rate (10s); slow approach to station, continued sounding for exact positioning for sampling; no whale watch possible due to darkness	cg	Single Pulse	10	20 kHz / 4 kHZ	Ctr. Paras. PHF	Start of station work PS128_56, Lon: 59.589843°E , Lat:-65.126448 °S, WD =3991 m Ausnahmegenehmigung (§17,Abs.2 Satz 1 AUG, V.)3.))
	Feb.	16	21:17		Resume sounding with normal ping rate after station end	cg	Single Pulse	0	20 kHz / 4 kHZ	Ctr. Paras. PHF	End of station work PS128_56
	Feb.	16	01:27		Start Parasound survey	jh	Single Pulse	0	20 kHz / 4 kHZ	Ctr. Paras. PHF	Start HS/PS-Survey after PS128_56
	Feb.	17	04:10	PS128_57	Reduced ping rate (10s); slow approach to Station, continued sounding for exact positioning for sampling; with whale watch during all station work	ew	Single Pulse	10	20 kHz / 4 kHZ	Ctr. Paras. PHF	Start of station work PS128_57, Lon: 59.169739°E, Lat: -64.546652 °S WD = 3915 m
	Feb.	17	05:54		stopp sounding and logging, because ship stopped for some hours for further station work	ew	off	off			
	Feb.	17	08:51		Resume sounding with reduced ping rate after station end; after 15 min. whale watch minimum	ew	Single Pulse	10	20 kHz / 4 kHZ	Ctr. Paras. PHF	End of station work PS128_57; soft start wait time 10 s
	Feb.	17	08:58		Resume sounding with normal ping rate after soft start,with whale watch during all station work	ew	Single Pulse	0	20 kHz / 4 kHZ	Ctr. Paras. PHF	Normal ping rate after soft start; wait time 0 s

Year	Month	Day	Time UTC	Station	**Action** (e.g. “Start; Stop...”) **–and Reason** (e.g. „Station reached; Whale Stop;...“)	Ob-server	**Modus** (Single Pulse or QED)	Puls rate waiting time	**Frequencies** PHF / SLF	System Depth Source	Comments
	Feb.	17	10:34	PS128_58	Reduced ping rate (10s); slow approach to Station, continued sounding for exact positioning for sampling; with whale watch during all station work	jh	Single Pulse	10	20 kHz / 4 kHZ	Ctr. Paras. PHF	Start of station work PS128_58 at 10:50 Lon: 58.601398°E, Lat: -64.471512 °S WD = 3926 m
	Feb.	17	13:18		Resume sounding with normal ping rate after soft start,with whale watch during all station work	jh	Single Pulse	0	20 kHz / 4 kHZ	Ctr. Paras. PHF	End of station work PS128_58
	Feb.	18			information from ELO, that Parasound Depth is not stored in DSHIP since Feb. 2021 (last system maintainance)	ew					information from Jörn Ewert and ELO Thorsten, that Parasound Depth is not stored in dship since Feb. 2021 (last system maintainance)
	Feb.	19	18:54		Stop MMO watches north of 60°S. Continued sounding and logging with normal ping rate.	cg	Single Pulse	0	20 kHz / 4 kHZ	Ctr. Paras. PHF	Stop MMO watches north of 60°S. Continued sounding and logging with normal ping rate but stop watch keeping because leaving area of Antarctic Treaty System; Lon:39° 07.326'E, Lat: 59° 59.996' S.
	Feb.	20	09:00		Remote maintainance by Jörn Ewert to store and display Parasound depths in DSHIP again	ew					Remote maintainance (Fernwartung) by Jörn Ewert to store and display Parasound depths in DSHIP again, assisted by ELO Thorsten

Year	Month	Day	Time UTC	Station	**Action** (e.g. “Start; Stop...”) **–and Reason** (e.g. „Station reached; Whale Stop;...“)	Ob-server	**Modus** (Single Pulse or QED)	Puls rate waiting time	**Frequencies** PHF / SLF	System Depth Source	Comments
	Feb.	21				ew					Increasing storm and seastate (swell) in evening
	Feb.	22	13:00		Sounding and logging for survey of bathymetry and sediment echolot	ew	Single Pulse	0	20 kHz / 4 kHZ	Ctr. Paras. PHF	survey during heavy sea, and rough topography
	Feb.	22	15:17		reduce ping rate, possible station reached	ew	Single Pulse	10	20 kHz / 4 kHZ	Ctr. Paras. PHF	possible station reached, reduce ping rate during waiting for better wether conditions, 52.6020°S 24.5304°E WD for PHF= 3370.9, SLF= 3393.7, Other(Hydro)=3326.5
	Feb.	22	20:03		Resume sounding and logging with normal ping rate for further survey, station not started	ew	Single Pulse	0	20 kHz / 4 kHZ	Ctr. Paras. PHF	Station PS128_59 cancelled, because of heavy sea and strong wind.
	Feb.	24	08:00	n/a	Remote service by Jörn Ewert and tests of new software concerning PDS -system of Parasound AND Hydrosweep	ew					
	Feb.	24	16:00		Remote service not finished	ew					
	Feb.	25	ca.10:00		Continuation of remote service by Jörn Ewert and tests of new software concerning PDS -system of Parasound AND Hydrosweep	ew					

Year	Month	Day	Time UTC	Station	**Action** (e.g. "Start; Stop...") **–and Reason** (e.g. „Station reached; Whale Stop:...")	Ob-server	**Modus** (Single Pulse or QED)	**Puls rate waiting time**	**Frequencies** PHF / SLF	**System Depth Source**	**Comments**
			ca. 18:00		Remote service finished ?	ew					> Clip of 0.5 mV on SLF signal; > Bottom TVG 0.15 dB/m on SLF; > New Window: Absolute Beam ? Settings made by remote service
	Feb	26	05:38		Tick out of Clip and Bottom TVG SLF signal because recording of original data is requested	ew					Tick out of Clip and Bottom TVG SLF signal because recording of original data is demanded by AWI (Catalina Gebhard)
					No message by Jörn Ewert if remote service was finished successfully	ew					
	Feb	27	04:01		Stop sounding and logging because EEZ of South Africa is reached	ew					Stop sounding and logging because EEZ of South Africa is reached Start of last processing and backups
	Feb	27	04:01		copy PS128 to MDM	ew					
					Observer (Watch-Keeper): ew = Estella Weigelt, cg = Christoph Gaedicke, jh = Jakob Hamann						Temporary during seismic survey: MCM = Matthieu Civel-Mazens, JM = Jule Müller, LLJ = Lester Lembke-Jene, HP = Hinner Preckel, AI = Alina Ivanova, BW = Bernd Wagner, Bernhard Diekmann = BD, Lea Fuchs = LF, Pa = Patricia Sonnemann, EN = Ebbe Nürnberg,

Year	Month	Day	Time UTC	Station	**Action** (e.g. "Start; Stop...") **–and Reason** (e.g. „Station reached; Whale Stop;...")	**Ob-server**	**Modus** (Single Pulse or QED)	**Puls rate waiting time**	**Frequencies** PHF / SLF	**System Depth Source**	**Comments**
						Files					
			File	Summary	PHF + SLF *.ps3	13390					
					PHF *.ps3	6698					
					SLF*.ps3	6692					
					ps32sgy	288					
					conv	576					
					nav	288					
					ukooa	288					

A.5.2 Parasound Station Profiles

Please find the A.5.2 Parasound Station Profiles of expedition PS128 as a supplement (Download: 269 mb)

A.5.3 Parasound File List

Tab. A.5.1: List of parasound files generated during expedition PS128 from Cape Town to Cape Town

File	min [s]	max [s]	Depth [s]	first shot	last shot	Remarks
2022_0107_144349.sgy	5.9	6.3	ok			
2022_0107_184352.sgy	6.15	6.5	ok			
2022_0107_224400.sgy	6.3	6.55	ok			
2022_0108_024409.sgy	6.15	6.6	ok	gutes Beispiel		
2022_0108_064419.sgy	1	6.6	ok			
2022_0108_104429.sgy	1	6.4	ok			
2022_0108_144435.sgy	4.7	6.8	ok			
2022_0108_184443.sgy	4.9	6.9	ok			
2022_0108_224456.sgy	5.4	6.7	ok			
2022_0109_024505.sgy	6.2	7.5	ok	viel Topographie		
2022_0109_064513.sgy	6.1	7	ok	„		
2022_0109_104526.sgy	6	6.95	ok	„		
2022_0109_144539.sgy	6	6.9	ok	„		
2022_0109_184548.sgy	5.6	7	ok	„		
2022_0109_224556.sgy	6	6.9	ok	„		
2022_0110_024603.sgy	1	6.4	ok	Sandile Seamount		
2022_0110_064615.sgy	1	6.3	ok	Sandile Seamount		
2022_0110_104624.sgy	4	6	ok			
2022_0110_144632.sgy	4	6	ok			
2022_0110_184641.sgy	5	6	ok			

File	min [s]	max [s]	Depth [s]	first shot	last shot	Remarks
2022_0110_224648.sgy	4.4	6.5	ok			
2022_0111_024651.sgy	4.8	6.1	ok			
2022_0111_064700.sgy	4.7	5.9	ok			
2022_0111_104708.sgy	4.55	5.45	ok			
				Bouvet Island stop sounding		
2022_0111_122124.sgy		no data				
2022_0112_211835.sgy	5.9	7.4	ok			
2022_0113_011848.sgy	5.9	7.4	ok			
2022_0113_051859.sgy	6.45	7.45	ok	good example Seamount+sedimentsaround		
2022_0113_091911.sgy	7	7.4	ok			
2022_0113_131926.sgy	6.6	7.5	ok			
2022_0113_171940.sgy	7.1	7.4	ok			
2022_0113_211951.sgy	7	7.4	ok			
2022_0114_011954.sgy	7.05	7.35	ok			
2022_0114_052003.sgy	6.9	7.2	ok			
2022_0114_092011.sgy	6.8	7.15	ok			
2022_0114_132020.sgy	6.7	7.05	ok			
2022_0114_172030.sgy	6.4	6.95	ok			
2022_0114_212044.sgy	6.4	6.8	ok			
2022_0115_012045.sgy	6.25	6.6	ok	-		
2022_0115_052055.sgy	6.3	6.5	ok	-		
2022_0115_092103.sgy	6.3	6.65	ok	-		
2022_0115_132117.sgy	4.15	6.55	ok	Whale, no sounding until start of next line		

File	min [s]	max [s]	Depth [s]	first shot	last shot	Remarks
2022_0115_173832.sgy	3.9	4.4	ok	-		
2022_0115_213841.sgy	3.55	4.4	ok	PS128-1		
2022_0116_013850.sgy	3.55	3.8	ok	Stat ion PS128-001, 02:37 UTC, -6.042, -69.048		
2022_0116_053859.sgy3.53.8ok	3.5	3.8	ok			
2022_0116_093922.sgy	3.5	3.8	ok			
2022_0116_133941.sgy	3.5	3.8	ok	end PS128-001, Profilfahrt WP4-WP5		
2022_0116_173957.sgy	2.4	3.8	ok	Profilfahrt WP4-WP5		
2022_0116_214003.sgy	2.4	2.7	ok	Station PS128-002, 21:52 UTC, -5.5887, -69.4107		
2022_0117_014006.sgy	0.3	3.8	ok	Profilfahrt WPA1-WPA13, Failure in waterdepth 2022-0117-0510 to 2022-0117-0535		
2022_0117_054021.sgy	2.8	3.8	ok			
2022_0117_094029.sgy	1.3	3.4	ok	PS128_14, PS128_15, PS111_13-4		
2022_0117_134033.sgy	0.25	2	ok	-		
2022_0117_174036.sgy	0.25	0.65	ok	*Neumayer*_Between_2022-0117-16:30-20:37UTC, Survey_JohannK_WP1-WP15_Start_2022-0117-20:22 UTC		
2022_0117_214040.sgy	0.3	0.85	ok	Survey_JohannK_WP1-WP15, survey for Sites PS128_3, PS128_7, PS128_8, PS128_9		
2022_0118_014042.sgy0.5	0.5	0.8	ok	PS128_5		

File	min [s]	max [s]	Depth [s]	first shot	last shot	Remarks
2022_0118_054046.sgy	0.5	0.8	ok	-		
2022_0118_094050.sgy	0.5	0.8	ok	PS128-4		
2022_0118_134100.sgy	0.5	0.8	ok	PS128-5, PS128-6		
2022_0118_174117.sgy	0.5	0.7	ok	PS128-7, PS128-8		
2022_0118_214119.sgy	0.4	1.5	ok	PS128-6, PS128-7, PS128-9, PS128-10		
2022_0119_014131.sgy	1.1	3.8	ok	-		
2022_0119_054135.sgy	3.05	3.75	ok	-		
2022_0119_094141.sgy	3	3.85	ok	PS128-11		
2022_0119_134154.sgy	2.15	3.8	ok	PS128-11		
2022_0119_174207.sgy	1.6	3.9	ok	PS128_13		
2022_0119_214209.sgy	2.45	4.3	ok	PS128_12	survey profile, from SP-1437 to SP-1550, wrong depth, interruption of sounding because of complete signal loss, stuck in ice = Rammfahrt (back and forth), likely ice around sensor, no signals on hydrosweep as well	
2022_0120_014217.sgy	3.45	4.3	ok	PS128_12	often signal loss, stuck in ice = Rammfahrt (back and forth)	
2022_0120_054225.sgy	1.95	3.8	ok	PS128_13		
2022_0120_094235.sgy	1.9	2.9	ok	PS128_13		

File	min [s]	max [s]	Depth [s]	first shot	last shot	Remarks
2022_0120_134239.sgy	1.3	2.3	ok	PS128_14		
2022_0120_174246.sgy	2	2.75	ok	PS128_14, PS128_15, PS111_13-4		
2022_0120_214256.sgy	2.45	2.75	ok	PS128_15		
2022_0121_014309.sgy	2.5	2.75	ok	PS128_15		
2022_0121_054323.sgy	2.65	3.05	ok	PS128_16		
2022_0121_094327.sgy	2.8	3	ok	PS128_16		
2022_0121_134341.sgy	2.8	3	ok	PS128_16		
2022_0121_174401.sgy	2.8	3	ok	PS128_16		
2022_0121_214421.sgy	2.75	3.5	ok	PS128_16, PS128_17		
2022_0122_014427.sgy	2.95	3.25	ok	PS128_17		
2022_0122_054438.sgy	2.95	3.25	ok	PS128_17		
2022_0122_094453.sgy	2.9	3.7	ok	PS128_17		
2022_0122_134505.sgy	2.9	4.25	ok			
2022_0122_174509.sgy	3.1	4.75	ok			
2022_0122_214517.sgy	3.9	4.4	ok	PS128_19		
2022_0123_014522.sgy	3.85	4.15	ok	PS128_19		
2022_0123_054544.sgy	3.85	4.14	ok	PS128_19		
2022_0123_094609.sgy	3.85	4.3	ok	PS128_19		
2022_0123_134625.sgy	2.55	4.3	ok	Strömungskolk, SP 1000, lon: -6.4014°, lat: -68.8968°		
2022_0123_174631.sgy	2.35	2.8	ok	PS128_20		
2022_0123_214633.sgy	2.4	2.65	ok	PS128_20		
2022_0124_014655.sgy	2.35	2.8	ok	PS128_20		

File	min [s]	max [s]	Depth [s]	first shot	last shot	Remarks
2022_0124_054710.sgy	2	3.9	ok			
2022_0124_094715.sgy	1.2	3.15	ok	Gap, signal loss during icebreaking		
2022_0124_134719.sgy	0.3	1.8	ok	PS128_10		
2022_0124_174722.sgy	0.6	0.95	ok			
2022_0124_214725.sgy	0.35	0.9	ok	Seismik, Lines 20220101, 20220103		
2022_0125_014727.sgy	0.4	2.2	ok			
2022_0125_054730.sgy	0.85	2.85	ok			
2022_0125_094734.sgy	0.85	2.85	ok			
2022_0125_134737.sgy	0.25	1.5	ok			
2022_0125_174741.sgy	0.4	1.5	ok			
2022_0125_214745.sgy	0.15	0.95	ok			
2022_0126_014747.sgy	0.2	0.55	ok			
2022_0126_054751.sgy	0.25	2.3	ok			
2022_0126_094755.sgy	0.75	2.25	ok			
2022_0126_134758.sgy	1.2	3.05	ok			
2022_0126_174803.sgy	0.95	3.75	ok			
2022_0126_214809.sgy	0.1	1.5	ok			
2022_0127_014810.sgy	0.4	0.75	ok	PS128_23, PS128_24		
2022_0127_054814.sgy	0.85	3.75	ok	PS128_25		
2022_0127_094826.sgy	1.55	3.75	ok	PS128_25		
2022_0127_134838.sgy	1.5	3.75	ok	PS128_13		
2022_0127_174842.sgy	2.35	3.65	ok			
2022_0127_214848.sgy	2.6	4.35	ok			

File	min [s]	max [s]	Depth [s]	first shot	last shot	Remarks
2022_0127_120314.sgy	1.5	3.75	PS128_13	Test1-conv-no-resample-faktor1		
2022_0127_160327.sgy				Test1-conv-no-resample-faktor1		
2022_0127_200332.sgy				Test1-conv-no-resample-faktor1		
2022_0128_014849.sgy	3.35	4.4	ok			
2022_0128_054854.sgy	2.5	3.95	ok			
2022_0128_094859.sgy	2.9	4.6	ok	PS128_26		
2022_0128_134909.sgy	3.35	4.8	ok			
2022_0128_174924.sgy	2.65	4.55	ok			
2022_0128_214927.sgy	2.5	4.25	ok	nice outcrops		
2022_0129_014930.sgy	3.75	5.05	ok	PS128_27		
2022_0129_054937.sgy	4.2	5	ok			
2022_0129_094948.sgy	1.9	4.55	ok			
2022_0129_134956.sgy	1.55	3.5	ok			
2022_0129_175000.sgy	3.3	4.4	ok			
2022_0129_215004.sgy	4	4.6	ok	outcrop at SP340		
2022_0130_015007.sgy	4.4	5.9	ok	PS128_28		
2022_0130_081103.sgy	4.4	5.9	ok	PS128_28		
2022_0130_121118.sgy	4.4	5.9	ok			
2022_0130_161123.sgy	4.4	5.5	ok			
2022_0130_201128.sgy	4.55	5.45	ok			
2022_0131_001129.sgy	4.55	5.45	ok			

File	min [s]	max [s]	Depth [s]	first shot	last shot	Remarks
2022_0131_041133.sgy	3.8	5.2	ok	PS128_29		
2022_0131_105531.sgy	0.6	5.15	ok	PS128_29		
2022_0131_145546.sgy	0.4	0.85	ok			
2022_0131_185550.sgy	0.4	2.3	ok			
2022_0131_225552.sgy	0.85	3.8	ok			
2022_0201_025557.sgy	2.1	5	ok	Gulli (Ralfs gulli)		
2022_0201_065605.sgy	1.25	5.5	ok	Station PS128_30, Fishlot_ WD=3920m=ok, Parasound_ WD=1050m=wrong		
2022_0201_150329.sgy	4.05	6	ok			
2022_0201_190343.sgy	3.05	5.45	ok			
2022_0201_230347.sgy	3.4	5.3	ok			
2022_0202_030354.sgy	0.9	3.9	ok			
2022_0202_070400.sgy	0.5	1.4	ok	stopp off *Molodezhnaya*		
2022_0202_151018.sgy	0.3	2.7	ok			
2022_0202_191021.sgy	2	3.35	ok			
2022_0202_231022.sgy	1.9	3.7	ok			
2022_0203_031028.sgy	2.5	5	ok	PS128_31		
2022_0203_071036.sgy	3.6	4.95	ok	PS128_31		
2022_0203_111043.sgy	2.6	4.2	ok			
2022_0203_151048.sgy	1.9	4.2	ok			
2022_0203_191052.sgy	1.75	4.45	ok	nice sediment layers		
2022_0203_231053.sgy	4	5.15	ok			
2022_0204_055544.sgy	3.25	5.2	ok	PS128_32		

File	min [s]	max [s]	Depth [s]	first shot	last shot	Remarks
2022_0204_095558.sgy	3.9	5	ok			
2022_0204_135607.sgy	4.6	5.25	ok			
2022_0204_175617.sgy	4.7	5.35	ok			
2022_0204_215624.sgy	4.35	5	ok			
2022_0205_015627.sgy	4.7	5.5	ok			
2022_0205_055634.sgy	4.95	5.45	ok			
2022_0205_095643.sgy	4.95	5.45	ok	slump		
2022_0205_135650.sgy	4.85	5.2	ok	Gulli-25m-tief		
2022_0205_175701.sgy	4.35	5.1	ok			
2022_0205_215710.sgy	4	4.6	ok	Absenkung-mit-20 m-Sedimente		
2022_0206_015712.sgy	3.8	4.4	ok	Incisions ~170 m deep		
2022_0206_055717.sgy	3.8	4.8	ok			
2022_0206_095724.sgy	4.35	5.05	ok			
2022_0206_135734.sgy	4.4	4.75	ok	22 m Sedimente		
2022_0206_175743.sgy	4.45	4.75	ok	PS128_33_start		
2022_0207_063143.sgy	4.05	4.8	ok	from end PS128_33 to start PS128_34		
2022_0207_103203.sgy	4.1	4.35	ok	PS128_34_on-station		
2022_0207_143221.sgy	4.1	4.35	ok	PS128_34_end		
2022_0207_183238.sgy	4.1	4.9	ok	PS128_35-red-salon-banana_ start		
2022_0207_223246.sgy	3.9	4.65	ok	PS128_35-red-salon-banana_ end		
2022_0208_023249.sgy	3.2	4.5	ok	50m vertical displacement		

File	min [s]	max [s]	Depth [s]	first shot	last shot	Remarks
2022_0208_063255.sgy	2.4	3.5	ok	rough topographie, 20-30 m-vertical displacements, nearly sediments		
2022_0208_103301.sgy	2.8	4	ok	rough topographie, 20-30 m-vertical displacements, few sediments		
2022_0208_143306.sgy	2.55	3.55	ok	PS128_36		
2022_0208_185124.sgy	0.1	3	ok	shallow shelf 95 m !		
2022_0208_225139.sgy	0.05	1.35	ok	PS128_37-1_Start parasound-survey: rough topographie, vertical displacements, very thin sediments		
2022_0209_025140.sgy	0.65	1.4	ok	PS128-37-2_End-of-Parasound survey: thick sediments, PS128_38, PS128_39, PS128_40, PS128_41, PS128_42		
2022_0209_065144.sgy	0.65	1.4	ok	PS128_38-1, PS128_38-2		
2022_0209_105150.sgy	0.2	1.25	ok	PS128_39		
2022_0209_145207.sgy	0.6	1.3	ok	PS128_39, PS128_40		
2022_0209_185221.sgy	0.65	1.3	ok	PS128_40		
2022_0209_225233.sgy	0.45	1	ok	PS128_41, PS128_42, PS128_37-2 (end point of Parasound-Survey)		
2022_0210_025237.sgy	0.45	1		amplitude loading test		
2022_0210_025235.sgy	0.15	0.7	ok	PS128_45		
2022_0210_065239.sgy	0.2	1.25	ok	PS128_43, PS128_44		

File	min [s]	max [s]	Depth [s]	first shot	last shot	Remarks
2022_0210_105243.sgy	0.2	1.1	ok	PS128_44, PS128_45		
2022_0210_145255.sgy	0.3	1.1	ok	PS128_47		
2022_0210_185259.sgy	0.15	0.7	ok	PS128_46, PS128_47		
2022_0210_225303.sgy	0.45	2.9	ok			
2022_0211_025305.sgy	1.7	3.45	ok	PS128_48, PS128_49		
2022_0211_065309.sgy	2	3.2	ok	PS128_48, PS128_49		
2022_0211_105317.sgy	2.8	3.5	ok	PS128_49		
2022_0211_145331.sgy	2.9	4	ok	PS128_50		
2022_0211_185348.sgy	3.6	4	ok	PS128_50		
2022_0211_225403.sgy	2.6	4.25	ok			
2022_0212_025405.sgy	3.3	4.3	ok	PS128_51		
2022_0212_065412.sgy	3.7	4.8	ok	PS128_51		
2022_0212_105428.sgy	4.2	5.6	ok			
2022_0212_145439.sgy	4.75	5.6	ok			
2022_0212_185446.sgy	4.6	5.15	ok	PS128_54 thick sediments on slope		
2022_0212_225449.sgy	4.15	5.35	ok			
2022_0213_025456.sgy	2.8	4.5	ok	30m Sedimente on slope, hard surface		
2022_0213_065503.sgy	0.65	4.5	ok			
2022_0213_105508.sgy	0.55	2.9	ok			
2022_0213_150040.sgy	0.7	3.1	ok			
2022_0213_190043.sgy	0.45	3.3	ok	26 m Sedimente in ca. 1080m Tiefe		
2022_0213_230046.sgy	0.3	1.85	ok			

File	min [s]	max [s]	Depth [s]	first shot	last shot	Remarks
2022_0214_030049.sgy	0.25	1.3	ok	Bsp. Für Tiefenscheiben		
2022_0214_070053.sgy	0.2	0.6	ok	*Molodezhnaya*		
2022_0214_125745.sgy	0.2	1.35	ok	PS128_52, After *Molodezhnaya*		
2022_0214_165747.sgy	0.3	1.15	ok			
2022_0214_205751.sgy	0.4	2.3	ok			
2022_0215_005754.sgy	1.4	2.65	ok	PS128_53		
2022_0215_045758.sgy	0.4	3.25	ok			
2022_0215_085804.sgy	0.65	2.3	ok			
2022_0215_125809.sgy	0.6	2.95	ok			
2022_0215_165813.sgy	0.75	4.8	ok			
2022_0215_205816.sgy	3.3	4.85	ok	gutes zeitscheiben-bsp		
2022_0216_005820.sgy	4.6	5.45	ok	PS128_54		
2022_0216_105631.sgy	4.56	5.15	ok	PS128_55		
2022_0216_145652.sgy	5	5.7	ok	PS128_55, PS128_56		
2022_0216_185715.sgy	5.3	5.7	ok	PS128_56		
2022_0216_225717.sgy	5.13	5.5	ok	PS128_57		
2022_0217_025725.sgy	5.13	5.5	ok	PS128_57		
2022_0217_085115.sgy	5.13	5.5	ok	PS128_57, PS128_58		
2022_0217_125130.sgy	5.35	5.9	ok			
2022_0217_165148.sgy	5.75	6.4	ok			
2022_0217_205159.sgy	5.75	6.7	ok			
2022_0218_005208.sgy	6.05	6.3	ok			

File	min [s]	max [s]	Depth [s]	first shot	last shot	Remarks
2022_0218_045212.sgy	6.25	6.65	ok			
2022_0218_085224.sgy	6.55	6.7	ok			
2022_0218_125235.sgy	6.3	6.7	ok			
2022_0218_165149.sgy	6.35	6.65	ok			
2022_0218_205153.sgy	6.55	6.85	ok			
2022_0219_005202.sgy	6.75	7.05	ok			
2022_0219_045214.sgy	6.93	7.08	ok			
2022_0219_085224.sgy	7	7.12	ok			
2022_0219_125233.sgy	7.03	7.15	ok			
2022_0219_165243.sgy	7.05	7.17	ok			
2022_0219_205258.sgy	7.05	7.2	ok			
2022_0220_005312.sgy	7.05	7.2	ok			
2022_0220_045326.sgy	7.07	7.2	ok			
2022_0220_085341.sgy	7.07	7.23	ok			
2022_0220_125350.sgy	7.1	7.25	ok			
2022_0220_165401.sgy	7.15	7.35	ok			
2022_0220_205409.sgy	7.22	7.4	ok			
2022_0221_005419.sgy	7.25	7.5	ok			
2022_0221_045425.sgy	7.25	7.4	ok			
2022_0221_085438.sgy	7.25	7.38	ok			
2022_0221_125450.sgy	6.7	7.4	ok			
2022_0221_165506.sgy	4.8	7.5	ok			
2022_0221_205514.sgy	5.65	7.55	ok			
2022_0222_005526.sgy	4	7.3	ok			
2022_0222_045536.sgy	3.4	7.5	ok			

File	min [s]	max [s]	Depth [s]	first shot	last shot	Remarks
2022_0222_085543.sgy	2.7	7.9	ok			
2022_0222_125555.sgy	3.3	4.7	ok	PS128_59_cancelled		
2022_0222_165603.sgy	4.38	4.83	ok			
2022_0222_205611.sgy	3.65	4.8	ok			
2022_0223_005617.sgy	2.7	6.2	ok			
2022_0223_045623.sgy	2	5.3	ok			
2022_0223_085627.sgy	3	5.25	ok			
2022_0223_125637.sgy	2.8	6.4	ok			
2022_0223_165648.sgy	3.25	5.25	ok			
2022_0223_205657.sgy	3.95	5.7	ok			
2022_0224_005714.sgy	4.45	6.05	ok			
2022_0224_045723.sgy	4.5	6.6	ok	data strong amplitude-loss at end		
2022_0224_085737.sgy	4.75	6.25	ok			
2022_0224_125745.sgy	5	6.7	ok			
2022_0224_165758.sgy	5.5	6.9	ok			
2022_0224_205807.sgy	5.45	6.9	ok			
2022_0225_005820.sgy	5.7	6.9	ok			
2022_0225_045828.sgy	5.05	6.3	ok			
2022_0225_085837.sgy	5.6	6.2	ok			
2022_0225_125845.sgy	5.9	6.6	ok			
2022_0225_165857.sgy	5.9	6.7	ok			
2022_0225_205909.sgy	6.3	6.9	ok			
2022_0226_005920.sgy	6.4	6.9	ok			
2022_0226_045932.sgy	5.9	7.4	ok			

File	min [s]	max [s]	Depth [s]	first shot	last shot	Remarks
2022_0226_085945.sgy	6.1	7.6	ok			
2022_0226_125953.sgy	6.3	6.75	ok	ca. 70 m Sediments on base-reflector		
2022_0226_170006.sgy	6.1	7	ok			
2022_0226_210015.sgy	5.6	7	ok			
2022_0227_010029.sgy	6.2	6.6	ok			

A.6 MARINE GEOLOGY

A.6.1 Core Images PS128

A.6.2 Litho Logs PS128

A.6.3 Smear Slide Analyses PS128

A.6.4 Coarse Fraction Analyses PS128

A.6.1 Core Images PS128

PS128_1-5

69°2.9’ S 6°23.05’ W 2661 m Depth

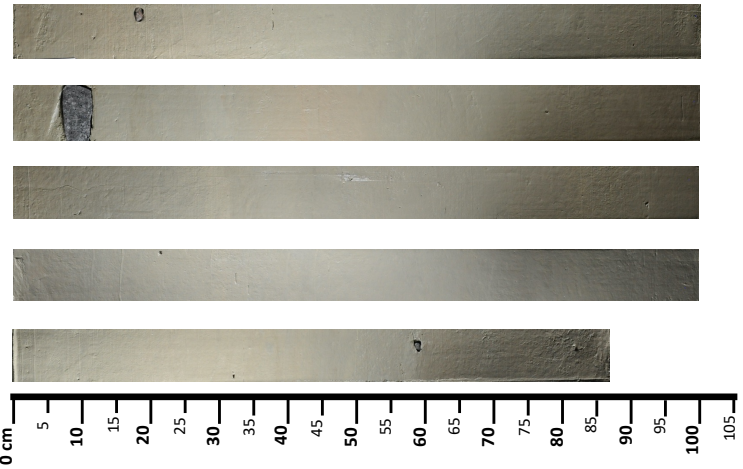


PS128_2-2
69°24.69' S 5°35.38' W 1819 m Depth
0 - 55
55 - 155
155 - 255
255 - 355
355 - 439
0 cm
5
10
15
20
25
30
35
40
45
50
55
60
65
70
75
80
85
90
95
100
105

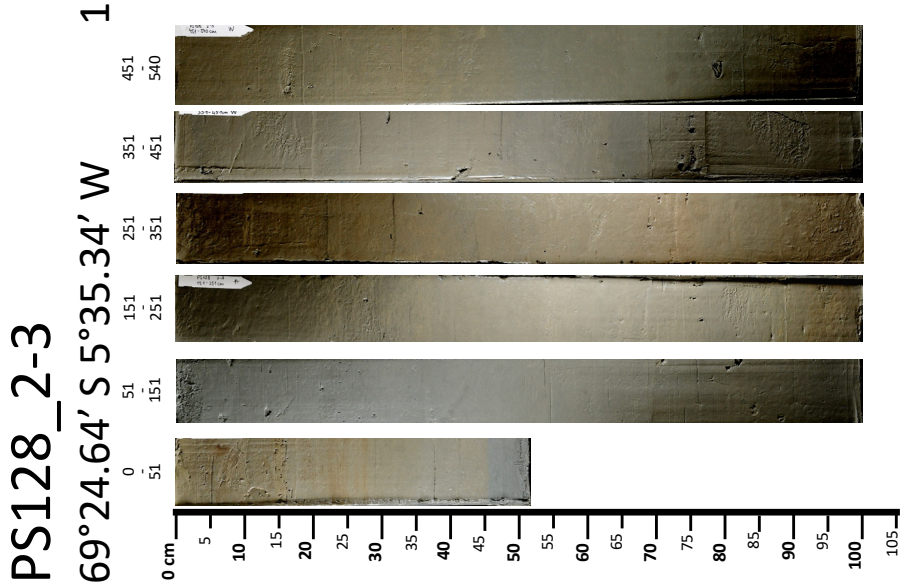
PS128_2-3
69°24.64' S 5°35.34' W
1834 m Depth
0 - 51
51 - 151
151 - 251
251 - 351
351 - 451
451 - 540
0 cm
5
10
15
20
25
30
35
40
45
50
55
60
65
70
75
80
85
90
95
100
105

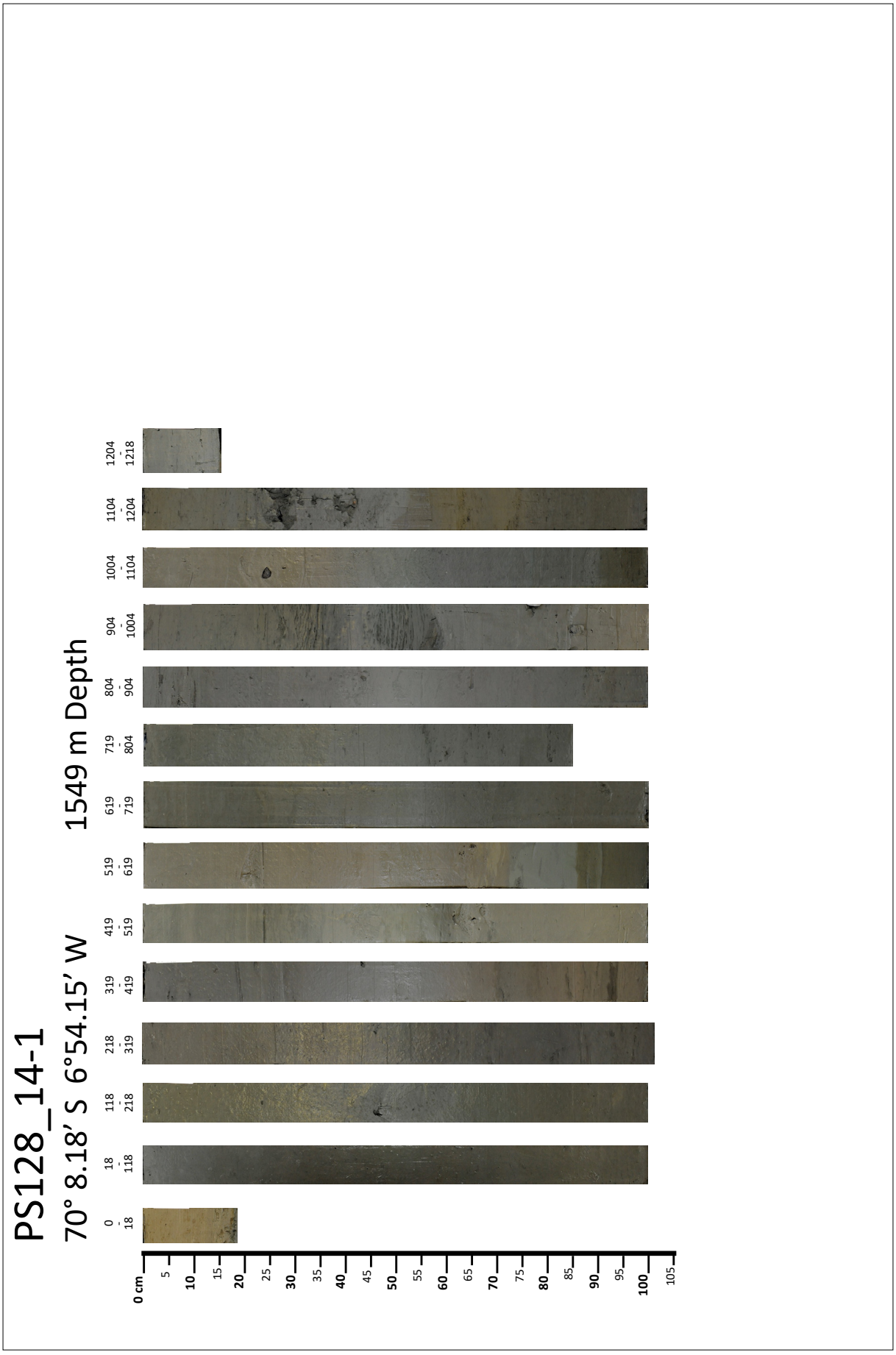
PS128_14-1
70° 8.18' S 6°54.15' W
1549 m Depth
0 - 18
18 - 118
118 - 218
218 - 319
319 - 419
419 - 519
519 - 619
619 - 719
719 - 804
804 - 904
904 - 1004
1004 - 1104
1104 - 1204
1204 - 1218
0 cm
5
10
15
20
25
30
35
40
45
50
55
60
65
70
75
80
85
90
95
100
105

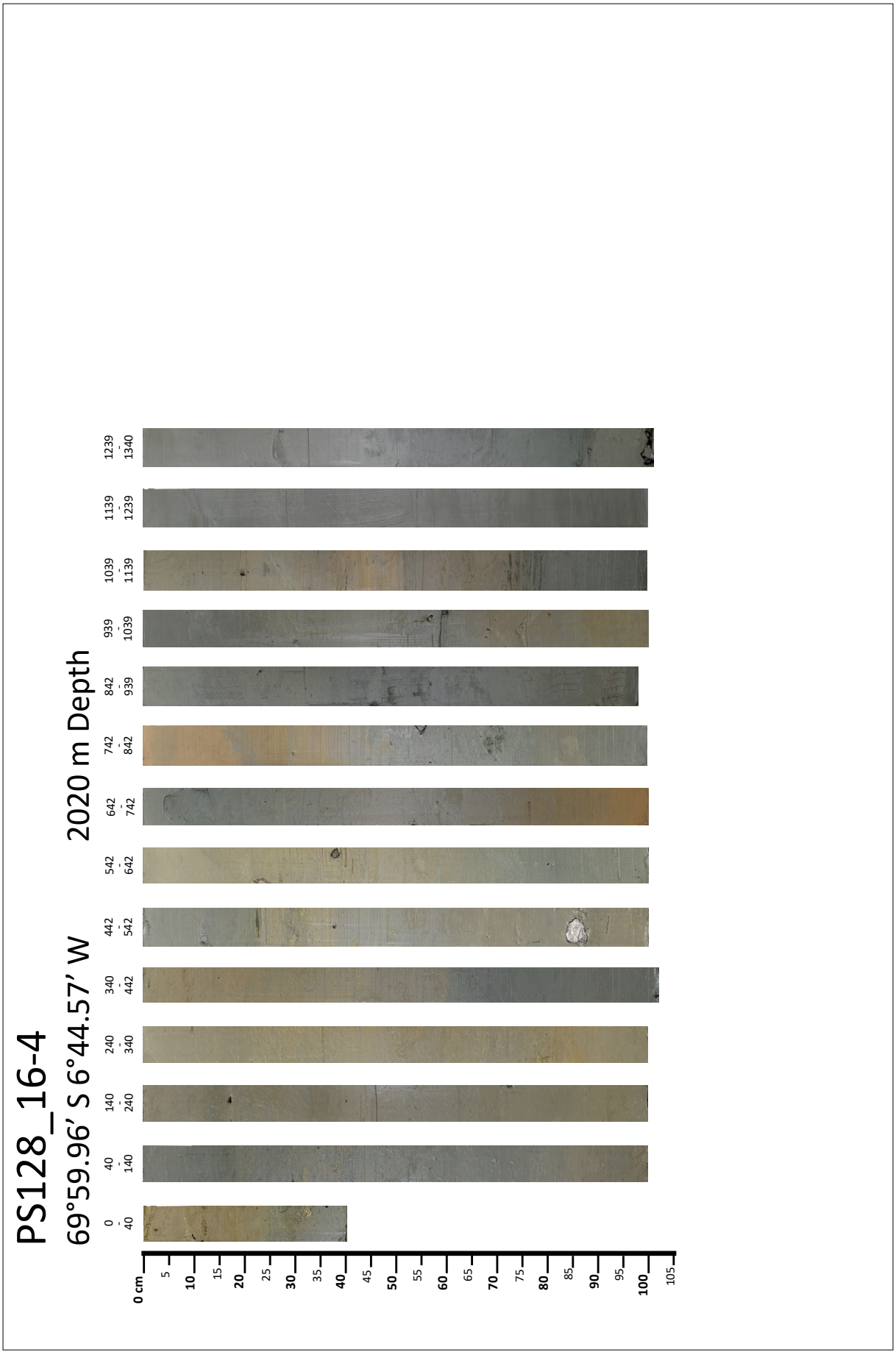
PS128_16-4
69°59.96’ S 6°44.57’ W
2020 m Depth
0 - 40
40 - 140
140 - 240
240 - 340
340 - 442
442 - 542
542 - 642
642 - 742
742 - 842
842 - 939
939 - 1039
1039 - 1139
1139 - 1239
1239 - 1340
0 cm
5
10
15
20
25
30
35
40
45
50
55
60
65
70
75
80
85
90
95
100
105

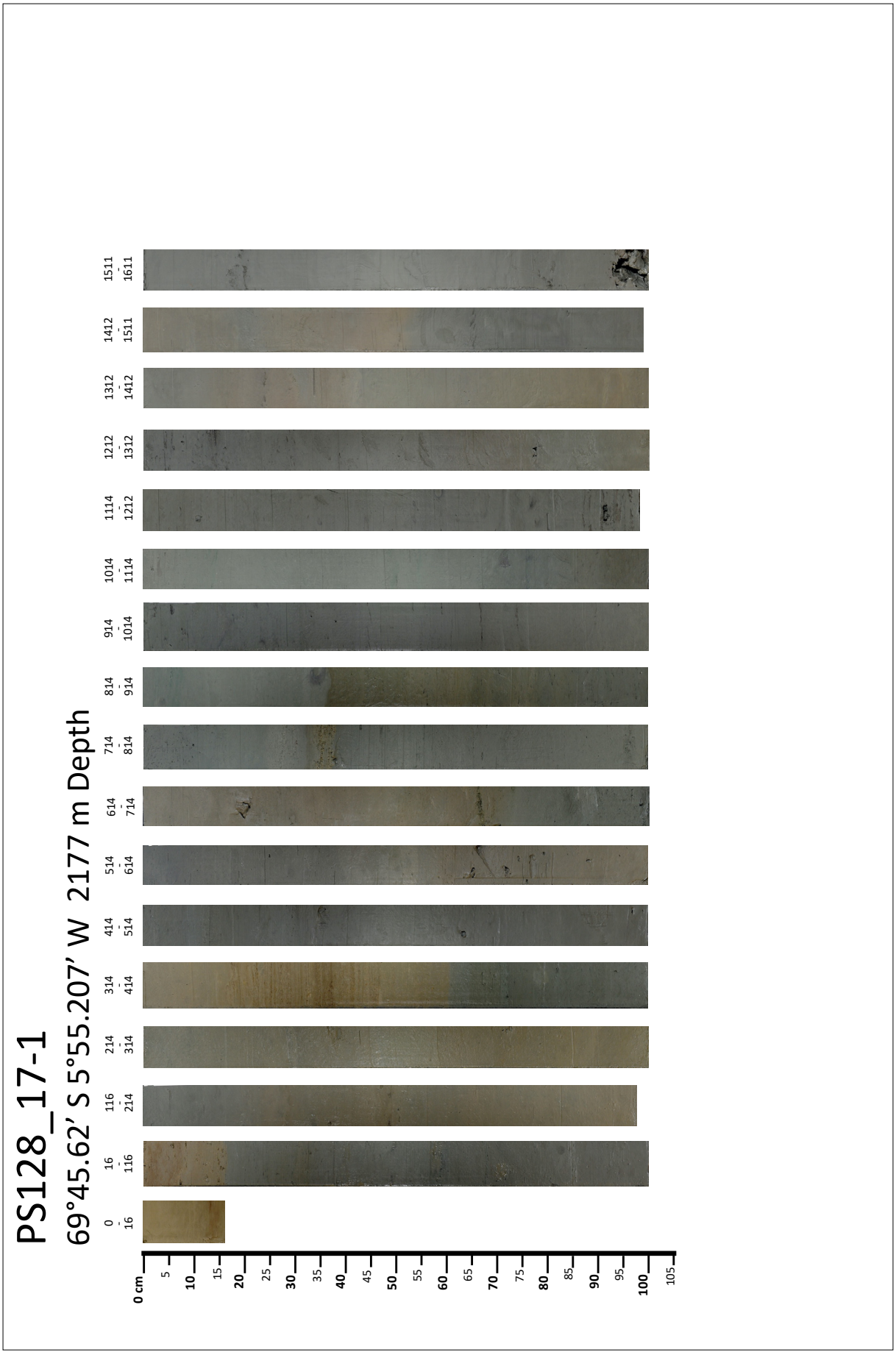
PS128_17-1
69°45.62' S 5°55.207' W 2177 m Depth
0 - 16
16 - 116
116 - 214
214 - 314
314 - 414
414 - 514
514 - 614
614 - 714
714 - 814
814 - 914
914 - 1014
1014 - 1114
1114 - 1212
1212 - 1312
1312 - 1412
1412 - 1511
1511 - 1611
0 cm
5
10
15
20
25
30
35
40
45
50
55
60
65
70
75
80
85
90
95
100
105

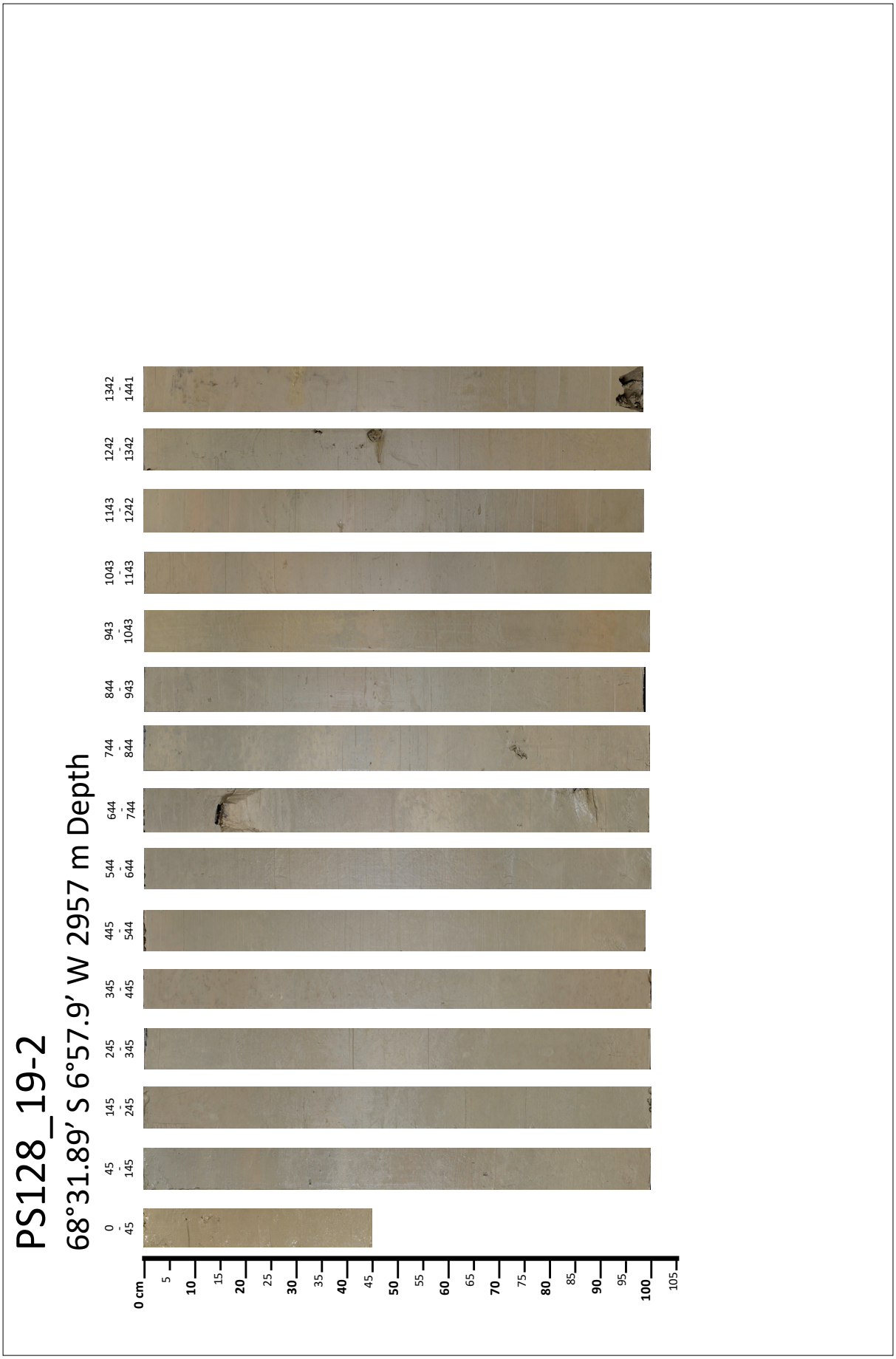
PS128_19-2
68°31.89' S 6°57.9' W 2957 m Depth
0 45
45 145
145 245
245 345
345 445
445 544
544 644
644 744
744 844
844 943
943 1043
1043 1143
1143 1242
1242 1342
1342 1441
0 cm
5
10
15
20
25
30
35
40
45
50
55
60
65
70
75
80
85
90
95
100
105

PS128_23-2

70°27.366' S 9°07.229' W 376 m Depth

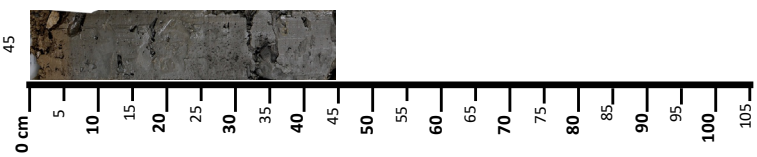

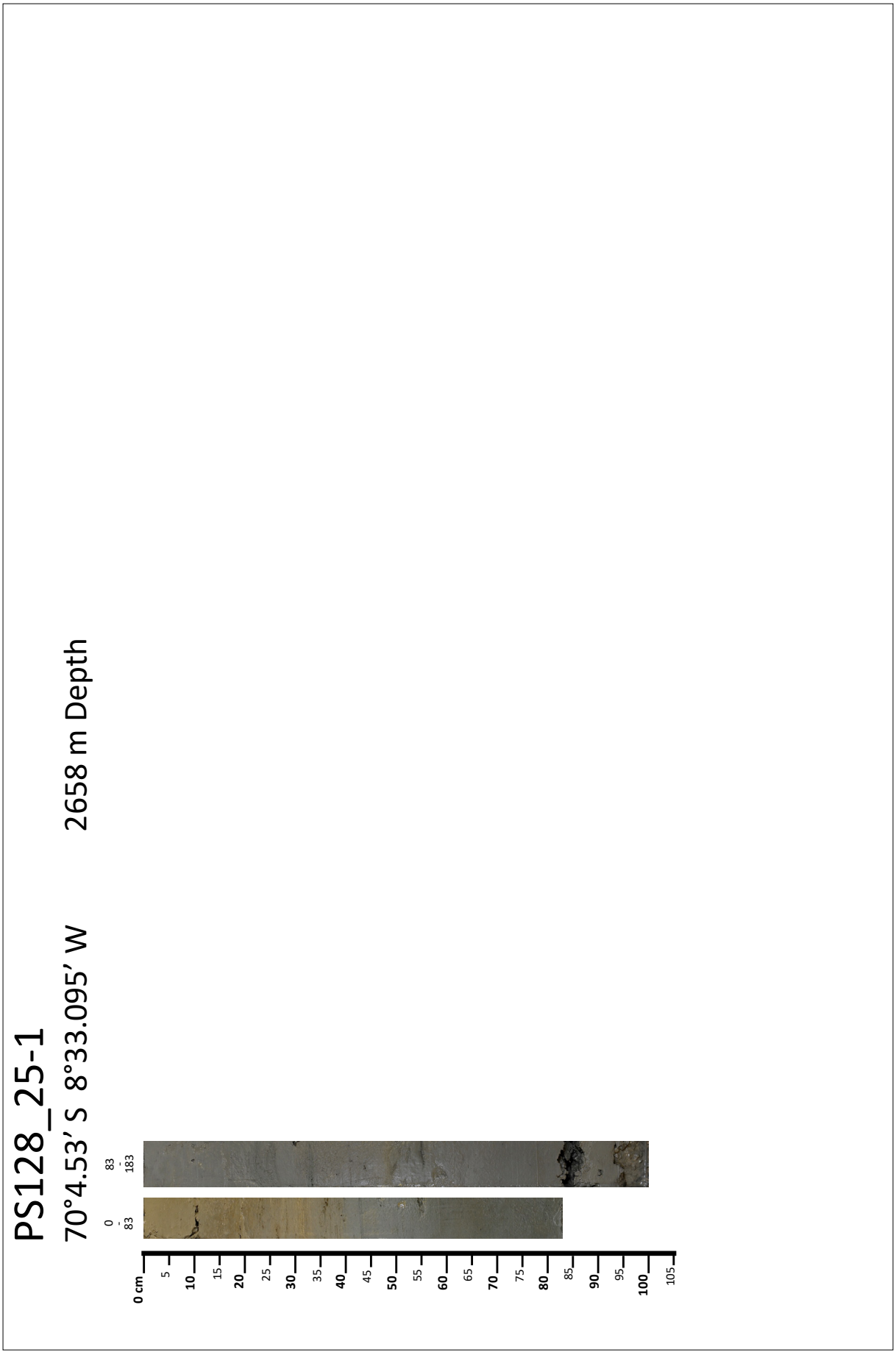
PS128_25-1
70°4.53' S 8°33.095' W
2658 m Depth
0 - 83
83 - 183
0 cm
5
10
15
20
25
30
35
40
45
50
55
60
65
70
75
80
85
90
95
100
105

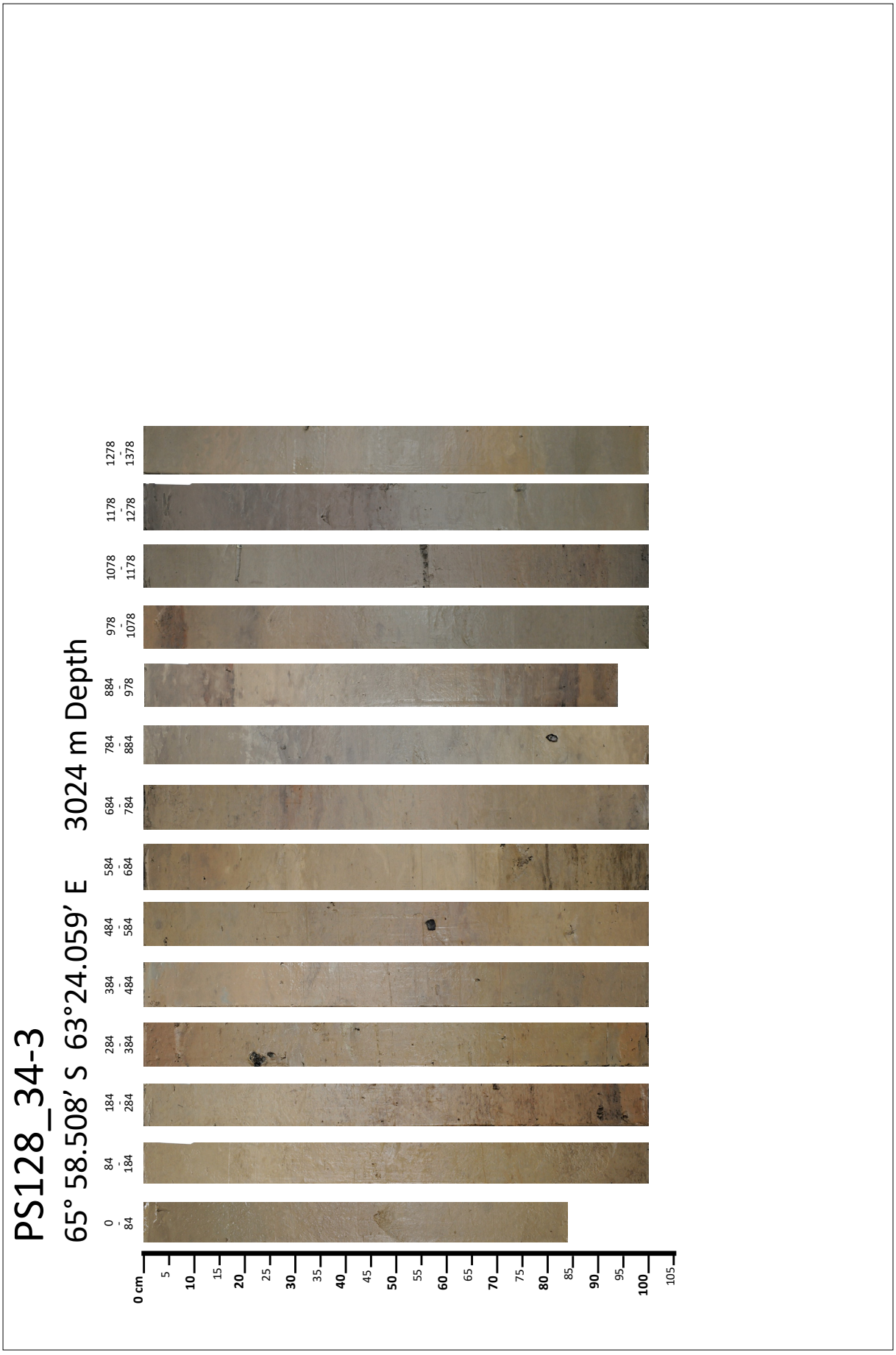
PS128_34-3
65° 58.508' S 63°24.059' E 3024 m Depth
0 - 84
84 - 184
184 - 284
284 - 384
384 - 484
484 - 584
584 - 684
684 - 784
784 - 884
884 - 978
978 - 1078
1078 - 1178
1178 - 1278
1278 - 1378
0 cm
5
10
15
20
25
30
35
40
45
50
55
60
65
70
75
80
85
90
95
100
105

A.6.2 Litho Logs PS128

Please find the A.6.2 Litho Logs of expedition PS128 as a supplement.

A.6.3 Smear Slide Analyses PS128

Floral and faunal description based on smear slide observations during EASI-1

January – Febuary 2022

Species, taxa, groups observed during the expeditions are reported down below as a supplementary information to the mission report. Smear slides were taken at the base of each section for each core when possible. The following information thus only concerns the bottom of each section. Additionally, the quantity of sediment used to prepare smear slides varied from section to section and no protocol for equal repartition of microfossils on the slide was used. Therefore, information on abundances and percentages presented are preliminary estimations and require further investigation.

PS128_1-5

Core catcher

Diatoms: *Fragilariopsis kerguelensis* dominates the assemblage (around 70%) / Fragments of *Thalassiosira lentiginosa* / *Thalassiotrix antarctica* / *Eucampia antarctica* / *Thalassiosira tumida*

Radiolarians: *Artostrobus annulatus* / *Antarctissa denticulata* / *Siphocampe arachnea* (only few specimens)

Remark: Presence of foraminiferals. Diatom assemblage mostly dominated by species associated to the Permanent Open Ocean Zone (POOZ). Few diatoms associated to the Sea Ice Zone (SIZ). Radiolarian species associated to water masses below 0˚C

Section 1

Nothing except minerals and fragments

Section 2

Nothing except minerals and fragments

Section 3

Diatoms: *Fragilariopsis curta* (SIZ)

Radiolarian: *Cenosphaera cristata*

Remark: Very low productivity and few specimens. No forams. Probably glacial signal.

Section 4

Nothing except minerals and fragments

Section 5

Maybe one foram chamber but nothing else, except minerals and fragments.

PS128_1-6

Core Catcher

Foraminiferals

Section 1

Foraminiferals

Section 2

Section Nothing except minerals and fragments

Section 3

Diatoms: *Fragilariopsis kerguelensis*, *F. sublinearis* and *F. obliquecostata*, *Thalassiosira lentiginosa*, *Eucampia antarctica*.

Remark: Species associated to the POOZ dominate.

Section 4

Foraminiferals and sponge spicules

Section 5

Nothing except minerals and fragments

Section 6

Diatoms: *F. kerguelensis* (fragments), *F. cylindrus*, *F. curta*, *F. obliquecostata*, *F. ritscheri*, *Thalassiotrix antarctica*.

Remark: Species mostly associated to Sea Ice environment, colder signal than section 3.

Surface

Remark: Foraminiferals (including bi-seriated benthics). No or few diatoms/radiolarians.

PS128_2-2

Section 1

Diatoms: Presence of *Fragilariopsis sublinearis*, *Fragilariopsis kerguelensis*, *Thalassiotrix antarctica*, *Thalassiosira lentiginosa*, *Eucampia antarctica* (*var. recta*)

Remark: Presence of forams, mix between POOZ and coastal diatom species. Rather warm signal.

Section 2

Remark: Presence of forams (benthic species, *Epistominella exigua*). No radiolarian nor diatom.

Section 3

Diatoms: *Eucampia antarctica*, *Actinocyclus actinochilus*, *Thalassiotrix antarctica*, *Fragilariopsis curta*, *F. ritscheri*, *F. kerguelensis* (dominates), *Thalassiosira* sp.

Radiolarian: *Actinomma leptoderma*

Remark: Diatom species associated to POOZ dominate. High abundance.

Section 4

Diatoms: *Rhizosolenia* sp., *F. kerguelensis*, *Thalassiotrix antarctica*

Remark: More forams (including *E. exigua*) than diatoms. Diatoms in very low abundance.

Section 5

Diatoms: *Actinocyclus actinochilus*, *Eucampia antarctica*, *Thalassiosira lentiginosa*, *F. kerguelensis*

Radiolarian: *Annulatus artostrobus*

Remark: More diatoms than in section 4 but still low occurrence. No forams. *F. kerguelensis* dominates the assemblage (~ 70%)

PS128_2-3

Core catcher

Diatoms: Presence of *Fragilariopsis sublinearis*, *Fragilariopsis obliquecostata* (Sea Ice Zone)

Section 1

Diatoms: *F. kerguelensis* fragments (POOZ)

Radiolarian: *Antarctissa strelkovi*

Remark: Many forams, interglacial signal

Section 2

Remark: Forams, and radiolarian *Cenosphaera* sp.

Section 3

Remark: Forams and sighting of *F. kerguelensis* (fragments)

Section 4

Diatoms: *Eucampia antarctica*, *F. kerguelensis*, *Thalassiosira lentiginosa*, *Thalassiosira oliverana*, *Actinocyclus curvatulus*, *Denticulopsis* sp.

Remark: *F. kerguelensis* dominates assemblage. Warm signal (relative to the core location)

Section 5

Remark: Forams and sighting of *F. kerguelensis* (fragments)

Section 6

Radiolarian: *Botryostrobus auritus*, broken spumellarian

Diatoms: *Eucampia antarctica*, *F. kerguelensis*, *Th. lentiginosa*, *Th. oliverana*, *Actinocyclus actinochilus*, *Chaetoceros* Resting Spores (CRS), *Coscinodiscus occulus-irridis*,

Surface

Diatoms: *Eucampia antarctica*, *F. kerguelensis*, *Thalassiosira lentiginosa*, *F. curta*, *Actinocyclus* actinochylus, *Thalassiotrix antarctica*, *F. obliquecostata*, *Thalassiosira antarctica*, benthic diatoms.

Radiolarian: *Stylodictya acuelata*, *Stylodictya tenuispina*, *Siphocampe arachnea*, *Cenosphaera* sp., *Antarctissa strelkovi*, *Antarctissa denticulata*, *Actinomma popofskii*, *Artostrobus joergenseni*, *Hexapyle dodecantha*, *Tetrapyle octacantha*

Remark: Presence of Radiolarian species associated to subantarctic zone environments, this suggests a warm period, interglacial. POOZ diatom species dominate the assemblage.

PS128_4-4

Core Catcher + Section 1 + Section 2

Nothing except minerals and fragments

Surface

Presence of *Coscinodiscus oculus-irridis*

Remark: Not much to see in this core in terms of microfossils.

PS128_5-1

Surface

Diatoms: *Eucampia antarctica*, *Fragilariopsis curta*, *F. kerguelensis*, *F. obliquecostata*, *F. rhombica*, *Actinocyclus actinochilus*, *Paralia sulcata*, *Porosira glacialis*, *Stellarima microtrias*, *Thalassiosira antarctica*, *Thalassiosira gracilis*, *Th. oliverana*.

Remark: High abundance and diversity of diatoms in the surface with species associated to POOZ and SIZ. No diatoms were seen in the other sections of the core.

PS128_6-1

Core Catcher

Remark: Sightings of foraminiferals and fragments of *F. obliquecostata* and *F. kerguelensis*.

Section 1

Remark: Forams (*N. pachyderma*)

Surface

Diatoms. *Fragilariopsis curta*, *F. kerguelensis*, *F. rhombica*, *F. obliquecostata*, *F. sublinearis*, *Thalassiosira oliverana*, *Th. antarctica*, *Th. gracilis*, *Th. tumida*, *Porosira glacialis*, *Actinocyclus curvatulus*, *Rhizosolenia antennata var. semispina*, *Porosira glacialis*, CRS.

Remark: High abundance and diversity of diatoms in the surface with species associated to POOZ and SIZ.

PS128_7-1

Core Catcher

Nothing but minerals, no forams

Surface

Diatoms: *Actinocyclus actinochilus*, *F. kerguelensis*, *F. separanda*

PS128_8-1

Core Catcher

Nothing except minerals and fragments

Surface

Diatoms: *Eucampia antarctica*, ***F. kerguelensis, F. curta***, *F. obliquecostata*, *F. ritscheri*, *F. sublinearis*, *F. separanda*, *Actinocyclus actinochilus*, *Asteromphalus hyalinus*, *Thalassiosira antarctica*, *Th. gracilis*, ***Th. lentiginosa***

Remark: High abundance and diversity of diatoms in the surface with species associated to POOZ and SIZ. Presence of silicoflagellates and forams (including benthics).

PS128_9-1

Core Catcher

Remark: Sponge spicules, no diatoms, fragments of *Antarctissa* (radiolarians), minerals.

Surface

Remark: Presence of *Thalassiosira oliverana*

PS128_10-1

Core catcher

Diatoms: *F. kerguelensis*, *Eucampia antarctica*, *Thalassiosira oliverana*, *Thalassiosira gracilis*, *Fragilariopsis curta*, *Actinocyclus actinochilus*, *Fragilariopsis rhombica*, *F. obliquecostata*, *Th. antarctica*

Remark: Average abundance and diversity of diatoms in the surface with species associated to POOZ and SIZ. *F. kerguelensis* dominates the assemblage. Presence of silicoflagellates.

PS128_12-1

Core Catcher

Nothing except fragments and minerals, presence of *Coscinodiscus* sp. (diatom).

PS128_13-2

Core Catcher slide 1 and 2

Nothing except minerals and fragments

Section 1

Diatoms: *Actinocyclus ingens* (16 – 0.6 Myrs), Central diatom with honeycomb porosity (maybe *Th. kolbei*), fragment of *Actinocyclus actinochilus* (First appearance at 2.75 Myrs), *Thalassiosira lentiginosa* (first appearance 4Myrs), *Thalassiosira elliptopora* (3.3 – 0.7 Myrs), *Denticulopsis* sp.

Radiolarian: *Dipylissa bensoni*

Remark: *F. kerguelensis* has been the dominant species so far, its absence from this sample suggests that the sample is probably older than 2.3 Myrs (first appearance of *F. kerguelensis*). The presence of *Actinocyclus actinochilus* in this sample suggests an age close to Plio-Pleistocene boundary.

Sections 2 and 3

Nothing except minerals and fragments

Section 4

Remark: Presence of *Actinocyclus ingens* and forams (*N. pachyderma* and other species)

Section 5

Presence of foraminiferals.

Section 7

Section 8

Radiolarian: *Larcoid* sp.

Section 9

Diatom: *Eucampia antarctica*

Remark: Many Foraminiferals (*Cibicidoides pachyderma*, *Epistominella exigua*, *N. pachyderma*, *Globorotalia menardii*)

Section 10

Radiolarians: *Antarctissa strelkovi* / *A. denticulata*

Diatoms: *Eucampia antarctica*, *Fragilariospsis kerguelensis*, *Cocconeis costata*, *Thalassiosira oliverana*, *Actinocyclus actinochilus*, *Thalassiosira gracilis*

Remark: The presence of *F. kerguelensis* suggests an age younger than 2.3 Myrs

PS128_14-1

Section 1

Diatoms: *Fragilariopsis obliquecostata*, *Porosira glacialis*, *Fragilariospsis kerguelensis*, *Eucampia antarctica*

Section 2

Diatoms: *F. kerguelensis*, *A. actinochilus*, *Thalassiosira antarctica* (vegetative and spores), CRS, *Asteromphalus parvulus*, *F. separanda*, *Eucampia antarctica*, *F. obliquecostata*, *Rouxia leventarae*, *Thalassiotrix antarctica*

Remark: High abundance of diatoms

Section 3

Diatoms: *Thalassiosira lentiginosa*, broken *F. kerguelensis*

Remark: Extremely low presence of diatoms, only two specimens were observed.

Sections 4 and 5

Nothing except minerals and fragments

Section 6

Diatoms: *Fragilariopsis kerguelensis*, *Actinocyclus actinochilus*, *Eucampia antarctica*, *Asteromphalus parvulus*, *Thalassiotrix antarctica*, *F. sublinearis*, *F. obliquecostata*, *F. vanheurcki*, *F. curta*

Remark: Much more diatoms than before but many fragments and poor preservation. *F. kerguelensis* widely dominates (~70%), POOZ conditions. Sea Ice diatoms are in very low numbers.

Section 7

Diatoms: *F. kerguelensis*, *F. obliquecostata*, *F. separanda*, *Thalassiosira oliverana*, *Th. lentiginosa*, *Th. antarctica*, *Th. gracilis*, *Actinocyclus curvatulus*, *Eucampia antarctica*, *Cocconeis costata*, *Thalassiotrix antarctica*, *Rhizosolenia* sp., *Denticulopsis* sp.

Remark: *F. kerguelensis* dominates the assemblage by far (~70%). Lots of diatoms, less sea ice species than in the previous section, and they have lower abundances.

Sections 8 and 9

Nothing except minerals and fragments

Section 10

Diatoms: *Fragilariopsis kerguelensis*

Remark: Only 3 diatoms were observed, nothing else. Many broken valves.

Section 11

Diatoms: *F. kerguelensis* (~60-80%), *F. ritscheri* / *F. sublinearis* / *F. obliquecostata* (~10%), *Thalassiosira oliverana*, *Actinocyclus actinochilus* (~5-10%), *Rhizosolenia* sp., *Thalassiosira antarctica*, *Porosira glacialis*, *Eucampia antarctica*.

Remark: Abundant diatoms. *F. kerguelensis* dominates the assemblage by far.

Section 12

Diatoms: *F. kerguelensis* (~60-80%), *F. ritscheri*, *Thalassiosira lentiginosa*, *Th. Antarctica*, *Th. oliverana*, *Coscinodiscus oc.-ir.*, *Eucampia antarctica*, *Actinocyclus actinochilus*

Remark: Sea Ice diatoms are less abundant than in the previous smear slide, suggesting warmer conditions.

Section 13

Diatoms: *Thalassiosira oliverana* (~10%), *Th. antarctica*, *Th. lentiginosa*, *F. kerguelensis* (~60-80%), *Eucampia antarctica* (~10-20%), *F. obliquecostata*, *Actinocyclus actinochilus*

Remark: Sea Ice diatoms are even less abundant than before, *E. antarctica* drastically increased in abundance.

PS128_15-3

Core Catcher:

Diatoms: *F. kerguelensis*, *Eucampia antarctica*, *Actinocyclus* actimochilus, *Thalassiosira lentiginosa*.

PS128_16-3

Core Catcher

Remark: presence of Forams

Section 1

Remark: Forams and one *F. kerguelensis*

Section 2

Remark: Sighting of a *F. kerguelensis* fragment, no forams.

Section 3

Remark: Presence of Forams.

Sections 4 and 5

Nothing except minerals and fragments

Section 6

Remark: Fragments of a central diatom (unidentified), nothing else.

Section 7

Diatoms: *F. kerguelensis*, *Actinocyclus actinochilus*, *Eucampia antarctica*, *Thalassiotrix antarctica*, *Thalassiosira lentiginosa*, *Thalassiosira oliverana*.

Remark: Sediment looked like diatom rich mud upon section cutting, many fragments of diatoms

Section 8

Remark: sighting of a *F. kerguelensis* fragment and a central diatom (broken unidentified).

PS128_16-4

Core catcher

Nothing except minerals

Section 1

A couple of forams, very few. Nothing else.

Section 2

Very few forams nothing else

Section 3

Nothing except minerals

Section 4

Idem

Section 5

A few forams and broken needles

Section 6

Nothing except minerals

Section 7

Nothing except minerals

Section 8

Eucampia antarctica, *Coscinodiscus oc-ir*, *Thalassiosira lentiginosa* (dominant), *Th. oliverana*, *Fragilariopsis kerguelensis* (low abundance)

Siphocampe arachnea, *Spongopyle osculosa*

Needles, no forams, low abundance of diatoms, only two rads.

Section 9

Nothing except minerals

Section 10

Nothing except broken needles

Section 11

Nothing except broken needles

Section 12

One foram and one diatom (*Th. lentiginosa*)

Section 13

Nothing except a fragment of a central diatom

Section 14

F. kerguelensis (dominates), *Eucampia antarctica*, *Actinocyclus actinochilus*, *Th. lentiginosa*, *Th. oliverana*

Needles

Diatoms somewhat abundant and preserved. No rad or foram

Surface

F. kerguelensis, *Th. lentiginosa*, *Euc. antarctica*, *Th. oliverana*,

*Larcoid*s, *Cenosphaera*, *Stylodictya tenuispina*, *Ant. strelkovi*, *Triceraspyiris antarctica*, *Didy tetra*, *Larc. buetschlii*, *Lithelius nautiloides*.

Many diatoms, radiolarians, and needles. A ton.

PS128_17-1

Core was opened and smear slides were done at various depths, observations for this station are mostly based on these slides.

0 cm

Diatoms: *F. kerguelensis*, *Eucampia antarctica*, *Actinocyclus actinochilus*, *Th. oliverana*, *Th. lentiginosa*

Radiolarians: *Antarctissa strelkovi*, *Actinomma leptoderma*

Remark: Sighting of sponge spicules. Diatoms relatively abund*ant.*

222 cm

Nothing except fragments and minerals

350 cm

Diatoms: Thalassiora lentiginosa, *Fragilariopsis kerguelensis*, *Eucampia antarctica*, CRS, *F. curta*, *F. obliquecostata*, *Actinocyclus actinochilus*, *Odontellia weissflogi*, *Thalassiosira antarctica*, *F. vanheurcki*, *Rouxia leventarae*

Remark: The assemblage and the abundance of diatoms suggest a warm period. Assemblage observations compared to the sediment magnetic susceptibility signal suggests that this samples is from MIS 5e. The presence of a dissolved and broken valve of *Rouxia leventarae* (2.5 – 0.13 Myrs) further strengthen this hypothesis.

376 cm

Similar assemblage as “350 cm” plus an unidentified *Rouxia* sp.

500 cm

Nothing except fragments and minerals

600 cm

Nothing except fragments and minerals

749 cm

Diatoms: *Fragilariopsis kerguelensis*, *Thalassiosira oliverana*, *Eucampia antarctica*, *Rouxia leventarae*

890 cm

Diatoms: *F. kerguelensis* (~ 60-70%), *F. rhombica*, *F. separanda*, *F. ritscheri*, *Th. lentiginosa*, *Rouxia leventarae*.

1045 cm

Nothing except fragments and minerals

1320 cm

Diatoms: *Eucampia antarctica*, *F. kerguelensis*

Remark: Only few diatoms, low abundances

1360 cm

Nothing except fragments and minerals

1375 cm

Nothing except fragments and minerals

Remark: Sponge spicules and a fragment of *F. kerguelensis*.

PS128_17-2

Core Catcher:

Diatoms: *F. kerguelensis*, *Eucampia antarctica*, *Thalassiotrix antarctica*, *Thalassiosira oliverana*, *Thalassiosira lentiginosa*, *Actinocyclus actinochilus*, *F. obliquecostata*, *F. curta*, *F. separanda*, *F. ritscheri*, *Thalassiosira gracilis*, *Chaetoceros* sp.

Radiolarians: *Botryostrobus* sp. (broken cephalis) and *Siphocampe arachnea*.

PS128_19-2

Section 2

Nothing except minerals and fragments

Section 3

Nothing except minerals and fragments

Section 4

Nothing except minerals and fragments

Section 5

Nothing except minerals and fragments

Section 6

No slide

Section 7

Foraminiferals and sponge spicules

Section 8

Foraminiferals

Section 9

Foraminiferals (*N. pachyderma* dominates the assemblage)

Section 10

Some foraminiferals but less than in previous sections

Section 12

Nothing except minerals and fragments

Section 13

Forams are present again and are abundant

Section 14

Some forams but in lower quantities than in the slide for section 13

Section 15

No slide

Surface

Sighting of many foraminiferals.

Algea from the ship's pump

Fragilariopsis kerguelensis, Rhizosolenia antennata var. semispina, *Fragilariopsis curta*, sponge spicules, *Thalassiosira lentiginosa*.

Remark: Species mostly associated to the **POOZ/PFZ**

PS128_20-1

Core Catcher

Remark: *N. pachyderma* dominates assemblage and other foram species observed, no diatoms or radiolarian.

Section 2

Remark: Very few diatoms, fragmented. Sightings of fragments of *Thalassiosira lentiginosa*, *Th. oliverana*, *Actinocyclus ingens* (16 – 0.6 Myrs)

Section 3

Nothing except minerals and fragments

Sections 4 and 5

Many foraminiferals, various species, nothing else

Section 6

Many foraminiferals, various species, nothing else, *N. pachyderma* dominates

Sections 7 and 8

Nothing except minerals and fragments and a few forams

Section 9

Many foraminiferals, various species, nothing else, *N. pachyderma* dominates

Section 10

Nothing except minerals and fragments and a few forams

Section 11

Many foraminiferals, various species, nothing else

Section 12

Nothing except minerals and fragments

Remark: Sighting of a fragment of *Actinocyclus ingens*

Section 13

Nothing except minerals and fragments and a few forams

Section 14

Nothing except minerals and fragments

Section 15

Nothing except minerals and fragments

Surface

Diatoms: F.kerguelensis, *Eucampia antarctica*, *Th. lentiginosa*, *Th. oliverana*, *Actinocyclus actinochilus*, *Th. gracilis*

Radiolarians: *Spongopyle osculosa*, *Antarctissa denticulata*, *Actinomma medianum*, *Stylodictya tenuispina*

Remark: Many diatoms but very broken, not well preserved. *F. kerguelensis* dominates the assemblage. A few radiolarians. Species from subsurface-surface (no deep water species.)

PS128_23-1

Core Catcher

Nothing except minerals and fragments

PS128_23-2

Core Catcher

Nothing except minerals and fragments

Surface

Diatoms: *Eucampia antarctica*, *Porosira pseudodenticulata*, *Actinocyclus actinochilus*, *Thalassiosira tumida*, *F. kerguelensis*, *F. sublinearis*, *Th. antarctica*, *F. curta*.

Remark: Too many coarse grains, very sandy sediment, NOA didn't paste the slide correctly. Difficult to identify species but diatoms are present. Sea ice diatoms are somewhat abund*ant.* Forams are present as well.

PS128_25-1

Core Catcher

Diatoms: *F. kerguelensis*, ***F. ritscheri***, *Th. antarctica*, *Eucampia antarctica*, ***F. cylindrus***, *Th. oliverana*, ***Actinocyclus actinochilus, F. curta***

Remark: Sighting of forams. **Sea Ice Zone** signal from the diatom assemblage.

Section 2

Diatoms: *F. kerguelensis* (~60-80%), *Th. oliverana*, *Th. lentiginosa* (~10-20%), *Eucampia antarctica*, *Actinocyclus actinochilus*, *Coscinodiscus oc.-ir.*, *F. curta*, *Corethron cryophilum*, *Th. tumida*

Remark: Sea ice diatoms less abundant than in the core catcher, warmer conditions.

Sea ice sample from Molodezhnaya

Fragilariopsis curta dominates the assemblage (80-90%), *Navicula* sp. (probably *N. glacei*), *Synedropsis fragilis*, *F. cylindrus*, maybe *F. vanheurcki*.

PS128_34-2

Core Catcher

Radiolarian: *Antarctissa strelkovi*/*A. denticulata*, *Actinomma medianum*, *Artostrobus annulatus*, *Actinomma* sp., *Larcopyle buetschlii*, *Pseudodictyophimus gracilipes*

Diatoms: *Eucampia antarctica*, *F. obliquecostata*, *F. sublinearis*, *Actinocyclus ingens*, *F. separanda*, *Rouxia constricta* (1.4 – 0.3 Myrs), *Rouxia antarctica* (5-1.5Myrs), *Th. oliverana*, *Th. lentiginosa*, *Stellarima microtrias*, *F.bohatyi*, *Actinocyclus actinochilus*,

Remark: Not sure whether this is *R. antarctica* or *R. constricta*.

Section 2

Radiolarian: *Antarctissa denticulata*, *Druppatractus variabilis*

Diatoms: *Actinocyclus ingens*, *Eucampia antarctica*, *Denticulopsis* sp., *Th. gracilis*, *Stellarima microtrias*, Central diatom unidentified

Remark: very few diatoms, everything is very dissolved and broken

Section 3

Radiolarian: *Siphocampe arachnea*, *Antarctissa denticulata*, *Actinomma medianum*, *Cornutella profunda*, *Larnacilla typus*, *Cycladophora cornutoides*, *Saccospyris antarctica*, *Hexapyle dodecantha*, *Didymorcitis tetralamus*, *Pseudodictyophimus bicornis*, *Artostrobus annulatus*, *Saccospyris* conythorax, *Cenosphaera* sp., *Spongodiscus biconcavus*

Diatoms: *Th. oliverana*, *Actinocyclus actinochilus*, *Rouxia antarctica*, *Stellarima microtrias*, *Actinocyclus ingens*, *Trichotoxon reinboldii*, *F. separanda*

Remark: The diversity of radiolarian species suggests interglacial oceanographic settings. Presence of radiolarian species that would never appear during a glacial (i.e., *S. conythorax* or *H. dodecantha*).

Section 4

Diatoms: *Actinocyclus ingens* (16 – 0.6 Myrs), *Trichotoxon reinboldii*, *Eucampia antarctica*, *Rhizosolenia* sp., *F. kerguelensis*, *Actinocyclus curvatulus*, *Actinocyclus actinochilus*, *F. obliquecostata*, *Coscinodiscus occulus-irridis*

Radiolarian: *Stylodictya acuelata*, *Antarctissa strelkovi*, *Botryostrobus* sp., *Actinomma antarcticum*, *Pseudodictyophimus platycephalus*, *Artostrobus annulatus*, *Zygocircus* sp.

Remark: The presence of *A. ingens* and *F. kerguelensis* suggests that this sample could be from older than 0.6Myrs, but definitely Quaternary.

Section 5

Radiolarian: *Antarctissa denticulata*, *Siphocampe arachnea*

Remark: Tons of *N. pachyderma*

Section 6

Diatoms: *Coscinodiscus occulus-irridis*, *Thalassiosira lentiginosa*, *Thalassiosira oliverana*, *Actinocyclus ingens*, *F. sublinearis*, *Th. elliptopora* (maybe), *Eucampia antarctica*, *F. curta*, *F. ritscheri*, *Actinocyclus actinochilus*, *Thalassiotrix antarctica*, *Rhizosolenia* sp., *F. kerguelensis*, *Porosira glacialis*.

Radiolarian: *Actinomma popofski*, *Actinomma boreale*, *Larcopyle pylomaticus*, *Spongodiscus resurgens*

Remark: Presence of forams (*N. pachyderma*). *F. ritscheri* is very abundant. The diatom assemblage has a strong SIZ signal.

Section 7

Remark: Low productivity and abundance of radiolarians and diatoms. Presence of *Actinocyclus ingens* (16 – 0.6 Myrs).

Section 9

Diatoms: *F. kerguelensis*, *Thalassiosira elliptopora* (3.3 Myrs – 0.7 Myrs), *Actinocyclus actinochilus*, *Denticulopsis* sp.

Remark: Low productivity and abundance of diatoms. No radiolarian. Sample older than 0.7 Myrs.

Section 10

Denticulopsis sp., Central diatom (unidentified)

Remark: Low abundance of diatoms. No radiolarian.

Section 12

Diatoms: *F. kerguelensis* (dominates), *Eucampia Antarctissa*, *Thalassiosira oliverana*, *Actinocyclus ingens* (16 – 0.6 Myrs)

Radiolarian: *Antarctissa strelkovi*, *Annulatus artostrobus*.

Remark: Presence of silicoflagellates (*Distephanus* sp.)

Section 14

Diatoms: *Eucampia antarctica*, *Thalassiosira oliverana*, *F. kerguelensis*, *F. sublinearis*, *Paralia sulcata*, *Actinocyclus actinochilus*, *Thalassiosira lentiginosa*

Radiolarians: *Antarctissa strelkovi*, *Larcopyle buetschlii*, *Siphocampe arachnea*

Top (Sieved 63-250µm)

Radiolarian. *Antarctissa denticulata*/*A. strelkovi*, *Chromyechinus antarctica*, *Cenosphaera* sp., *Saccospyris antarctica*, *Lacopyle weddellium*, *Larcopyle pylomaticus*, *Stylodictya tenuispina*, *Spongodiscus glacialis*, *Actinomma* sp., *Lithelius nautiloides*, *Dictyophimus mawsoni*, *Phormospyris antarctica*, *Actinomma leptoderma*, *Schizodiscus stylotrochoides*, *Actinomma sol*, *Actinomma boreale*, *Actinomma popofski*, *Cycladophora davisiana*.

Remark: Rads are concentrated due to sieving. Some species with intermediate-deep water ecology, clearly interglacial signal despite the presence of very cold Radiolarian species.

Top (not sieved)

Diatoms

Paralia sulcata, *F. kerguelensis*, *F. curta*, *Eucampia antarctica*, *F. sublinearis*, *Actinocyclus actinochilus*, *F. separanda*, *Th. antarctica*, *Th. oliverana*, *Th. tumida*

Remark: *F. kerguelensis* dominates the assemblage. Many diatoms.

PS128_34-3

Core Catcher

Diatoms

Actinocyclus karstenii (… - 2.1 Myrs), *Eucampia antarctica*, *Fragilariopsis barronnii*, *Rhizosolenia* sp., *Th. elliptopora*, *Denticulopsis* sp., *F. obliquecostata*, *F. sublinearis*, *Th. lentiginosa*, *Rouxia* sp. (*R. antarctica*?), *Th. tumida*, *Actinocyclus* sp., *Th. tetraoestrupii var. reimeri*

Remark: Many diatoms and sponge spicules, some radiolarians (*Siphocampe arachnea*, *Larcoid*)

Section 3

Sponge needles

Antarctissa denticulata

Actinocyclus karstenii, *Actinocyclus ingens*

Very few diatoms

Section 4

Actinocyclus ingens, fragment of *Actinocyclus actinochilus*, *Eucampia antarctica*, *Th. lentiginosa*

Fragment of *Cycladophora davisiana*

Very few diatoms. Fragmented

Section 5

Actinocyclus ingens, *F. kerguelensis* (first sighting, appeared at 2.3 Myrs), *Th. lentiginosa*, *F. obliquecostata*

Very few diatoms (sighting of a broken spumellarian)

Section 6

Actinocyclus ingens, *F*. kerguelensis, *Actinocyclus actinochilus*, *Stellarima microtrias*, *Eucampia antarctica*, *F. barronii – F. kerguelensis* transitional form

More diatoms than before

Section 7

Actinocyclus ingens, *F. kerguelensis*, *Eucampia antarctica*, *F. obliquecostata*, *F. ritscheri*, *Th. lentiginosa*, *Th. tumida*, *Actinocyclus* sp., *Stellarima microtrias*, *F. sublinearis*, *Coscinodiscus* oc. Ir., fragment of *Actinocyclus actinochilus*

Many needles, silicoflagellates

Diatoms are abundant

Section 8

Actinocyclus actinochilus, *Th. lentiginosa*

Artostrobus annulatus, Fragment of *Antarctissa denticulata*

Very few diatoms

Section 9

Coscinodiscus oc.-ir., *Th.* inura (5 – 1.8 Myrs), *Th. tumida*

Antarctissa denticulata, *Lithelius nautiloides*

Very few diatoms and rads

Section 10

F. kerguelensis fragment

*Larcoid*s, *Spongotrochus* sp.

Silicoflagellates, broken needles, very few fossils and little biogenic content

Section 11

Only broken needles, nothing to see

Section 13

Eucampia antarctica, *F. kerguelensis*, *Th. lentiginosa*, *Denticulopsis* sp.

Many fragments, not well preserved, not many full diatoms

Section 14

F. kerguelensis, *Eucampia antarctica*, *Th. lentiginosa*

Larcopyle buetschlii

Many fragments, not well preserved, not many full diatoms

Top

F. kerguelensis, *F. separanda*, *Th. lentiginosa*, *Actinocyclus actinochilus*, *F. curta*, *Thalassiotrix antarctica*, *Asteromphalus parvulus*, *Th. oliverana*, *F. sublinearis*, *F. rhombica*, *Th. antarctica*

Silicoflagellates, F. kerg dominates the assemblage by far.

PS128_39-1

Core catcher + Section 2

Diatoms

Eucampia antarctica, *Coscinodiscus occulus-irridis*, *Thalassiosira oliverana*, *F. kerguelensis*, *Thalassiosira lentiginosa*, *F. sublinearis*, *Th. gracilis*.

Section 4

Remark: Low abundance of diatoms. Presence of *Triceratium* sp. (triangular diatom, coastal signal).

Section 7

Diatoms

F. kerguelensis, *F. curta*, *F. sublinearis*, *Coscinodiscus oc.-ir.*, *Actinocyclus actinochilus*, *Corethron cryophilum*, *Porosira glacialis*, *F. separanda*, *F. obliquecostata*, *Rhizosolenia antennata var. semispina*, *F. ritscheri*, *Cocconeis costata*.

PS128_40-2

Core Catcher

Diatoms

Odontella weissflogi, *F. kerguelensis*, *F. sublinearis*, *F. obliquecostata*, *F. ritscheri*, *F. curta*, *F. rhombica*, *Thalassiosira oliverana*, *Th. tumida*, *Th. lentiginosa*, *Actinocyclus actinochilus*, *Eucampia antarctica*, *Corethron cryophilum*, *Coscinodiscus oc-ir.*, *Rhizosolenia antennata var. semispina*, *Asteromphalus hookeri*, *Cocconeis costata*, *Porosira glacialis*

Radiolarians

Antarctissa strelkovi

Remark: Presence of silicoflagellates. The core is mainly composed of diatom ooze, reflectors suggested that the core covers the late Holocene. Diatom assemblage suggests coastal and SIZ conditions.

Section 5

Same species were observed

Section 11

Same species were observed, *Corethron cryophilum* dominates the assemblage which may suggest an early spring bloom signal.

Section 14b

Similar observation, *Corethron* greatly dominates.

Section 20

95% *Corethron cryophilum*, no radiolarian was observed in this core.

PS128_41-1

Core Catcher

Diatoms

Eucampia antarctica

fragments of *F. kerguelensis*, *A. actinochilus* and *Th. oliverana*.

Remark: Presence of silicoflagellates (*Distephanus* sp.), very few diatoms and generally poor preservation.

Section 5

Diatoms

Eucampia antarctica, *Actinocyclus actinochilus*, *Corethron cryophilum*, *Fragilariopsis curta*, *F. ritscheri*, *F. sublinearis*, *F. separanda*, *F. rhombica*, *F. kerguelensis*, CRS, *Thalassiosira antarctica*, *Thalassiosira maculata*, *Th. oliverana*, *Th. gracilis*, *Th. tumida*, *Porosira pseudodenticulata*, *Paralia sulcata*, *Chaetoceros* bulbosum, *Chaetoceros atlantica*, *Rhizosolenia* sp.

Radiolarian

Antarctissa strelkovi
Remark: Lots of diatoms, high abundances, assemblage similar to core 40-2

PS128_42-1

Core Catcher

Diatoms

Eucampia antarctica, *Fragilariopsis kerguelensis*, *F. ritscheri*, *F. curta*, *F. sublinearis*, *Thalassiosira antarctica*, *Th. oliverana*, *Th. gracilis*, *Actinocyclus actinochilus*

Section 2

Diatoms

Fragilariopsis kerguelensis, *F. ritscheri*, *Thalassiosira* sp., *Th. oliverana*, *Eucampia antarctica*, *Cocconeis antarctica*

Section 3

Diatoms

Thalassiosira oliverana, *Th. lentiginosa*, *Eucampia antarctica*, fragments of *F. kerguelensis*.

Remark: Few diatoms poor preservation.

Section 4

Diatoms

Fragilariopsis kerguelensis, *F. curta*, *Thalassiosira Antarctissa*, *Th. gracilis*, *Th. oliverana*, *Actinocyclus actinochilus*

Remark: More diatoms than in section 3, still not very abundant (may depend on the amount of sediment used to make the slide).

Section 5

Radiolarian

Antarctissa denticulata, *A. strelkovi*

Remark: Diatom ooze, diatoms extremely abundant, same cold, SIZ, and coastal species. Similar assemblage as what was observed for core 40-2.

PS128_44-1

Core Catcher

Diatoms

Thalassiosira oliverana, *Central* sp., *Denticulopsis* sp., *Actinocyclus actinochilus*

Section 1

Diatoms

Eucampia antarctica, fragments

Remark: Poor preservation, not much to see.

Section 2

Diatoms

Eucampia antarctica, *Actinocyclus Actinocyclus*, *Triceratium* sp., *Cocconeis* sp., *Paralia sulcata*, *Fragilariopsis kerguelensis*, *F. ritscheri*, *Thalassiosira oliverana*, benthic diatom (unidentified), *Porosira glacialis*

Radiolarians

Chromyechinus antarctica

Remark: More diatoms than in section 1

Section 3

Diatoms

Stellarima microtrias, *Actinocyclus actinochilus*, benthic diatom (unidentified), *Fragilariopsis ritscheri*, *F. curta*, *F. obliquecostata*, *F. separanda*, *F. kerguelensis*, *Thalassiosira tumida*, *Th. oliverana*

PS128_46-1

Core Catcher

Diatoms

Thalassiosira oliverana, *Th. lentiginosa*, *Fragilariopsis curta*, *F. rhombica*, *F. kerguelensis*

Remark: Not many diatoms in this sample

Section 3

Diatoms

Fragilariopsis kerguelensis, *F. curta*, *F. obliquecostata*, *F. ritscheri*, *F. sublinearis*, CRS, *Porosira glacialis*, *Thalassiosira oliverana*, *Th. tumida*, *Th. antarctica*, *Actinocyclus actinochilus*, *Eucampia antarctica*, *Odontellia weissflogi*, *Rhizosolenia* simplex

Remark: Many diatoms (very abundant), and a lot of biogenic silica (sponge spicules, silicoflagellates), no radiolarians were observed. Very little sediment was used for this smear slide and rads maybe present if more material is used.

PS128_47-1

Core Catcher

Diatoms

Porosira glacialis, *Fragilariopsis kerguelensis*, *Eucampia antarctica*, *Denticulopsis* sp., *Actinocyclus actinochilus*

Remark: Few diatoms and many fragments, poor preservation. Presence of silicoflagellates.

Section 2

Diatoms

Eucampia antarctica, *Thalassiosira oliverana*, *Fragilariopsis kerguelensis*, *F. obliquecostata*, *F. sublinearis*, *Actinocyclus actinochilus*, CRS, *Rhizosolenia simplex*.

Section 4

Diatoms

F. kerguelensis, *F. ritscheri*, *F. obliquecostata*, *F. rhombica*, *Th. oliverana*, *Th. tumida*, *Eucampia antarctica*, *Coscinodiscus oc-ir.*, *Actinocyclus actinochilus*, *Porosira glacialis*, *Asteromphalus hookeri*, *Corethron cryophilum*

Remark: High abundance of silicoflagellates and diatoms

Surface

Diatoms

Eucampia antarctica, *Thalassiosira gracilis*, *Th. oliverana*, *Th. tumida*, *Th. lentiginosa*, *Fragilariopsis kerguelensis*, *F. curta*, *F. ritscheri*, *F. obliquecostata*, *F. sublinearis*, *Asteromphalus hookeri*, *Rhizosolenia antennata var. semispina*, *Coscinodiscus oc.-ir.*, *Porosira glacialis*,

Cocconeis costata, *Corethron cryophilum*

Remark: Lots of diatoms, very abundant.

PS128_49-2

Core Catcher

Diatoms

Eucampia antarctica, *Thalassiosira oliverana*, *Th. lentiginosa*, *Th. tumida*, *Th. antarctica*, *Fragilariopsis kerguelensis*, *F. curta*, *F. ritscheri*, *F. sublinearis*, *F. rhombica*, *F. separanda*, *Thalassiotrix antarctica*, CRS, *Cocconeis costata*, *Paralia sulcata*, *Rouxia leventarae* (2.5 – 0.13 Myrs)

Radiolarian

Didymocyrtis tetralamus

Remark: A lot of minerals and diatoms. *Rouxia leventarae* is very abundant in this sample, suggesting in situ production and not reworking. This sample is probably older than MIS 5e

Section 2

Diatoms

Eucampia antarctica, *Coscinodiscus* oc.ir., *F. kerguelensis*, *F. ritscheri*, *F. obliquecostata*, *F. sublinearis*, *F. curta*, *F. rhombica*, *Actinocyclus actinochilus*, *Thalassiosira gracilis*, *Th. oliverana*, *Th. lentiginosa*, *Asteromphalus hookeri*, CRS, *Stellarima microtrias*, *Porosira glacialis*.

Radiolarian

Antarctissa strelkovi

Remark: *F. kerguelensis* dominates the diatom assemblage.

Section 3

Diatoms

Fragilariopsis obliquecostata, *F. kerguelensis*, *F. sublinearis*, *F. ritscheri*, *F. curta*, *Eucampia antarctica*, *Actinocyclus actinochilus*, *Thalassiosira lentiginosa*, *Th. oliverana*, *Paralia sulcata*, benthic (unidentified), CRS, *Rhizosolenia simplex*, *Rhizosolenia antennata var. semispina*, *Cocconeis costata*, *Odontellia weissflogi*.

Radiolarian

Antarctissa denticulata, *Antarctissa strelkovi*

Remark: Diatoms are very abund*ant.* Presence of silicoflagellates.

Section 4

Diatoms

Fragilariopsis kerguelensis (dominant), *F. sublinearis*, *F. obliquecostata*, *F. ritscheri*, *F. rhombica*, *Th. oliverana*, *Th. lentiginosa*, *Th. gracilis*, *Eucampia antarctica*, *Actinocyclus actinochilus*, *Rhizosolenia* sp., *Rhizosolenia antennata var. semispina*, *Porosira glacialis*, CRS, *Asteromphalus parvulus*, *Cocconeis costata*, *Denticulopsis* sp.

Radiolarians

Actinomma sp., *Larcopyle buetschlii*.

Remark: *F. kerguelensis* dominates the diatom assemblage by far, suggesting open ocean conditions, thus rather warm conditions relative to the core location.

Section 5

Diatoms

Eucampia antarctica, *F. sublinearis*, *F. ritscheri*, *F. obliquecostata*, *F. kerguelensis*, *Thalassiosira oliverana*, *Th. antarctica*, *Rhizosolenia* sp., *Thalassiotrix antarctica*, CRS.

Remark: Lower diatom count and abundance compared to the previous sections.

Section 7

Diatoms

Eucampia antarctica, *Fragilariopsis kerguelensis*, *Actinocyclus actinochilus*, *Thalassiosira oliverana*, *F. obliquecostata*, *F. sublinearis*, *F. ritscheri*, *Thalassiosira antarctica*, *Thalassiosira lentiginosa*, *Asteromphalus hookeri*, *F. curta*, *Cocconeis costata*, *Coscinodiscus oc.-ir.*, *Thalassiosira tumida*, benthic diatom (unidentified), *Stellarima microtrias*, *Th. gracilis*

Remark: Diatoms are more abundant in section 7 than in section 5 and the assemblage may suggest warmer conditions.

PS128_53-1

Core Catcher

Diatoms

F. kerguelensis

Remark: Not much to see, very fragmented. Fragments of *Th. oliverana*.

Section 2

Diatoms

Th. antarctica, *Actinocyclus actinochilus*

Remark: Not much to see, very fragmented. Fragments of *Eucampia antarctica*, *F. kerguelensis*, *Th. oliverana*

Section 3

Eucampia antarctica (abundant), *Th. lentiginosa*, *F. kerguelensis*

Remark: Not much to see, very fragmented. Fragments of *Denticulopsis* sp., *Actinocyclus actinochilus*, *Th. oliverana*, *Th. antarctica*

Section 4

Th. lentiginosa, *F. kerguelensis* (~60%), *Thalassiotrix antarctica*, *F. obliquecostata*, *F. ritscheri*, *F. sublinearis*, *Th. oliverana*, *Actinocyclus actinochilus*, *Eucampia antarctica*, *F. rhombica*, *Coscinodiscus oc.-ir*.

Remark: Differences between *F. sublinearis*, *F. obliauecostata* and *F. ritscheri* very marked. Easy to differentiate them.

Section 5

Eucampia antarctica, *Th. oliverana*, *Paralia sulcate*, *F. kerguelensis*

Remark: Not much to see, very fragmented. Fragments of *Th. lentiginosa*, *Actinocyclus actinochilus*, *Th. gracilis*, *Actinocyclus ingens* (16 – 0.6 Myrs). The latter may indicate reworking.

Section 6

No slide

Section 7

Remark: Not much to see, very fragmented. Fragments of *Th. oliverana*, *F. kerguelensis*, *Th. lentiginosa*

Section 8

Remark: Not much to see, very fragmented. Fragments of *Th. oliverana*, *F. kerguelensis*, *Th. lentiginosa*

Section 9

Diatoms

Eucampia antarctica, *Thalassiosira oliverana*

Remark: Not much to see, very fragmented. Fragments of *F. kerguelensis*, *Th. lentiginosa*

Section 10

Diatoms

F. kerguelensis, *F. curta*, *F. sublinearis*, *F. ritscheri*, *F. rhombica*, *Eucampia antarctica*, *Thalassiosira oliverana*, *Th. gracilis*, *Actinocyclus actinochilus*, *Th. lentiginosa*, *Th. tumida*, *Corethron cryophilum*, CRS

Remark: Many diatoms with full valves. *F. kerguelensis* dominates the assemblage. Overview of the core: All diatoms were very broken suggesting transport and not in situ productivity, there could be some reworking as well.

PS128_54-1

Core Catcher

Diatoms

F. kerguelensis, *Th. lentiginosa*, *Actinocyclus ingens* (16-0.6 Myrs), *Th. oliverana*, *Denticulopsis* sp., CRS, *Eucampia antarctica*, *Th. elliptopora* (3.3 – 0.7 Myrs), *Actinocyclus actinochilus*

Radiolarian

Spum indet (Spongious and spherical), *Larnacilla typus*, *Antarctissa* sp., *Stylodictya acuelata*, *Annulatus artostrobus*, *Prunopyle* sp., *Stylodictya tenuispina*, *Antarctissa denticulata*, *Actinomma* sp., *Hexacontium giganthum* (?)

Section 2

Diatoms

Thalassiosira elliptopora, *F. kerguelensis*,

Remark: Not many *F. kerguelensis*, lots of sponge spicules

Section 3

Diatoms

Denticulopsis sp., *Actinocyclus ingens* (several specimen), *F. kerguelensis*, *F. rhombica*, *F. sublinearis*, *Th. lentiginosa*, *Th. oliverana*, *Actinocyclus actinochilus*

Remark: Very few kerguelensis, many fragments. Fragments of *Euc. antarctica*

Section 4

Diatoms

F. obliquecostata, *Actinocyclus ingens* (broken valve)

Remark: Not much and many fragments of centric diatoms

Section 5

Diatoms

F. kerguelensis (abundants), *Th. lentiginosa* (abundant ~30%), *Th. oliverana*, *Actinocyclus ingens*, *Eucampia antarctica*, *Coscinodiscus oc.-ir*.

Remark: Many diatoms, assemblage dominated by *F. kerguelensis* and *Th. lentiginosa*

Section 6

No slide

Section 7

Diatoms

Actinocyclus actinochilus, *F. curta*, *Eucampia antarctica*, *Denticulopsis* sp., *Coscinodiscus oc.-ir.*, *Th. lentiginosa*, *F. kerguelensis*, *F. obliquecostata*, *F. ritscheri*, *F. separanda*, *Actinocyclus* sp., *Rouxia leventarae*

Radiolarians

Siphocampe arachnea

Remark: Less diatoms than in section 5. Very fragmented, particularly sea ice diatoms, *F. kerguelensis* dominates the assemblage.

Section 8

Diatoms

F. kerguelensis, *F. ritscheri*, *Actinocyclus ingens*, *Th. lentiginosa*, *Denticulopsis* sp., *F. obliquecostata*, fragments of *Actinocyclus actinochilus*, *F. cylindrus*, fragment of *Paralia sulcata*

Radiolarians

Saccospyris conythorax, cephalis of *Antarctissa* (probably *A. denticulata*)

Remark: Radiolarian specimen very silicified. Few diatoms.

Section 9

Diatoms

Th. oliverana, *Thalassiotrix antarctica*, *F. kerguelensis* (dominates, ~60%), *F. sublinearis*, *F. obliquecostata*, *Th. tumida*, *Th. lentiginosa*, *Eucampia antarctica* (a lot), *Th. gracilis*, fragments of *Actinocyclus actinochilus*, *Actinocyclus ingens* (1 specimen), *Rhizosolenia* sp.

Radiolarians

Larcoid sp., Spum indet (same spongious species as in the core catcher), *Larcopyle weddelium*, *Botryostrobus auritus*, *Antarctissa denticulata*, *Antarctissa strelkovi*, *Artostrobus annulatus*, *Lithomelissa* spA.

Remark: A lot of siliceous microfossils, sponge spicules and silicoflagelates.

Section 10

Diatoms

Th. oliverana, *Eucampia antarctica*, *Actinocyclus actinochilus*, *Th. lentiginosa*, *F. obliquecostata*, *F. kerguelensis*, *F. ritscheri*, *Triceratium* sp., *Stellarima microtrias*, *Denticulopsis* sp., CRS, *Chaetoceros* sp.

Radiolarians

Antarctissa denticulata, *Antarctissa strelkovi*, *Cycladophora davisiana*

Remark: Sighting of a fragment of *Actinocyclus ingens*

Section 12

Diatoms

Triceratium sp., *Th. oliverana*, *Th. lentiginosa*, *Th. tumida*, *Th. gracilis*, *Eucampia antarctica*, *Actinocyclus actinochilus*, *F. kerguelensis*, *Actinocyclus ingens* (1 specimen), *Coscinodiscus oc.-ir.*, *F. separanda*, *Porosira glacialis*, *Asteromphalus parvulus*, *Stellarima microtrias*, *F. separanda*

Radiolarians

Antarctissa denticulata, *Stylodictya tenuispina*, *Antarctissa strelkovi*, *Lithomelissa* spA, *Artostrobus annulatus*, *Actinomma leptoderma*, *Actinomma* sp., *Cycladophora davisiana*, *Lithocampe furcaspiculata*,

Remark: Radiolarians very silicified again.

Section 13

Diatoms

Asteromphalus hookeri, *F. kerguelensis*, *Th. oliverana*, *Th. lentiginosa*, *Eucampia antarctica*, *Actinocyclus actinochilus*, *Th. gracilis*, Ast. parvulus, *F. curta*, *F. obliquecostata*, *F. sublinearis*, *Proboscis* sp., *Denticulopsis* sp., *Paralia sulcata*

Radiolarian

Artostrobus annulatus, *Siphocampe arachnea*, *Antarctissa denticulata*, *Larcopyle weddellium*, *Cycladophora davisiana*, *Artostrobus annulatus*, *Lithomelissa* spA, *Zygocircus* sp.

Section 14

Diatoms

Eucampia antarctica, *Rhizosolenia* sp., *F. kerguelensis*, *Th. lentiginosa*, *Th. oliverana*, *Cocconeis costata*, Benthic diatom, *F. curta*, *Actinocyclus actinochilus*, *F. rhombica*, *Porosira glacialis*, *F. ritscheri*, *Paralia sulcata*, *Th. antarctica*

Radiolarians

Antarctissa strelkovi, *Zygocircus* sp.

PS128_54-2

Core Catcher

F. kerguelensis, Fragments of *F. obliquecostata*, *Denticulopsis* sp. (many)

PS128_57-1

Core catcher

Diatoms

Actinocyclus ingens, *Th. lentiginosa*, *Th. oliverana*, *Th. tetraoestrupii var reimeri*, *F. kerguelensis*, *Actinocyclus actinochilus*, *Thalassiosira elliptopora* fragments, *F. cylindrus*, *Denticulopsis* (at least 2 different species)

Remark: diatoms quite abundant

Section 2

Diatoms

Actinocyclus ingens, *Denticulopsis* sp. (many specimen), fragments of *F. kerguelensis*, CRS, *Rouxia* fragments, *Rouxia leventarae*, *Actinocyclus actinochilus*, *Rhizosolenia ant. var. semispina*, *F. curta*, *F. obliquecostata*

Radiolarians

Siphocampe arachnea

Remark: Much less diatoms than in the core catcher slide. Very fragmented.

Section 3

Diatoms

Th. tumida, *Th. lentiginosa*, *Actinocyclus ingens*, *Th. tetraoestrupii var reimeri*, *Rhizosolenia* sp., CRS, fragments of *Actinocyclus actinochilus*

Radiolarians

Siphocampe arachnea, *Artostrobus annulatus*

Remark: Diatoms are abundant again, but very fragmented.

Section 4

Diatoms

Eucampia antarctica, *F. kerguelensis*, *Th. lentiginosa*, *Actinocyclus actinochilus*, *Porosira glacialis*, *Denticullopsis* sp., *F. obliquecostata*, *Th. oliverana*, *Actinocyclus ingens*, *Rouxia constricta*

Radiolarians

Zygocircus sp.,

Remark: Fewer diatoms, silicoflagellates.

Section 5

F. kerguelensis, *Th. lentiginosa*, *Th. oliverana*, *Eucampia antarctica*, *Actinocyclus ingens*, *Th. tumida*, fragments of *F. sublinearis* and *F. obliquecostata*/ritscheri, *Thalassiotrix antarctica*, *Hemidiscus karstenii* (0.42-0.2 Myrs), *F. ritscheri*, *Th. tumida*

Lithocampe furcaspiculata, *Antarctissa denticulata*, *Actinomma leptoderma*, *Larcopyle buetschlii*, *Botryopyle inflata*, *Arachnocorys dubius*, *Antarctissa strelkovi*, *Siphocampe arachnea*,

Remark: Slide with the most diatoms so far. *Hemidiscus karstenii* so far south is strange but no doubt about the species, several specimens were observed.

Section 7

Diatoms

Eucampia antarctica, *Fragilariopsis kerguelensis* (dominates), *Actinocyclus actinochilus*, *Th. oliverana*, *Cocconeis costata*, *Th. lentiginosa*, fragment of *Actinocyclus ingens* (16-0.6 Myrs), *Stellarima microtrias*, *F. ritscheri*, *Rhizosolenia* sp., *Th. gracilis*

Radiolarians

Botryostrobus auritus, *Cycladophora davisiana*, Cornutoides profunda, *Botryopyle inflata*, *Artostrobus joergenseni*, *Artostrobus annulatus*, *Antarctissa strelkovi*, *Acanthosphaera* sp., *Tholospyris gephyristes*, *Saccospyris antarctica*, *Siphocampe arachnea*, *Larcopyle pylomaticus*, *Larcopyle weddelium*

Remark: Presence of *Actinocyclus ingens* may suggest reworking because the radiolarian assemblage appears modern.

A.6.4 Coarse Fraction Analyses

PS128_17-1 Depth [cm]	Forams	Biosilicate	Silt	Clay	Comment
0	-	+	+	+	
28	-	+	+	+	
40	-	+	++	++	
95	-	(+)	+	++	
222	(+)	(+)	+	+	
350	-	++	+	+	
366	-	++	+	+	
376	-	+	+	++	
382	-	(+)	+	++	
388	-	+	+	++	
500	-	(+)	+	++	
526	(+)	(+)	+	++	
600	(+)	-	+	+	
750	-	++	+	++	
810	-	+	+	+	
831	-	++	++	+	
854	-	++	++	+	
890	-	++	++	+	
894	-	++	++	+	
940	-	+	+	+	
970	(+)	-	+	++	
1024	-	-	+	++	
1045	-	-	+	++	
1060	-	-	+	++	
1110	-	-	+	++	
1200	-	-	+	++	
1220	-	-	+	++	
1250	-	-	+	++	
1280	+	-	+	++	
1320	-	-	+	++	
1355	-	-	-	-	Sand Layer
1375	(+)	-	+	+	
1400	-	-	+	+	
1420	-	-	+	+	
1440	-	-	+	+	
1450	(+)	-	+	+	
1460	-	-	+	+	
1513	(+)	-	++	++	
1530	-	-	+	++	
1560	-	-	+	++	
1600	(+)	-	+	++	

PS128_19-2 Depth [cm]	Forams	Biosilicate	Silt	Clay	Comment
0	+	-	++	+	
84	++	-	+	+	
135	++	-	+	+	
155	+	-	+	++	
275	+	-	+	++	
370	++	-	+	+	
437	++	-	+	++	
500	++	-	+	+	
580	++	-	+	+	
665	++	-	+	+	
702	+	-	+	+	
731	+	-	+	+	
789	++	-	+	+	
885	+	-	+	+	
929	+	-	++	++	
1054	(+)	-	+	++	
1061	(+)	-	+	++	
1154	(+)	-	+	++	
1261	(+)	-	+	+	
1453	(+)	-	++	+	

PS128_54-2 Depth [cm]	Forams	Biosilicate	Silt	Clay	Comment
2	-	+	+	+	
52	-	++	++	+	
89	-	++	++	+	
170	-	++	++	+	
210	-	+	+	+	
250	-	+	+	+	
280	-	++	++	+	
320	-	++	++	+	
400	-	++	++	+	
460	-	+	+	+	
523	-	+	++	+	
590	-	++	++	+	
620	-	++	++	+	
660	-	+	+	+	
684	-	+	+	++	
700	-	+	+	++	
730	-	+	++	++	
780	-	++	++	+	
800	-	++	++	+	

PS128_54-2 Depth [cm]	Forams	Biosilicate	Silt	Clay	Comment
880	-	+	++	+	
930	-	++	+++	+	
1036	-	+	+	+	
1048	-	-	++	++	Mud-Clast
1064	-	+	+	++	
1084	-	+	++	++	
1087	-	+	+	++	
1090	-	+	+	++	
1120	-	+	+	++	
1185	-	+	++	++	
1140	-	(+)	+	++	
1220	-	++	++	++	
1260	-	++	++	++	
1280	-	++	++	++	
1286	-	++	++	++	
1310	-	+	+	++	
1360	-	++	++	++	

Die **Berichte zur Polar- und Meeresforschung** (ISSN 1866-3192) werden beginnend mit dem Band 569 (2008) als Open-Access-Publikation herausgegeben. Ein Verzeichnis aller Bände einschließlich der Druckausgaben (ISSN 1618-3193, Band 377-568, von 2000 bis 2008) sowie der früheren **Berichte zur Polarforschung** (ISSN 0176-5027, Band 1–376, von 1981 bis 2000) befindet sich im electronic Publication Information Center **(ePIC)** des Alfred-Wegener-Instituts, Helmholtz-Zentrum für Polar- und Meeresforschung (AWI); see https://epic.awi.de. Durch Auswahl "Reports on Polar- and Marine Research" (via "browse"/"type") wird eine Liste der Publikationen, sortiert nach Bandnummer, innerhalb der absteigenden chronologischen Reihenfolge der Jahrgänge mit Verweis auf das jeweilige pdf-Symbol zum Herunterladen angezeigt.

The **Reports on Polar and Marine Research** (ISSN 1866-3192) are available as open access publications since 2008. A table of all volumes including the printed issues (ISSN 1618-3193, Vol. 377-568, from 2000 until 2008), as well as the earlier **Reports on Polar Research** (ISSN 0176-5027, Vol. 1–376, from 1981 until 2000) is provided by the electronic Publication Information Center **(ePIC)** of the Alfred Wegener Institute, Helmholtz Centre for Polar and Marine Research (AWI); see URL https://epic.awi.de. To generate a list of all Reports, use the URL http://epic.awi.de and select "browse"/"type" to browse "Reports on Polar and Marine Research". A chronological list in declining order will be presented, and pdf-icons displayed for downloading.

Zuletzt erschienene Ausgaben:

Recently published issues:

764 (2022) The Expedition PS128 of the Research Vessel POLARSTERN to the Weddell Sea, Lazarew Sea, Riiser-Larsen Sea, Cosmonaut Sea, and Cooperation Sea in 2022, edited by Ralf Tiedemann and Juliane Müller with contributions of the participants

763 (2022) The MOSES Sternfahrt Expeditions of the Research Vessels ALBIS, LITTORINA, LUDWIG PRANDTL, MYA II and UTHÖRN to the Elbe River, Elbe Estuary and German Bight in 2021, edited by Ingeborg Bussmann, Norbert Anselm, Holger Brix, Philipp Fischer, Götz Flöser, Elisabeth von der Esch, Norbert Kamjunke

762 (2022) 28th International Polar Conference Polar Regions, Climate Change and Society, Potsdam, 01 – 05 May 2022 German Society for Polar Research, edited by H. Kassens, D. Damaske, B. Diekmann, F. Flisker, G. Heinemann, J. Herrle, U. Karsten, N. Koglin, F. Kruse, R. Lehmann, C. Lüdecke, C. Mayer, B. Sattler, M. Scheinert, C. Spiegel-Behnke, and R.Tiedemann

761 (2022) The Expedition PS127 of the Research Vessel POLARSTERN to the Atlantic Ocean in 2021/22, edited by Laura Hehemann with contributions of the participants

760 (2022) Messungen des oberflächennahen Ozons an Bord von Forschungsschiffen im Atlantik und an der Georg-von-Neumayer-Station in der Antarktis von 1977 bis 1996, by Peter Winkler

759 (2022) The Expedition AMD2104 of the Research Vessel CCGS AMUNDSEN to the Arctic Ocean in 2021, edited by Lisa Bröder, Matt O'Regan, Michael Fritz, Bennet Juhls, Taylor Priest, Julie Lattaud, Dustin Whalen, Atsushi Matsuoka, André Pellerin, Thomas Bossé-Demers, Daniel Rudbäck, Antje Eulenburg, Thomas Carson, Maria-Emilia Rodriguez-Cuicas, Paul Overduin, and Jorien Vonk

758 (2021) Expeditions to Antarctica: ANT-Land 2020/21 NEUMAYER STATION III, Kohnen Station, Flight Operations and Field Campaigns, edited by Tanja Fromm, Constance Oberdieck, Tim Heitland and Christine Wesche with contributions of the participants

757 (2021) The Expedition PS126 of the Research Vessel POLARSTERN to the Fram Strait in 2021, edited by Thomas Soltwedel with contributions of the participants

ALFRED-WEGENER-INSTITUT
HELMHOLTZ-ZENTRUM FÜR POLAR-
UND MEERESFORSCHUNG

BREMERHAVEN

Am Handelshafen 12
27570 Bremerhaven
Telefon 0471 4831-0
Telefax 0471 4831-1149
www.awi.de

HELMHOLTZ